SLOVAK GEOLOGICAL MAGAZINE

VOLUME 20 NO 1 ISSN 1335-096X

SELECTED MODELLING APPROACHES IN GEOSCIENCES

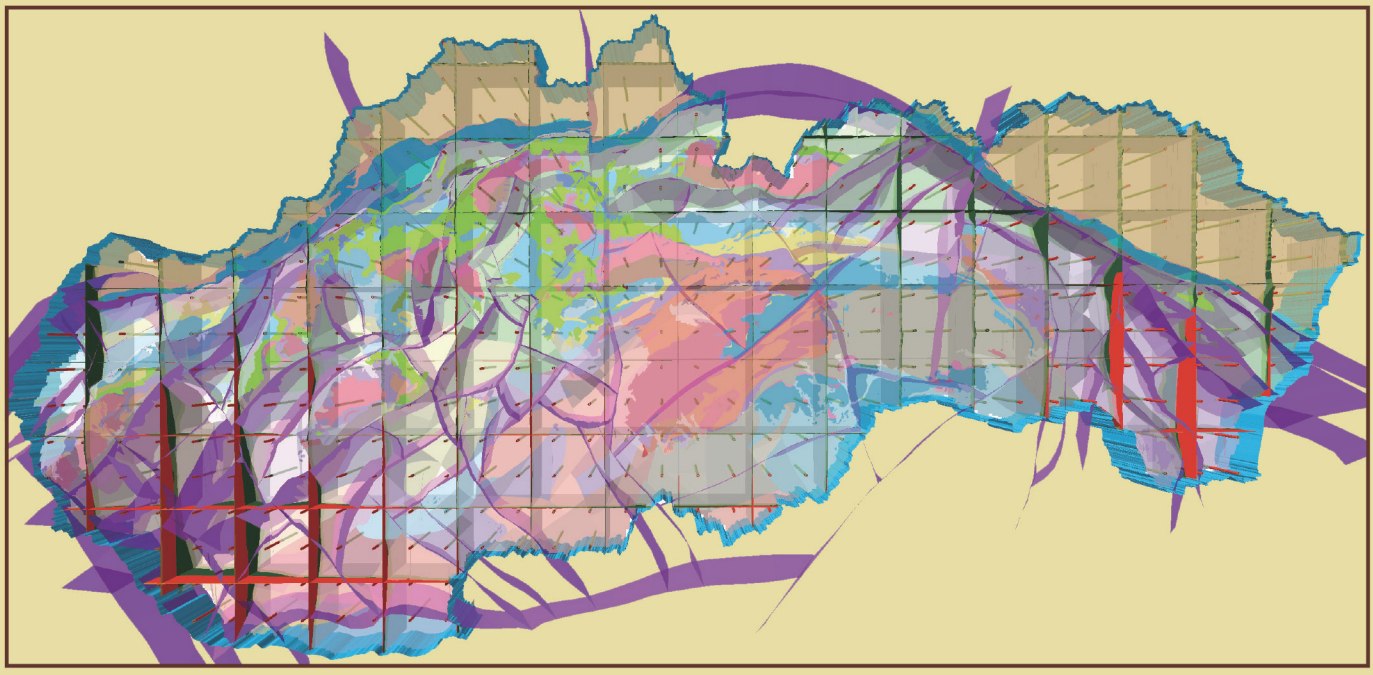

State Geological Institute of Dionýz Štúr Bratislava

1/2020

SLOVAK GEOLOGICAL MAGAZINE

Periodical journal of the State Geological Institute of Dionýz Štúr is a biyearly presenting the results of investigation and researches in wide range of topics:

- regional geology and geological maps
- lithology and stratigraphy
- petrology and mineralogy
- palaeontology
- geochemistry and isotope geology
- geophysics and deep structure
- tectonics and structural geology
- geology of raw minerals deposits
- hydrogeology and geothermal energy
- environmental geochemistry
- engineering geology and geotechnology
- geological hazards and risks
- geoinformatics
- geotourism

The journal is thematically focused in the issues of the Alpine-Carpathian region.

Bratislava, June 2020

Address of Editorial Office: State Geological Institute of Dionýz Štúr, Mlynská dolina 1, 817 04 Bratislava, Slovak Republic, IČO 31753604. The journal is indexed in the list of periodicals of the Ministry of Culture of the Slovak Republic under registration number EV 5006/14.
Printed at State Geological Institute of Dionýz Štúr Bratislava, Slovak Republic.
Online: https://www.geology.sk/slovak-geological-magazine/

ISSN 1335-096X

Content

SLOVAK GEOLOGICAL MAGAZINE

20 (2020) • 1
ISSN 1335-096X

SELECTED MODELLING APPROACHES IN GEOSCIENCES

Content

Edited by:

RNDr. Marian Zlocha, CSc.

Ing. Branislav Fričovský, PhD.

Reviewers:

Ing. Veronika Blanárová, PhD.

RNDr. Radovan Černák, PhD.

Dr. Enrico Guastaldi

Mgr. Balász Kronome, PhD.

Ing. Jozef Mižák

Doc. RNDr. František Staněk, CSc.

ISSN 1335-096X

Preface

The aim of the natural and social sciences is to know the objective reality, to find the laws that govern the processes in nature and society in order to understand and use them. An effective means of the cognitive process is the modelling of objects of interest in space and time.

By a term *model* we understand a simplified representation of the object that is the subject of modelling. However, the model displays only some selected features of the original, because the studied phenomena represent objects of infinite complexity. We therefore proceed with integration by parts – *per partes* – and create partial theories (models) for a limited class of selected observed phenomena. The right choice of modelled properties is the first and at the same time the basic element of a model construction.

Not every model representing a certain theory can be considered acceptable, a theory (model) is good provided it describes a large number of observations based on a small amount of input data and predicts the future behaviour of the object of modelling. Each model is temporary, no matter how many times it has been confirmed by various measurements and observations, we can never be sure that no discrepancy will arise in the future. It can be refuted by a single (verified) observation if the result does not agree with the predictions. On the contrary, every measurement, experiment, that agrees with the model, increases our belief in its accuracy.

Creating *optimal models*, i.e. those that comprehensively meet the required purposes, is not easy. There is no set of rules leading to the unambiguous creation of an ideal model. The model exists only in our minds and has no other reality. The system approach in its creation consists in the analysis of the template, leading to the compilation of a series of partial models and the subsequent synthesis of individual knowledge in order to know the template as a whole. The system approach does not have its own special methods, formal apparatus and technical means. To solve the problem, it combines the methods of various scientific disciplines, so it is characterized by a comprehensive view of natural and social objects and phenomena. The process of creating a model is not a mechanical activity, but always a creative work. It often requires a broad cooperation and knowledge of experts from several scientific and technical disciplines.

There are many reasons for modelling and using models. The main reason is the fact that the modelled display is one of the ways to cope with the complexity of real templates. There are also more pragmatic reasons: working with a model can be easier and safer than with the original, and it may not even be available; experimenting with the original can be costly and time consuming. The models also serve as an aid for understanding the known behaviour of the system as a tool for testing hypotheses, we use models to transfer the behaviour of the system when conditions change and, last but not least, we can use interactive work with computer technology.

The question of the *veracity* of the model is often discussed. In general, it is not possible to judge whether the model is true or false. The model is not a duplicate of the original, but a purposeful simplification. The aim of the modelling process is therefore the effort to obtain a suitable model, i.e. one on which it is possible to solve the required tasks with an accuracy suitable for the purpose.

At the State Geological Institute of Dionýz Štúr, a number of scientists have been modelling natural (mainly geological) phenomena in a broader sense for decades. These are works in the fields of laboratory work (ATNS KE), engineering geology, hydrogeology and in recent years also in the field of regional geology. In the presented issue of the Slovak Geological Magazine, we publish some of the results of recently completed projects in the field of 3D regional modelling of geological structures and geothermal hydrogeology.

The article "3D geological model of the Turčianska kotlina Basin at a scale of 1: 50,000" presents findings from the creation of the first regional 3D model in the Slovak Republic, the methodological procedure used, evaluation of modelling results with recommendations for similar regions modelling. The project of the geological task was completed in 2014. The article "3D Geological model of the Slovak Republic at scale 1: 500,000" presents the results of a geological task, completed in 2019, in which a national 3D geological model of the area was created for the first time on this scale and in this detail. In addition to the modified methodology and the creation of spatial interfaces of the modelled complexes, a web application was created, with the help of which it will be possible to view the 3D model created on the SGIDŠ website. In the contribution „Analytical pseudo lumped-parameter model for reservoir response and recovery assessment: case study for the Ďurkov Depression hydrogeothermal structure, Košice Basin, Slovakia" authors address complexity of model construction enhancing reliability of a model in a given case of lack of production data to forecast reservoir response and recovery. Besides overview on reservoir dynamics during production and reclamation, a clear goal is set to assess a baseline for field production opening, at a rate safe of breakthrough unless sound monitoring is carried, allowing model calibration and further decision making. The paper „Use of Geostatistical Simulation in Reservoir Thermodynamics Assessment and Interpretation at the Ďurkov Hydrogeothermal Structure, Slovakia" reviews use of geostatistical and simulation techniques in approaching thermodynamic quality classification and reservoir description of the Ďurkov Depression, the one amongst most perspective geothermal fields in Slovakia. A paper compares steady-state reservoir thermodynamic conditions given by numerical Turning-bands simulations with state of selected fields worldwide.

Marian Zlocha & Branislav Fričovský

LIST OF ACRONYMS

AHS	Atmosphere Harmful Substances
ALPM(s)	Analytical Lumped-Parameter Model(s)
Ascii	American Standard Code for Information Interchange
ATNS KE	Department of Applied Technology of Raw Materials in Košice
Cdf	Cumulative Distribution Function (Curve)
DDHS	Ďurkov Hydrogeothermal Structure
Dmr	Digital Relief Model
DP	Definition Point
Esri	Environmental Systems Research Institute
Fm.	Formation
GIS	Geographical Information System
IDF	Inverse Distribution Function (Curve)
LPM	Lumped Parameter Model
Mb.	Member
Mcs	Monte Carlo Simulation
NS	Nonconditional Simulation
Pss	Pseudo-Steady State
S-Jtsk	Krovak East North (*System of Uniform Trigonometric Cadastral Network*)
SExI	Specific Exergy Index
TB	Turning Band
TDS	Total Dissolved Solids
UK	Universal Kriging
VES	Vertical Electrical Sounding
2D	Two-Dimensional
3D	Three-Dimensional
1TER	1-Tank Temperature and Energy Recovery (Model)
1TIQ	1-Tank Temperature Response Model with Heat Influx and Reinjection.

Slovak Geol. Mag., 20, 1 (2020), 5 – 32

1. 3D Geological Model of the Turčianska kotlina Depression at Scale 1: 50,000

Zlocha Marian & Nagy Alexander

State Geological Institute of Dionýz Štúr, Mlynská dolina, Bratislava, Slovak Republic; marian.zlocha@geology.sk

Abstract: 3D modelling of the Turčianska kotlina Depression was elaborated within the project Turčianska kotlina Depression - three-dimensional geological modelling in 2013 and 2014 (Nagy et al., 2014) in order to create a quality regional model at a scale of 1: 50,000, which could also be used as an input data for hydrogeological modelling, etc.

To create a 3D geological model of the area, data from published works were used, such as analog geological profiles from the geological map at a scale of 1: 50,000 (Gašparik & Halouzka, 1993), maps of the pre-Tertiary basement of the Atlas of Geothermal Energy (Franko et al., 2010) and geophysical works (Bielik et al., 2013), but for the required quality it was also necessary to use data from 1,300 VES probes that were interpreted in 34 profiles. The creation of the model itself would still not be possible without the external intervention of an experienced geologist, so it is possible to say that the so-called an explicit approach was applied, where a geologist and a 3D expert interactively co-create a 3D model using computer technology.

In this work we present a methodical procedure for solving the problem, i.e. the exact procedure from the creation of a catalog of modelled layers/formations and processing of input data, through the creation of a tectonic model to the creation of 3D surfaces with respect to the tectonic structure.

The results of modelling are documented by individual modelled formations and layers and in a separate chapter also by individual tectonic segments, where the projection areas and cubatures of individual modelled bodies are calculated. Both the procedure and the modelling results are documented by tables and a number of figures.

The conclusions provide a summary of the work and recommendations for modelling other regions of the Slovak Republic.

The work used a 3D modelling package Petrel® in version 8.4 from the company Schlumberger.

Keywords: 3D modelling, geological model, sedimentary basin, vertical electrical sounding

1.1 Introduction

Already at the beginning of the computer age, after mastering elementary computational operations and verifying the speed of computations for a larger amount of input data, effective algorithms began to be developed and subsequently applied, which helped to perform demanding tasks in a reasonable time. In addition to the great interest of the military, new opportunities have opened up for science and research and the application of their results in various areas of human activity, not excluding geology.

From the beginning, the investments in geological prospecting and of mining companies have pushed the development forward, from various 2D interpolation methods (kriging, splines), through simulations, mining optimization to the current state with fantastic possibilities in 3D (calculations, visualizations) and virtual reality. Such tools, robust 3D packages, were gradually available to the wider professional public, and thus enabled also SGIDŠ to participate in the field of 3D model creation more than ten years ago.

The first task in this area was the project "Upper Nitra Basin - three-dimensional geological modelling of the exposed area" (Kotuľová et al., 2010). The methodological results of this project were followed by the task "3D geological model of the Turčianska kotlina Depression at a scale of 1: 50,000" (Nagy et. al., 2014) in order to create a three-dimensional geological model of the area and other superstructure 3D models of the basin together with morphology and lithological content of the pre-Cenozoic bedrock and the overlying Cenozoic sedimentary fill.

1.2 Sequence of the 3D model creation

At work, we relied on previous experience and know-how. We have already solved the problems of calculating the reserves of mineral resources, or solving the spatial distribution of useful components in the magnesite deposit of the Dúbrava Massif, but these problems were solved mainly in a 2D way along individual mining horizons and profiles.

The use of the Petrel® 8.4 program from the Schlumberger Company enabled us to create a geological model in a truly spatial way, assuming we are based on the methodological procedure and philosophy of the Petrel® program model creating.

Since our task was to create a 3D model of the sedimentary filling of the depression, we did not have to create new procedures, it was enough to prepare as much relevant input data as possible and proceed exactly within the defined methodology.

We proceeded from the creation of a tectonic structure, the selection of modelled interfaces, the creation of catalogs and databases, through the generalization and interpretation of input data to the actual modelling of individual 3D bodies (complexes). The resulting 3D model formed a set of 3D surfaces, including the tectonic structure of the area.

How did we proceed?

3D modelling was preceded by the preparation of input data (engineering geological boreholes, hydrogeological wells, deep boreholes, analog data from existing geological maps and geochemical atlas data, analog profiles from maps at a scale of 1: 50,000 (Fig. 1.1), existing digital data on the basement from geophysics results and the others, which we will present hereinafter).

The comparison of some existing models of the basement of the Turčianska kotlina Depression (geophysical model or data from the Atlas of Geothermal Energy, Fig. 1.2) showed that the situation was not unambiguous and we

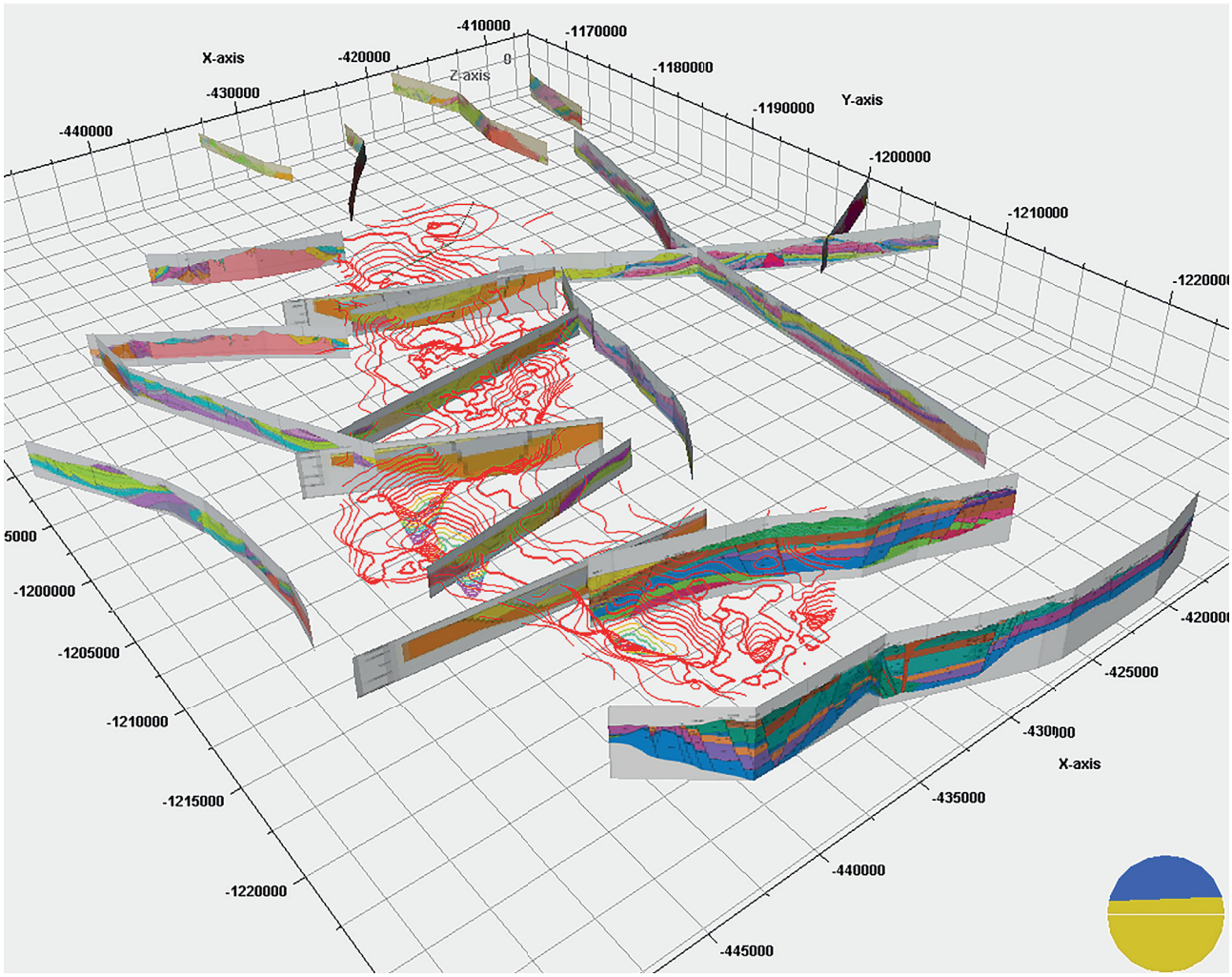

Fig. 1.1. *3D geological profiles from geological maps and basement depth (basement depth according to Bielik et al., 2013)*

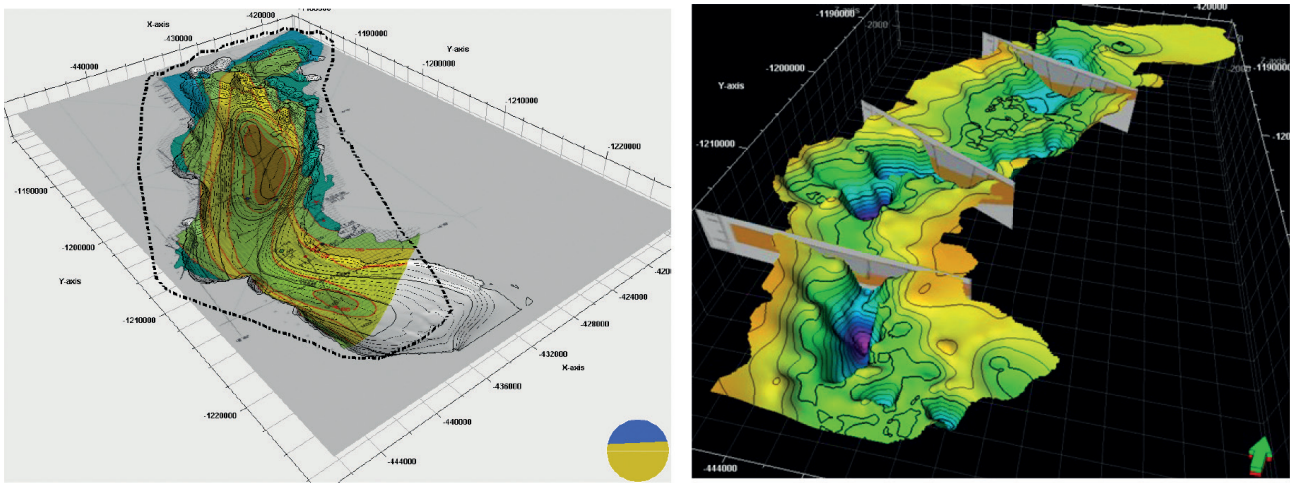

Fig. 1.2. *left: Basement depth according to data from the Atlas of Geothermal Energy, right: Basement depth according to (Bielik et al., 2013) and selected 3D geological profiles.*

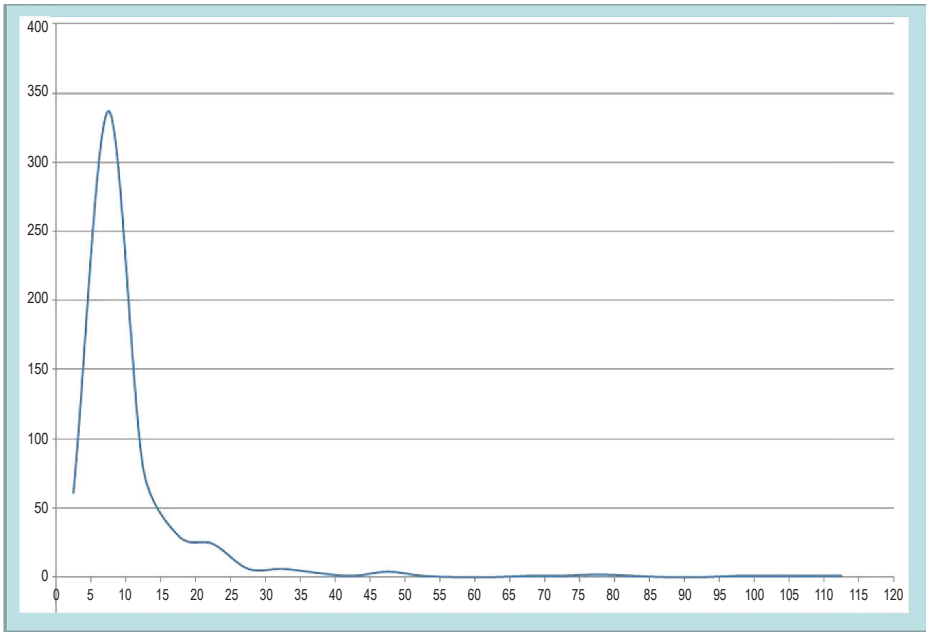

Fig. 1.3. *Number of boreholes depending on depth (histogram/ distribution). Existing, mostly shallow engineering geological and hydrogeological boreholes did not allow to model the area of the Turčianska kotlina Depression basin to a depth greater than 10-15 m.*

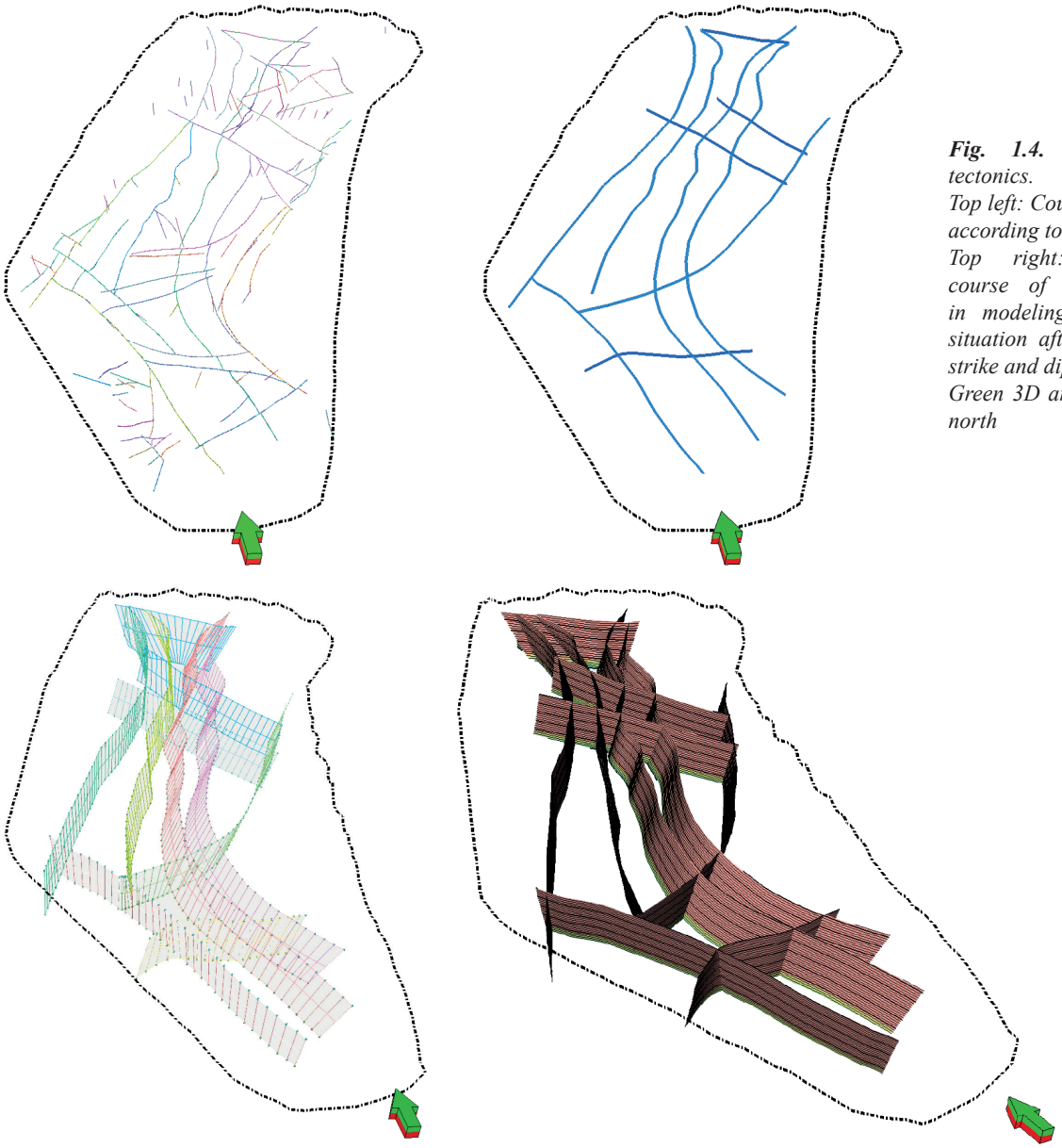

Fig. 1.4. *Modelling of tectonics.*
Top left: Course of all faults according to geologic maps, Top right: Generalizrd course of faults applied in modeling. Bottom: 3D situation after defining the strike and dip of the faults. Green 3D arrow pointed to north

had to critically evaluate the previously published results or create a basement model in a new way.

In addition, due to the spatial distribution of the above-mentioned input data (Figs. 1.1, 1.2, 1.3), it was not possible to create a more detailed, or sufficiently deep 3D geological model at a scale of 1: 50,000.

We proceeded to thicken the input data with data from existing VES profiles, which were obtained from company Geocomplex, a.s. Subsequently, more than 1,300 VES probes were processed and 34 *interpreted* geophysical profiles were created. From such 3D input data (i.e. from a sufficiently detailed set of geological profiles), it was already possible to create a sufficiently representative 3D model of the Turčianska kotlina Depression. This model was subsequently used as an input for the creation of a hydrogeological model of the area.

In the initial phase of the model creation, a legend was prepared, or the catalog in which the codes for the modelled layers and formations were defined (Tab.1.1).

Tab. 1.1. Explanations for the processed VES probes. We list the names of the layers and formations ("Original Name", the "Simplified name", and the "Code" used in the database).

Original Name	Simplified name	Code
Quaternary	Quaternary	0
orthogneiss	Granitoids/Crystalline complex	2
granitoid		
weathered granitoid		
Ramsau dolomite	Mesozoic	4-7
dolomitic limestone		
marly limestone, marl		
Algau+Gresten Members		
Borové Formation	Borové Fm.	10
Huty Formation	Huty Fm.	11
Rakša Formation	Rakša Fm.	14
fine grained tuff and tuffite	Fine grained tuff(ite)	16
epiclastic volcanic conglomerate	Epicl.conglom.	17
lava flow 1	Turčok Fm.	18.1
lava flow 2	Jastrabie Fm.	18.2
Bystričany Formation	Bystričany Fm.	19
Budiš Formation	Budiš Fm.	20
Abramovce Member	Abramovce Mb.	21
sandstone	>> Martin Fm.	22

The top boundary surface of the 3D model was created from the existing high-precision DMR in a 20x20 m grid (source: GeoIS SGIDŠ), which was recalculated and generalized to a 100x100 m network. This regular grid was used for all 3D visualizations.

The boundary of the modelled area and the geological map of the area at a scale of 1: 50,000 were digitally processed and georeferenced into 3D. Above the georeferenced map of the Turčianska kotlina Depression and the adjacent regions (Veľká Fatra, Malá Fatra, Kremnické vrchy Mts.), the faults were digitized, the most significant were selected for modelling purposes and they were generalized (Fig. 1.4).

Based on the VES probes (1,340 pcs.), 34 interpreted profiles with a legend (explanations) were created in accord with Tab.1.1. Subsequently, the slope of the individual faults was modelled according to the interpreted VES profiles so that it corresponded as accurately as possible to the geological and interpreted situation (Fig. 1.5).

The modelling of the tectonic structure completed the first stage of creating a 3D model, the so-called *fault modelling* - creation of model structural frame. In the next stages, this tectonic structure formed a skeleton not only for the subsequent creation of a 3D model, but also provided a solid structure during the interpretation and digitization of the input data. The space was divided into 14 segments by generalized faults (Fig. 1.6).

Originally nonlinear raster geological profiles were digitized with respect to generalized tectonics. The interfaces of the individual interpreted VES profiles were vectorized taking into account the created spatial faults and the existing legend of the individual complexes (i.e. their mutual stratigraphic position, Figs. 1.7, 8).

Tab. 1.2. Final explanations (catalog, database) for the processed VES probes from overburden to basement.

Simplified name	Code
Quaternary	0
Bystričany Fm.	19
Jastrabie Fm.	18.2
Martin Fm.	16-24
Abramovce Mb.	21
Epiclastic conglomerates	17
Turčok Fm.	18.1
Budiš Fm.	20
Rakša Fm.	14
Huty Fm.	11
Borové Fm.	10
Mesozoic undivided	4-7
Granitoids/Crystalline complex	2

Selected modelled complexes description:

Crystalline (code 2)

Crystalline rocks are involved in the geological structure of NW slopes of the Žiar mountain range, the western slopes of Lúčanská Malá Fatra Mts. and on the S slopes of Krivánska Malá Fatra Mts. The crystalline rocks of the Žiar and Malá Fatra core mountains are made of magmatites mainly, dominantly granitoid rocks. Metamorphic rocks, with the exception of Lúčanská Malá Fatra Mts., where paragneiss predominatea, are inferiorly represented in the Žiar Mts. and are absent in Krivánska Malá Fatra Mts.

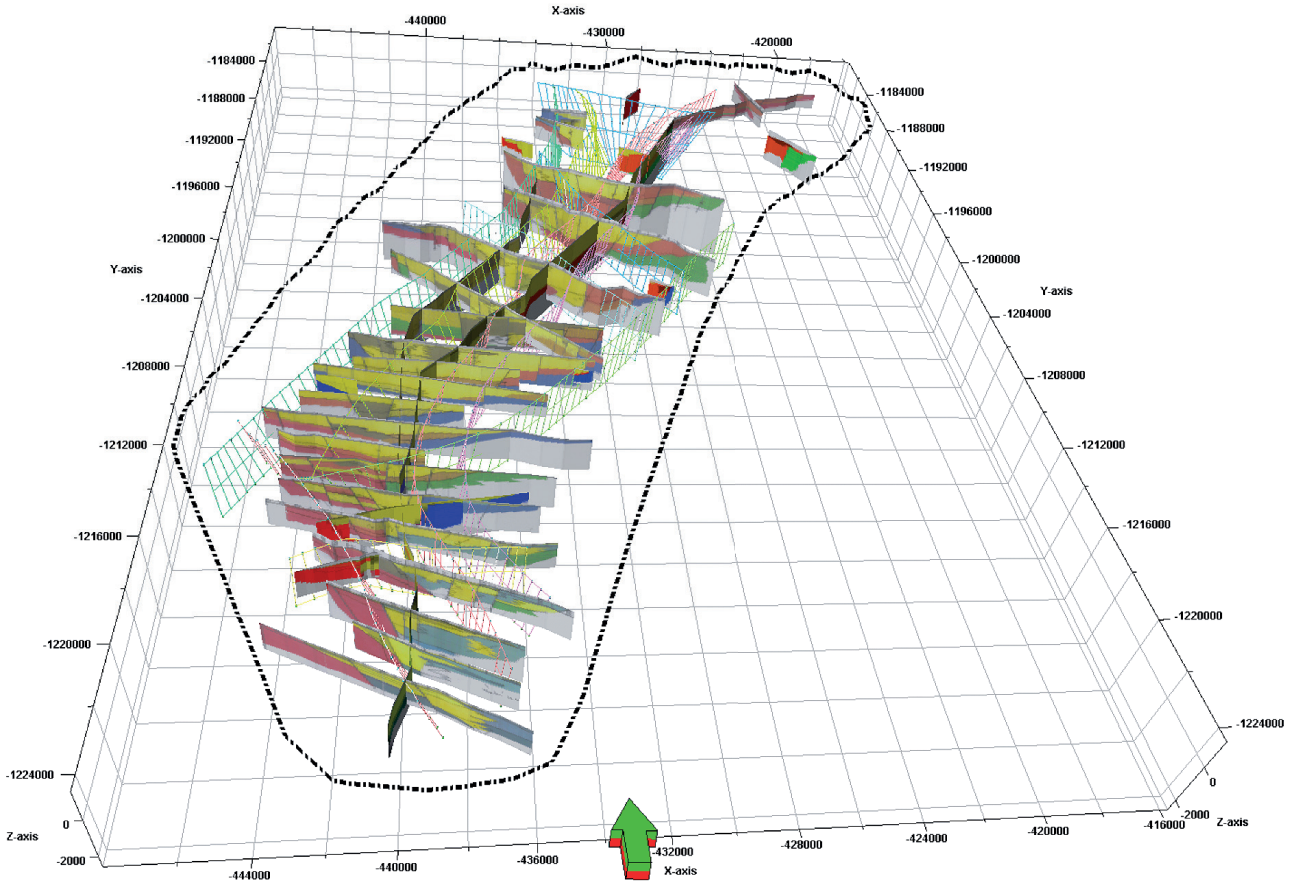

Fig. 1.5. *Resulting georeferenced interpreted 3D VES profiles with territory delineation and faults course depiction.*

Mesozoic undivided (code 4-7)

In the segment 1, only Hronicum rocks (age range Cretaceous-Valanginian to Triassic-Fasanian) represented by dolomites and marly shales of the Mráznica Formation, Gader Limestone and Wetterstein Dolomite.

The segment **2** includes Tatricum and Fatricum outcrops. The **Tatricum** (age range of the Early Triassic to the Cretaceous-*Early Albian-Middle Turonian* is represented by sedimentary clastic, carbonatic and shale rocks in the form of narrow strips (Lúžna Formation Gutenstein Mb., Ramsau Dolomite, Carpathian Keuper, Trlenský potok Fm., Allgäu Mb., Lučivná and Poruba Fms.).

The largest areas of Mesozoic **Fatricum** units (age range Triassic-*Anisian* to Cretaceous-*Early Cenomanian*) are made of calcareous rocks of the Mráznica Fm., then the Ramsau Dolomite and the least represented sediments of the Carpathian Keuper. The remaining sediments (Gutenstein Limestone, Podhradie Limestone, Lunz Mb., Haupt Dolomite, Fatra Mb., Kopienec Fm., Allgäu Mb., silica-rich Fleckenmergel, variegated radiolarian limestones and radiolarites, Jasenie Fm., Osnica Fm., organodetritic limestones, Nolčovo Mb. And Poruba Fm.) occupy an incomparably smaller area representing mostly occurrences in the form of strips.

The sgment **3** consists only of the **Hronicum** rocks (age range Triassic-*Anisian* to *Late Carnian-Norian*), of which the Wetterstein Dolomite, Gader Limestone and Ramsau Dolomite occupy the largest surface area. Others (Gutenstein Limestone, Wetterstein Limestone, Lunz Mb. and Haupt Dolomite) are represented to a much lesser extent.

The whole area of the segment 4 is represented by Fatricum rocks (age range Triassic-*Norian* to Cretaceous-*Early Cenomanian*) of which (Ramsau Dolomite, Carpathian Keuper, Fatra Mb., Allgäu Mb., variegated radiolarian limestones, Poruba Fm.) almost the entire territory is represented by dolomites and marly shales of the Mráznica Fm.

In the segment **5** of the edge of the basin of the pre-Cenozoic age, the Mesozoic rocks belong mainly to the Tatricum Žiar Succession. In the lithostratigraphic sequence (age range from the Early Triassic to the Cretaceous), larger continuous areas are formed only by clastic sediments of the Lúžna Formation, Gutenstein Limestone and limestones and claystones of the Allgäu Mb. Distribution of other carbonatic, shale and clastic sediments (Werfenian Mb., Carpathian Keuper, Kopienec Fm., Trlenský potok Fm., Hierlatz Limestone, siliceous Fleckenmergel, siliceous limestones and radiolarian limestones, Lučivná Fm. and conglomerates occurs in the form of relatively thin strips.

The Fatricum in the segment **6** is represented by the Zliechov Sequence (age range from the Middle Triassic to the Middle Cretaceous). The situation is complicated by a duplex structure, where on a Cretaceous flysch there

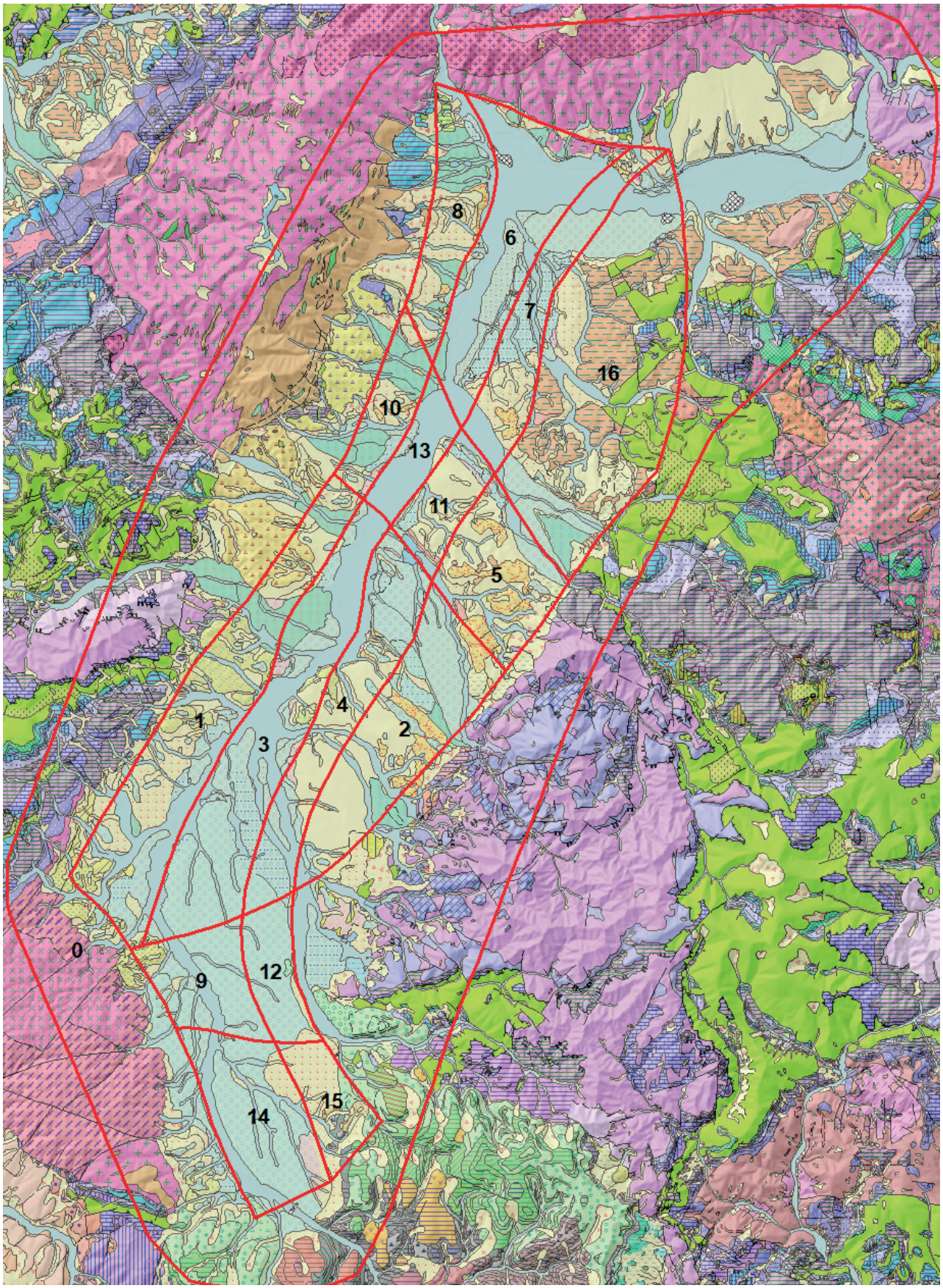

Fig. 1.6. *Area segmentation (according to generalized faults).*
Segments 2 to 14 are bound by tectonics from all sides, segments 91-93 form auxilliary segments, bound by tectonics from three sides. segment 1 forms an boundary area on the digital geological map at a scale 1: 50 000, map portal SGIDŠ [online].

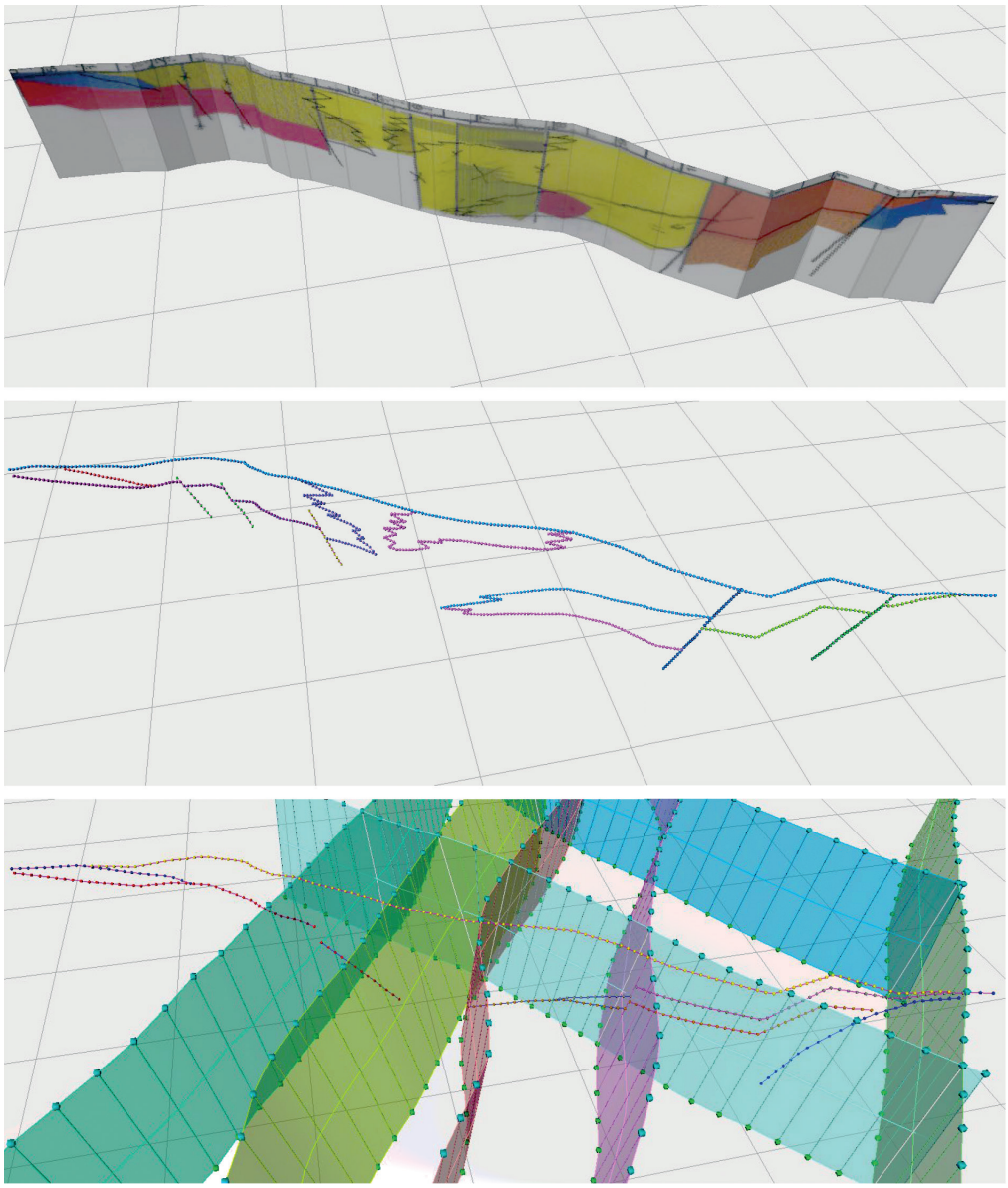

Fig. 1.7. *Digitization of raster 3D profiles - detail of works.*
Top: Raster interpreted VES profile georeferenced in 3D (1st stage)
In the centre: Digitization of interfaces into vector form in space (2nd stage).
Bottom: Final interpretation (stage 3).

is again a layered sequence of Neocomian age overlain by the Hronicum tectonic outliers. Larger continuous areas consist only of Ramsau Dolomite and Cretaceous carbonates. The remaining carbonatic, clayey and clastic sediments (Gutenstein-type limestone, Podhradie Limestone, Carpathian Keuper, Kopienec Fm, Allgäu Mb., siliceous Fleckenmergel, radiolarans and flyschoid formation) occur in the form of relatively thin stripes.

The Hronicum rocks (age range Triassic-Anisian to Norian) in the segment **7**, consist of two elements. The lower structure is composed of Gutenstein Limestone, Ramsau Dolomite and Haupt Dolomite and marginally by Lunz Mb. The upper one is formed by the so-called tectonic outlier "Studenec", represented by Gutenstein Limestone and Wetterstein Dolomite, marginally also by Schreyaralm Limestone. The Wetterstein and then the Haupt Dolomite occupy the largest area.

The segment **8** is formed by rocks of the Fatricum and Hronicum. The oldest and at the same time the lowest parts of the Fatricum belong to the Middle Triassic sequences. The setting is complicated by the unevenly developed duplex structure, in which the sequence of the Middle Cretaceous age lies again on the Early Cretaceous. The Fatricum sediments are also exposed in small isolated islands between the Valčianska dolina Valley and Lázky in the narrow strip of NE direction.

The Fatricum sediments (age range of Triassic-*Anisian* to Cretaceous-*Aptian*) are represented by carbonatic, clastic and clayey rocks (Ramsau Dolomite, Lunz Shale, Carpathian Keuper, Kössen Mb., Kopienec Fm., Allgäu Mb., siliceous limestones, radiolarian limestones, marls and marly limestones).

The minor tectonic outliers of the Mesozoic Hronicum units, represented by the Ramsau Dolomite and the Gutenstein Limestone, rest either on the first thrust slice or on the duplex block.

In the segment **9**, the Mesozoic Tatricum units are situated in small occurrences on the SE slopes of Lúčanská Malá Fatra Mts. They overlie directly the crystalline rocks. They consist only of clastic sediments of the

Lúžna Formation and of Gutenstein Limestone (age range Triassic-*Scythian* to *Anisian*).

Among the Mesozoic formations of the Fatricum (age range from Triassic-*Rhethian* to the Cretaceous-*Hauterivian*), the Allgäu Mb. is the most widespread. In addition to it, there are also carbonatic, organodetritic and shale sediments (Kopienec Fm., Fatra Mb.).

Borové Fm. (Lutetian, code 10)

It consists of conglomerates, breccias and organogenic limestones.

Huty Fm. (Priabonian, code 11)

It is made of shales, sandstones and menilite claystones.

Rakša Fm. (Eggenburgian, code 14)

The Rakša Fm. is the oldest Neogene sediments complex, formed by brecciated conglomerates of carbonate rocks and layers of sandy limestones with a fauna of molluscs.

Budiš Fm. (Sarmatian-Pannonian, code 20)

The formation occurs only in the southern part of the basin, in forefront of the Žiar mountain range. The deposits have the character of a flood cone (sediments of planar torrents or a braided river). The main rock component are washed-out granite deluvia transported over short distances and erosion products of the packaging Mesozoic. They are mainly sands - sandstones of arkose-like character with varying degrees of lithifying from loose to dense or slightly cemented.

Turčok Fm. (code 18.1)

The Turčok Fm. (*Late Badenian*) is made of epiclastic conglomerates, tuffs, pyroclastic breccias and lava flows of various varieties of andesite volcanism.

Abramovce Mb. (Pannonian-Pontian, code 21)

The main rock type are gravel - gravel sands of exclusively carbonate composition. These are sediments of dense gravitational flows (debris flow) settled in the form of fans.

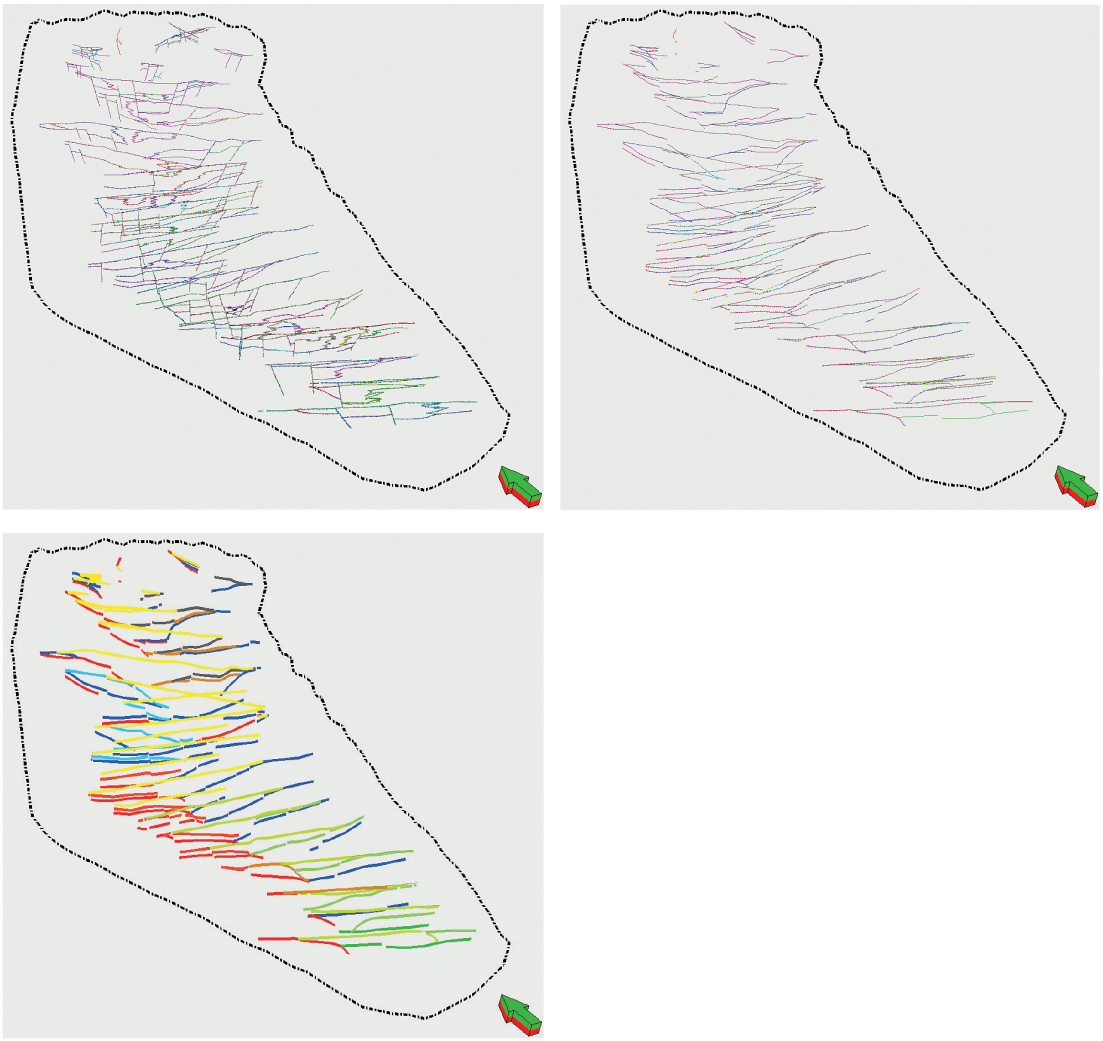

Fig. 1.8. *From digitization to 3D database.*
Top left: vector interfaces by profiles 2nd stage.
Top right: vector interfaces by profiles 3rd stage.
Below: Colour-indicated interfaces of overburdens of selected complexes (see Tab. 1.2).

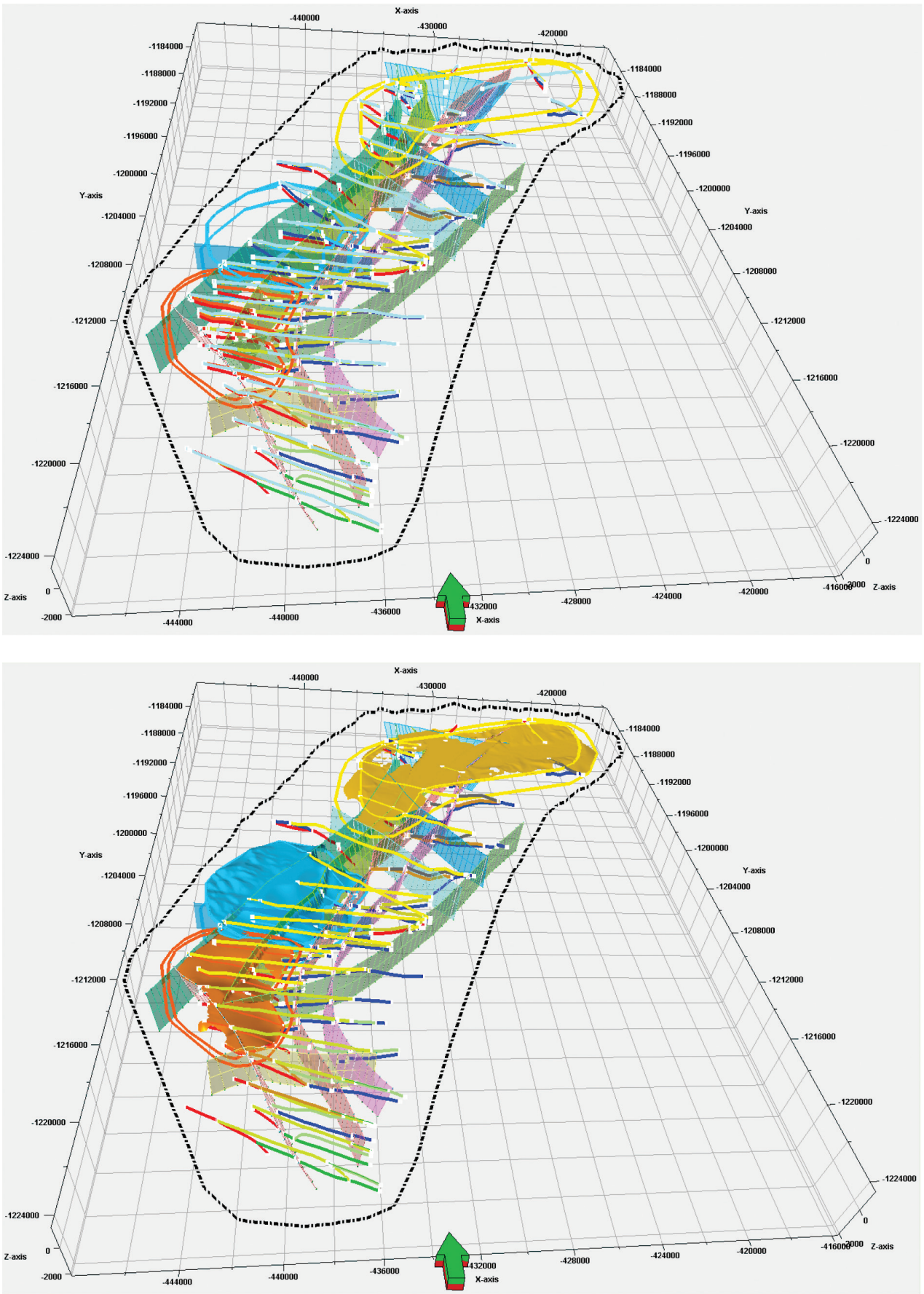

Fig. 1.9. *Interfaces and their occurrence.*
Above: 3 selected complexes are displayed: Budiš Fm., Abramovce Mb. and Bystričany Fm. and their probable wedging out. The selected units are shown below as a 3D modelled surface.

Martin Fm. (Sarmatian-Pontian, code 16-24)

The formation forms the main part of the Neogene filling of the basin. In terms of lithofacies it is variable, with the main component being clays with different proportions of sandy admixture. Furthermore, there occur so-called coaly clays, lignite seams, clayey sands to sands, rare sandstones, fine to medium-grained carbonate conglomerates and freshwater limestones and occasionally tuffites.

Jastrabská Fm. (code 18.2)

The Jastrabie Fm. (*Late Sarmatian-Early Pannonian*) consists of rhyolite epiclastic sandstones and breccias, tuffs, extrusions of rhyolites and their breccias and lava flows.

Bystričany Fm. (Pliocene, code 19)

It consists of coarse sediments of subaerial and subaquatic gravitational flows (debris flow) deposited in the form of fans. In contact with the crystalline massif of Lúčanská Malá Fatra Mts., these are rather breccias and boulder conglomerates with blocks of several m^3 in volume, made of dolomites and limestones. From the edge, the size of the pebbles gradually decreases. Unlike the Slovany and Abramovce Mbs., their composition is varied.

Quaternary (code 0)

Quaternary sediments have the largest area distribution in the Turčianska kotlina Depression. In the past, they were most completely studied by Halouzka (in Gašparik et al., 1995), according to whom the determining genotype of the Quaternary alluvial sediments in this basin are terrace-type sediments.

To each of the individual 3D boundary lines an attribute was assigned which characterized the modelled complex. These objects were grouped according to the modelled horizon (Tab. 1.2). Models of individual horizons were formed gradually from the base (granitoids). The 3D boundaries created faithfully corresponded to the data from the profiles (where they were at hand), but in areas where there was no data, their extrapolation was challenging (Fig 1.9). For this reason, it was necessary to include other expert information in the modelling, such as the probable wedging out of the layers, which was performed in a similar way as in the calculation of mineral reserves. (In the construction of 3D polygons, the wedging out was inserted within 1/2 of the distance between positive and negative occurrence in the profiles, respecting the morphology between the profiles and stratigraphy (Fig. 1.9).

Progressing from the base to the overburden, the errors of topological connections between objects, or various interpolation artifacts (extrapolation of the Mesozoic below the granitoids, the outcrop of a layer at the surface where it was not possible according to the geological map and interpreted profiles, etc.). Gradually, all modelled units were created in the form of 3D surfaces in this way (Figs. 1.10, 1.11).

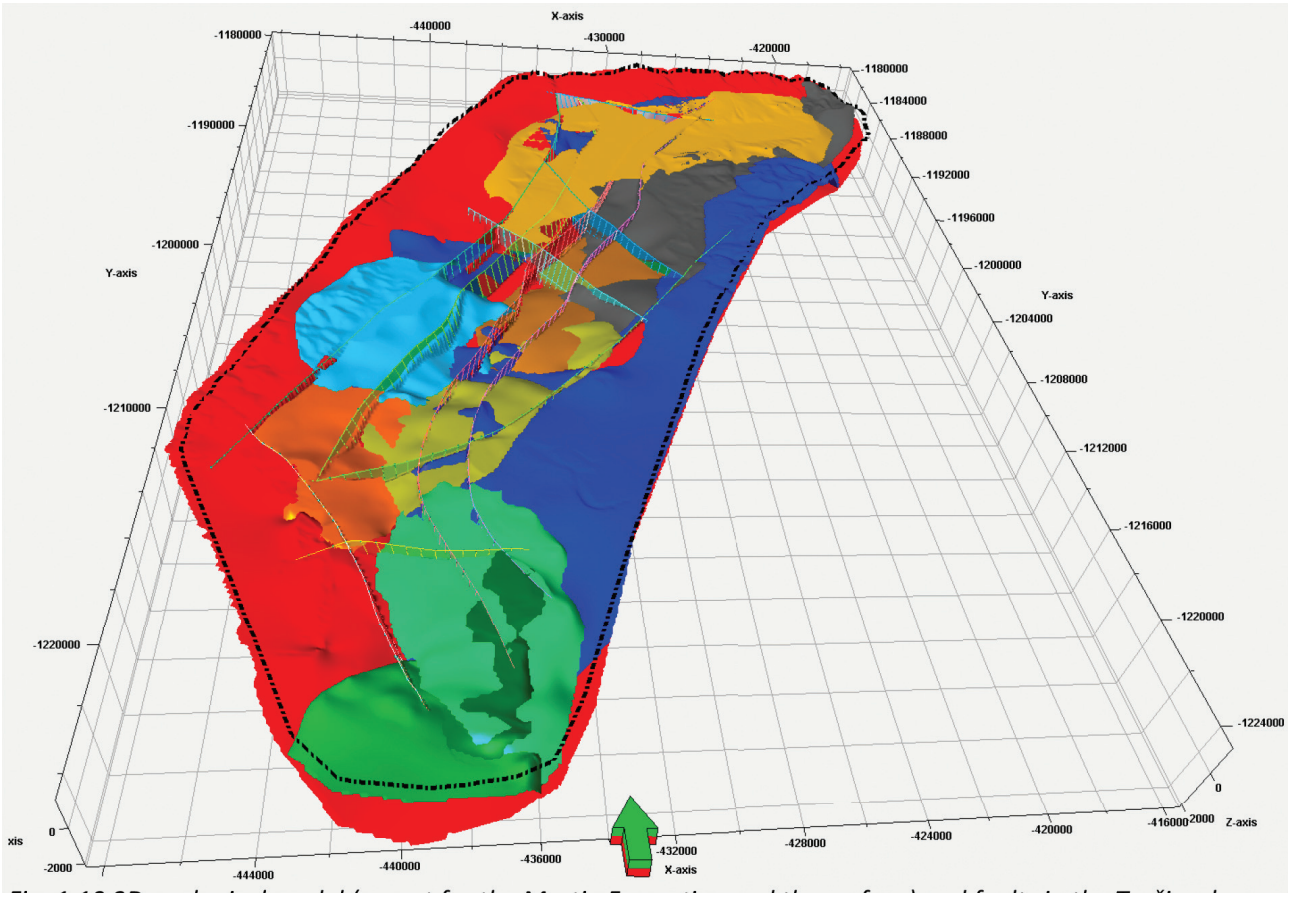

Fig. 1.10. *3D geological model (except for the Martin Formation and the surface) and faults in the Turčianska kotlina Depression.*

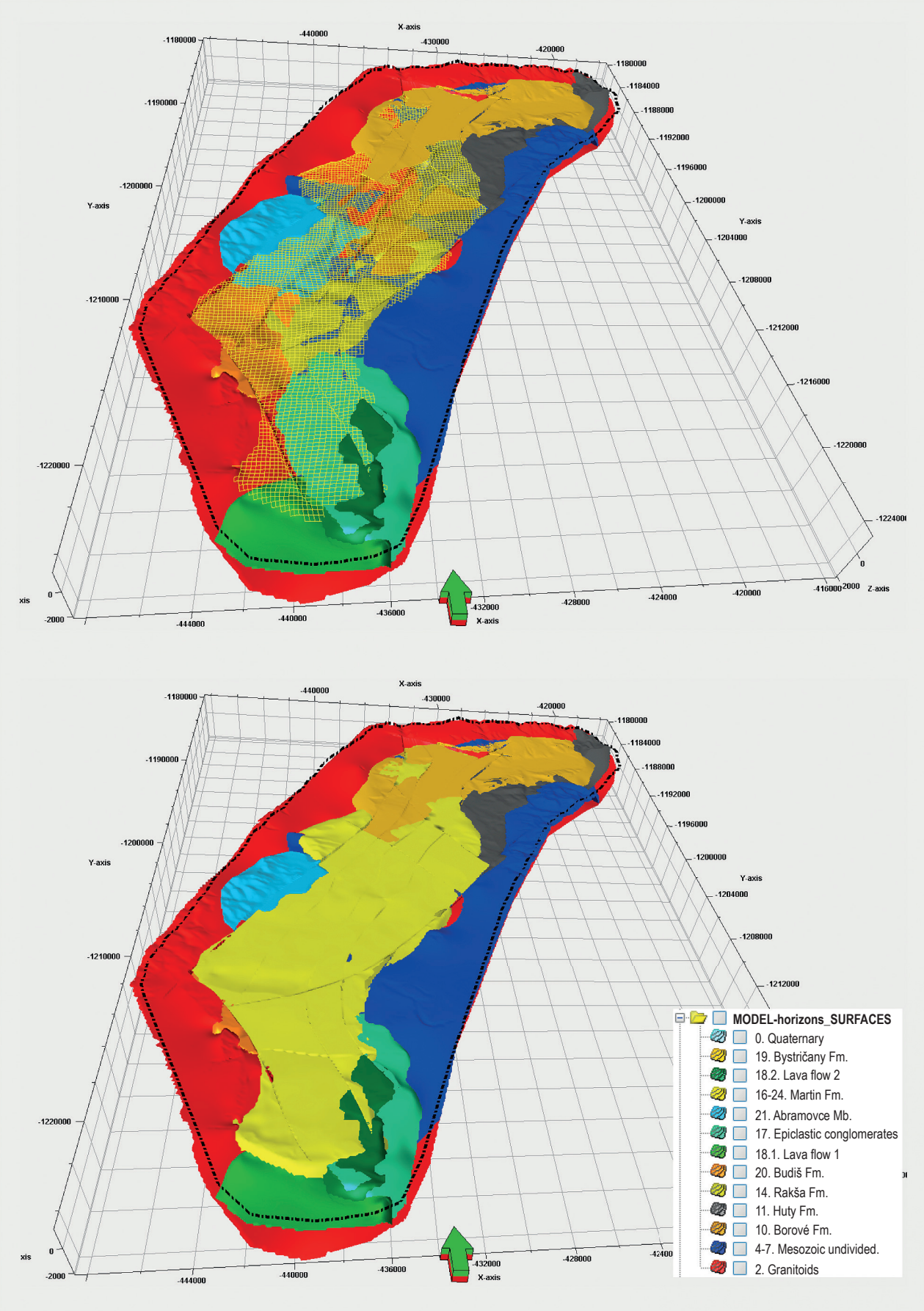

Fig. 1.11. *3D geological model of the Turčianska kotlina Depression.*
Above: exposed model (Martin Formation is shown in the form of a hatch).
Bottom: 3D geological model with legend (without Quaternary).

1.3 Results of the 3D modelling reflecting individual formations

In the following text, for the sake of clarity, the individual modelled complexes (except for granitoids) are shown as follows (Figs. 1.12-1.23).

At the top left is a view of the modelled unit (formation, layer) from SW, at the top right is a modelled unit loaded on the ***cumulative*** surface of the underlying layers. The bottom left shows the unit thickness in [m] and the bottom right its approximate modelled range projected onto the surface of the area with DMR and topography.

MESOZOIC

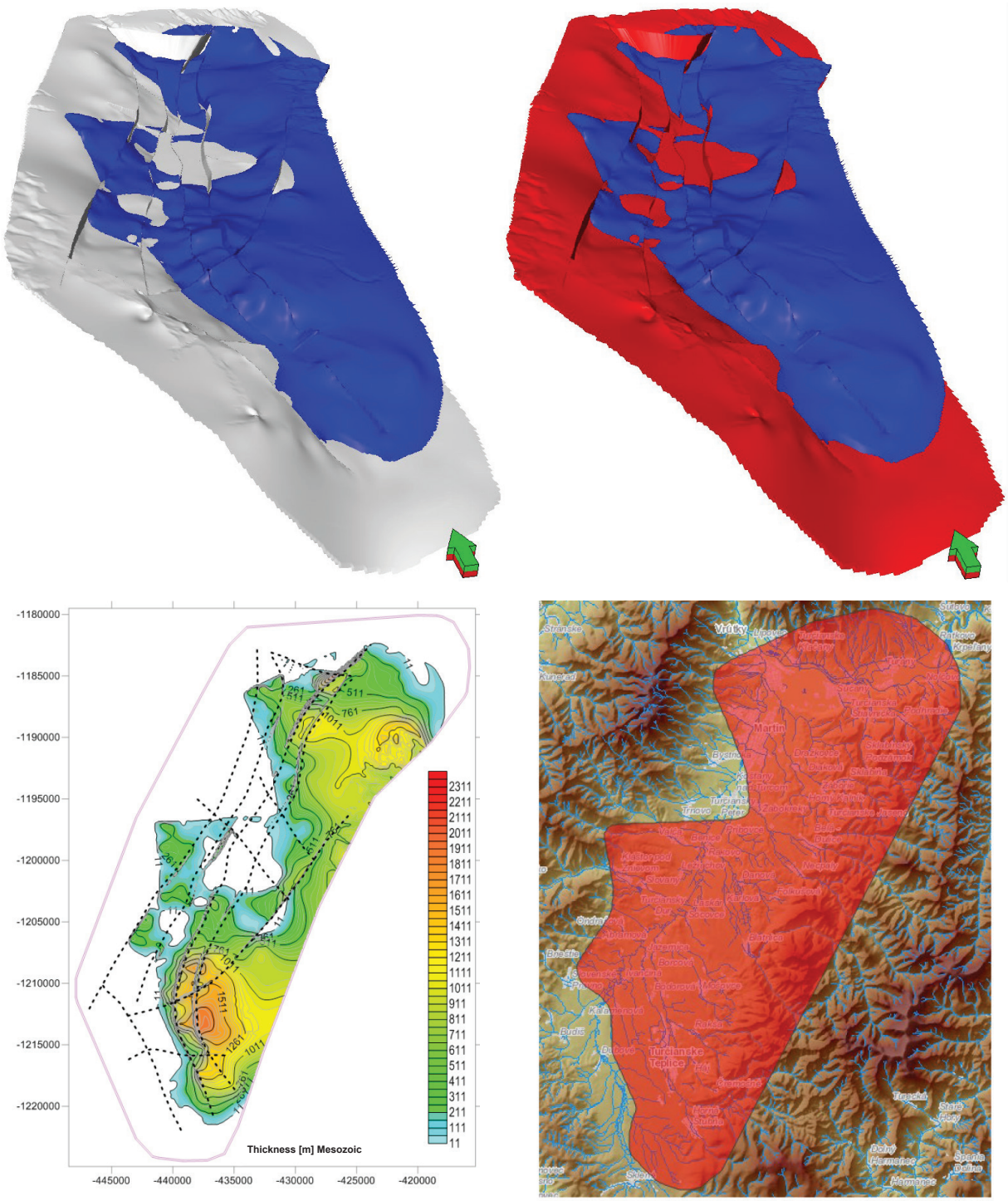

Fig. 1.12. *Mesozoic.*
Top left: view from SW, top right: loaded on the cumulative surface of the bedrock (here: granite), bottom left: thickness [m],bottom right: approximate extent projected onto the surface of the area with DMR and topography (display without scale).

BOROVÉ FORMATION

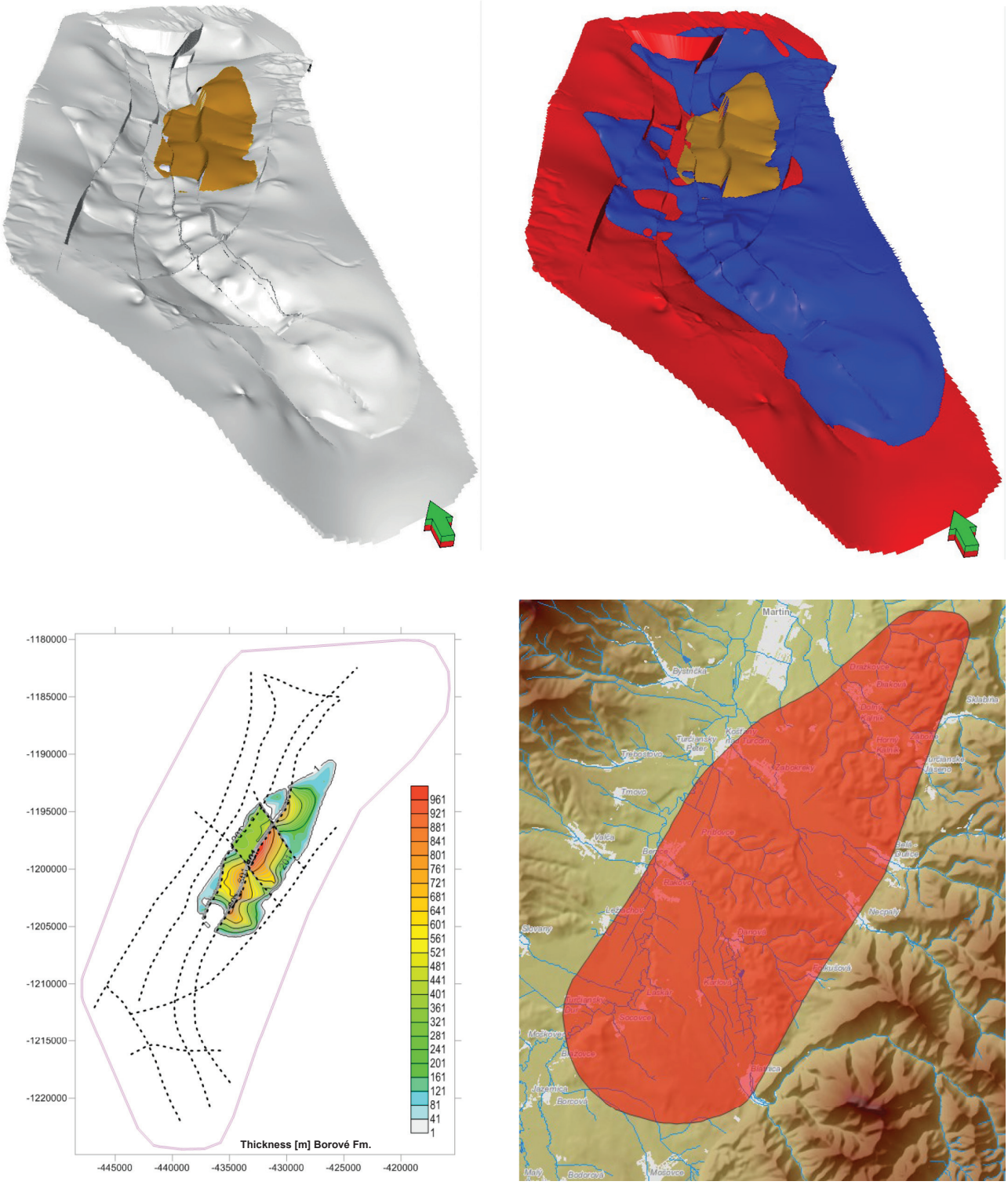

Fig. 1.13. *Borové Formation.*
Top left: view from SW, top right: loaded on the cumulative surface of the underlying formations (in this case: granite and Mesozoic), bottom left: thickness in [m],bottom right: approximate extent projected onto the surface of the area with DMR and topography (display without scale).

HUTY FORMATION

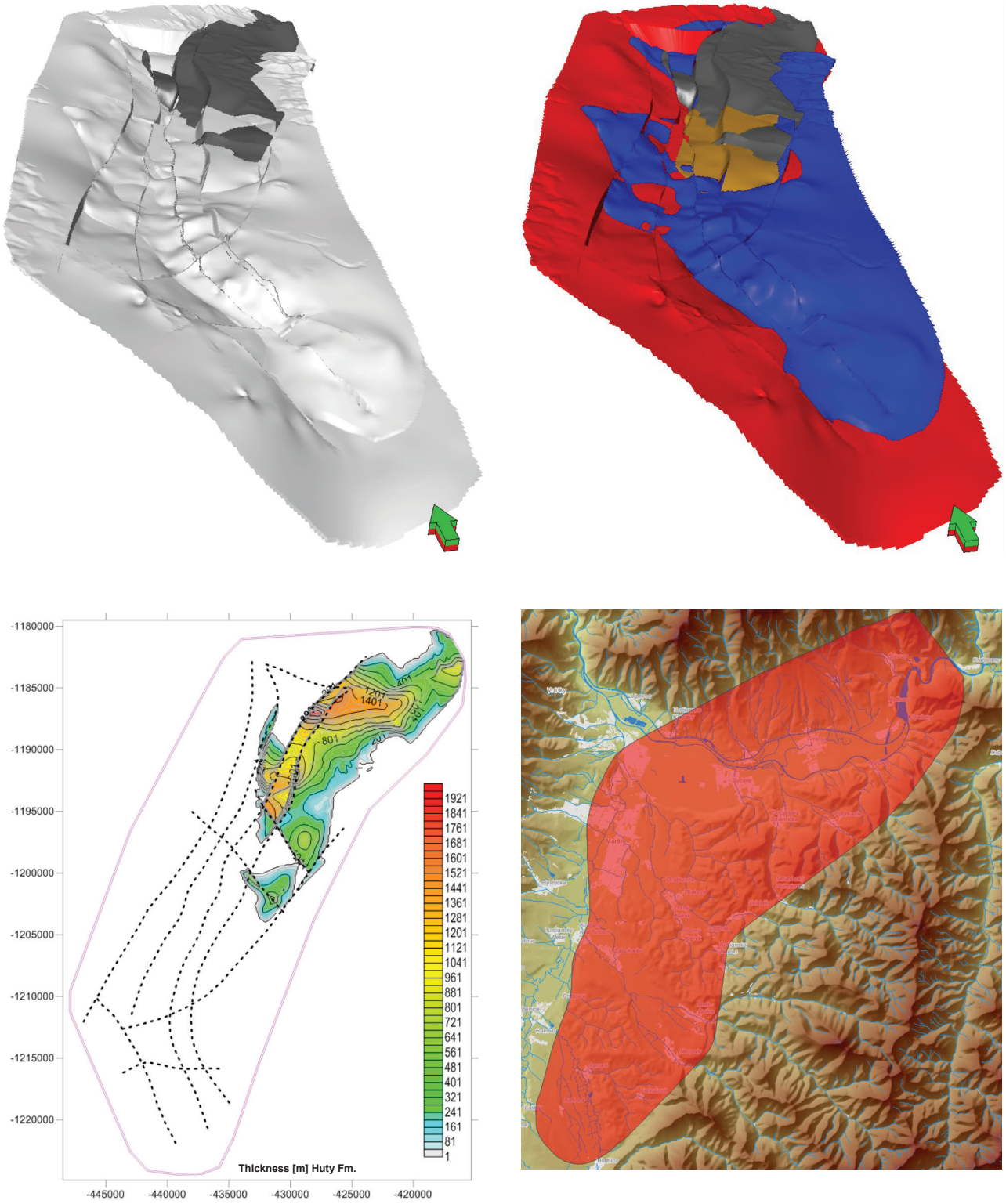

Fig. 1.14. *Huty Formation.*
Top left: view from SW, top right: loaded on the cumulative surface of the bedrock (in this case: previous complexes), bottom left: thickness in [m], bottom right: approximate extent projected onto the surface of the area with DMR and topography (display without scale).

RAKŠA FORMATION

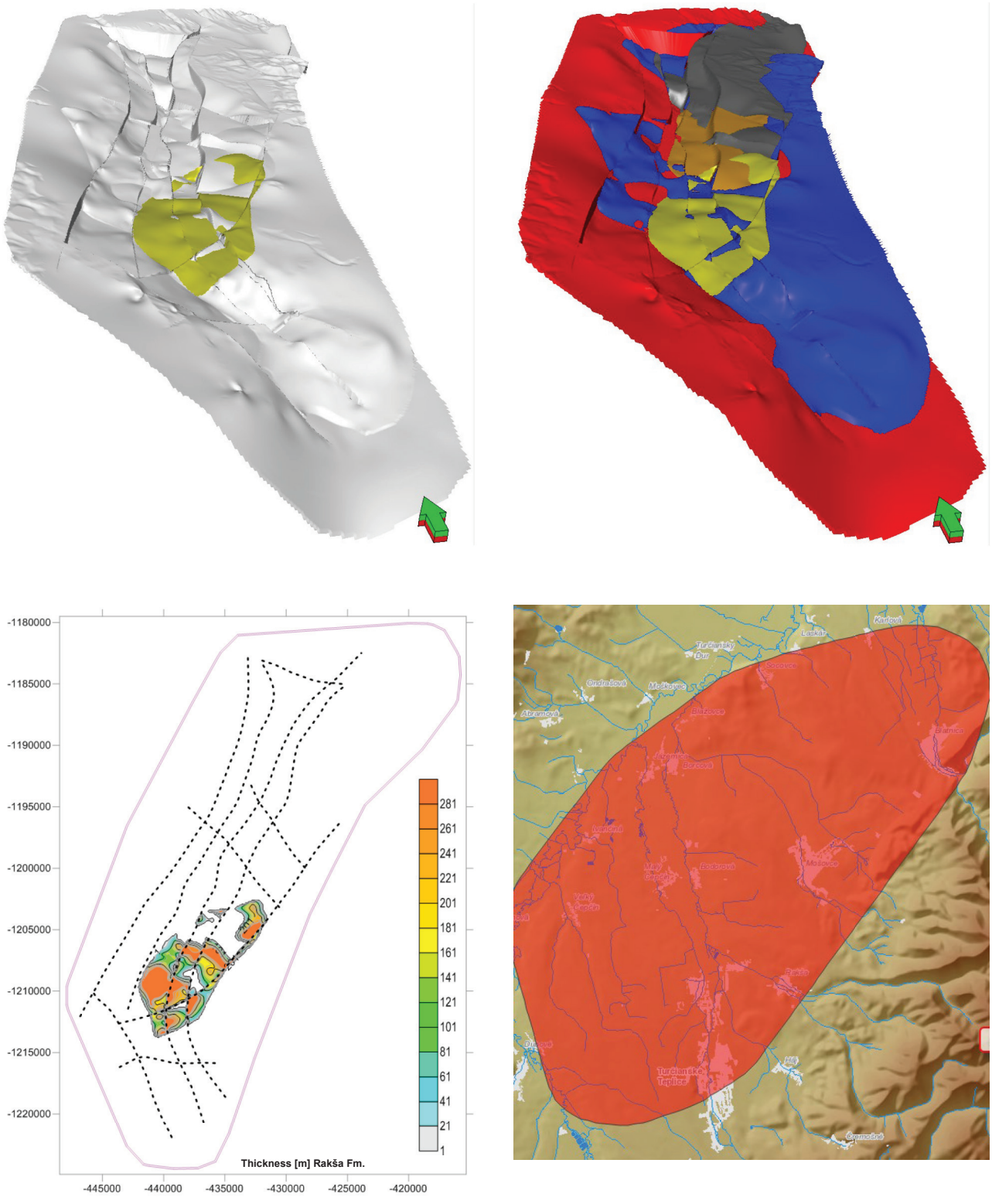

Fig. 1.15. *Rakša Formation.*
Top left: view from SW, top right: loaded on the cumulative surface of the bedrock (in this case: previous complexes), bottom left: thickness in [m], bottom right: approximate extent projected onto the surface of the area with DMR and topography (display without scale).

BUDIŠ FORMATION

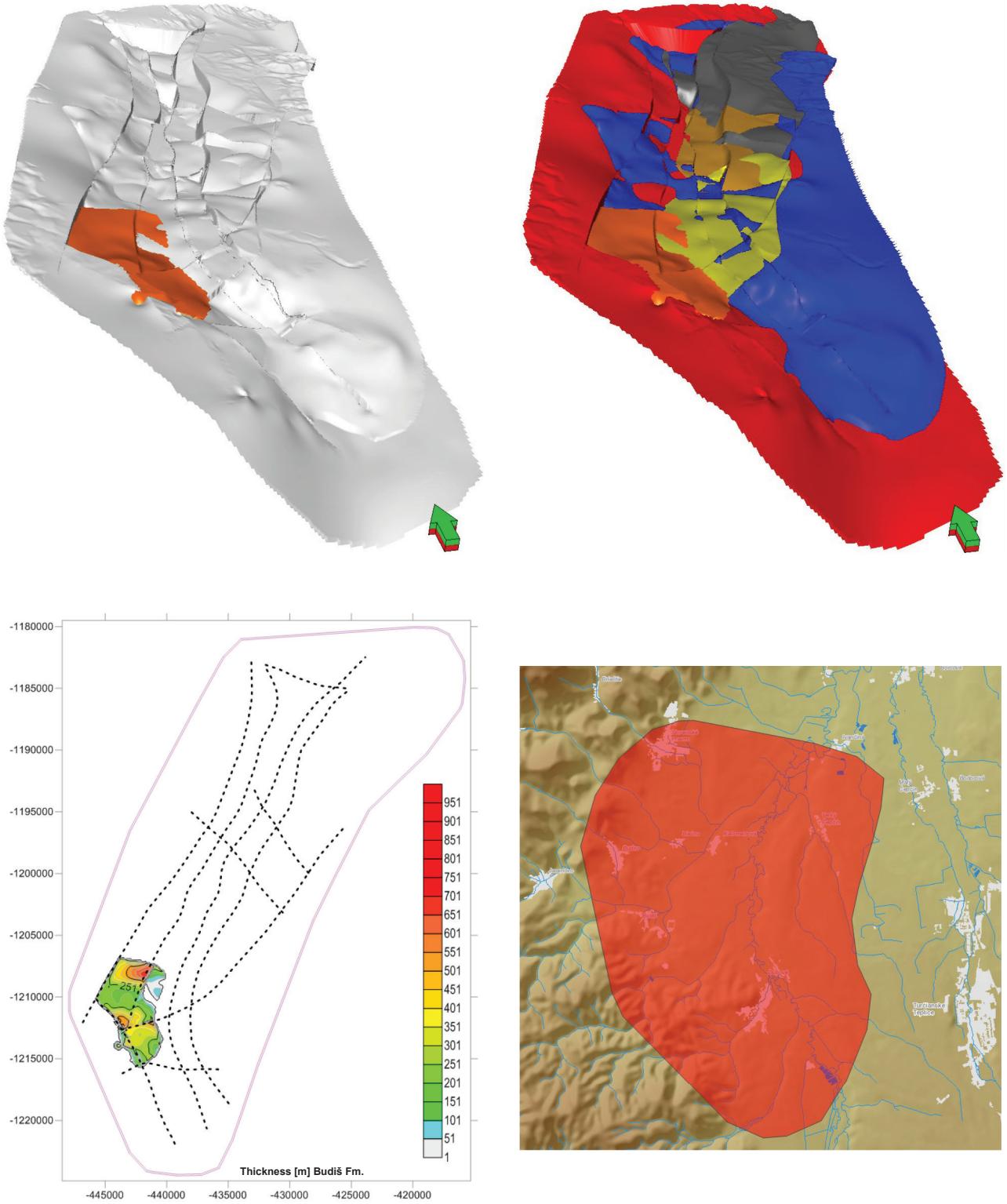

Fig. 1.16. *Budiš Formation.*
Top left: view from SW, top right: loaded on the cumulative surface of the bedrock (in this case: previous complexes), bottom left: thickness in [m], bottom right: approximate extent projected onto the surface of the area with DMR and topography (display without scale).

TURČOK FORMATION

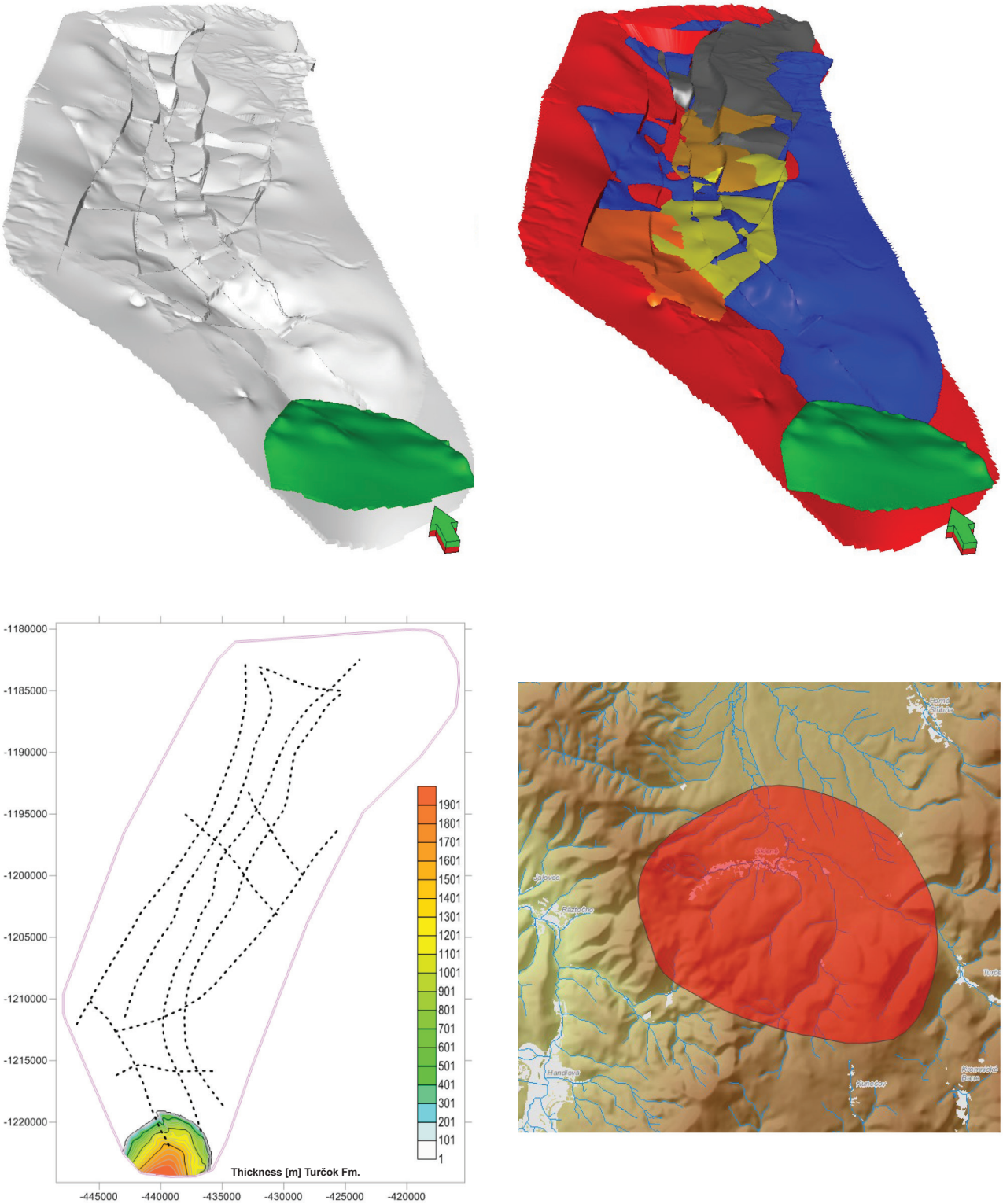

Fig. 1.17. *Turčok Formation.*
Top left: view from SW, top right: loaded on the cumulative surface of the bedrock (in this case: previous complexes), bottom left: thickness in [m], bottom right: approximate extent projected onto the surface of the area with DMR and topography (display without scale).

EPICLASTIC CONGLOMERATES

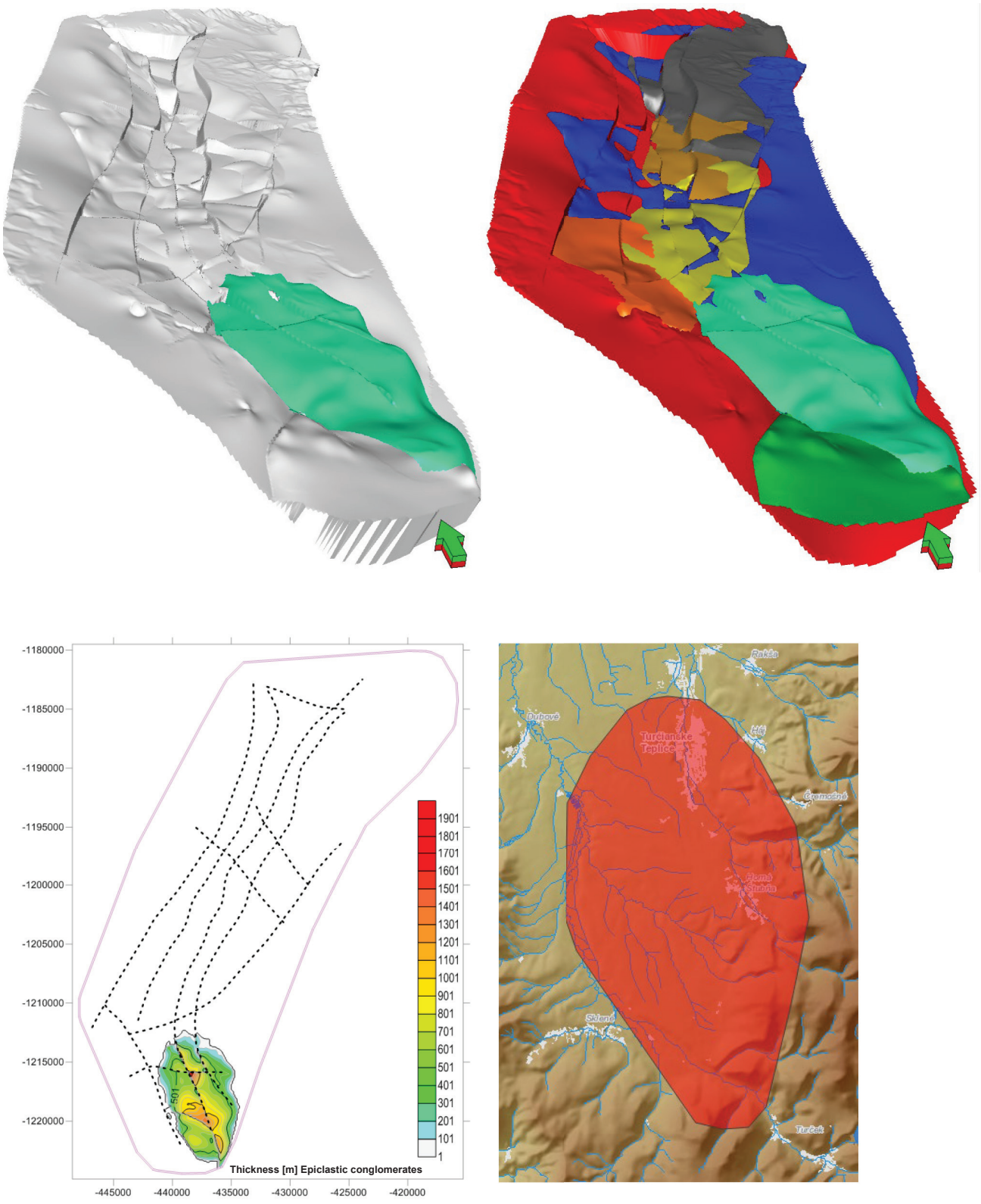

Fig. 1.18. *Epiclastic conglomerates.*
Top left: view from SW, top right: loaded on the cumulative surface of the bedrock (in this case: previous complexes), bottom left: thickness in [m], bottom right: approximate extent projected onto the surface of the area with DMR and topography (display without scale).

ABRAMOVCE MEMBER

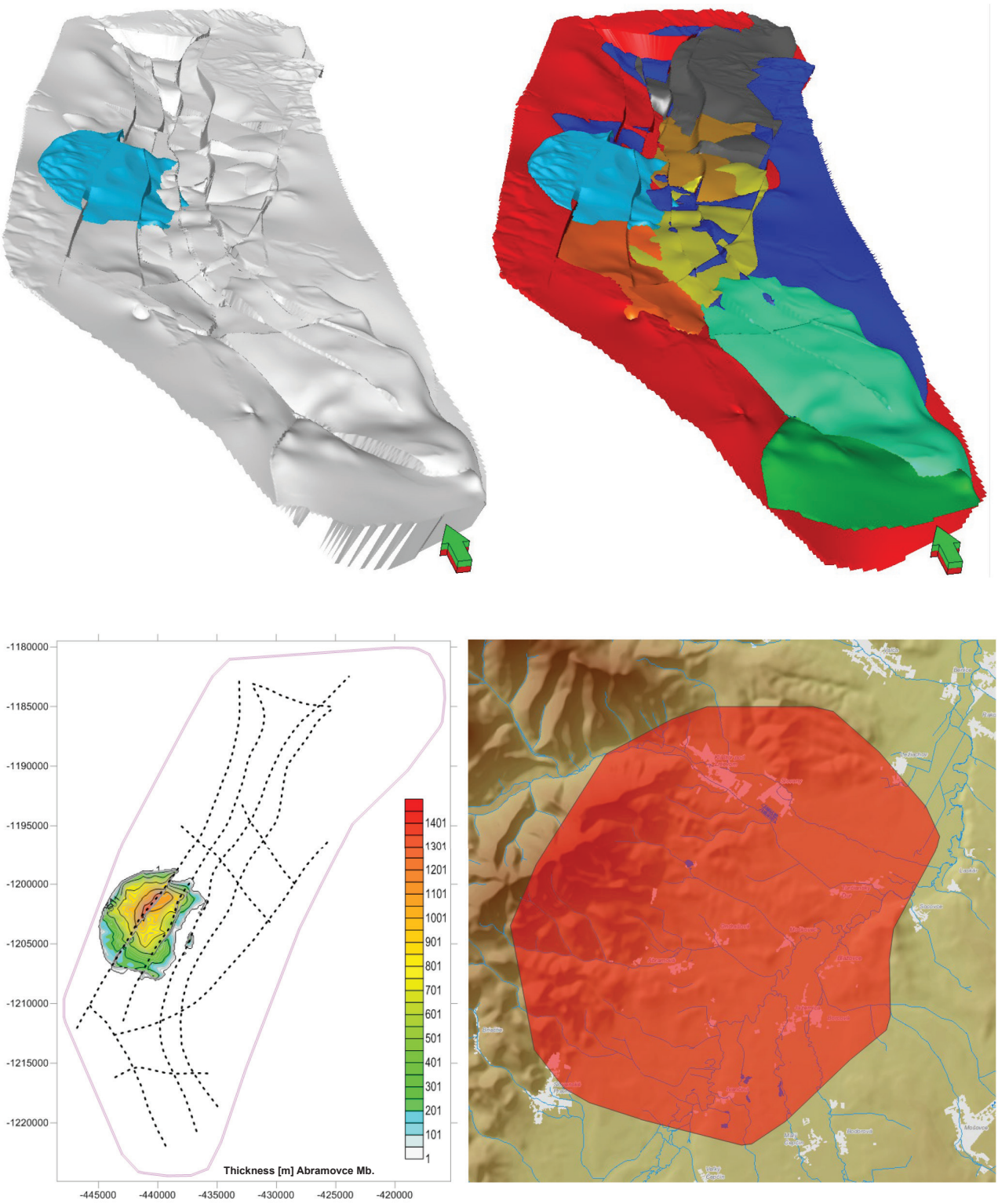

Fig. 1.19. *Abramovce Member.*
Top left: view from SW, top right: loaded on the cumulative surface of the bedrock (in this case: previous complexes), bottom left: thickness in [m], bottom right: approximate extent projected onto the surface of the area with DMR and topography (display without scale).

MARTIN FORMATION

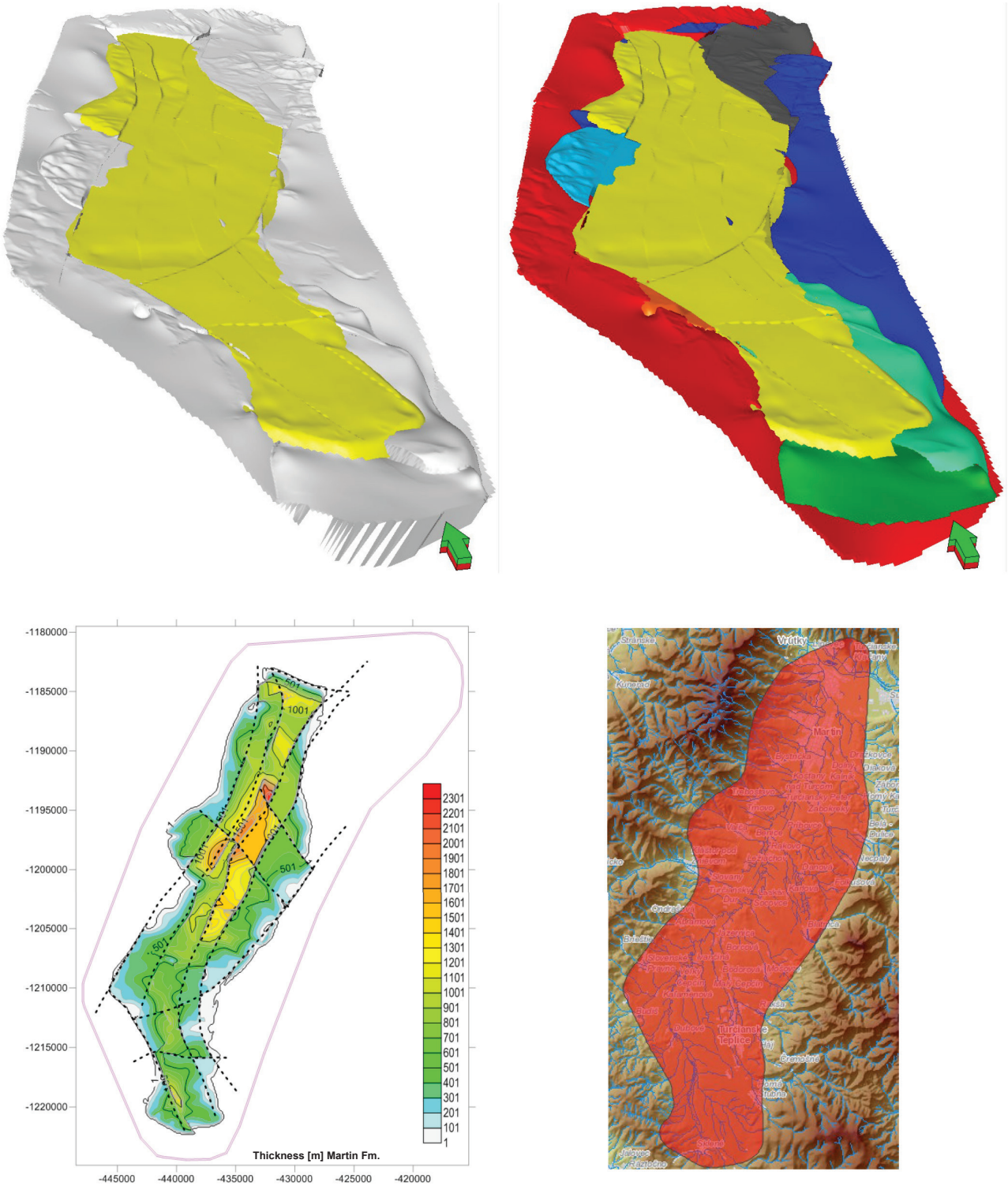

Fig. 1.20. *Martin Formation.*
Top left: view from SW, top right: loaded on the cumulative surface of the bedrock (in this case: previous complexes), bottom left: thickness in [m], bottom right: approximate extent projected onto the surface of the area with DMR and topography (display without scale).

JASTRABIE FORMATION

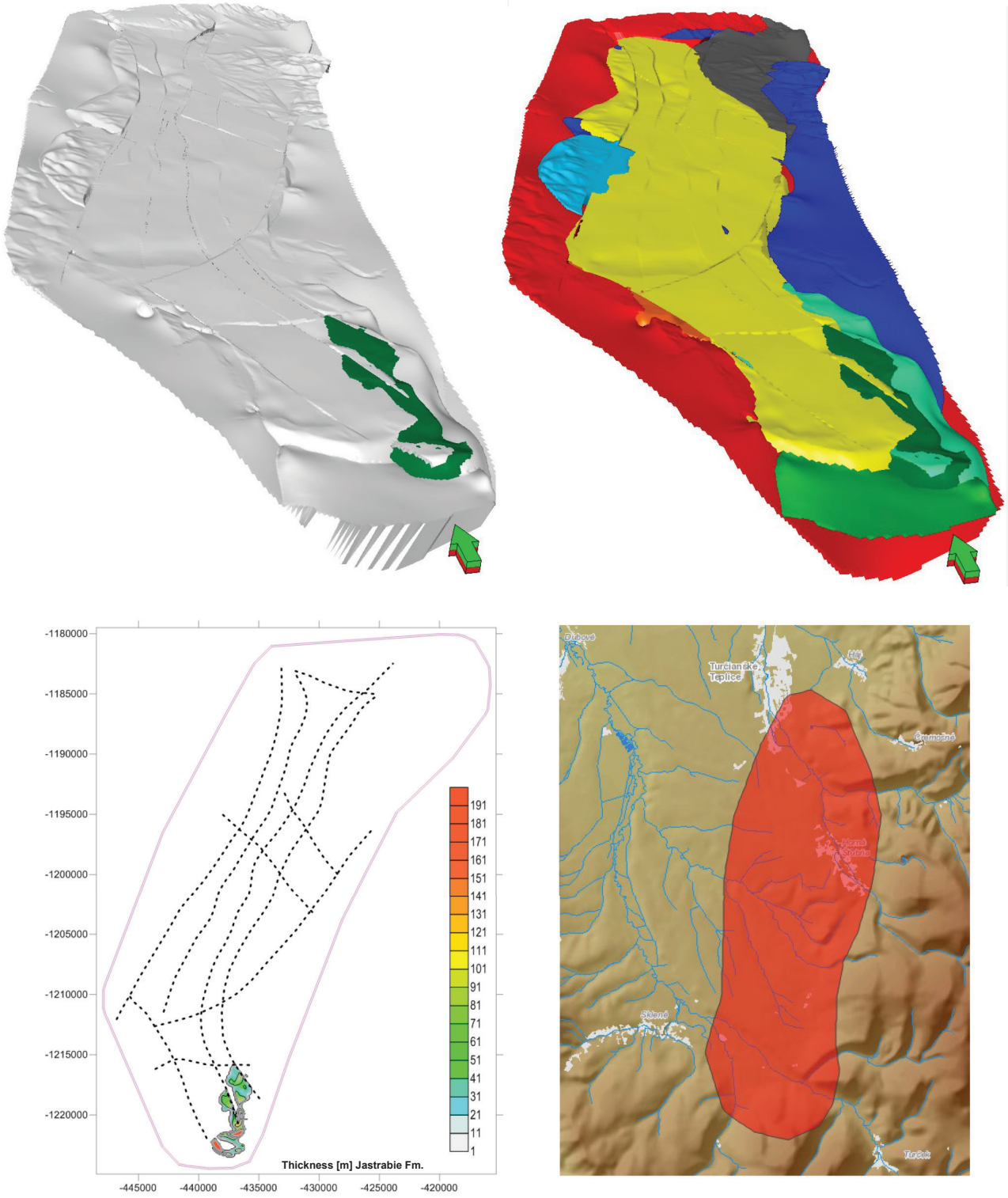

Fig. 1.21. *Jastrabie Formation.*
Top left: view from SW, top right: loaded on the cumulative surface of the bedrock (in this case: previous complexes), bottom left: thickness in [m], bottom right: approximate extent projected onto the surface of the area with DMR and topography (display without scale).

BYSTRIČANY FORMATION

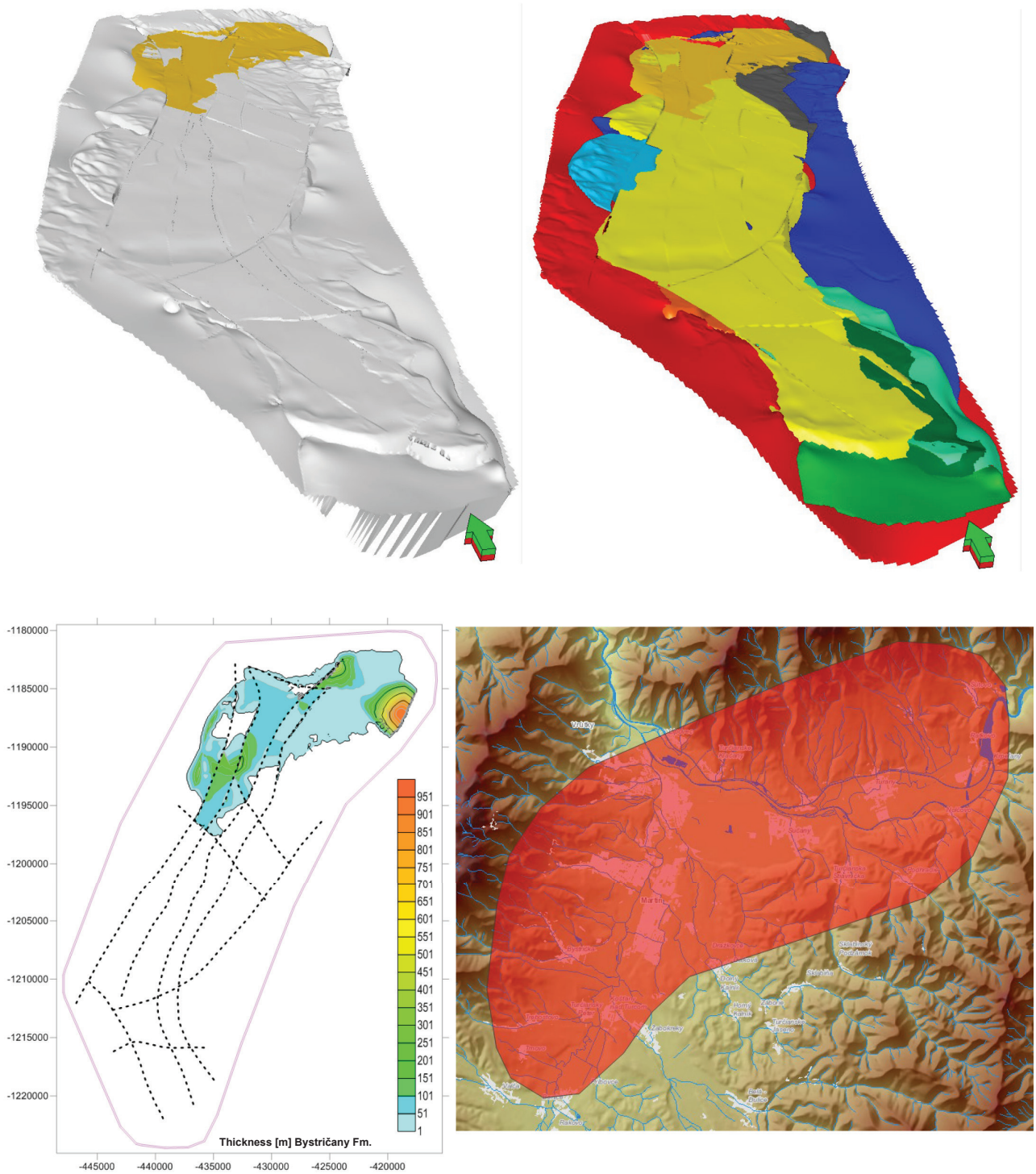

Fig. 1.22. *Bystričany Formation.*
Top left: view from SW, top right: loaded on the cumulative surface of the bedrock (in this case: previous complexes), bottom left: thickness in [m], bottom right: approximate extent projected onto the surface of the area with DMR and topography (display without scale).

QUATERNARY

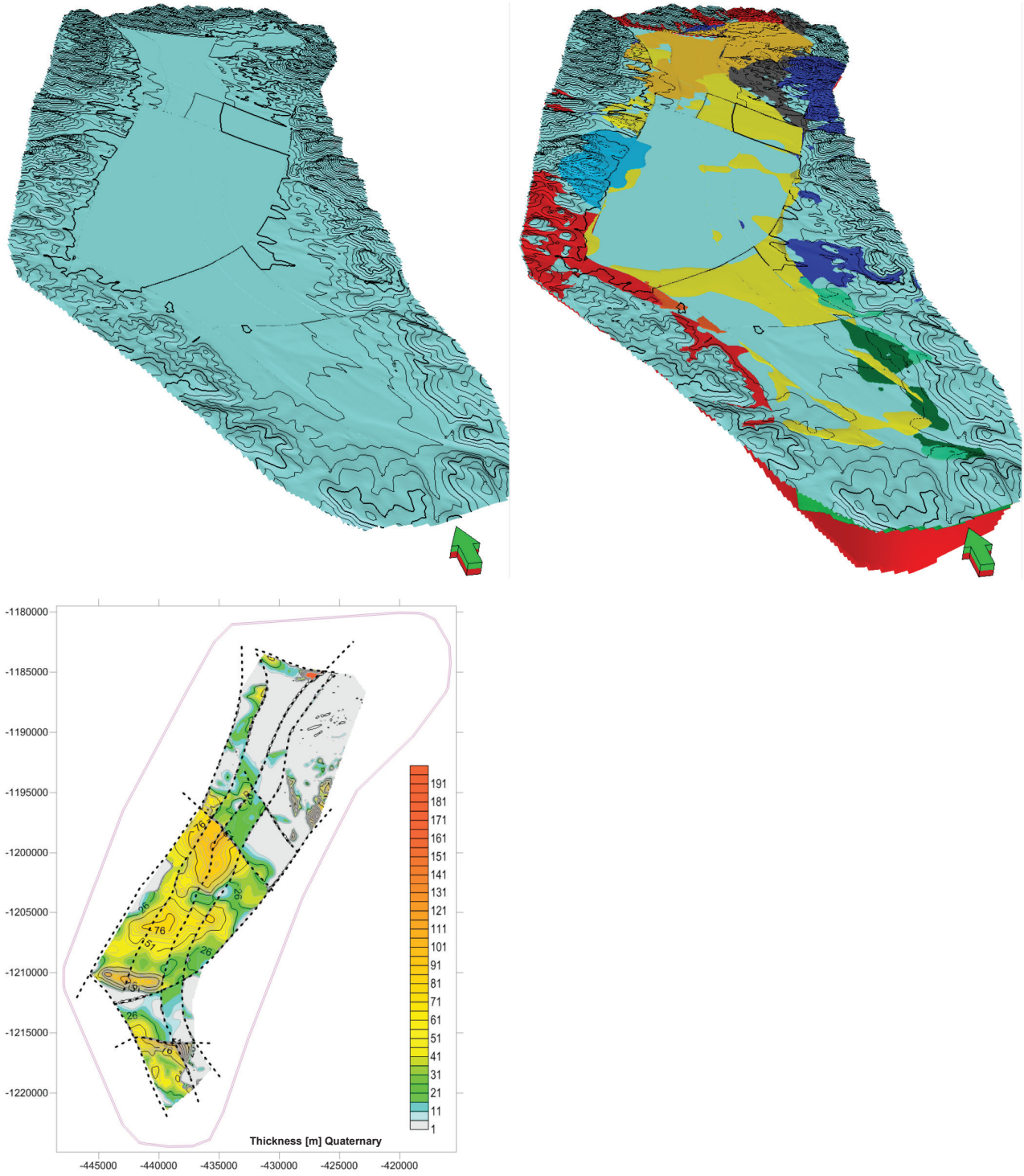

Fig. 1.23. *Quaternary (DEM).*
Top left: view from SW, top right: loaded on the cumulative surface of the bedrock (in this case: previous complexes), bottom left: thickness in [m].

Slovak Geol. Mag., 20, 1 (2020), 5 – 32

1.4 Results by individual segments

As we mentioned above, the 3D space of studied area was divided by generalized faults to tectonic segments (see Fig 1.24).

SEGMENT 1: The Segment 1 forms a marginal zone outside the central part up to the edge of the study area. It covers an area of 420.7 km^2 and contains all modelled complexes /formations, except the Borové and Rakša Fms.

SEGMENT 2: It covers an area of 37.36 km^2 and contains complexes/formations: Granitoids/Crystalline complex, Mesozoic undivided, Martin Fm., Budiš Fm. and Abramovce Mb.

SEGMENT 3: It covers an area of 26.45 km^2 and contains complexes/formations: Granitoids/Crystalline complex, Mesozoic undivided, Borové Fm., Huty Fm., Rakša Fm. and Martin Fm.

SEGMENT 4: It covers an area of 34.92 km^2 and contains complexes/formations:

Granitoids/Crystalline complex, Mesozoic undivided, Borové Fm., Rakša Fm., Martin Fm., Budiš Fm. and Abramovce Mb.

SEGMENT 5: It covers an area of 22.07 km^2 and contains complexes/formations:

Granitoids/Crystalline complex, Mesozoic undivided, Borové Fm., Huty Fm., Rakša Fm., Martin Fm. and Abramovce Mb.

SEGMENT 6: It covers an area of 16.43 km^2 and contains complexes/formations: Granitoids/Crystalline complex, Mesozoic undivided, Borové Fm., Huty Fm. and Martin Fm.

SEGMENT 7: It covers an area of 25.86 km^2 and contains complexes/formations: Granitoids/Crystalline complex, Mesozoic undivided, Huty Fm., Martin Fm. and Bystričany Fm.

SEGMENT 8: It covers an area of 16.52 km^2 and contains complexes/formations: Granitoids/Crystalline complex, Mesozoic undivided, Huty Fm., Martin Fm. and Bystričany Fm.

SEGMENT 9: It covers an area of 14.7 km^2 and contains complexes/formations: Granitoids/Crystalline complex, Mesozoic undivided, Huty Fm., Martin Fm. and Bystričany Fm.

SEGMENT 10: It covers an area of 11.9 km^2 and contains complexes/formations: Granitoids/Crystalline complex, Mesozoic undivided, Rakša Fm., Martin Fm., epiclastic conglomerates and Budiš Fm.

SEGMENT 11: It covers an area of 9.08 km^2 and contains complexes/formations: Granitoids/Crystalline complex, Mesozoic undivided, Martin Fm. and Bystričany Fm.

SEGMENT 12: It covers an area of 8.05 km^2 and contains complexes/formations: Granitoids/Crystalline

Fig. 1.24. *3D model of the territory. View from SW. Abramovce Mb. is shown by a thin grid (white), the Bystričany Fm. is shown by a dense grid (dark orange).*

complex, Mesozoic undivided, Borové Fm., Huty Fm. and Martin Fm.

SEGMENT 13: It covers an area of 8.15 km^2 and contains complexes/formations: Granitoids/Crystalline complex, Mesozoic undivided, Rakša Fm., Martin Fm. and epiclastic conglomerates and Budiš Fm.

SEGMENT 14: It covers an area of 6.97 km^2 and contains complexes/formations: Granitoids/Crystalline complex, Mesozoic undivided, Borové Fm., Martin Fm. and Bystričany Fm.

AUXILLIARY SEGMENT 91: It covers an area of 18.94 km^2 and contains complexes/formations: Granitoids/Crystalline complex, Mesozoic undivided, Martin Fm., epiclastic conglomerates, Turčok Fm., and Jastrabie Fm.

AUXILLIARY SEGMENT 92: It covers an area of 8.09 km^2 and contains complexes/formations: Granitoids/Crystalline complex, Mesozoic undivided, Martin Fm., epiclastic conglomerates and Jastrabie Fm.

AUXILLIARY SEGMENT 93: It covers an area of 54.60 km^2 and contains complexes/formations: Granitoids/Crystalline complex, Mesozoic undivided, Borové Fm., Huty Fm., Martin Fm. and Bystričany Fm.

The area and volume of individual modelled complexes were calculated for each of the 14 tectonic segments of the Turčianska kotlina Depression area delineated. The results are shown in Tab. no. 1.3.

Tab. 1.3. Representation of modelled complexes in individual segments. Material volume in km^3. The modelled complexes are defined with the help of database code for the sake of clarity of the table, the names are assigned to the codes below.

Row	Segment \ formation	2 [km^3]	4-7	10	11	14	16-24	17	19	20	21	18-1	18-2
1	2 [code]	74.55	3.63	-	-	-	14.84	-	-	4.50	12.48	-	-
2	3	45.98	12.82	5.71	0.84	2.35	10.41	-	-	-	-	-	-
3	4	60.69	6.10	0.58	-	2.94	27.14	-	-	1.56	3.22	-	-
4	5	25.38	10.82	5.01	0.09	1.67	21.80	-	-	-	0.03	-	-
5	6	29.12	4.02	7.43	1.39	-	7.26	-	-	-	-	-	-
6	7	35.47	8.92	-	4.85	-	23.80	-	2.12	-	-	-	-
7	8	11.92	8.60	-	19.34	-	7.57	-	0.46	-	-	-	-
8	9	28.94	2.22	-	0.15	-	10.28	-	0.51	-	-	-	-
9	10	24.41	1.27	-	-	0.36	6.42	1.30	-	1.91	-	-	-
10	11	17.61	0.01	-	-	-	7.86	-	12.63	-	-	-	-
11	12	8.56	0.05	3.32	0.42	-	11.33	-	-	-	-	-	-
12	13	8.96	9.85	-	-	0.49	2.50	2.56	-	-	-	-	-
13	14	9.06	0.03	0.46	-	-	10.52	-	0.15	-	-	-	-
14	91	30.05	3.04	-	-	-	9.45	9.88	-	-	-	4.33	0.09
15	92	9.54	8.08	-	-	-	0.57	6.46	-	-	-	-	0.20
16	93	85.80	42.09	4.57	27.21	-	2.45	-	0.06	-	-	-	-
17	Sum1 [r. 1 to 16]	506.06	121.55	37.07	65.29	21.80	174.23	37.19	34.94	27.96	36.73	4.33	0.30
18	continuation		block 1		block 1		block 1	block 1	block 1		block 1	block 1	block 1
19	In directions		NW		NW		W	E	W, NW		W	W, S	S
20	1 - edge	1,000.65	130.90	-	33.07	-	13.55	9.15	8.33	0.36	13.30	26.31	0.35
21	Sum2 [r. 17 + 20]	1,506.71	252.45	37.07	98.37	21.80	187.78	46.35	43.27	28.32	50.02	30.63	0.64

Formation [code]	Name
2	Granitoids/Crystalline complex
4-7	Mesozoic undivided
10	Borové Fm.
11	Huty Fm.
14	Rakša Fm.
16-24	Martin Fm.

Formation [code]	Name
17	Epiclastic conglomerates
19	Bystričany Fm.
20	Budiš Fm.
21	Abramovce Mb.
18.1	Turčok Fm.
18.2	Jastrabie Fm.

Explanations to the Tab. 1.3:
Interpretation in rows: e.g. Segment 6 involves 29.12 km^3 of the Crystalline rocks (code 2), 4.02 km^3 Mesozoic rocks (code 4-7), 7.43 km^3 rocks of Borové Fm. (code 10), 1.39 km^3 rocks of Huty Fm. (code 11) and 7.26 km^3 rocks of Martin Fm. (code 16-24),
Interpretation in columns: e.g. epiclastic conglomerates (code 17) are present in segments 10 (volume 1.3 km^3), 13 (volume 2.56 km^3), 91 (volume 9.88 km^3) and 92 (volume 6.46 km^3).

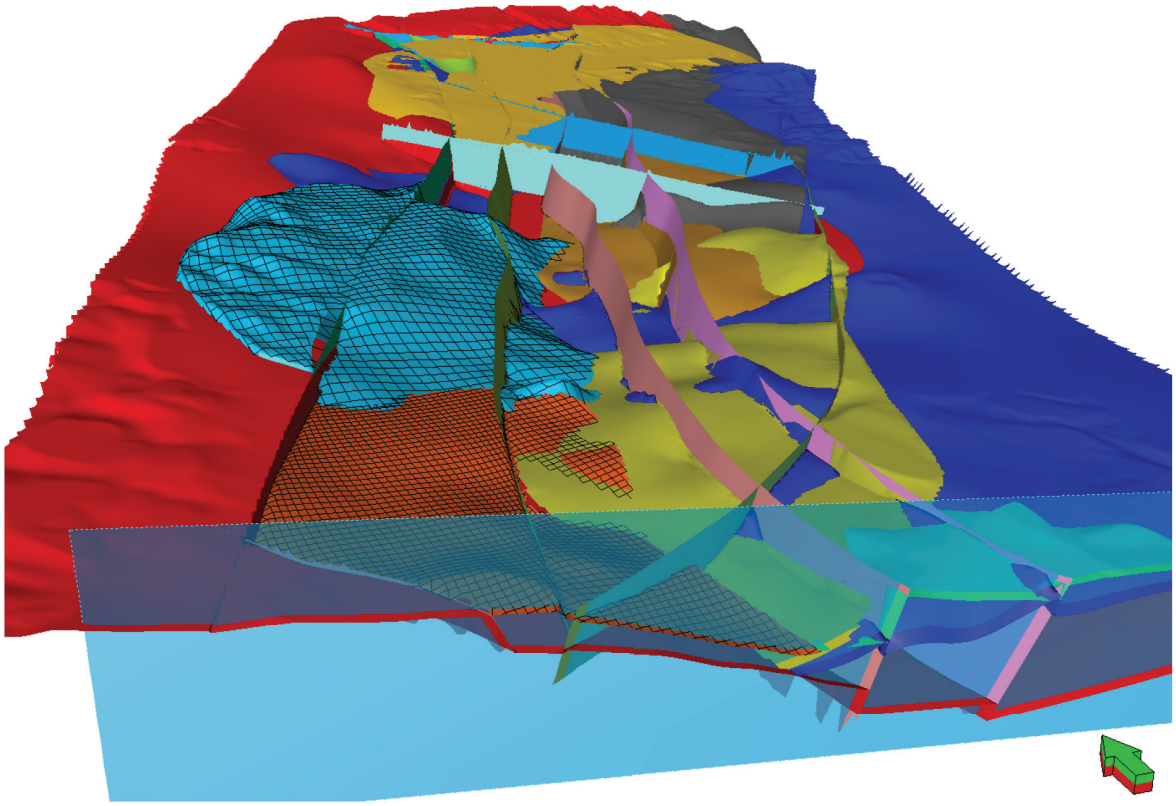

Fig. 1.26. *3D model of the territory. Transverse profile in the central part of the territory through the Budiš Fm. View from S.*

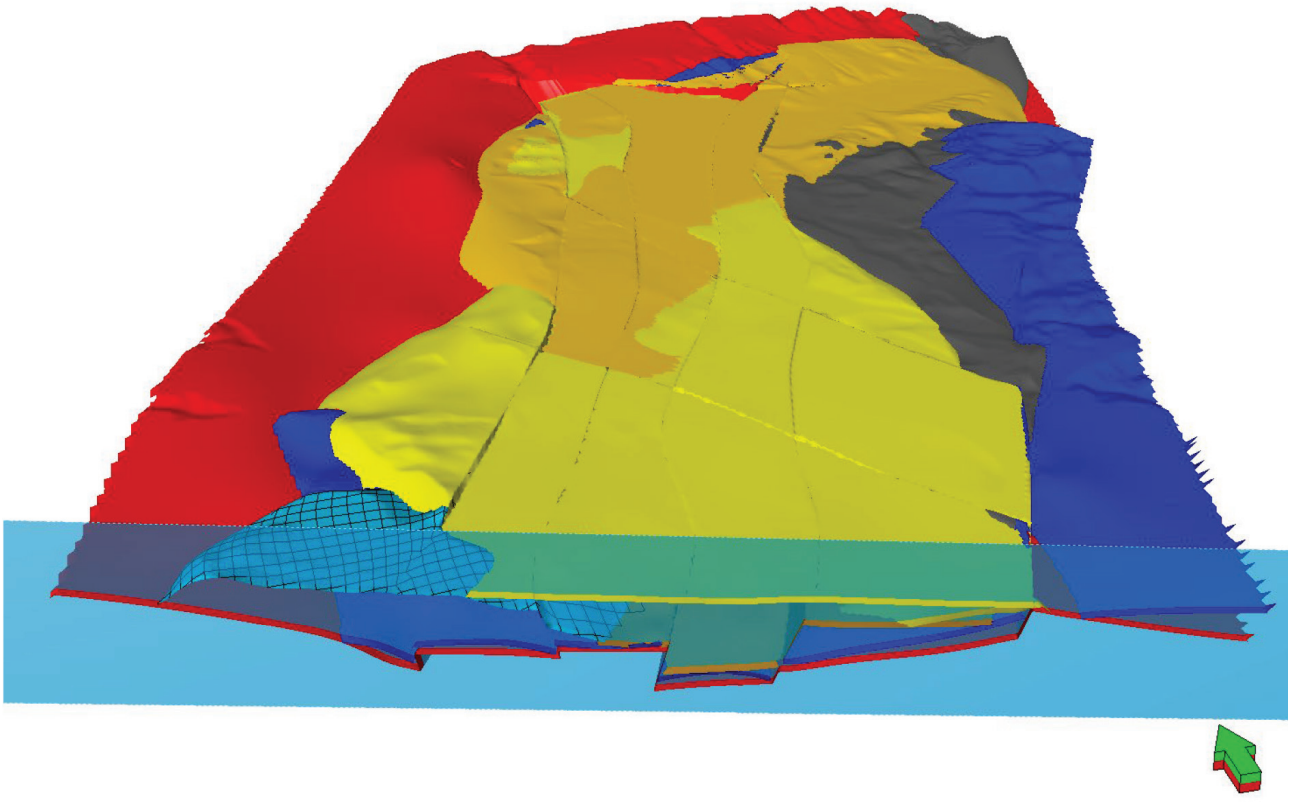

Fig. 1.27. *3D model of the territory. Transverse profile in the central part of the territory through the Abramovce Mb. View from S.*

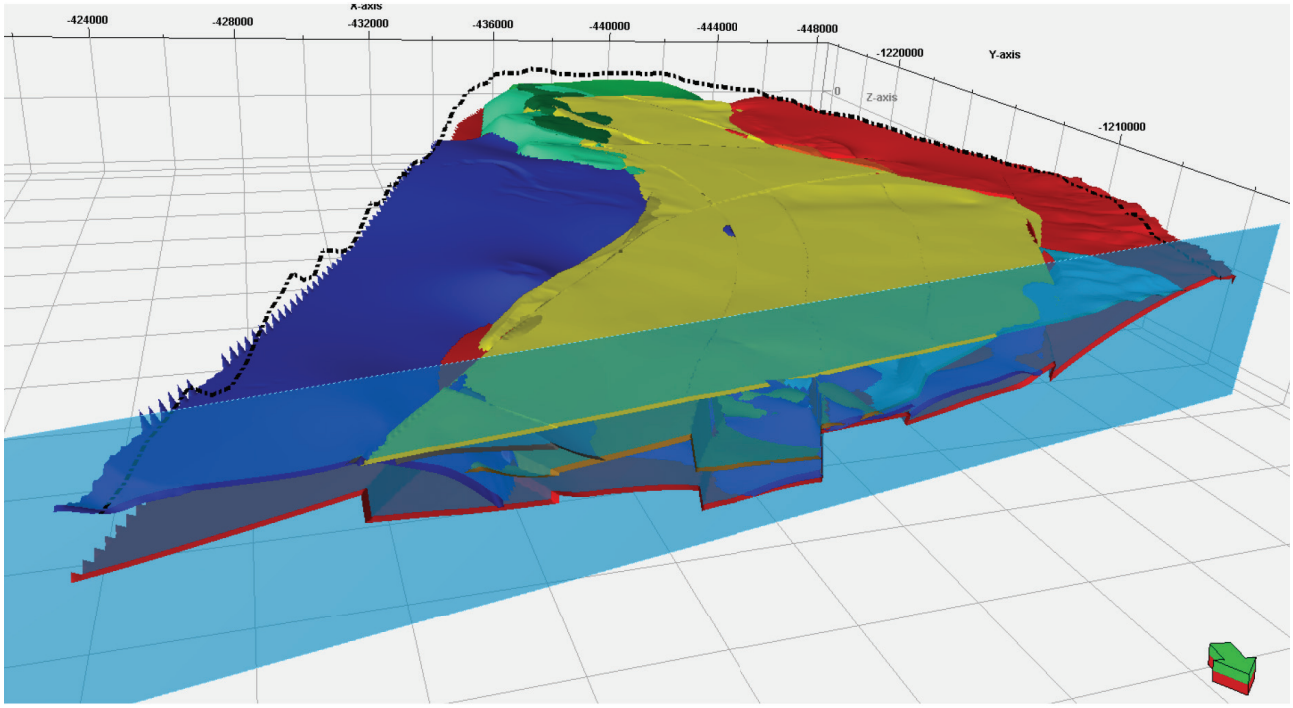

Fig. 1.28. *3D model of the territory. Transverse profile in the central part of the territory through the southern part of the Bystričany Fm. View from N.*

1.5 Visualization options for the 3D model

The visualization options are demonstrated in Figs. 1.24 to 1.28. In 3D models, it is possible to turn on and off individual layers, change their colour, transparency, display method (fill, grid, iso-planes, etc.). In the 3D model, it is possible to create a profile in any direction, a dynamic profile (gradual display of the following profiles with a defined step). The 3D model can be freely rotated, zoomed in/out. Above the created map view, it is possible to create various map compositions after adding a north, scale, legend.

1.6 Conclusion

3D modelling of the Turčianska kotlina Depression took place in several stages. The input data for modelling were deep boreholes and analog geological profiles of the area. When creating the model, it turned out that on the basis of such data it was not possible to model the volume of the basin with sufficient credibility (the quality of the model depends on the quality of input data, which is all the more true in multidimensional modelling) and it was necessary to thicken the input data based on the interpretation of VES profiles. Information from deeper boreholes for calibration of modelled curves was also taken into account in their interpretation. Despite the fact that we did not have any seismic data and the spatial distribution of boreholes and VES probes was not sufficiently uniform, using interpolation and extrapolation techniques, the 3D model of the entire Turčianska kotlina Depression with a depth range of approximately 2 km was created.

In comparison with the pioneer model of the area of the Upper Nitra Basin, where the area of interest occupied an area of 290 km^2 and the model area for 3D output about a quarter, in the Turčianska kotlina Depression the area subjected to three-dimensional geological modelling represented about 750 km^2. In addition to the 3D geological model, other models were created: a geological-geomorphological model of the whole area together with engineering geological characteristics of the rocks and a static hydrogeological model. For the first time in Slovakia, 3D modelling was applied to the basin development of a complete and delimited sedimentary pool.

Since this was the first task of this type, several procedures and algorithms were tested in the 3D modelling. The result of this research was the creation of a comprehensive ***methodological procedure*** for processing geological spatial data for sedimentary basins modelling. The process has been integrated into licensed software products such as ESRI® ArcGIS™ and Petrel® from Schlumberger. The spatial data processing (3D) methodology applied the following processing methods in consecutive steps:

- 3D georeferencing of objects (rasters);
- 3D vectorization (creation of polygons in space by 2D digitization and snapping to the corresponding spatial plane);
- 3D import of objects;
- 3D (spatial) modelling of the distribution of the observed phenomenon;
- 3D modelling of objects (vectors);
- 3D volume modelling;
- 3D visualization and 3D animation.

The resulting ***spatial model of the Turčianska kotlina Depression*** reflects, on the basis of currently known facts, all spatial relationships between the modelled complexes, while the main tectonic lines are also reflected

in it - which needs to be emphasized. From the created model, the volumes of individual modelled complexes were calculated, which can be used for further geological analyzes.

The Petrel® software package from Schlumberger was very suitable for the purposes of modelling the sedimentary basin and can be recommended for use in such areas in the future. All modelled objects in the form of 3D vector objects can be easily exported in ASCII format with coordinates and used directly as inputs for specialized programs (e.g. for hydrogeological modelling) or after simple modifications as inputs for other GIS programs, such as ESRI® ArcGIS™ or display some layers in Google Earth™, etc. This procedure was later used in the creation of a 3D geological model of the Slovak Republic at a scale of 1: 500,000, the results of which are presented in a separate article in this issue of the Slovak Geological Magazine (Zlocha et al., 2020, in press).

References

Bielik, M., Krajňák, M., Makarenko, I., Legostaeva, O., Starostenko, V.I., Bošanský, M., Grinč, M. & Hók, J. 2013: 3D gravity interpretation of the pre-Tertiary basement in the intramontane depressions of the Western Carpathians: a case study from the Turiec basin. Geol. Carpath. 64, 5, p. 399-408.

Franko, O., Remšík, A., Fendek, M. et al., 2010: Atlas geotermálnej energie Slovenska [*Atlas of Geothermal Energy of Slovakia*; online]. Bratislava: State Geological Institute of Dionýz Štúr.

Gašparik, J., Halouzka, R., Miko, O., Rakús, M., Bujnovský, A., Lexa, J., Panáček., A., Samuel., O., Gašpariková, A., Planderová, E., Snopková, P., Fendek, M., Hanáček, J., Modlitba, I., Klukanová, A., Žáková, E., Horniš, J. & Ondrejičková, A., 1995: Vysvetlivky ku geologickej mape Turčianskej kotliny 1 : 50 000 [*Explanations to the Geological Map of the Turčianska kotlina Basin 1: 50,000*]. Geological Institute of Dionýz Štúr, Bratislava, 196 p. In Slovak.

Map server of SGIDŠ, 2010: Digital geological map of Slovakia at scale 1: 50,000 [online]. Available from https://apl.geology.sk/gm50js/ [accessed on 20 January 2020].

Kotuľová, J., Švasta, J., Pauditš, P., Janega, A., Dananaj, I., Halmo, J., Elečko, M., Šimon, L., Zlocha, M., Šarkan, J., Fazekaš, J. & Müller, M., 2010: Horná Nitra, "Hornonitrianska kotlina - trojrozmerné geologické modelovanie exponovaného územia" [*Upper Nitra Basin - three-dimensional geological modelling of the area*]. Manuscript, Geofond archive, SGIDŠ, Bratislava.

Nagy, A., Zlocha, M., Kucharič, Ľ., Švasta, J., Olšavský, M., Zlinská, A., Fordinál, K., Šimon, L., Gaži, P., Dananaj, I., Buček, S., Baráth, I., Demko, R. & Liščák, P., 2014: Turčianska kotlina – trojrozmerné geologické modelovanie územia [*Turčianska kotlina Depression - three-dimensional geological modelling of the area*]. Manuscript, Geofond archive, SGIDŠ, Bratislava.

Zlocha, M., Vizi L., Kronome B., Cibula R., Nagy A., Fričovská J. & Surový M., 2020: 3D geological model of the Slovak Republic at scale 1: 500,000. Slovak Geological Magazine 1/2020, p. 33–48 of this issue.

Slovak Geol. Mag., 20, 1 (2020), 33 – 48

2. 3D Geological Model of the Slovak Republic at Scale 1: 500,000

Zlocha Marian, Vizi Ladislav, Kronome Balázs, Cibula Róbert, Nagy Alexander, Fričovská Jana & Surový Martin

State Geological Institute of Dionýz Štúr, Mlynská dolina, Bratislava, Slovak Republic; marian.zlocha@geology.sk

Abstract: The creation of digital 3D geological models has become relatively common in recent years with the development of computer technology, the deployment of powerful algorithms and the intense work of larger teams. Also at the State Geological Institute of Dionýz Štúr, several geological tasks were carried out in this area: "Upper Nitra Basin - Three-Dimensional Geological Modelling of the Exposed Area" (Kotuľová et al., 2010), as well as the multilateral International Project "TRANSENERGY" (Černák et al., 2012), "Turčianska kotlina Basin - Three-Dimensional Geological Modelling" (Nagy et al., 2014) and in the years 2016-2019 the task "3D Geological Model of the Slovak Republic at Scale of 1: 500,000" (Zlocha et al., 2019).

SGIDŠ's progressive approach to this issue in the last decade has been reflected not only in the use of explicit and implicit approaches to modelling, similarly to the world, but also in the development and application of its own methodological procedures and algorithms, implemented by its own applications.

The 3D geological model of the Slovak Republic at the scale of 1: 500,000 is one of the first national models at all. From commercial softwares, the following were used in its creation: Petrel® 8.4 and ISATIS™, for import / export of data, for creation of virtual boreholes, profiles and sections own applications and for visualization of results ArcScene™ of ESRI® company and own web application on ArcGIS™ Enterprise 10.7.1 platform with API for JavaScript.

In the article we briefly describe the process of creating a 3D geological model, source data and the methodology of their processing, the methodological procedure of the solution and the main results of 3D modelling with a number of attached images are provided.

Keywords: 3D modelling, geological model, virtual borehole profile, cross-section.

2.1 Introduction

In general, it is possible to observe a growing trend in decisions of the professional public based on spatial data. Typical examples include objectives relating to the health and safety of the population, the use of natural resources and wealth, etc. The fulfilment of these objectives requires, among other things, information obtained on the basis of geological research. For this reason, the share of geology in solving problems and finding solutions in the issues of energy, deposits of useful minerals, water resources as well as risks, hazards and infrastructure optimization is increasing. The global trend is to move from established practices to new approaches, which means a shift from classical 2D paper maps and publications to digital 3D models that can be integrated into systematic space-time monitoring.

The goal of today's geological services is the production of 3D computer images (models), which include information and properties such as thicknesses, strike and dip of bedding, heterogeneity of monitored parameters, reliability of results, etc. The renown geological services (e.g. in Poland, the Czech Republic and Austria, United Kingdom, Denmark, Finland, Germany, the Netherlands, Spain, Switzerland, Italy and Sweden and others) today provide not only modelling results within the lithostratigraphic setting of the study area, but also relevant properties and parameters of the rock environment such as petrophysical properties, contents of monitored elements, distribution of fractures of the rock mass and its disintegration and others, which are used for subsequent modelling of heat flow, landslide risk, groundwater quality, spatial planning and the like for sustainable development.

The issue of creating a 3D geological map is relatively new and it is not possible to consider it as a methodologically reliable and unambiguously solvable task. There are practically no 3D solutions for entire territories in a sufficiently detailed scale. In terms of methodology, detail and scale of processing, the British geological survey approach was a suitable inspiration.

At the State Geological Institute of Dionýz Štúr (hereinafter SGIDŠ), several geological tasks were performed in the field of 3D modelling in the past, e.g.: "Upper Nitra Basin - three-dimensional geological modelling of the exposed area" (Kotuľová et al., 2010), "TRANSENERGY" (Černák et al., 2012), "Turčianska kotlina Basin - three-dimensional geological modelling" (Nagy et al., 2014), etc. In the creation of these regional models, the interaction between a 3D expert using specialized 3D software and the geologist himself, whose knowledge was implemented in the model (so-called spatially explicit modelling approach).

The creation of a national 3D geological model of the Slovak Republic at a scale of 1: 500,000 in a relatively short period of time required, in addition to the above approach, significantly greater use of computer algorithms available in specialized software packages, as well as sophisticated geostatistical methods, especially in the field of interpolation and extrapolation of spatial data (so-called implicit modelling approach).

A web application was created to view the results of the 3D modelling, which will be available on the SGIDŠ map portal.

2.2 Methodology of the solution

When creating a 3D geological model of the Slovak Republic at a scale of 1: 500,000, we relied on previous experience gained from the 3D regional modelling and inspiration from published best practices, but last but not least we had to modify and expand the methodology for such a large area, including the development of new algorithms and their applications, test the resulting models on prototype areas and extend the procedures used for the entire area of the Slovak Republic.

A) Literature and archive search

We divided the input spatial data for the creation of the 3D model into 4 groups - map data, geological profiles, data from boreholes and other data.

– Map documents
  ○ Geological maps were used:
    • Geological map of the Slovak Republic at a scale of 1: 500,000 (Biely et al., 1996);
    • Geological map of the Western Carpathians and adjacent areas at a scale of 1: 500,000 (Lexa et al., 2000) (Fig. 2.1);
    • Tectonic map of the Slovak Republic at a scale of 1: 500,000 (Bezák et al., 2004);
    • Digital geological map of the Slovak Republic at a scale of 1: 500,000 (Káčer et al., 2005);
    • General geological map at a scale of 1: 200,000 (Bezák et al., 2008);
    • Digital geological map of the Slovak Republic at a scale of 1: 50,000 (Káčer et al., 2005).
      ▪ Analog maps at a scale of 1: 500,000
      ▪ Neotectonic map of the Slovak Republic at a scale of 1: 500,000 (Maglay et al., 1999a, b);
      ▪ Map of the Pre-Tertiary basement relief of the Inner Western Carpathians (Plančár et al., 1985);
      ▪ Tectonic map of the Pre-Tertiary basement relief of the Inner Western Carpathians (Fusán et al., 1987);
      ▪ Geological map of the basement of the covered areas of the southern part of the Inner Western Carpathians (Fusán et al., 1972);
      ▪ Geological map of the Quaternary of Slovakia at a scale of 1: 500,000" (Maglay et al., 2009).

– Geological cross-sections
  ○ Geological cross-sections from maps at scales of 1: 50,000, 1: 100,000 and 1: 200,000 were used for the 3D model creation (Fig. 2.2). A total of 240 profiles from 56 analog maps at the scale of 1: 50,000, 5 cross-sections from maps at the scale of 1: 100,000 and 2 profiles from the map at the scale of 1: 200,000 were processed.

– Data from wells
  For the needs of model creation, its calibration and control, a total of 462 boreholes drilled through Tertiary were used from the territory of the Slovak Republic out of almost 1,000 deep boreholes.

– Other data
  ○ formed the boundary of the 3D model in space
    ▪ in the direction [X, Y] it was the border of the Slovak Republic.
    ▪ in direction [Z]
      • overburden: digital relief model at scale 1: 50,000 (source: GIS SGIDŠ) generalized to scale 1: 500,000.
      • basement: variable depth range of the 3D model given by the depth of the input data (together with the *buffer*).

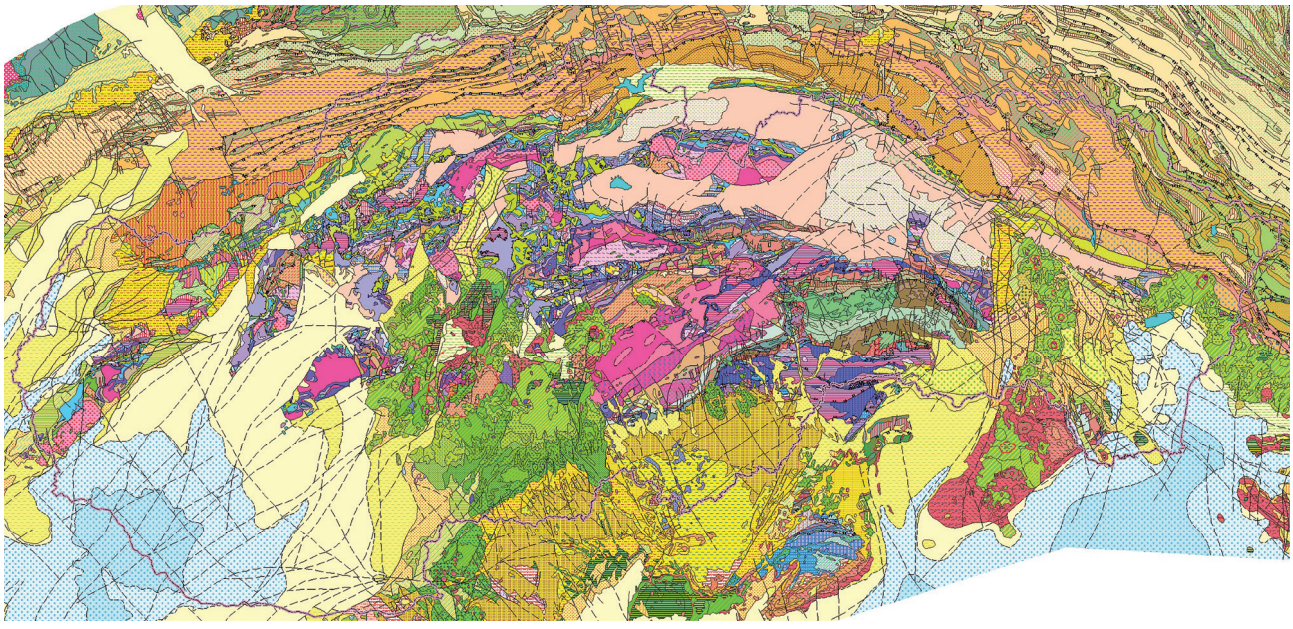

Fig. 2.1. *Geological map of the Western Carpathians and adjacent areas at a scale of 1: 500,000. (Lexa et al., 2000).*

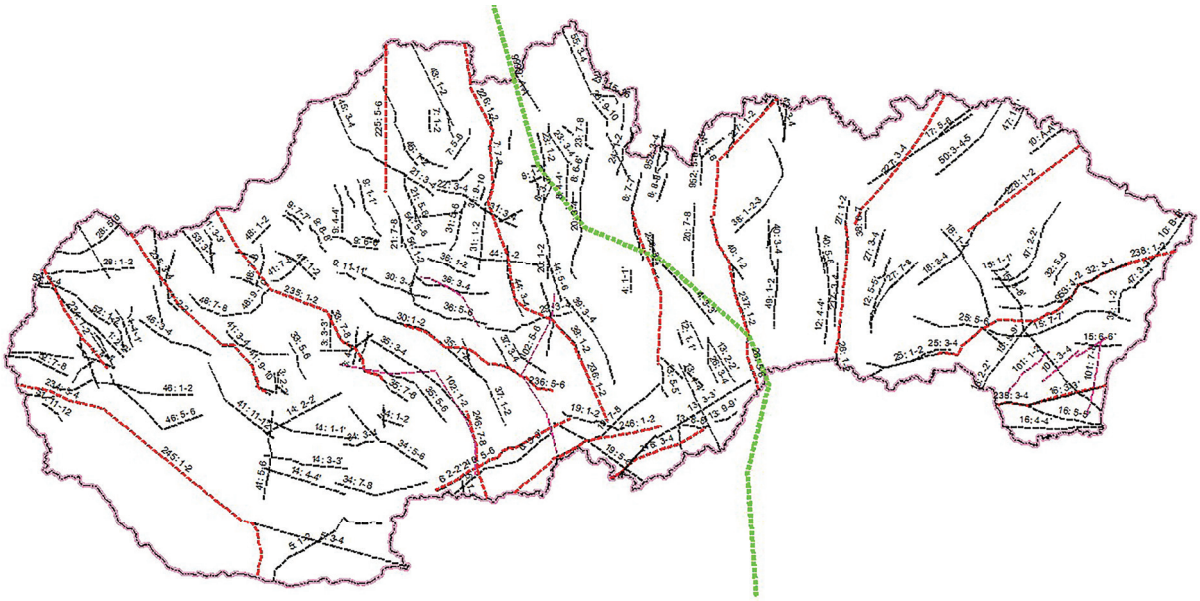

Fig.2.2. *Projection of used geological cross-sections from geological map 1: 50,000 (black), 1: 200,000 (red) and 1:500,000 (green).*

B) Digital processing of spatial data into 3D

- Digital maps were in the S-JTSK coordinate system, their geometries were taken over.
- Analog maps were scanned, georeferenced, selected objects were digitized into line and polygon objects (lines, e.g. depth isolines, tectonics, polygons, for instance geology).
- A separate issue was Geological map of the Quaternary of Slovakia at a scale of 1: 500,000 (Maglay et al., 2009). The attributes of this map existed in the form of intervals (e.g. depth sections 20-50 m, 50-100 m), which had to be recalculated by special geostatistical methods into a regular raster network.
- Data from geological profiles of scale 1: 50,000 were generalized after analysis with respect to the used basement (geological map 1: 500,000). Interface vectorization was performed manually on 3D georeferenced substrates, or by 2D semi-automatic vectorization and rotation of the obtained objects into space based on the known [XYZ] coordinates of the breakpoints vertices (Fig. 2.3). Short programs have been developed for this calculation.
- Data from geological boreholes were filtered for conditions of completeness of data (unambiguous identification by name, archive number, filled in values of collar coordinates, depths, drilling through Tertiary, etc. (Fig. 2.4)
- The legend to the Geological map of the Western Carpathians and adjacent areas (Lexa et al., 2000) was chosen to create a catalogue of attributes. According to this database, values were assigned to individual spatial objects.

C) 3D geological model creation

Even before modelling, the geological model of a large area required the creation of an idea/concept of how to approach spatial data with regard to the complexity of the geological setting on the one hand and the possibilities of 3D modelling tools on the other. This interpretive aspect, the subjective input of the geologist, with the strong support of modelling tools as an objective factor, is the principle for the whole modelling process.

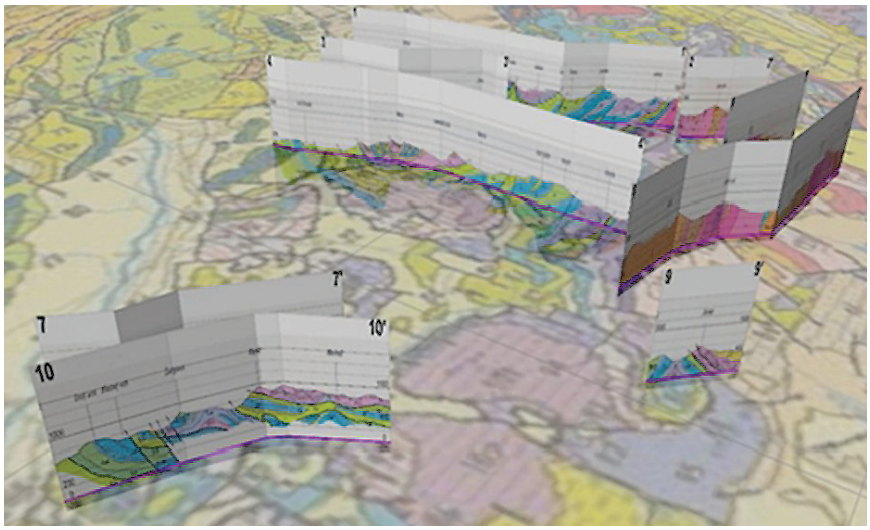

Fig. 2.3. *3D georeferencing of geological cross-sections.*

a) Model concept

The concept of the model was based on the tectonic setting, the structure of the input data, the goals and the scale of modelling. It determined which geological elements (units, faults, etc.) were included in the model, in what form and what is their mutual relationship (Fig. 2.5a). Given that the planned model includes the entire territory of Slovakia, we had to significantly simplify the geological setting, both in terms of lithological content and faults pattern. The model created was "hybrid": while in the pre-Cenozoic lower part the principle of tectonic units was used, in the higher Cenozoic, "basinal" part it was built mainly on the stratigraphic principle. A special group consisted of neovolcanics, where we had to distinguish up to three horizons, because especially in the East Slovak part, two periods of volcanic activity are relatively well distinguishable. A special group consists of subvolcanic bodies (Fig. 2.5b). The concept of the model also determined the entry of input data according to the requirements of the model: coalescence of some formations, re-evaluation and re-indexing of drilling data, connection of some faults into one line, etc.

b) Sequence of geological model creation

The pre-Cenozoic bedrock as an interface between the lower part of the model and its basinal sedimentary filling was created mainly on the basis of a map of Kilényi and Šefara (1989), but in areas where we had a newer and/or more accurate source, these input data were also used, e.g. Sub-Tatra Basin: (Szalaiová et al., 2008), Vienna Basin: Wessely (1988), Danube Basin: TRANSENERGY results (Černák et al., 2012). The horizon, which has not yet been disintegrated by faults, is shown in Fig. 2.6.

In the following phase, a structural model was created, in which the main fault lines describing the character of the entire failure zone were determined. By integrating tectonic elements into the modelled horizon, the final layer of the pre-Cenozoic bedrock was created (Fig. 2.7). We consider it to be one of the most significant results of the entire 3D geological model.

Other horizons - Neogene base, Palaeogene base, Lower Miocene/Badenian interface and Quaternary base were created gradually from existing elevation data, such as e.g. Map of the Tertiary base Plančár et al. (1985), Map of Quaternary thicknesses (Maglay et al., 2009) supplemented with data obtained from processed geological profiles. The most important information input into the modelling process was drilling data, which served as primary data (mostly from cross-section, partly also from maps) the relevant boundaries have been adjusted to respect drilling data (Fig. 2.8).

The modelling of spatial distribution was preceded by a thorough control of input data and error correction. The models were calculated by several interpolation methods,

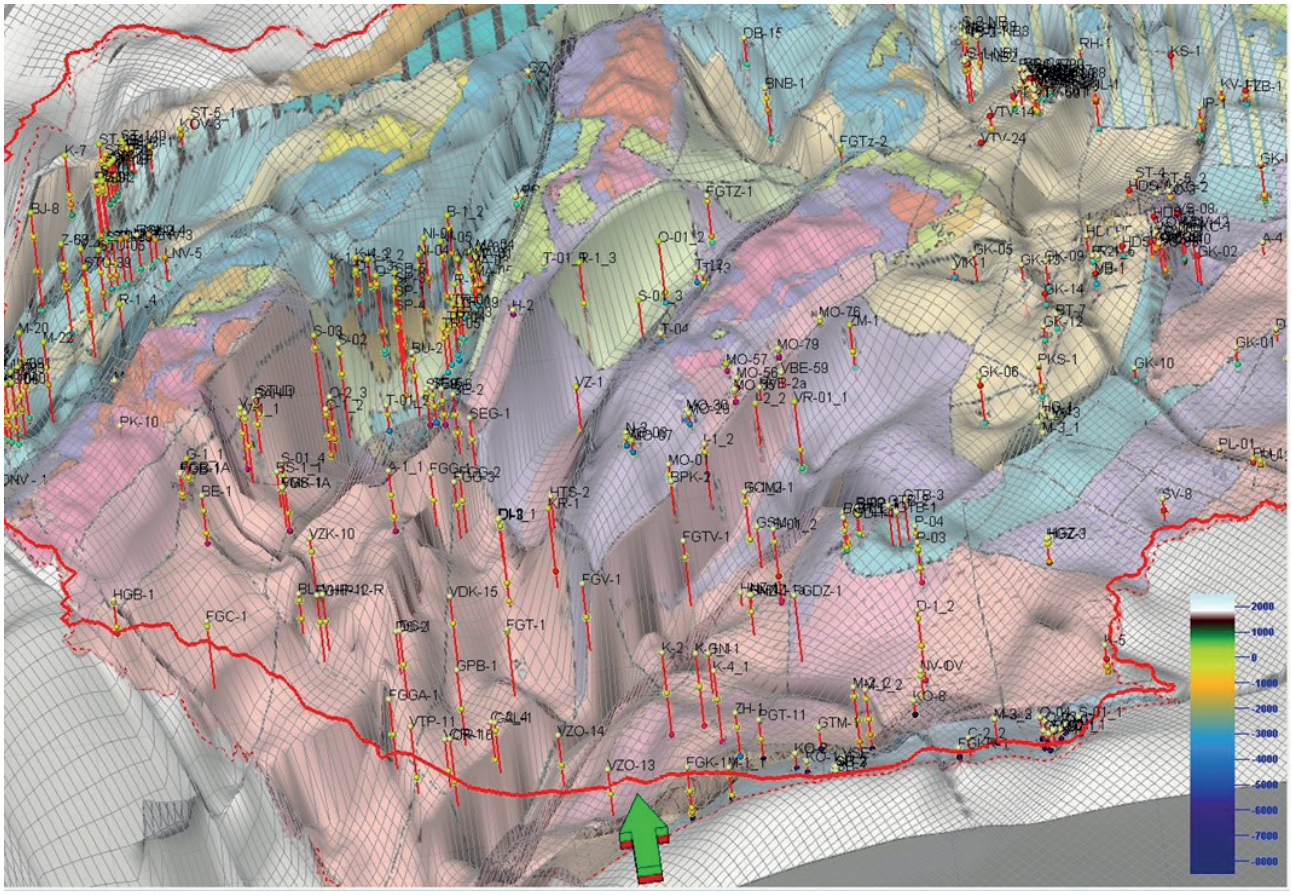

Fig. 2.4. *Deep geological boreholes with an associated legend, map of the interfaces in the Pre-Tertiary basement.*

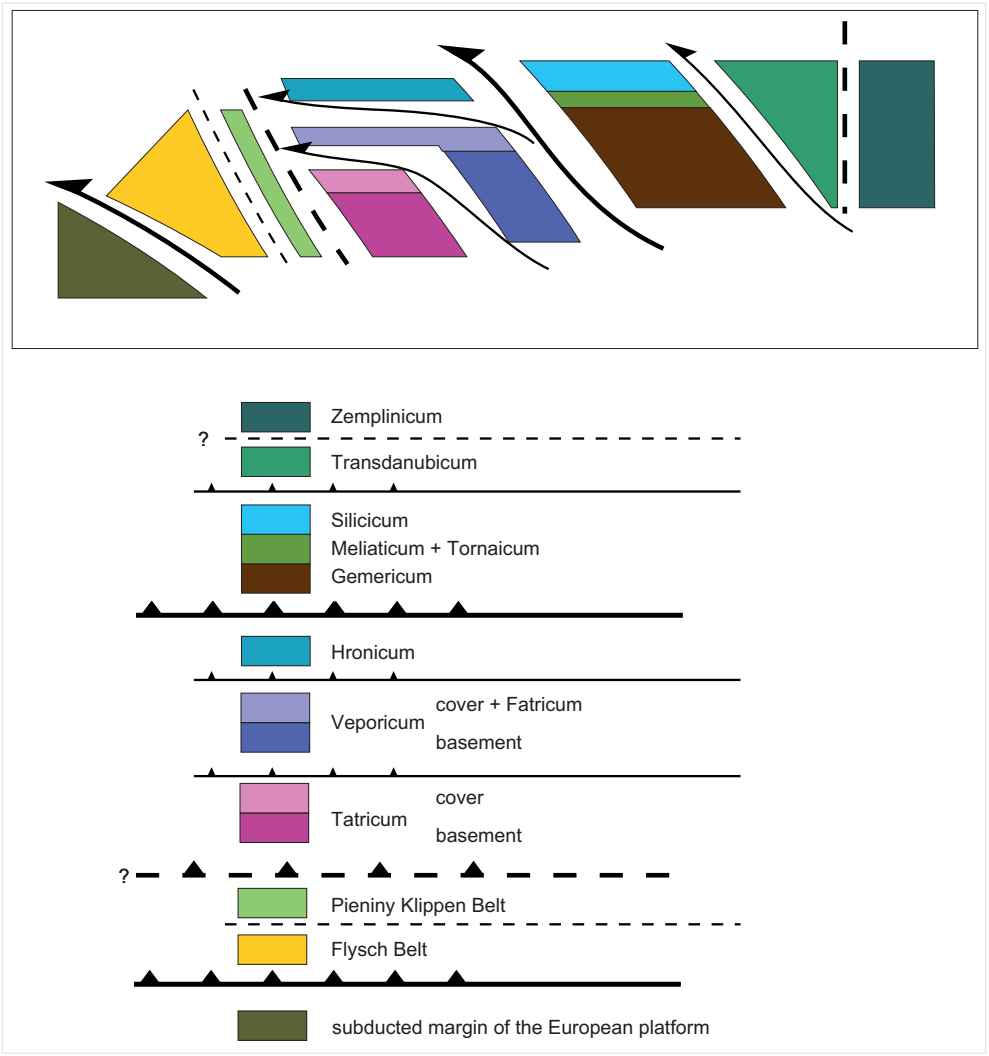

Fig. 2.5a. *Concept of the model of the pre-Cenozoic bedrock.*

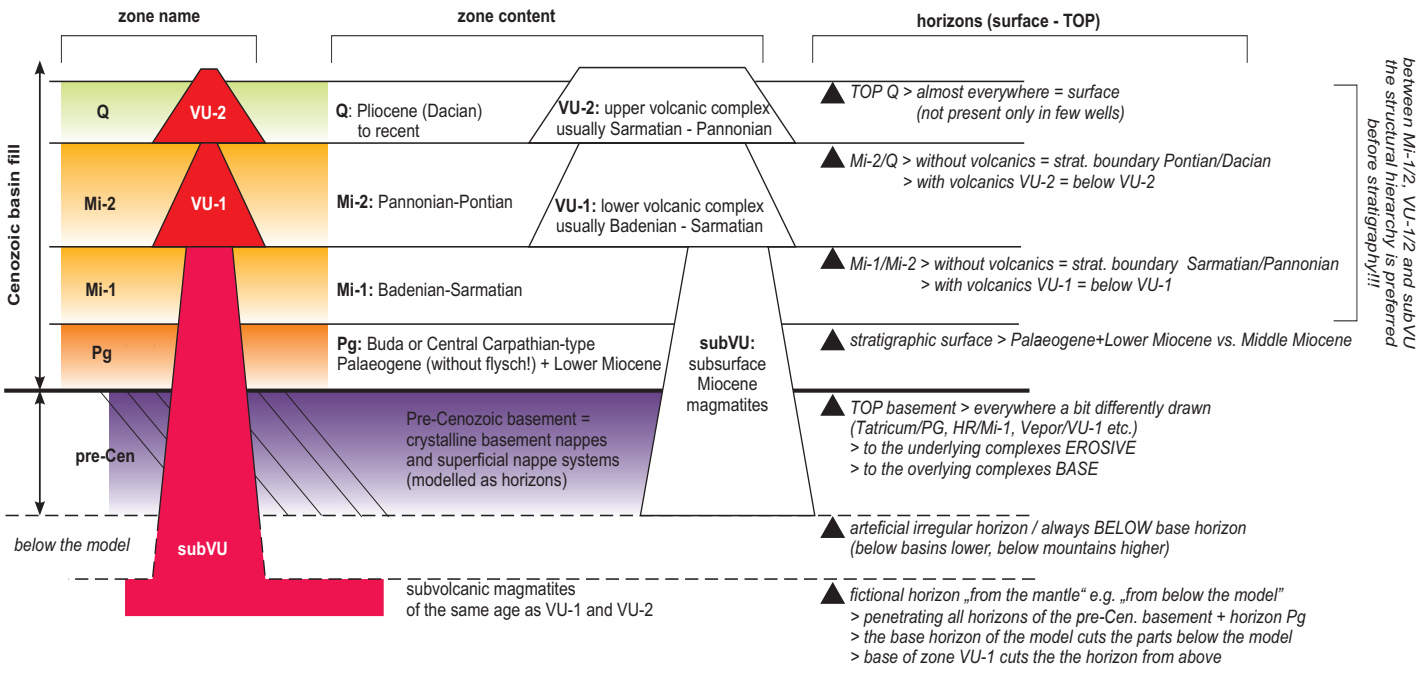

Fig. 2.5b. *Concept of the model of the Cenozoic basinal filling, including neovolcanics.*

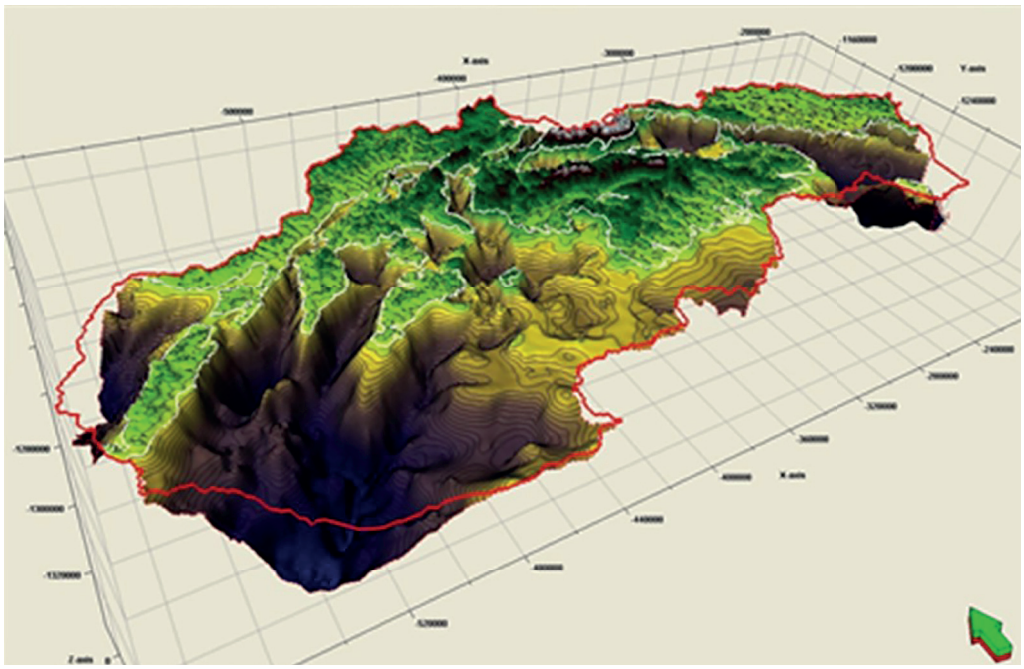

Fig. 2.6. *The "unfaulted" surface of the Cenozoic basement.*

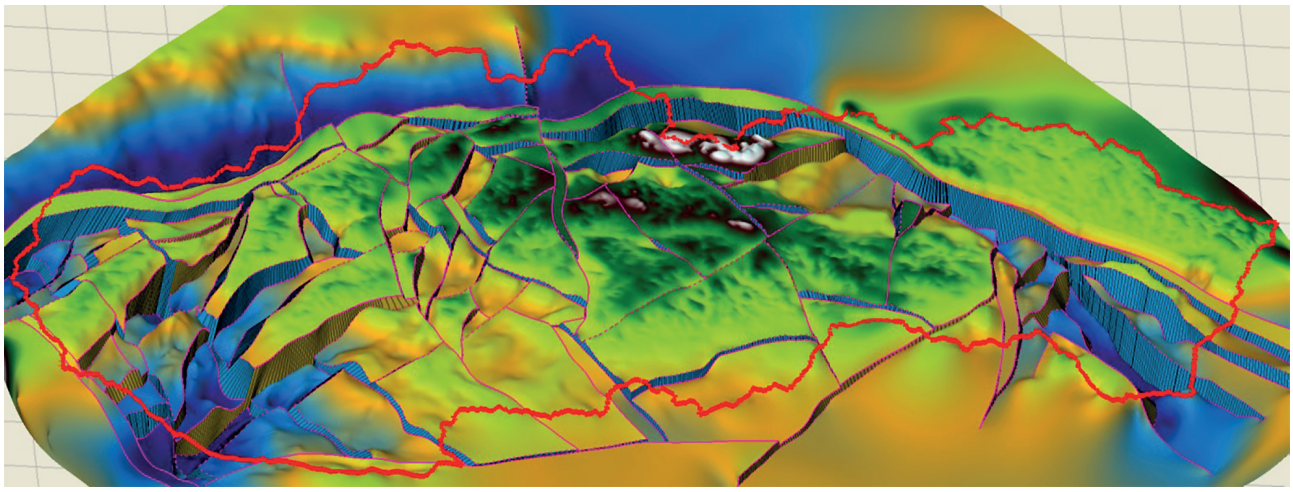

Fig. 2.7. *Fault-segmented horizon of the pre-Cenozoic basement.*

through ordinary kriging with various parameters (simple kriging with isotropic spherical variogram, anisotropic model of spherical type variability, etc.), triangulation method, square distances, splines and minimum curvature methods. However, none of these approaches gave satisfactory results, with undesired ripple of isolines and various computational artifacts in the calculations (Fig. 2.9).

The best results were finally achieved using methods of sliding or local geostatistics, in which the parameters entering the modelling were locally optimized: the direction and magnitude of the axes of the anisotropy ellipse as well as the impact of the autocorrelation of both axes of anisotropy.

The mutual position of individual modelled horizons was confronted with knowledge about their mutual stratigraphic position. For instance, the altitude of the Quaternary base had to be at any point in space *below* the Earth's surface. In general, the relative position of formations can be as follows:

- *Erosional*: the erosive surface at the surface of the modelled complex (e.g. the Earth's surface);
- *Discontinuous*: a layer intersecting all other layers/formations, e.g. erosive surface with hiatus in sedimentation, or the overthrust surface of a nappe;
- *Conformable*: inclined, the layer overlies the underlying stratum without intersecting, continuation of the sedimentation cycle;
- *Base*: the layer on which all other layers/formations of the sedimentation sequence lie, the basal layer.

Knowledge of these rules at individual horizons allowed us to make corrections for inaccuracies that arose due to insufficient density of input data, or as undesirable estimates of some values in interpolation.

The resulting 3D model contained the following *3D surfaces*:

- Digital relief model
- Tertiary basins filling:

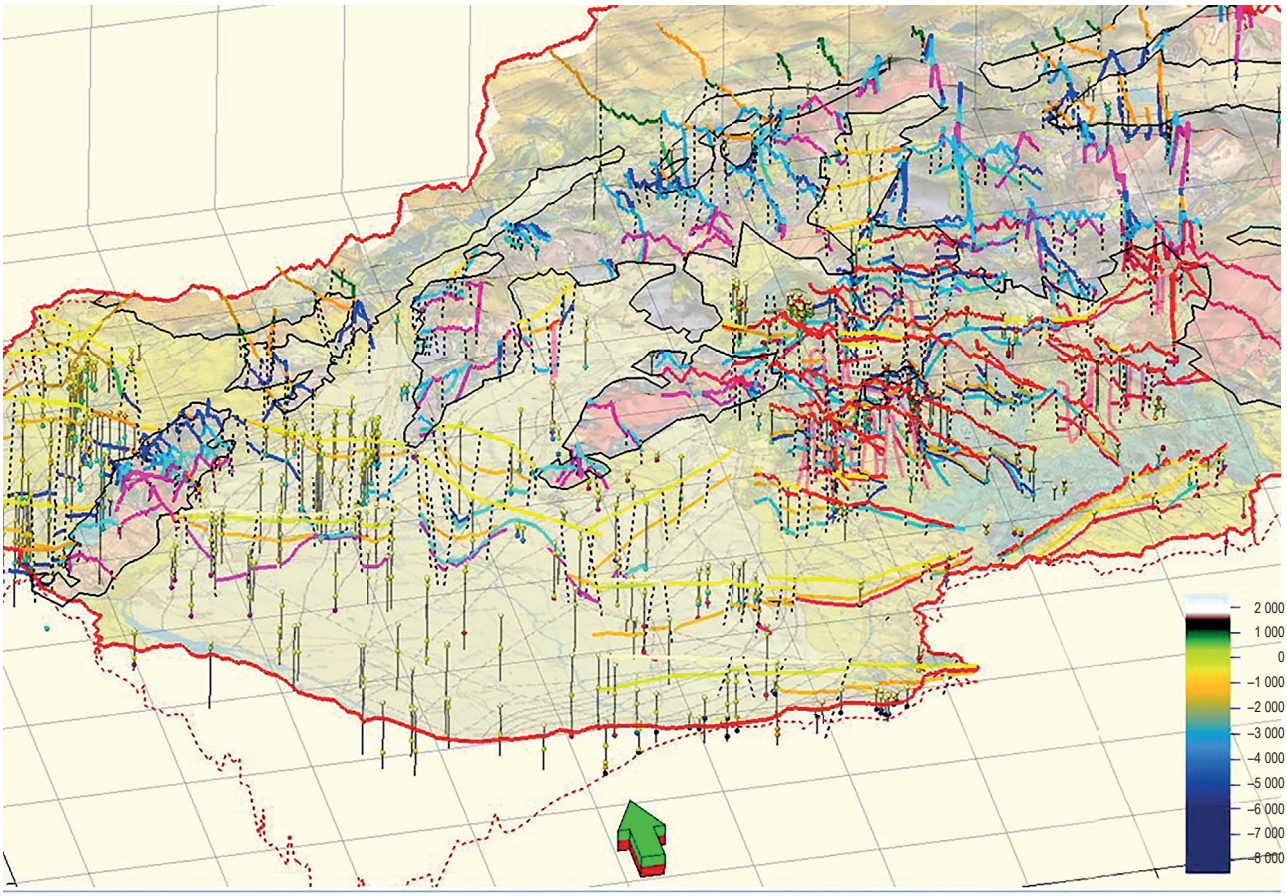

Fig. 2.8. *Deep geological boreholes with an associated legend, digitization of the interfaces. The territory of the western Slovakia.*

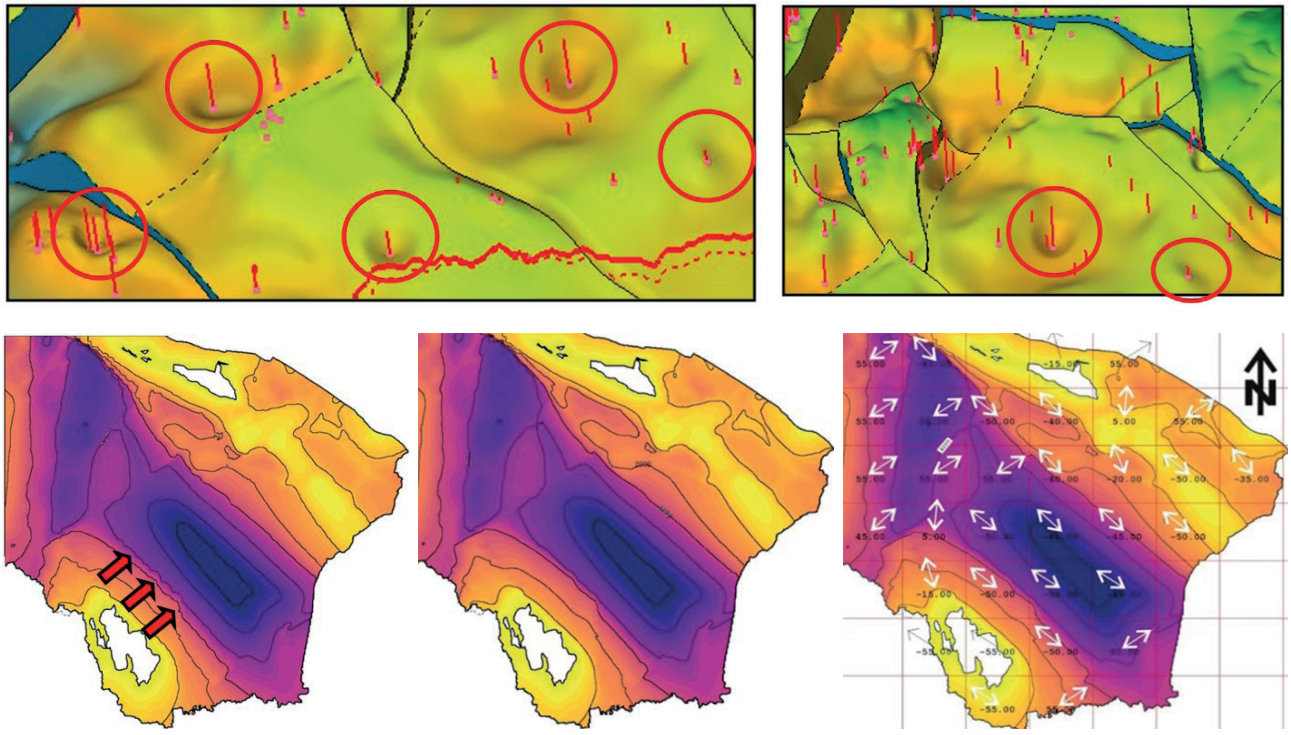

Fig. 2.9. *Artifacts around points created by interpolation (top), the use of sliding geostatistics methods to smooth interpolation curves (bottom).*

- Quaternary base;
- Miocene base;
- Palaeogene base;
- Neogene base (= pre-Tertiary)

– Tectonic structure

– Tectonic units subdivided as follows:
- the Gemericum;
- the Veporicum with cover;
- the Tatricum;
- higher tectonic units;

– Model base.

D) Voxel model creation

A true 3D model should provide information not only about the interfaces, represented in the form of 3D surfaces, but also information at any point of the modelled space. At this stage, our model was just the so-called box model, more suitable for visualization of buildings, etc. Due to the topological properties of the calculated 3D surfaces (given by their mutual position and interconnection), it was possible to assign to each point of the regular spatial network a value from the catalogue, i.e. determine its affiliation to a particular modelled entity. The set of this information then forms the so-called voxel model. This can be saved in one of the standard ASCII formats (e.g. for GeoModeler™), used as part of the spatial visualization of a real 3D geological model, or as an input parameter to some of the hydrogeological modelling softwares (ModFLOW, etc.) and last but not least as a data warehouse for quick and easy creation of some special geological functions, such as virtual wells, virtual profiles and virtual cross-sections.

E) Virtual functionalities creation: boreholes, profiles and cross-sections (Fig. 2.10)

At this stage the created 3D geological model with integrated 3D interfaces, tectonics and voxel information with a step 600x600 m in the direction [XY] for coarse visualizations, or 200x200 m for fine views, similarly in the direction of the axis [Z] 60 m, or 20 m was used for further calculations and visualizations.

The voxel's stored 3D model allowed simple and fast creation of arbitrarily localized boreholes (actually non-existent, they are "boreholes" in the sense of the perpendicular from the model overburden to its subsoil, so we term them *virtual*) with almost instant display of drilled formations in full volume and the appropriate legend, *virtual profiles* (defined by 2 points at the surface and then displayed in 3D with the appropriate legend) and *virtual cross-sections* (defined by the corners of the rectangle and the required altitude). These functionalities can be combined with each other, create e.g. *block-diagrams*, *radiator-like-diagrams* and other common visualizations. All layers were saved locally in ESRI® 3D SHP format.

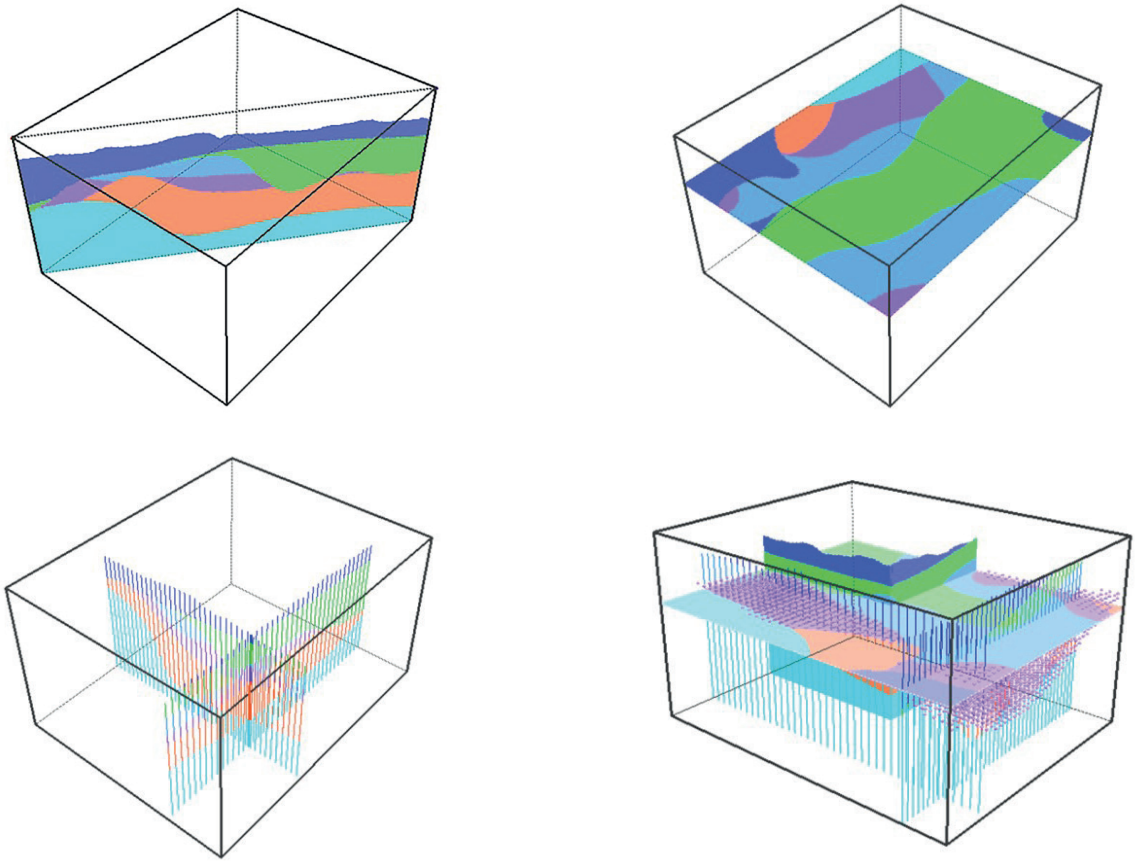

Fig. 2.10. *Virtual functionalities created from the voxel model: 3D profile (top left), 3D horizontal cross-section (top right), a set of boreholes in planes passing through a selected point (bottom left), a combination of several forms of 3D display (bottom right).*

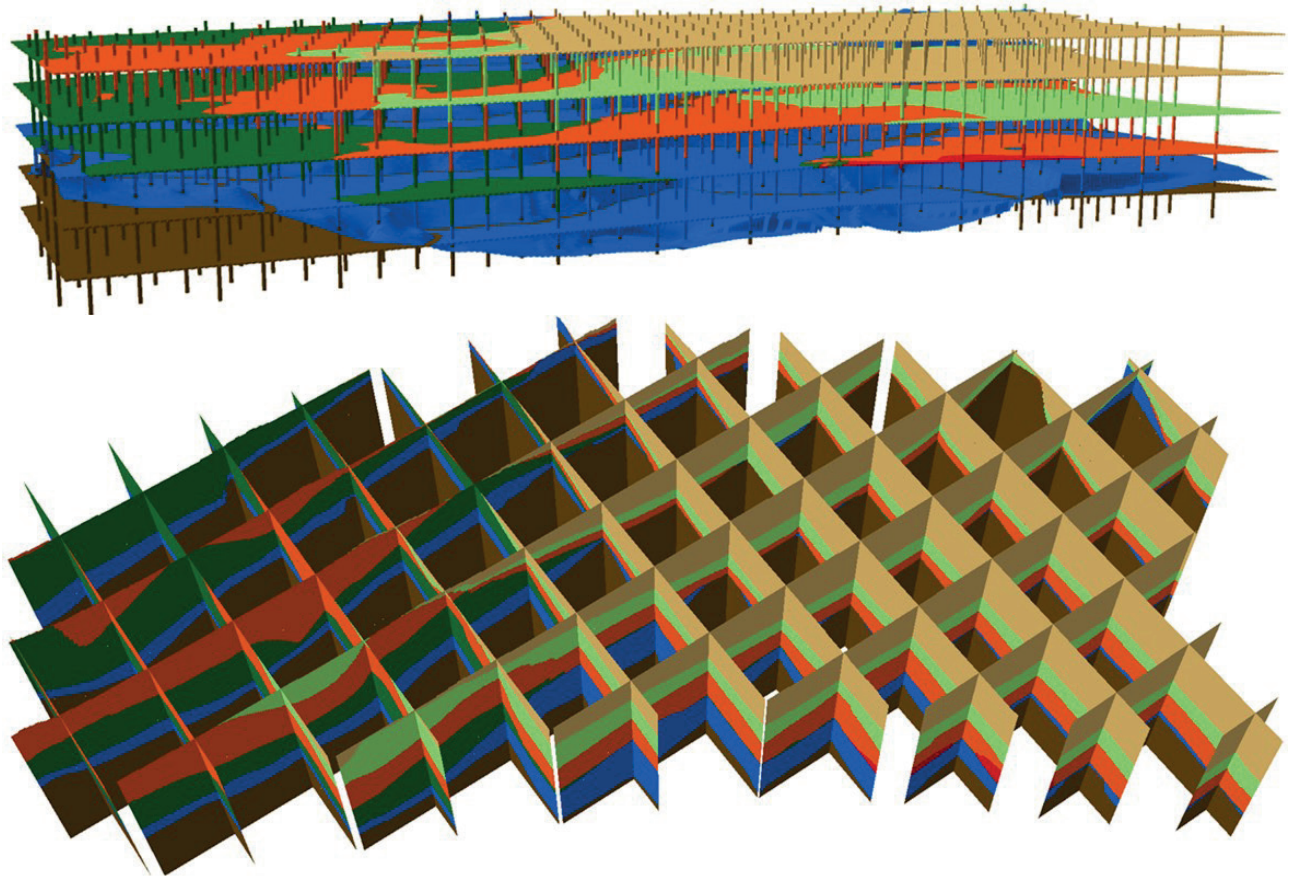

Fig. 2.11. *3D model of the test area (Východoslovenská nížina Lowland), visualization using a set of horizontal sections, boreholes and a selected surface (top), or sets of profiles in the direction of the X and Y axes (bottom).*

For the needs of visualization of the resulting model, a web application was created, which will be available on the website www.geology.sk. It currently offers a 3D interface display, tectonics, individually selected virtual borehole, profile or cross-section. The combination of individual views is being prepared for the future.

2.3 3D modelling results

The developed methodology of spatial geological data processing for the purpose of creating a 3D geological map was tested in selected already modelled regions, such as Turčianska kotlina Depression, Podunajská rovina Flat and Východoslovenská nížina Lowland (Fig. 2.11), solved in previous tasks: "Upper Nitra Basin - three-dimensional geological modelling of the exposed area" (Kotuľová et al., 2010), "TRANSENERGY" (Černák et al., 2012), "Turčianska kotlina Depression - three-dimensional geological modelling" (Nagy et al., 2014). The aim was to verify the methodology in these areas, testing the process steps from data pre-processing, through 3D modelling to visualization of results. The individual steps were used to fine-tune the display, response, testing and development of the functionality of the web application.

The results were very satisfactory. Users, limited in the past to working with specialized 3D modelling software packages, will be able to view the results of their work in real time with excellent response in a commonly used licensed ArcGIS™ environment (when ArcScene™ serves essentially only as a 3D viewer), or can easily visualize the calculated models using a web application on a regular PC and under a common internet connection speed.

Podunajská rovina Flat (TRANSENERGY)
/example of a regional 3D model for testing 3D methodology/

The territory of the Podunajská rovina Flat and adjacent areas (as part of the international project TRANSENERGY) was modelled in the environment of SW Petrel® 8.4. To create a 3D model of the area, 8 modelled horizons were defined, while the main fault lines were respected to during modelling. The individual modelled interfaces were (Figs. 2.12, 13):

- Earth surface;
- Upper Pannonian;
- Lower Pannonian;
- Sarmatian;
- Badenian;
- Badenian – volcanics;
- Palaeogene-Lower Miocene;
- pre-Cenozoic.

The result of the new modelling methodology was, in addition to 3D surfaces, also the voxel model, from

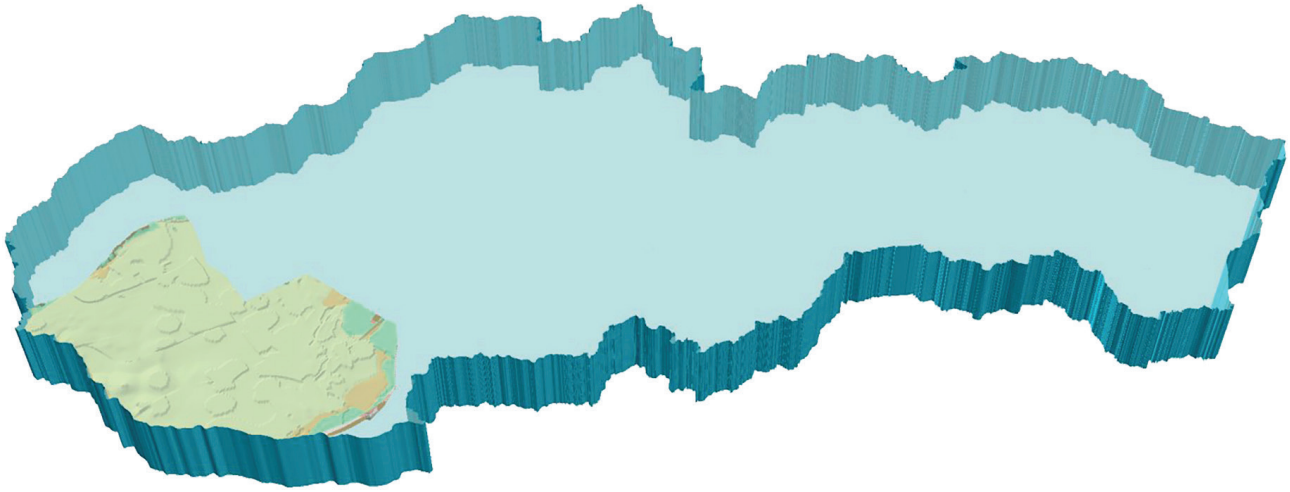

Fig. 2.12. *Localization of the modelled area of the Podunajská rovina Flat within the 3D space of the Slovak Republic.*

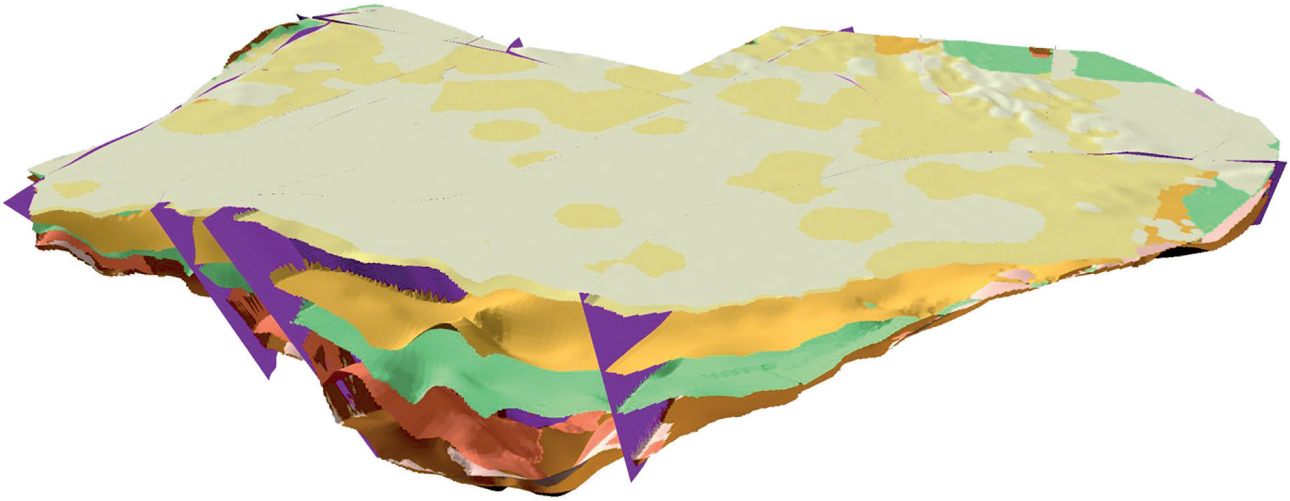

Fig. 2.13. *3D model of the Podunajská rovina Flat (TRANSENERGY), see legend below.*

which we present some extended visualization options, such as a set of sections in the direction of the X axis, or the Y axis, combined with the display of selected interfaces and tectonics (Fig. 2.14), or a combination of a set of horizontal sections, a cloud of virtual boreholes and selected interfaces (Fig. 2.15). The voxel model was calculated in a network of 500x500 m in vertical detail with a step of 50 m.

As can be seen from the attached images, the proposed methodology of data processing into a voxel model and derived virtual boreholes, profiles and sections, even at a voxel resolution of 500x500x50 m, illustrates spatial information about the spatial geological setting of the area, complements the display of information in the entire volume of the modelled 3D territory.

2.4 3D geological model of the Slovak Republic territory at scale of 1: 500,000

– The methodological part presented the method of creating a 3D geological model for the whole territory of the Slovak Republic. The boundary surfaces of the 3D model were:

– state border of the Slovak Republic;

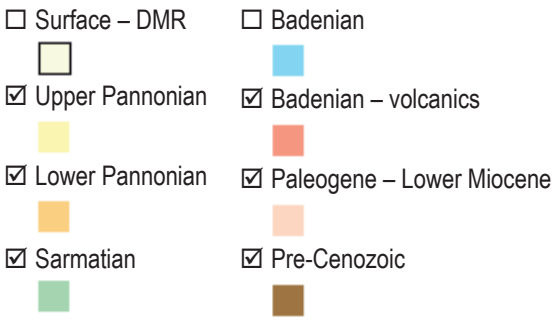

– the Earth's surface represented by a digital relief model (DMR);

– variable depth range of the model (according to the availability of input data calculated at the time of the model creating).

In the first step, the tectonic structure of the Slovak Republic was modelled as reliably as possible, with the support of the key experts in this field when drawing out the main fault lines (failure zones). The objects of faults were often edited, repaired not only for professional geological reasons, but the intersection of faults below the base also brought computational problems to correctly model the

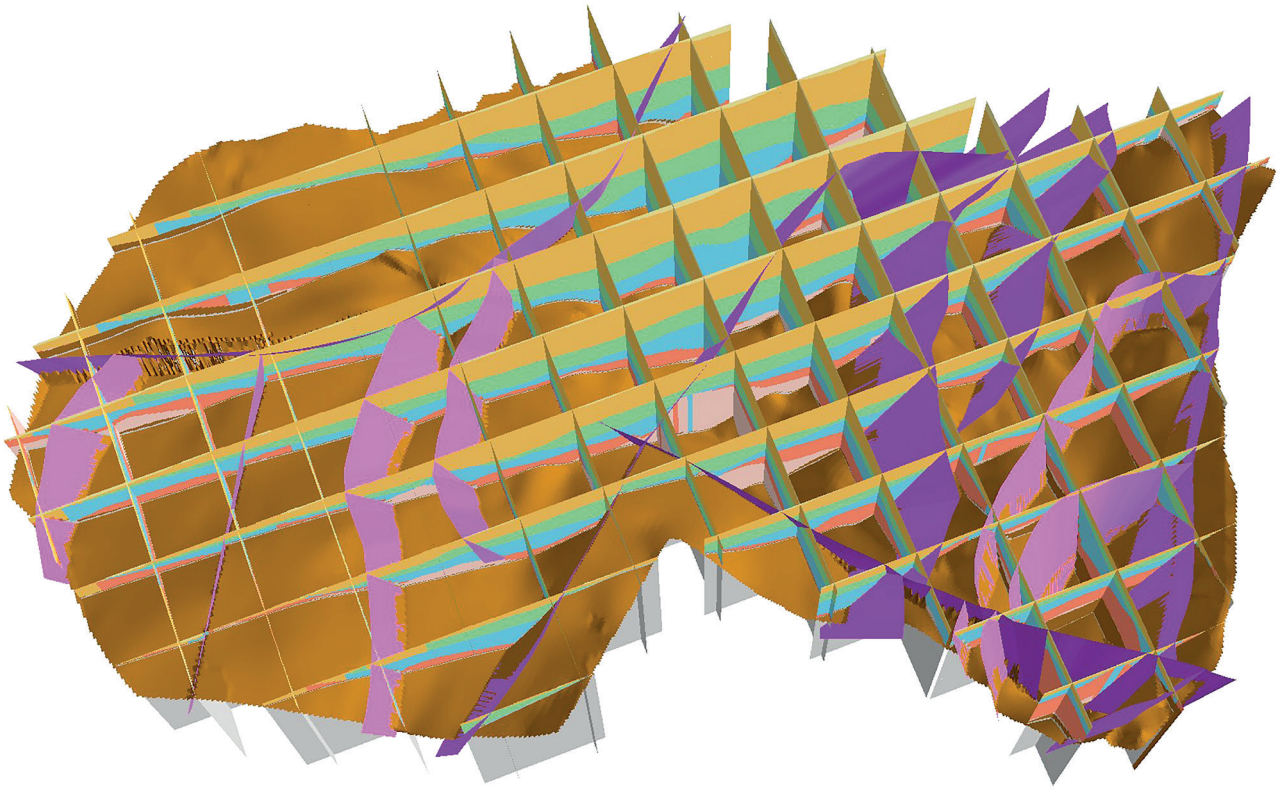

Fig. 2.14. *3D model of the Podunajská rovina Flat area with tectonics. Visualization using a set of profiles in the direction of the X and Y axes.*

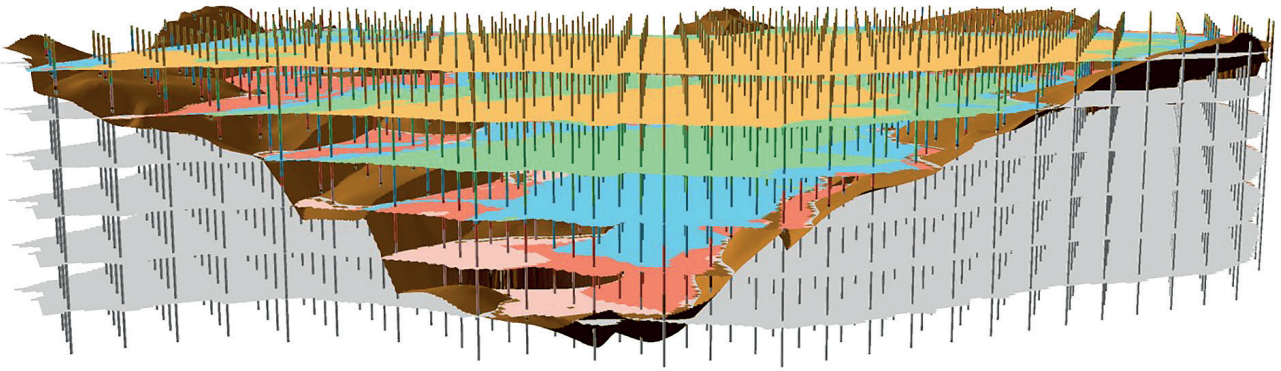

Fig. 2.15. *3D model of PR territory (TRANSENERGY). Visualization using a set of horizontal sections, boreholes and the surface of the pre-Cenozoic basement.*

spatial grid in these segments. This part of creating the 3D model was solved in the environment of the program Petrel® 8.4 of the company Schlumberger. The integrated methodology forced us to work in precisely defined steps and the internal logic of the Petrel® program, which brought many advantages, but also certain limitations.

The 3D tectonic structure of the territory of the Slovak Republic at a scale of 1: 500,000 forms the skeleton of further 3D modelling and we assume that in the future it will form the supporting structure of 3D models of this scale (e.g. when refining, updating the calculated model, but also when creating specialized geothermal models, etc.; Figs. 2.16a, 16b):

During the modelling of the course of 3D surfaces within the created tectonic structure, the individual segments were evaluated separately, or in a sophisticated way so as to respect spatial fault planes (Fig. 2.17).

The modelled space was divided in the depth direction by a layer of pre-Cenozoic basement. The layers below the pre-Cenozoic basement were modelled in the Petrel environment, the layers above this layer in the ISATIS™ program.

The very structural layer of the pre-Cenozoic basement was the main output of the solution of the 3D geological model of the Slovak Republic at the scale of 1: 500,000.

The resulting model was the spatial integration of all modelled 3D surfaces across the vector segments (Fig. 2.18, 19, 20, 21). Each layer was formed by a set of spatial triangles, integrated into a single spatial object with one attribute. Performance tests have shown that this form of

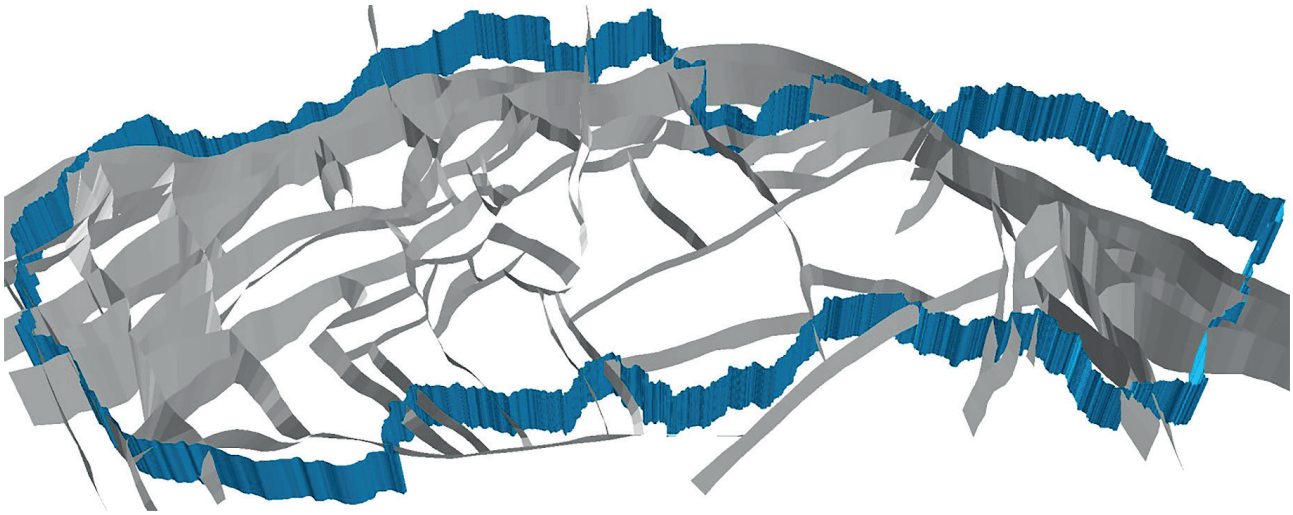

***Fig. 2.16a**. 3D tectonic structure of the Slovak Republic.*

***Fig. 2.16b.** 2D projection of 3D tectonic structure of the territory of the Slovak Republic.*

storage has been optimal. For the purposes of visualization, the spatial objects obtained in this way were divided into smaller parts on the basis of regional division.

A voxel structure was created from a set of spatial planes with a selected step. The resulting 3D grid was used to display a selected set of virtual functionalities, such as the creation of virtual boreholes, profiles and sections (Fig. 2.22, 23, 24). The selected set of objects is stored locally in a *multishape* format based on the query, similar to 3D surfaces. Separate applications have been created to create these functionalities.

In the future, direct support for the ESRI® platform for displaying voxel data is expected. Created applications are ready for this extension.

2.5 Discussion and Conclusions

The resulting 3D model of the geological setting of the Slovak Republic in the form of 3D surfaces (Fig. 2.24) will be available through a web application and in the form of a binary 3D voxel grid, from which it is possible to generate selected boreholes, profiles, sections and display them in one scene.

The 3D voxel model was calculated in a 200x200 m network and in a 600x600 m network with an optional depth resolution interval, e.g. 20 m for detailed views or 60 m for general views.

During modelling, it was found that the source data need to be re-evaluated applying a uniform methodology and using a single legend. A number of differences and inaccuracies were found in the mutual spatial superposition of the calculated surfaces. This was caused by the interpreted data themselves (e.g. the existing Pre-Tertiary basement map), which were formed as separate outputs without connection to other formations, or their surroundings. We have to note that opinions on the geological setting have also changed over time (the range of interpreted maps creation is up to 50 years). It is similar to the creation of classical geological maps, but in 3D there

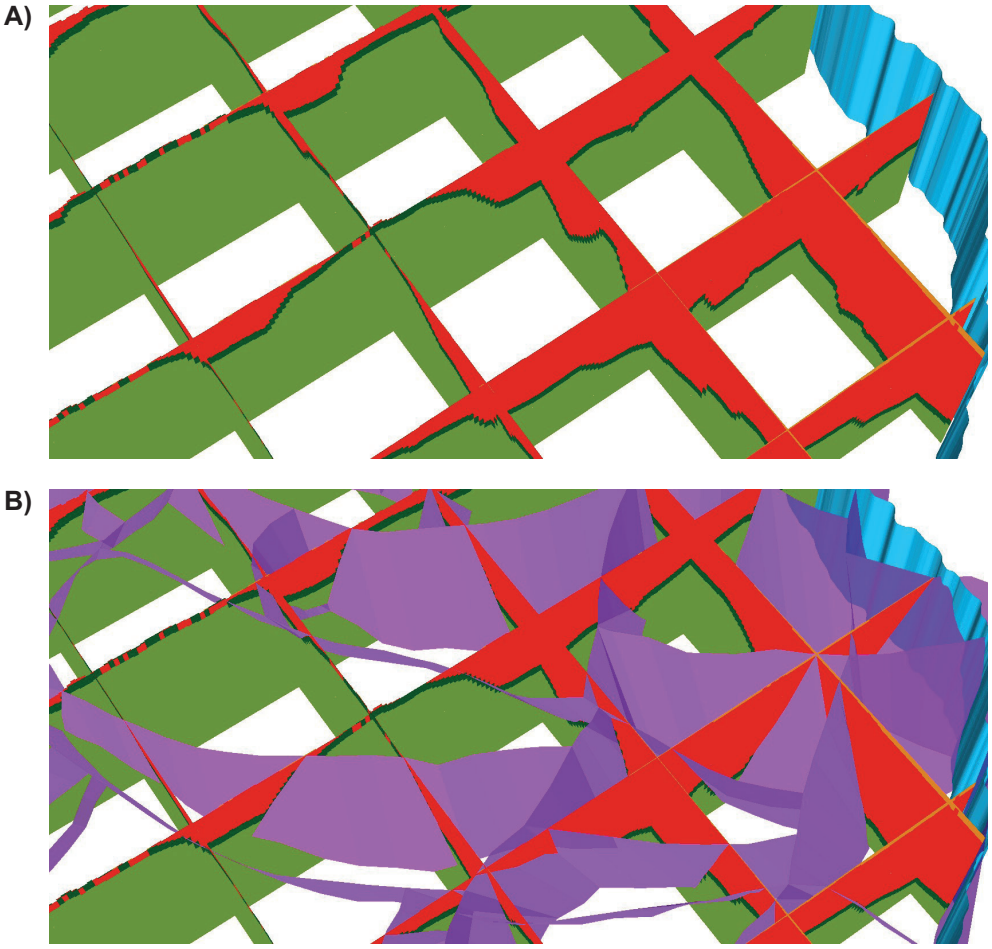

Fig. 2.17. *Comparison of the situation of imaging of the pre-Cenozoic basement with tectonics. A: tectonics off, B: tectonics displayed.*

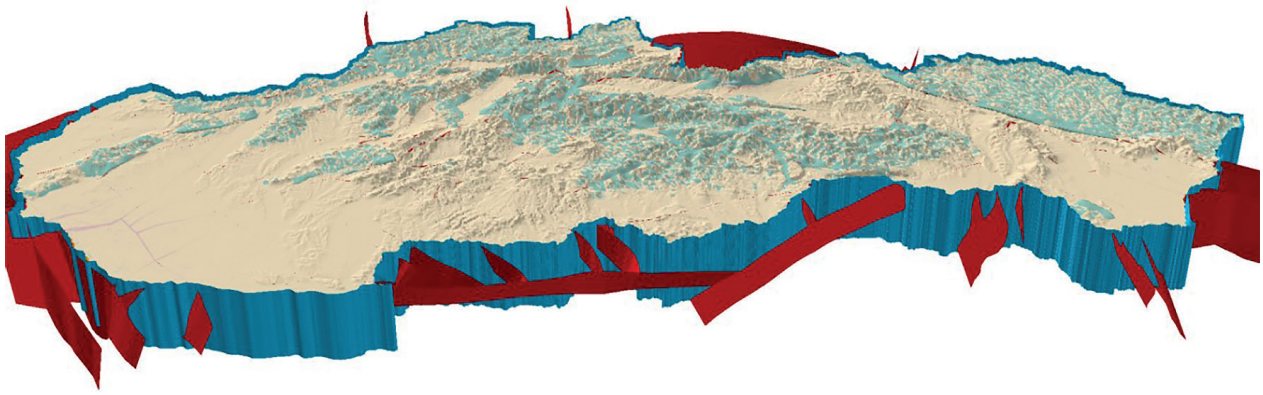

Fig. 2.18. *3D digital relief model in 600x600 m network. The faults are cut to their surface projection.*

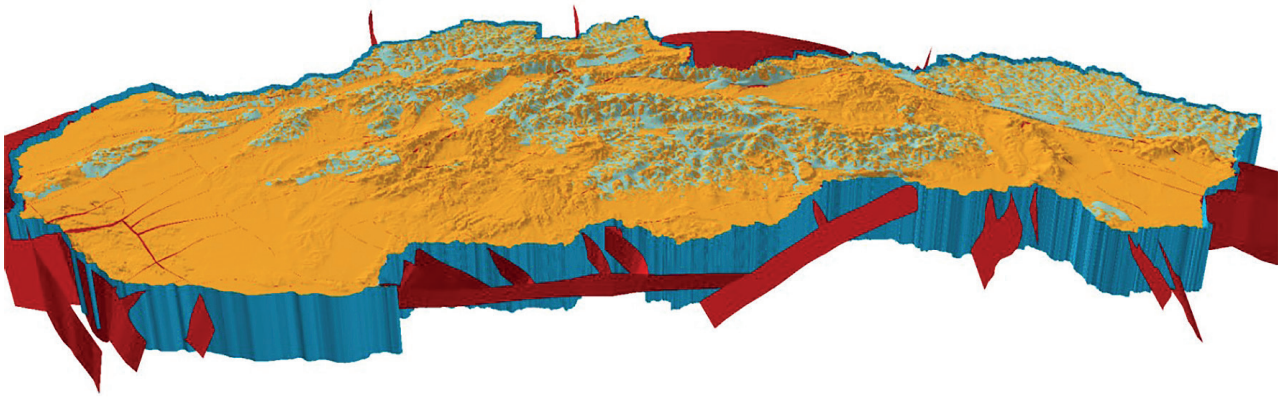

Fig. 2.19. *3D model of Quaternary depths in a 600x600 m network. The faults are cut to their surface projection.*

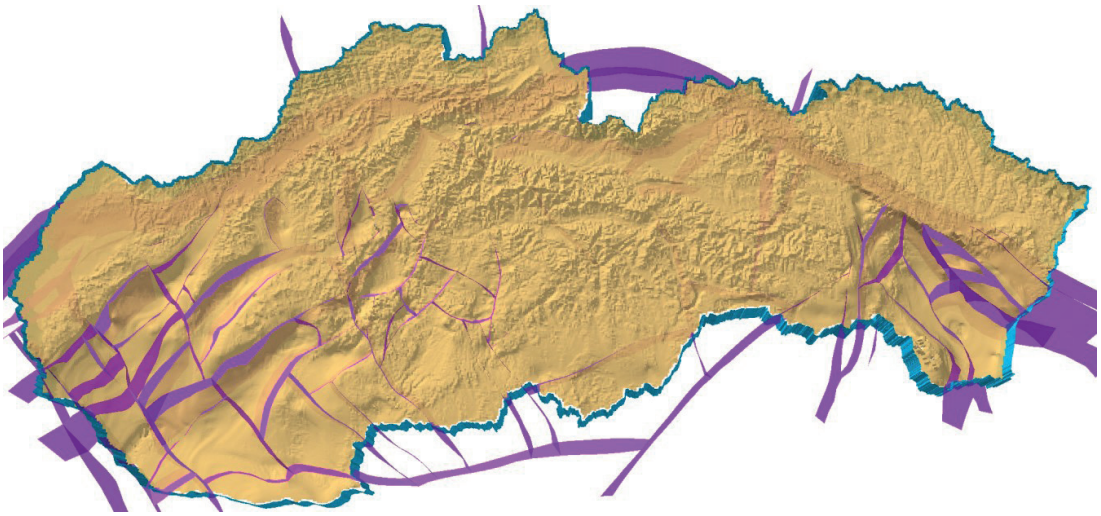

Fig. 2.20. *3D model of the depths of Neogene in a 600x600 m network. The faults are cut to their surface projection.*

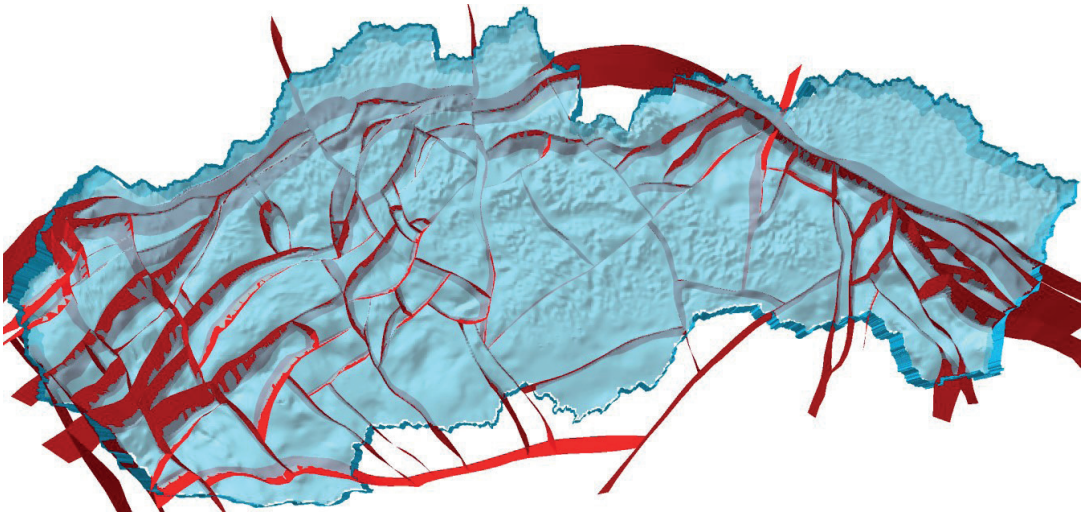

Fig. 2.21. *3D model of the pre-Cenozoic basement of the territory of the Slovak Republic with faults displayed.*

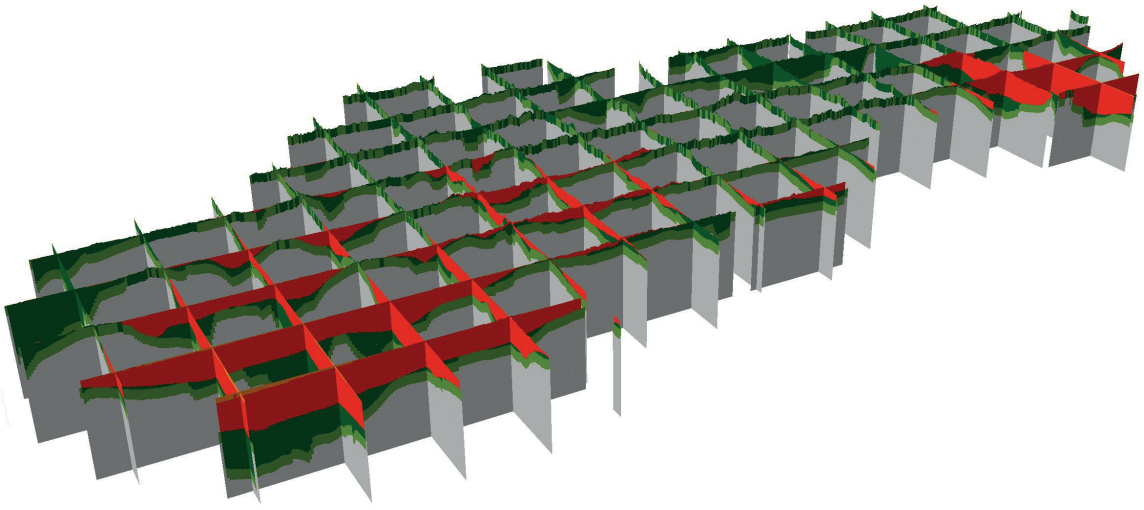

Fig. 2.22. *3D geological model with Neogene base.*
Layers: relief, Quaternary, Neogene base, pre-Cenozoic basement with tectonics, model base (1,000 m below the pre-Cenozoic), in a 600x600 m network. Displayed using virtual geological profiles in the direction of the X and Y axes.

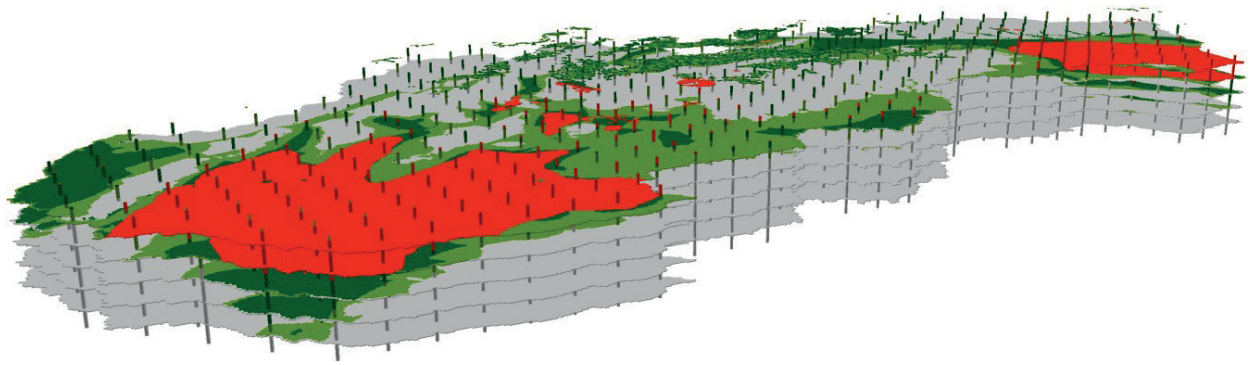

Fig. 2.23. *3D geological model with Neogene base, imaging using horizontal sections and boreholes.*
Layers: relief, Quaternary, Neogene base, pre-Cenozoic subsoil with tectonics, model base (1,000 m below the pre-Cenozoic), in a 600x600 m network.

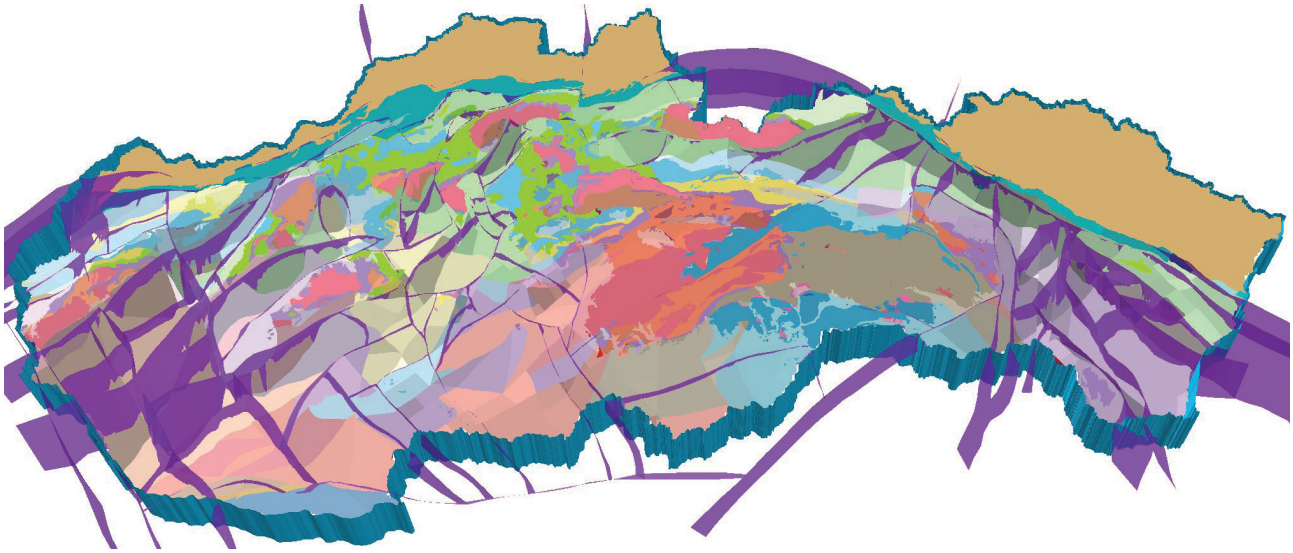

Fig. 2.24. *3D geological model with geological situation in the basement.*
Layers: pre-Tertiary basement, tectonics, geological situation in the basement.

are even more systematic and random inaccuracies and ambiguities in the data, very uneven spatial distribution of input data (boreholes), etc.

We encountered a number of problems at work, some of which we were unable to solve. The created 3D model corresponds in quality and accuracy to the input data from which it was created. We had the smallest amount of data in the northeastern part of Slovakia, as well as in the Outer Carpathians as such (Flysch Zone), the complicated geological structure of the Central Slovakia Neovolcanics Field (with typical younger dikes, penetrating through the older formations) had to be simplified. In the future, geophysical methods will also need to be applied for more reliable 3D modelling: VES, seismic sounding, etc.

The display of source data in space revealed all these discrepancies, which were more pronounced in 3D. In the case of intersecting profiles, it was clear whether the interfaces were drawn correctly or were bounced off, in the worst case non-coherent. A similarly created model compared to the drilling data had to correspond in a geologically acceptable way, it could not be a so-called *bull-eyes* (naming taken from 2D methodologies), etc. Troubleshooting was relatively easy, but the errors eradication was very complicated.

During 3D modelling, it was found that the 3D modelling packages we use (Petrel®, ISATIS™) could not create all the required functionalities so that they could be used in the web interface. Applications had to be created for data import/export, for the creation of virtual boreholes, profiles and sections, various forms of 3D model display had to be designed and tested (locally, but especially via a web application). The optimized procedure was tested on already completed regional models in various stress tests.

The result of the work was the creation of a comprehensive methodology from collection, through data processing, creation of tectonics scheme, structural map, modelling of individual 3D surfaces, creation of a voxel model, creation of boreholes, profiles and sections on request, creation of a web application to publish calculated results. In addition, the web application created over the ESRI® libraries will also support the voxel views themselves in the future.

The created 3D geological model of the Slovak Republic at a scale of 1: 500,000 represents the first attempt to provide a comprehensive 3D geological map for the entire territory of the Slovak Republic and is the most modern expression of a spatial geological setting. The 3D model may in the future be one of the bases for economic and administrative activities of the Slovak Republic and in addition to basic information on the geological setting of the region may provide data for compiling a wide range of purpose, thematic and general geological maps of scales 1: 500,000, 1: 1,000,000. Its selected layer - "3D model of the pre-Cenozoic basement" with a marked geological structure, can be printed plastically as a wall-hung exaggerated (or overlaid) 3D map.

By creating a 3D geological model at the state (national) level, we have become more widely involved in leading positions in this area. In the future, it will be appropriate to participate in international expert commissions and actively participate in the creation of catalogs and methodologies. Such possibilities would provide space for the creation of transnational 3D models in initiatives and projects of *OneGeology, GeoERA, GEOSS*, etc.

References

Bezák, V. (ed.), Broska, I., Ivanička, J., Reichwalder, P., Vozár, J., Polák, M., Havrila, M., Mello, J., Biely, A., Plašienka, D., Potfaj, M., Konečný, V., Lexa, J., Kaličiak, M., Žec, B., Vass, D., Elečko, M., Janočko, J., Pereszlényi, M., Marko, F., Maglay, J. & Pristaš, J., 2004: Tektonická mapa Slovenskej republiky 1: 500 000 [*Tectonic map of the Slovak Republic 1: 500,000*]. MoE SR, SGIDŠ, Bratislava.

Bezák, V., Elečko, M., Fordinál, K., Ivanička, J., Kaličiak, M., Konečný, V., Kováčik, M. (Košice), Maglay, J., Mello, J., Nagy, A., Polák, M., Potfaj, M., Biely, A., Bóna J., Broska, I., Buček, S., Filo, I., Gazdačko, Ľ., Grecula, P., Gross, P., Havrila, M., Hók, J., Hraško, Ľ., Jacko, S. ml., Jacko, S., st., Janočko, J., Kobulský, J., Kohút, M., Kováčik, M. (Bratislava), Lexa, J., Madarás, J., Németh, Z., Olšavský, M., Plašienka, D., Pristaš, J., †Rakús, M., Salaj, J., Siman, P., Šimon, L., Teťák, F., Vass, D., Vozár, J., Vozárová, A. & Žec, B., 2008: Prehľadná geologická mapa Slovenskej republiky 1: 200 000 [*General geological map of the Slovak Republic 1: 200,000*]. SGIDŠ, Bratislava.

Biely, A. (ed.), Bezák, V., Elečko, M., Kaličiak, M., Konečný, V., Lexa, J., Mello, J., Nemčok, J., Potfaj, M., Rakús, M., Vass, D., Vozár, J. & Vozárová, A., 1996: Geologická mapa Slovenskej republiky 1: 500 000 [*Geological map of the Slovak Republic 1: 500,000*]. 1st edition., MoE SR, Geological Survey of the Slovak Republic, Bratislava.

Černák R., Kronome, B., Baráth, I., Berka, R., Fordinál, K., Goetzl, G., Maglay, J., Maros, G., Mikita, S., Nagy, A., Švasta, J. & Uhrin, A., 2012: 3D geological model of the Danube Basin - outcome of the international project TRANSENERGY. / - In: Environmental, Structural and Stratigraphical Evolution of the Western Carpathians. 8th Conference 2012. Abstract book, 6th-7th December, Bratislava. Comenius University, 2012. - ISBN 978-80-223-3335-1, 26 p.

Káčer, Š. (Ed.), Polák, M., Bezák, V., Hók, J., Teťák, F., Konečný, V., Kučera, M., Žec, B., Elečko, M., Hraško, Ľ., Kováči, M., Pristaš, J., Káčer, Š., Antalík, M., Lexa, J., Zvara, I., Fritzman, R., Vlachovič, J., Bystrická, G., Brodnianska, M., Potfaj, M., Madarás, J., Nagy, A., Maglay, J., Ivanička, J., Gross, P., Rakús, M., Vozárová, A., Buček, S., Boorová, D., Šimon, L. & Mello, J., 2005: Digitálna geologická mapa Slovenskej republiky v M 1: 50 000 a 1: 500 000, [*Digital Geological map of the Slovak Republic at scales 1: 50,000 and 1: 500,000*], Geofond archive Nr. 86510, 42 p.

Kilényi, E. & Šefara, J. (Eds.), 1989: Pre-tertiary Basement Contour Map of the Carpathyan Basin Beneath Austria, Czechoslovakia and Hungary. Carpatho-Balkan region. Scale = 1: 2 000 000. ELGI, Budapest.

Kotuľová, J., Švasta, J., Pauditš, P., Janega, A., Dananaj, I., Halmo, J., Elečko, M., Šimon, L., Zlocha, M., Šarkan, J., Fazekaš, J. & Müller, M., 2010: Horná Nitra, „Hornonitrianska kotlina - trojrozmerné geologické modelovanie exponovaného územia" [*Upper Nitra Basin - three-dimensional geological modelling of the area*]. Manuscript, Geofond archive, SGIDŠ, Bratislava.

Lexa, J., Bezák, V., Elečko, M., Mello, J., Polák, M., Potfaj, M., Vozár, J. (eds.), Schnabll, G.W., Pálenský, P., Császár, G., Ryłko, W. & Mackiv, B. (coeds.), 2000: Geologická mapa Západných Karpát a priľahlých území – [*Geological Map of the Western Carpathians and Adjacent Areas* 1: 500,000]. MoE SR and SGIDŠ, Bratislava.

Maglay, J., Halouzka, R., Baňacký, V., Pristaš, J. & Janočko, J., 1999a: Neotektonická mapa Slovenska v mierke 1: 500 000 [*Neotectonic map of Slovakia at scale 1: 500,000*]. Bratislava, MoE SR – GS SR.

Maglay, J., Halouzka, R., Baňacký, V., Pristaš, J., Janočko, J. & Hók, J., 1999b: Vysvetlivky k neotektonickej mape Slovenska v mierke 1: 500 000 [*Explanations to the neotectonic map of Slovakia at scale 1: 500,000*]. GSSR, Bratislava.

Maglay, J., Pristaš, J., Kučera, M. & Ábelová, M., 2009: Geologická mapa kvartéru Slovenska, Genetické typy kvartérnych uloženín 1: 500 000 [*Geological map of Quaternary of Slovakia, Genetic types of Quaternary deposits 1: 500,000*]. Bratislava, MoE SR – SGIDŠ.

Nagy, A., Zlocha, M., Kucharič, Ľ., Švasta, J., Olšavský, M., Zlinská, A., Fordinál, K., Šimon, L., Gaži, P., Dananaj, I., Buček, S., Baráth, I., Demko, R. & Liščák, P., 2014: Turčianska kotlina – trojrozmerné geologické modelovanie územia [*Turčianska kotlina Depression - three-dimensional geological modelling of the area*]. Manuscript, Geofond archive, SGIDŠ, Bratislava.

Plančár, J., Ibrmajer, J. & Fusán, O., 1985: Mapa reliéfu predterciérneho podložia vnútorných Západných Karpatoch, 1: 500 000 [*Map of the relief of the pre-Tertiary basement of the Inner Western Carpathians, 1: 500,000*]. SGIDŠ, Bratislava.

Szalaiová, E., Bielik, M., Makarenko, I., Legostaeva, O., Hók, J., Starostenko, V., Šujan, M. & Šefara, J., 2008: Calculation of a stripped gravity map with a high degree of accuracy: a case study of Liptovská Kotlina Basin (Northern Slovakia). Geol. Quart., 52 (2): p. 103–114, Warszawa.

Wessely, G., 1988: Structure and Development of the Vienna Basin in Austria. - [in:] Royden, L. H. & Horvath, F. (eds.): The Pannonian System. A study in basin evolution. - Amer. Assoc. Petrol. Geol. Mem. 45, p. 333–346, Tulsa (Oklahoma).

Zlocha, M., Vizi, L., Kronome, B., Cibula, R., Nagy, A., Fričovská, J. & Surový, M., 2019: 3D geologická mapa Slovenskej republiky v mierke 1: 500 000 [*3D geological map of the Slovak Republic at scale 1: 500,000*]. 102 p., Manuscript, Geofond archive, SGIDŠ, Bratislava.

Slovak Geol. Mag., 20, 1 (2020), 49 – 84

3. Analytical Pseudo Lumped-Parameter Model for Reservoir Response and Recovery Assessment: Case Study for the Ďurkov Depression Hydrogeothermal Structure, Košice Basin, Slovakia

Fričovský Branislav, Vizi Ladislav, Fordinál Klement, Surový Martin & Zlocha Marian

State Geological Institute of Dionýz Štúr, Mlynská dolina, Bratislava, Slovak Republic, branislav.fricovsky@geology.sk

Abstract: Use of analytical and lumped parameter models (ALPMs) meets multiple limits in praxis given by many necessary assumptions and generalizations simplifying complexity of geothermal reservoir. Ability to adjust assumptions to local conditions through analytical function is, though, a robust advantage of ALPMs where relevant field production, observation and monitoring data are missing or are of unsound quality. The paper presents construction, upscaling and discussion to results of a complex ALPM model of thermal breakthrough, reservoir response and recovery estimator. A thermal breakthrough model shows a constant production of P_{th} = 38 MWth as a critical capacity to avoid cooling of production zone as long as D = 800 m and T_{inj} = 65 °C ($t_B > t_{prod}$ = 100 yrs). Introduction of tolerable cooling at a rate of $T_{wh,t(crit)} = 0.9T_{wh}$ = 122 °C so that a shut-in realizes at $t_{si} = t_{Twh,t(crit)}$ increases the capacity towards P_{th} = 51 MWth, yet more conservative proposal of P_{th} = 49 MWth is subjected to a case-study, matching results of energy balance based sustainability classification. Case studies document well a stepwise field development can reduce risks of incidental shut-in. Recovery model conservatively estimates energy recovery in a production zone as long as $T_{top,crit} \geq 80$ °C, $T_{res,t} \geq 138$ °C and $t_{reco} = t_{si} \geq 60$ yrs. Under sustainable production limitations, a system may be capable to produce $E_{TH(122)}$ = 45 – 46 TWh,th at the $t_{prod} = t_{si}$ = 100 yrs.

Key words: sustainability, reservoir response, reservoir recovery, lumped parameter models, Ďurkov Depression, Slovakia

3.1 Introduction

Geothermal energy is repeatedly reported a renewable and sustainable resource (Axelsson, 2010, 2011). Numerous examples worldwide show both can easily be exposed once excessive production is launched or maintained over a certain period of time. Concerns on sustainability and renewability resulted in a fair definition of sustainable reservoir production (Axelsson et al., 2001), according to that *"for each geothermal system and each mode of production there is a certain level of maximum energy production – E_0 below which it will be possible to maintain constant energy production for a very long time (100 – 300 years). Geothermal energy production below or equal the E_0 is termed sustainable production, while production greater than E_0 is termed excessive production"*. The frame of 100 to 300 years is further discussed in Axelsson et al., (2002, 2004); or Axelsson (2011, 2012a,b). The 100 years period is a compromise between longevity of a resource operation (meeting plural of "future generations" as defined in definition of sustainable development), and a period over which mankind development (including technologies) is somewhat predictable. This is, though, considerably longer period than that of 30 – 50 years set typically according to amortized lifetime of geothermal projects (e.g. Sanyal, 2005; Fridleifsson et al., 2008). Note the definition of sustainability addresses an impact on how a resource is used. Renewability, instead, describes a system for which "*the energy removed from the resource is continuously replaced by more energy on time scales similar to those required for energy removal and those typical of technological or societal systems*" (Rybach et al., 1999; Rybach & Mongillo, 2006; Rybach, 2007). Essentially, this rather addresses the resource characteristics and energy balance in the system, i.e. natural aspects. Conservation of renewability could, thus, be achieved through optimizing a resource production for a level a system would be capable to simultaneously (or in an equal period of time) replace removed energy, including restoration of initial state, such is distribution of heat flow anomalies, heat flux endmembers contribution etc.

Indeed, progressive growth in research, exploration and development of geothermal fields has challenged issues on a resource renewability and sustainability; crucial as long as geothermal energy is considered amongst resources to supply worldwide primary energy mixes according to a scheme of sustainable development (Stefansson, 2005; Fridleifsson et al., 2008; Rybach, 2010a,b). Numerous fields worldwide have, however, observed unexpected changes in reservoir and state conditions (e.g. cooling, phase transition, changes in chemistry), such is an example of The Geysers, Matsukawa, Laugaland, Ytri-Tjarnir or Cerro Prieto (DiPippo, 2005; Flóvenz et al., 1995, 2010; Yasukawa & Sasada, 2015; Gutiérrez & Negrín, 2005). Solutions on questionable production longevity have been approached either through contribution of reservoir engineering or energy / withdrawal or customers' policies (e.g. Flóvenz et al., 1995). These examples, amongst dozens of others, demonstrated that both, renewability and sustainability of geothermal resources can instantly be adjusted to their natural state, yet so easily can be questioned during production.

A role of geothermal reservoir engineering is, thus, not only in a design of reservoir operation, but takes significant contribution to:

- approaching a compromise between longevity and feasibility of production; and
- research and approval of capacity / deliverability a system is able to maintain for a long-term production.

Both issues can be tackled through combination of reservoir monitoring, modelling and simulations. Dozens of concepts on geothermal reservoir simulation and modeling were developed through decades that vary in magnitude of complexity, simplification, mathematical and geostatistical background (extensive reading in O'Sullivan et al., 2001; Burnell et al., 2015) or scope. Complex numerical models provide a way better screen on reservoir parameters and plausible response (e.g. Blöcher et al., 2010; Brehme et al., 2014; Bujakowski et al., 2016). On the other hand, they also require a sound input databasis from prospection and production monitoring (Axelsson, 2012b), including repeating recalibration (e.g. O'Sullivan et al., 1998), turning them time consuming. Lumped parameter or analytical models (e.g. Axelsson, 1989; Alkan & Satman, 1990; Sarak et al., 1995; Hyashi et al., 1999; Onur et al., 2008) apply robust simplifications to reservoir parameters (Sanyal & Sarmiento, 2005; Grant & Bixley, 2011). Still, they also provide a fair hint on prediction analysis especially at situations with lack of reliable or long-term monitoring data; where numerical models would yield robust uncertainties. Not regarding to what kind of model is constructed, each new data accessible subsequently urge its testing and recalibration.

Use of models (simulations) capable to predict (at a given confidence level) reservoir behavior in a response to its production is an exact example on application of modeling strategies in approaching concept of sustainable geothermal production and sustainable development. There is, however, an extensive group of models (frameworks; more reading in Shortall et al., 2015a,b) that scope sustainability of geothermal production or projects differently, e.g. through:

- balancing recent operation to probable reserves at a site – the reserve capacity ratio (Bjarnadottir, 2010; Fričovský et al., 2020a) on regional or national scales;
- evaluation of the project interaction with the environment (physical, chemical, biota) and society (economical, cultural, societal, technical); such is the rapid impact assessment matrix (Pastakia & Jensen, 1998; Ijäs et al., 2008) used in geothermal applications (e.g. Arevalo, 2003; Yousefi et al., 2009; Phillips, 2010a,b; González et al., 2015);
- thermodynamic optimization using efficiency analysis, exergoeconomics and derived indexes, i.e. the sustainability index, improvement potential etc. (e.g. Ozgener et al., 2007; Utlu & Hepbasli, 2008; Gungor et al., 2011).

The Ďurkov Depression hydrogeothermal structure (DDHS) is considered perspective since pioneering prospection on oil and gas in the Košice Basin from 70's (Vranovská et al., 1999a). Conduction of first hydrogeothermal evaluation in late 90's (Vranovská & Bodiš, 1999; Vranovská et al., 1999a,b, 2002) proved high thermal energy potential of the site, installing three geothermal wells (GTD-1 to GTD-3) to assess a potential of 41.8 MWth in overflow regime and 92.6 MWth obtainable by pumping, including need of reinjection. Applied studies emerged soon, whether aimed at heat supply for the city of Košice (e.g. Halás et al., 1999; Vranovská et al., 2000) or at possibilities on binary cogeneration cycles and working fluid selections (Popovičová & Holoubek, 2011; Kukurugyová et al., 2015a,b) and their tentative environmental impact through CO_2 emission reduction (Fričovský et al., 2013). Geothermal field and hydrogeothermics were approached through 3D (matrix driven) modelling (Pachocká et al., 2010); conceptual models on reservoir fluid origin and chemistry (Bodiš & Vranovská, 2012; Vranovská et al., 2015); crustal-scaled (Majcin et al., 2017) or regional thermal field modelling (Jacko et al., 2014); reservoir heat flow analysis (Fričovský et al., 2018b,c); or reservoir thermodynamics (Fričovský et al., 2019; Vizi et al., 2020).

A first production sustainability assessment at a site was conducted in 90's using TOUGH2 code (Giese, 1998, 1999). The model used orthogonal regular grid and borehole data, considering purely conductive environment for 2:1 producer – injector scheme scheduled to operate at a scale of 40 years and at a rate of 225 $l.s^{-1}$. Reinjection temperature was set to T_{inj} = 25 °C. A models shows no thermal breakthrough at a given capacity, implying thermal output of P_{th} = 92.6 MWth sustainable under given conditions. Recently Fričovský et al. (2019) presented results of geothermal reserves booking in combination with reserve capacity ratio (Bjarnadottir, 2010) applied to the DDHS, challenging a thermal output of P_{th} = 49 MWth as critical capacity considering reservoir production sustainability through energy balance.

The paper presents complete reconstruction and upscaling of analytical pseudo lumped-parameter models (ALPMs) at comprehensive theoretical background (Axelsson, 1989; Sarak et al., 2005; Onur et al., 2008; Tureyen et al., 2009; Satman, 2010, 2011; Tureyen & Akyapi, 2011; Satman & Tureyen, 2012) for the Ďurkov Depression hydrogeothermal structure. The entire module consists of:

- thermal breakthrough estimator using advective production-based model for doublets (Ungemach et al., 2005, 2009), involving propagation retardation through conductive effective thermal-exchange profile heating from surroundings (Sauty et al., 1980; Menjoz & Sauty, 1982);
- 1TIQ (1-tank closed ALPM with heat influx and reinjection) model for reservoir response during production since breakthrough (t_B); and
- 1TER (1-tank closed ALPM) model for energy recovery after production shut-in (t_{si}).

The entire estimator module is designed as non-linear and non-isothermal, i.e. production characteristics at time t+1 are function of a reservoir state at time t; and thermal field is subjected to plausible variation in contribution of convection and conduction, while radiogenic heat production is left constant. Both, 1TIQ and 1TER algorithms are designed to cover a desired period of production of t_{prod} = 100 yrs to match theory beyond a concept of sustainable reservoir production (Axelsson et al., 2001). Unlike apparently conventional boundary shut-

in condition given by breakthrough, the 1TIQ and 1TER work on invoking a tolerated cooling rate $T_{wh,t(crit)}$ (Tester et al., 2006; Sutter et al., 2011; Fox et al., 2013; Williams, 2007, 2014), i.e. as long as temperature at a wellhead at time t falls beneath 90 % of a steady-state, i.e. $t_{si} = t_{Twh,t(crit)}$.

In following, both algorithms are tested in a range of optional constant production scenarios P_{th} = 1 – 240 MWth, referenced to a return temperature of T_{inj} = 65 °C, as well as a case of step-wise field development is presented. Besides response of temperature, estimates on thermal field dynamics and response are presented in terms of heat flow end-members contribution and variation. This is crucial when searching for fluid phase stability during considered production.

Note that models have not been history-matched, limiting gained representativeness. Authors do not consider, however, accessible monitoring data from 21-days long pumping tests reliable, hence during production, multiple drawdowns were induced. Instead, more focus has been given to field and heat flow analysis. Use of analytical functions in a single module allow easy recalibration as long as new and sound data are available from (pre) production monitoring. Up to authors best knowledge, any other isothermal, nor non-isothermal lumped parameter modelling has been carried to study the DDHS.

Gained results must, thus, not be considered definitive. Instead, a goal of carried study is to set a baseline at given reliability level for initial production opening considerations, providing safe time span to carry sound reservoir monitoring campaign, recalibrate models, and, finally, optimize production; approaching sustainable and renewable use of a geothermal resource.

3.2 Site description

The DDHS (Fig. 3.1) represents a depressed morphostructure of multiply dissected Mesozoic carbonates underlying Neogene sedimentary fill of the Košice Basin, a NE promontory of the Pannonian Basin (Pereszlenyi et al., 1999). At an approximate area of 33.6 km^2 the system is defined structurally at subsurface extension of Neogene complexes of the Slanské vrchy Mts., whilst terminates along tectonic lines with the Bidovce depression (N), or elevated (uplifted) Mesozoic bedrock (the Vyšný Čaj – Oľšovany – Ďurďošík and Ruskov – Vyšný Čaj junction) to the W and S (Vranovská et al., 1999a, 2000).

A vertical profile (Fig. 3.2) begins with polygeneous Quaternary accumulations at small (< 10 m) thickness, essentially neglected in deep structural models.

Neogene succession reaches up to 2,000-3,000 m; with Sarmatian clays (200 to 1,200 m thick) and rare andesite to rhyolite volcanism products atop Badenian carbonate sandy clays intercalated rarely with tuffites and shales (thickness up to 1,500 m). Karpatian conglomerates that transit to carbonate clays and evaporates form a base of the profile (Pereszlenyi et al., 1999; Vranovská et al., 1999a, 2000).

Mesozoic carbonates are considered as analogue to the Krížna Nappe series of the Western Carpathians (Vranovská & Bodiš, 1999). Transiet varieties, i.e. the carbonate dolomites and dolomitic carbonates prevail. Brecciation and karstification reflects pre-Tertiary uplift and paleo-karstification (Činčura & Köhler, 1995) diminishing towards the base of the reservoir. Thickness of carbonates increases quasi-axially from peripheries (200 m) to central part of the structure (Vranovská et al., 1999a,b) (2,200 m). A top of the reservoir is at 1,660-2,600 m.b.t., a base sinks o 1,960-4,000 m (Vranovská et al., 1999; Fričovský et al., 2018a). Tectonic dissection of the morphostructure owes to three generations of faults in the SW-NE, NW-SE and N-S direction (Bodiš & Vranovská, 2012). A few is known about pre-Mesozoic basement, however, analogously to the Western Carpathians, crystalline complex (magmatites

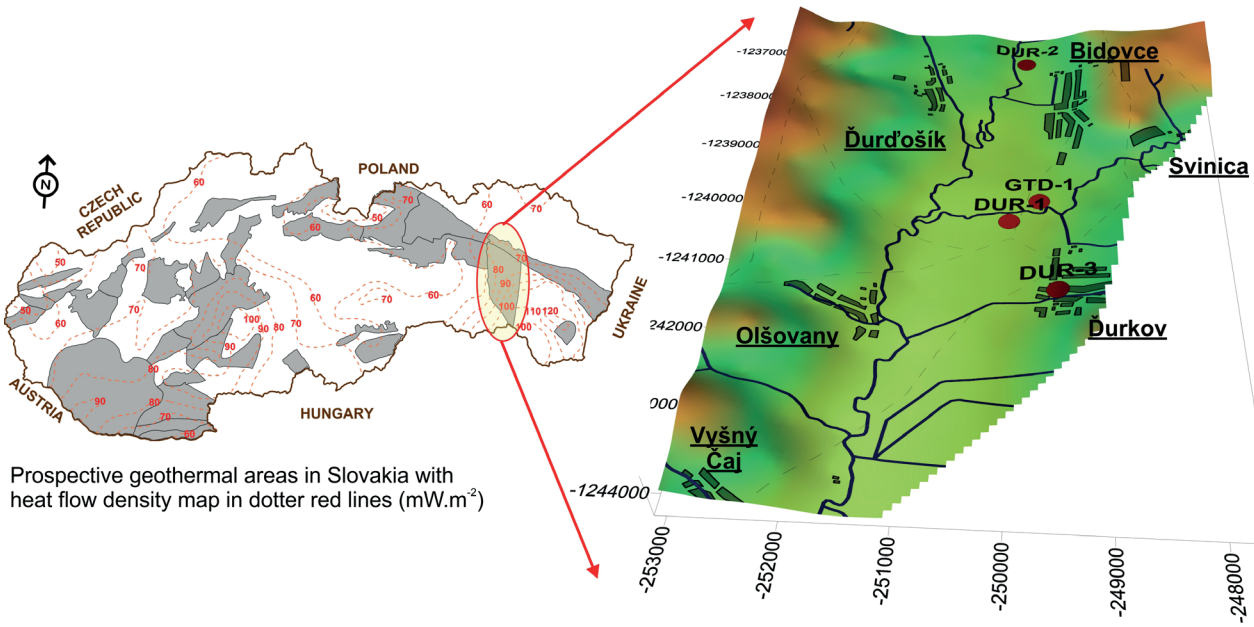

Fig. 3.1. Position of the Ďurkov Depression hydrogeothermal structure within geothermal water bodies of the Slovakia and surface heat flux density distribution. Note resolution is not enough to identify all GTD wells, too close to position of GTD-1.

and metamorphites) of the Veporic unit is expected instantly beneath (Pereszlenyi et al., 1999). The entire crust is roughly 30 km thick (Bielik, 1999).

Saturated geothermal water forms a resource of low to moderate-low thermodynamic quality, i.e. specific exergy index is estimated for SExI = 0.04-0.25 (a mean of 0.11) and moderate temperature / enthalpy, T_{res} = 80-180 °C (Vranovská et al., 1999b; Fričovský et al., 2018a) at TDS of 20.4 to 33.1 g.l^{-1} (Bodiš & Vranovská, 2012).

Geothermal brine originated as infiltrated meteoric water seeped to Neogene strata, dissolving evaporates and reacting with Hg-As-Sb type mineralization prior reaching Mesozoic carbonates. Hence signs on recent reservoir media degradation are missing, the system is generally considered closed. Brines are high in arsenic content, i.e. 19-36 mg.l^{-1} and total dissolved solids, up to 31 g.l^{-1} (Vranovská et al., 2015).

A surface heat flow density is 105-115 mW.m^{-2}. A mean geothermal gradient differs of 51.2 °C.km^{-1} for Neogene and 29.4 °C.km^{-1} for Mid Triassic horizon (Vranovská et al., 2015). Neither temperature distribution (Fig. 3.3), nor use of linear stability analysis at horizontal (Fričovský et al., 2018b; Vizi et al., 2020) or inclined (Fričovský et al., 2018c) conditions proven existence of complex convective zones. Instead, if any, stable, insulated cells may form in deepest parts of the system, limited within particular blocks, restraining progressive adiabatic boiling. Yet this system is off any geodynamically active zone, it meets concepts of conductive plays of orogenic belt type (Moeck, 2014; Moeck & Beardsmore, 2014).

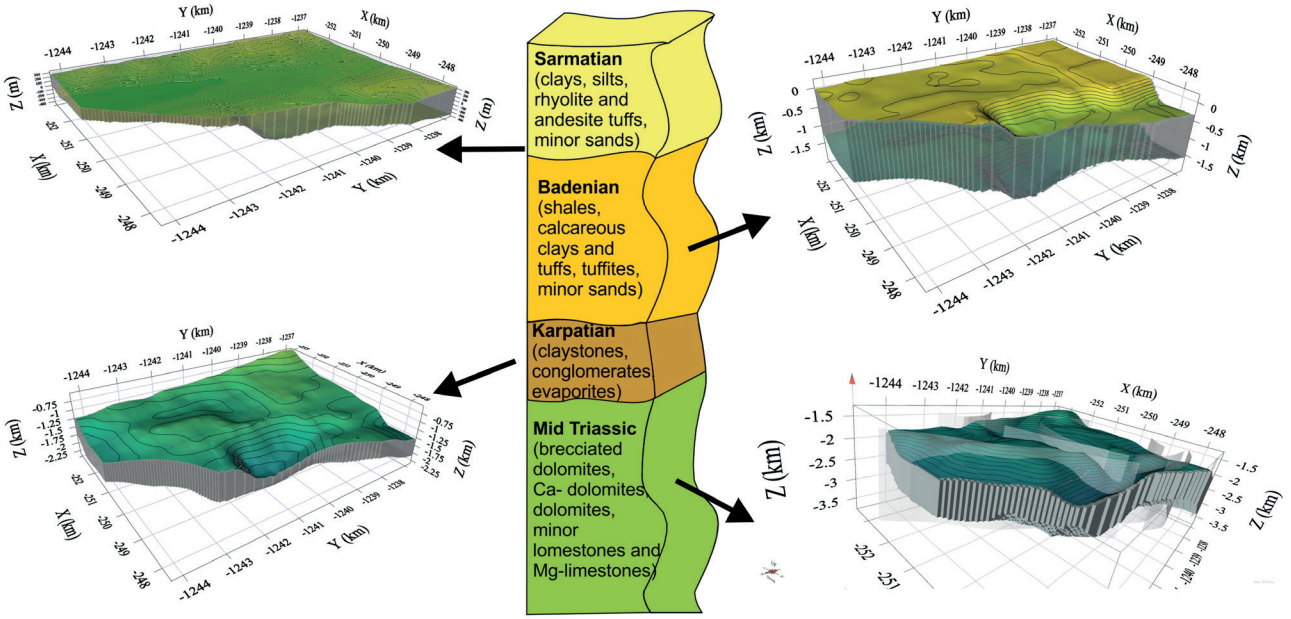

Fig. 3.2. *Deep geological profile of the Ďurkov Depression hydrogeothermal structure.*

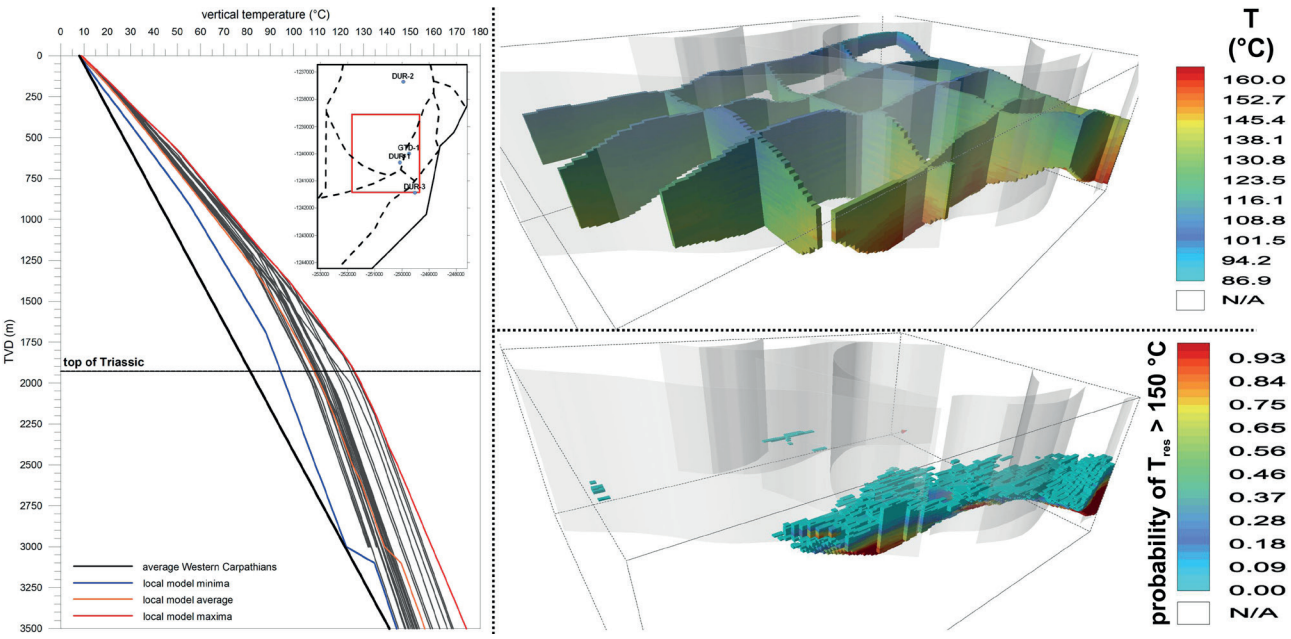

Fig. 3.3. *Horizontal and vertical temperature distribution.*

3.3 Analytical pseudo lumped-parameter model – theory beyond

Lumped parameter models (LPMs) "simplify" a hydrogeothermal system into one "tank" (1T) or multiple "tanks" representing different parts of the system or reservoir and the recharge zone connected to a constant-pressure recharge zone (open - O) or having a point-source reinjection at a margin (closed - C) – see generalized scheme on Figure 3.4.

LPMs have been developed to substitute numerical models in reservoir pressure changes simulations under a lack of adequate data that subsequently yields errors due to many necessary approximations. Early LPMs tackled simulation as an inverse problem, fitting analytical response function to observed data by non-linear iterative least-square techniques (Axelsson, 1989), later replaced by Levenberg-Marquardt method based algorithm for history matching and objection function error mitigation (Sarak et al., 2003a).

At their very beginning, LPMs assumed negligible temperature changes in reservoir, turning this approach applicable to low or moderate enthalpy systems (Onur et al., 2008). Although several non-isothermal LPMs were designed later (Onur et al., 2008; Tureyen et al., 2009, 2014; Tureyen & Akyapi, 2011), they all consider a single phase, liquid (water) dominated reservoir media. Some insights into two-phase and vapor-dominated models were carried by Alkan & Satman (1990) or Hosgor et al. (2013).

3.3.1 Model configuration (number of tanks) selection

Although multiple options were available, we consider a *one (single) closed – tank model* as representative at local conditions. The configuration is justified according to:

- closed hydrogeological character (uplift at faults is up to 400 m, no geochemical indices on chemistry degradation through natural recharges - i.e. Mg^{2+} increase or Cl^- decay); and
- necessary reinjection (producer / production well PW to injector / injection well IW distance ca. 800 m, geothermal brine chemistry).

On Figure 3.4, the reservoir represents a productive part of targeted formation at given hydraulic and geothermal conditions. Aquifer stands for distal, peripheral parts of system in connection to reservoir itself, be it, e.g. a transition zone. Both are, however, "capacitors", i.e. simulate tank with capacity to accumulate a fluid. Hydraulic "conductors" describe capacity of a system to transit the fluid from periphery (recharge zone, injector) towards producer.

3.3.2 Mass balance in one-tank closed model

The reservoir mass balance during production can be assessed through a current mass M_c equation (1) modified for the closed system equaling $M_{rech} = 0$ (2) as there is no recharge

$$M_c = M_{ini} - M_{prod} + M_{rech} + M_{inj} \tag{1}$$

$$M_c = M_{ini} - M_{prod} + M_{inj} \tag{2}$$

The fluid is a single-phase, saturated water, degassed artificially (e.g. Fričovský et al., 2018a,b), at conditions of compressed water expandable with decline in pressure (3). Differentiation of (2) and (3) to time using isothermal compressibility C_t defines the mass flow rate (Sarak et al., 2003a) in a closed tank as (4), assuming compressibility of water as a function of density (5) and compressibility of matrix (6) as function of porosity:

$$M_c = V_{res}.\phi_{res}.\rho_{w,res} \tag{3}$$

$$-\overset{\square}{m}_{prod} + \overset{\square}{m}_{inj} = V_{res}.\phi_{res}.C_{th}.\frac{dp}{dt} \tag{4}$$

$$C_{w,res} = \frac{1}{\rho_{w,res}}.\left(\frac{d\rho_{w,res}}{dp}\right)_{T_{res}} \tag{5}$$

$$C_m = \frac{1}{\phi_{res}}.\left(\frac{d\phi_{res}}{dp}\right)_{T_{res}} \tag{6}$$

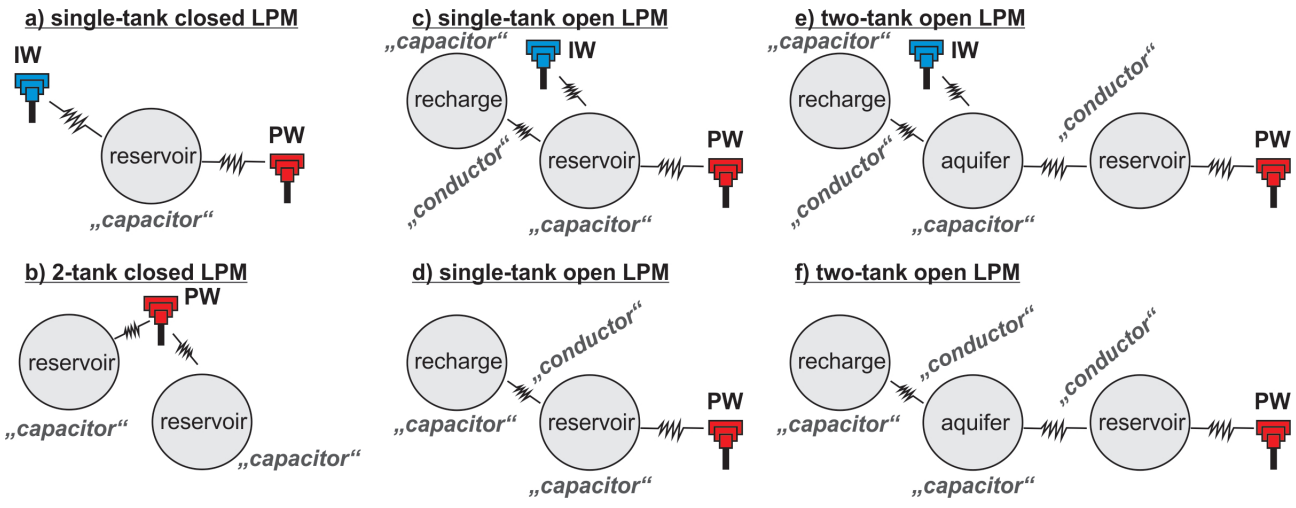

Fig. 3.4. *Schematics of lumped parameter models.*

If constant pressure boundary is assumed, the term of net production (7) characterizes a balance in reservoir mass per unit pressure change with time (8) for closed system:

$$\dot{m}_{prod} - \dot{m}_{inj} = \dot{m}_{net} \tag{7}$$

$$\dot{m}_{net} = V_{res}.\phi_{res}.\rho_{w,res}.C_t.\frac{dp}{dt} \tag{8}$$

The balance does not account for transient reservoir effects, nor extension of reinjection-induced cold-front propagation, essentially modifying reservoir matrix and media properties. Reduction of a problem to isothermal model is yet more accented as reinjection (due to robust temperature differences to the reservoir conditions) causes extensive non-isothermal changes especially when injection / production ratio is high (Sarak et al., 2005).

Now adjusting reinjection proportional to pressure difference between producer and injector (9) allows maintaining production / reinjection ratio constant and equal, so that $Q_{prod} = Q_{inj} = 1:1$, and so that net productivity (8) transforms to (10), with net reservoir storage capacity κ_{res} described as by Eq. 11 (Sarak et al., 2003a):

$$\dot{m}_{inj} = \Psi_{res}.\left(p_{inj} - p_{res}\right) \tag{9}$$

$$\dot{m}_{net} = \Psi_{res}.\left(p_{inj} - p_{res}\right).\kappa_{res}.\frac{dp_{res}}{dt} \tag{10}$$

$$\kappa_{res} = V_{res}.\phi_{res}.\rho_{w,res}.C_t \tag{11}$$

Assuming injection pressure constant (p_{inj} = const. as the $Q_{prod} = Q_{inj} = 1:1$ = const.), and pressure difference is $\Delta p = p_{inj} - p_{res}$, a first-order ordinary differential equation (Sarak et al., 2005) is obtained (12), solved according to initial conditions for reservoir pressure (13) or pressure difference (14):

$$\frac{\dot{m}_{net}}{\kappa_{res}} = \frac{d\Delta p}{dt} + \frac{\Psi_{res}}{\kappa_{res}}.\Delta p \;\Bigg|\; \begin{matrix} p_{res}(t=0) = p_{inj} \\ \Delta p(t=0) = 0 \end{matrix} \tag{12}$$

$$p_{res}(t) = p_{inj} - \frac{\dot{m}_{net}}{\Psi_{res}}.\left[1 - \exp\left(-\frac{\Psi_{res}.t}{\kappa_{res}}\right)\right] \tag{13}$$

$$\Delta p(t) = \frac{\dot{m}_{net}}{\Psi_{res}}.\left[1 - \exp\left(-\frac{\Psi_{res}.t}{\kappa_{res}}\right)\right] \tag{14}$$

3.3.3 Energy and mass flow in one-tank closed model

Alike shallow groundwater sources, the energy flux in the geothermal reservoir is of an essential importance. At initial (natural, undisturbed) conditions, the energy flow in the system is generally given by a balance between an energy inflow E_{IN} and outflow E_{OUT}. When the system is produced (Satman, 2010), the energy that is extracted through reservoir fluid removal is accounted. Rewritten to a term of cumulative energy, the balance becomes (15):

$$E_{prod} - E_{rech} - E_{inj} - E_{IN} - E_{OUT} = E_{ini} - E_{(t)} \tag{15}$$

Because $E_{IN} = -E_{OUT}$ in quasi-stable conductive environment, cumulative energy added and lost from the system are neglected in a balance. Simplification of (15) into (16) requires:

- to set energy produced E_{prod} (17) as function of a fluid withdrawal $Q_{prod,t}$ and change in wellhead temperature $T_{wh,t}$
- to mitigate natural energy recharge E_{rech} (18) to a system ($E_{rech} = 0$) as long as a tank is closed
- to adjust energy increment / removal to the system through reinjection E_{inj} (19) as function of mass withdrawal Q_{prod} and a time tprod as long as $Q_{prod} = Q_{inj}$ and T_{inj} = const. during production, or to turn $E_{inj} = 0$ after shut in as $Q_{prod} = Q_{inj} = 0$ during reclamation
- definition of initial reservoir energy content E_{ini} (20) as given by reservoir volume V_{res} and accumulated heat γ_a at initial conditions, i.e. $T_{res(t=0)}$; and
- to account an effect of reinjection on energy content and balance at time $t \neq 0$ $E_{t=i}$ as function of gradient between actual $T_{res,t}$ and reinjection T_{inj} temperature (21):

$$E_{prod} - E_{inj} = E_{ini} - E_{(t)} \tag{16}$$

$$E_{prod} = Q_{prod}.c_{w,wh}.\int_0^t \Delta T dt \tag{17}$$

$$E_{rech} = c_{w,rech}.\int_0^t Q_{rech}.\Delta T dt \tag{18}$$

$$E_{inj} = Q_{inj}.c_{w,inj}.T_{inj}.t \tag{19}$$

$$E_{ini} = V_{res}.\gamma_a.\Delta T_{t=0} \tag{20}$$

$$E_{t=i} = Q_{inj}.c_{w,inj}.\Delta T_{t=i} \tag{21}$$

Combining (16) to (21) yields different analytical models for a reservoir depending on a production management. For a *closed system with production only* (Satman, 2011) the energy – mass balance is proportional between the energy / fluid stored and its removal (22), expecting a temperature to decrease exponentially with abstraction of a heat in place (23 – 24):

$$V_{res}.\gamma_{a,res}.\frac{dT}{dt} = -Q_{prod}.c_{w,wh}.T_{wh} \tag{22}$$

$$T_{(t)} = T_{ini}.e^{-a.t} \tag{23}$$

$$a = \frac{Q_{prod}.c_{w,wh}}{V_{res}.\gamma_{a,res}} \tag{24}$$

A modification of a balance (22) can be made *adding reinjection* into a scheme (25). The reinjection

temperature T_{inj} is far less than that in the reservoir T_{res}. Fluid management balances reservoir pressure but so it induces cooling. For $Q_{prod} = Q_{inj}$ the rate of cooling (26) is proportional to a difference between $T_{res,t}$ and T_{inj} (T_{inj} = const.) during production, non-linearly increasing as cold-front propagates towards producers. At given specifications, the balance (25) and analytical functions for a single, closed tank model with reinjection are (Satman, 2011):

$$V_{res}.\gamma_{a,res}.\frac{dT}{dt} = -Q_{prod}.c_{w,wh}.T_{wh} + Q_{inj}.c_{w,inj}.T_{inj} \quad (25)$$

$$\Delta T = T_{ini} - T_{(t)} \rightarrow \Delta T = \left(T_{ini} + \frac{g}{a}\right).\left(1 - e^{-a.t}\right) \quad (26)$$

$$T_{(t)} = T_{ini}.e^{-a.t} - \frac{g}{a}.\left(1 - e^{-a.t}\right) \quad (27)$$

$$g = \frac{Q_{inj}.c_{w,inj}.T_{inj}}{V_{res}.\gamma_{a,res}} \quad (28)$$

Reservoir exploitation represents all but a natural state of a reservoir, with plausible formation of cooling-induced gradient within. A *closed system with production and heat increment model* (Satman, 2010) accounts the energy influx E_n in a general balance on a stored-heat site (29), set proportional to a heat gradient in the reservoir (30 to 32):

$$V_{res}.\gamma_{a,res}.\frac{dT}{dt} = -Q_{prod}.c_{w,wh}.T_{wh} + E_n \quad (29)$$

$$\Delta T = T_{ini} - T_{(t)} \rightarrow \Delta T = \frac{a.T_{ini} - x}{a}.\left(1 - e^{-a.t}\right) \quad (30)$$

$$T_{(t)} = T_{ini} - \frac{a.T_{ini} - x}{a}.\left(1 - e^{-a.t}\right) \quad (31)$$

$$x = \frac{E_n}{V_{res}.\gamma_{a,res}} \quad (32)$$

Essentially, the E_n substitutes the $E_{IN} - E_{OUT}$ balance. While at natural state the $E_{IN} - E_{OUT} = 0$ because $E_{IN} = E_{OUT}$, there is a heat gradient formation between the undisturbed zone (surroundings) and the effective heat-exchange profile (i.e. part of a reservoir body assumed dynamic according to pressure depression build-up and connectivity where reinjected fluid propagates to producer) during reservoir production.

Apparently, when combining equations (22), (25) and (29), an analytical model for a *single-tank, closed system with reinjection and a heat increment* is given by (33), with following functions (34 – 35) for temperature change and its function with time (Satman, 2011):

$$V_{res}.\gamma_{a,res}.\frac{dT}{dt} = -Q_{prod}.c_{w,wh}.T_{wh} + Q_{inj}.c_{w,inj}.T_{inj} + E_n \quad (33)$$

$$\Delta T = T_{ini} - T_{(t)} \rightarrow \Delta T = T_{ini}.\left(1 - e^{-a.t}\right) - \left[\frac{g'}{a}.\left(1 - e^{-a.t}\right)\right] \quad (34)$$

$$T_{(t)} = T_{ini}.e^{-a.t} - \frac{g'}{a}.\left(1 - e^{-a.t}\right) \quad (35)$$

$$g' = \frac{Q_{inj}.c_{w,inj}.T_{inj}}{V_{res}.\gamma_{a,res}} + \frac{E_n}{V_{res}.\gamma_{a,res}} \quad (36)$$

The solution of (33) to (36) (Satman, 2010, 2011) represents a general form of ALMP used to simulate estimates on reservoir response to production. A discussion on upscaling to adjust the general model to local conditions is provided in following chapter.

3.3.4 Energy recovery

In (33) to (36) the rate of reservoir cooling decreases with E_n, standing for a heat that is available in a reservoir when all its losses are subtracted from a balance (O'Sullivan & Mannington, 2006). As such, it is the sum of the heat that flows to the system, and is transported within the system by all available endmembers (37):

$$E_n = E_{CD} + E_{CV} + E_{RG} - E_{OUT} - E_{PROD} \quad (37)$$

The heat increment into produced part of a reservoir (profile of effective heat exchange) is definitely not constant. During production, the E_n increases with decline in $T_{res,t}$ and drop in temperature at top of the reservoir $T_{top,crit}$ as thermal gradient forms. At shut-in (t_{si}) the $E_{PROD} = 0$, and $T_{res,r}$ and $T_{top,r}$ starts to recover according to a state of $E_{n(t=tsi)}$. Recovery of $T_{res,r}$ and $T_{top,r}$ towards $T_{res,r} = T_{res}$ and $T_{top,r} = T_{top}$ causes an induced gradient to vanish. The E_n decreases, thus, simultaneously with approaching an initial state during reclamation (38). A rate of recovery (39) is, thus, proportional to thermal gradient ceasing, formulated as (Satman, 2011):

$$E_n = V_{res}.\gamma_{a,res}.\frac{d\Delta T}{d\Delta t} \quad \left| \begin{array}{l} \Delta T = T_{reco} - T_{top} \\ T_{top} = \text{const.} \\ T_{reco} = T_{si} \\ T_{reco} = T_{ini} \end{array} \right. \quad (38)$$

$$T_{reco} = T_{si} + x.\Delta t \rightarrow T_{si} + x.t_{reco} \quad (39)$$

Equations (32 and 39) require reservoir area and thickness equal for radiogenic heat production (E_{RG}), convection (E_{CV}) and conduction (E_{CD}). This yields a robust approximation, as e.g. in conductive low- or moderate- enthalpy basin systems convection cells may develop as insulated and limited in extension (such is a case of DDHS – Fričovský et al., 2018b,c), so that $V_{(CD)} >> V_{(CV)}$. Consequently, necessary upscaling changes a form (32) into (40) accounting on heat endmember geometry limitations:

$$\sum x = x_{(CD)} + x_{(CV)} + x_{(RG)} = \frac{E_{CD}}{A_{CD}.H_{CD}.\gamma_{a,CD}} + \frac{E_{CV}}{A_{CV}.H_{CV}.\gamma_{a,CV}} + \frac{E_{RG}}{A_{RG}.H_{RG}.\gamma_{a,RG}} \quad (40)$$

Thermal recovery terminates at thermal equilibrium, i.e. at $T_{res,r} = T_{res}$ and $T_{top,r} = T_{top}$ at a time t_{reco}, when heat flux into the system is balanced by natural heat losses such is a surface heat flux or heat transmission to surroundings

according to $E_n = E_{CD} + E_{CV} + E_{RG} \rightarrow lim\ E_{OUT}$. For closed-tank model, the analytical solution to search for a t_{reco} is (41):

$$t_{reco} = \frac{T_{ini} - T_{si}}{x} \quad (41)$$

3.3.5 Thermal breakthrough

The thermal breakthrough is an essential feature of reservoir response to production, whether considering natural recharge and/or reinjection. Selection of model to predict a breakthrough gains considerable credits in reservoir engineering especially when question of production longevity is considered, yet not necessarily causing a shut-in. Instead, a rate of cooling is questioned through concept of sustainability according to boundary conditions defined at a level of tolerable drop in reservoir / wellhead temperature (e.g. Williams, 2007).

Numerous analytical models have already been introduced in past, different in accounting heat transfer endmembers to contribute on cooling and its retardation. As based on local geothermal settings and data quality, an advective model with diffuse retardation for doublet systems (Gringarten & Sauty, 1975; Ungemach et al., 2005, 2009) was applied. The model is based on parametrical heat transfer equation (42), assuming hydraulical insulation of a reservoir at a top and a base and matrix homogeneity (Gringarten & Sauty, 1975). Cone-shaped cold-front propagation during time t_B (43) at a distance D and thickness H_{eff} (Ungemach et al., 2005) is assumed. Thermal diffusion slows cooling at a contact of injected fluid with matrix, increasing with D. A front cools the effective profile adjectively, accenting a rate of reinjection Q_{inj} at constant T_{inj}. A rate of thermal diffusion is given by a coefficient of heat exchange Λ_{CD} (44), implying minimum conductive retardation for $\Lambda_{CD} \rightarrow \lim\infty$ and rapid diffuse slowing of advective cold-front transport for $\Lambda_{CD} \rightarrow \lim 0$ (Gringarten, 1978; Sauty et al., 1980):

$$div\left(\lambda_B \nabla T\right) - div\left(\rho_{w,inj}.c_{w,inj}.v_D.T_{inj}\right) = \gamma_{a,res}.\frac{dT}{dt} \quad (42)$$

$$t_B = \frac{\pi}{3}.\frac{c_{w,inj}.\rho_{w,inj}}{\gamma_{a,res}}.\frac{Q_{inj}.H_{eff}}{D^2} \quad (43)$$

$$\Lambda_{CD} = \frac{c_{w,inj}.\rho_{w,inj}.\gamma_{a,res}}{\lambda_B.\rho_m.c_m}.\frac{Q_{inj}.H_{eff}}{D^2} \quad (44)$$

3.4 Analytical pseudo lumped-parameter model – upscaling

3.4.1 Production scheme

The model represents a one-tank closed system, localized within the Ďurkov Depression hydrogeothermal structure. In reference studies (e.g. Vranovská et al., 1999a,b; Giese, 1998, 1999), the producer – injector scheme is considered 2:1. Constructed ALPM simplifies a situation neglecting number of production and injection wells (Fig. 3.5).

The *distance D* is calculated as horizontal distance of the borehole tip in the reservoir level between GTD-2/GTD-3 (producers) and GTD-1 (injector) for D = 800 m, accounting angle of borehole inclination. A *wellhead temperature* T_{wh} is given by pumping tests (e.g. Vranovská et al., 1999a,b; Halás Sr et al., 2016) as averaged mean yearly temperature T_{wh} = 135 °C. *Reinjection temperature* T_{inj} is assumed for T_{inj} = 65 °C (Vranovská et al., 1999b) scheduled for a free-flow, however, considered reasonable according to chemistry of geothermal brine. Although lowering T_{inj} (such as T_{inj} = 25 °C calculated in Halás Sr et al., 2016) may generate ancillary benefits through building up a thermal gradient for P_{th}, subsequently requiring less yield (45), a risk of intense corrosion / scaling occurs. Maintaining the T_{inj} = 65 °C appears thus, a conservative scenario, yet more realistic.

Simulation of thermal breakthrough, reservoir response (1TIQ) and reclamation (1TER) is carried on a wide range of constant production scenarios (P_{th} = const.) obtained from combining the geothermal reserves booking (Sanyal – Sarmiento, 2005; Fričovský et al., 2019) with reserve capacity ratio classification (Bjarnadottir, 2010; Fričovský

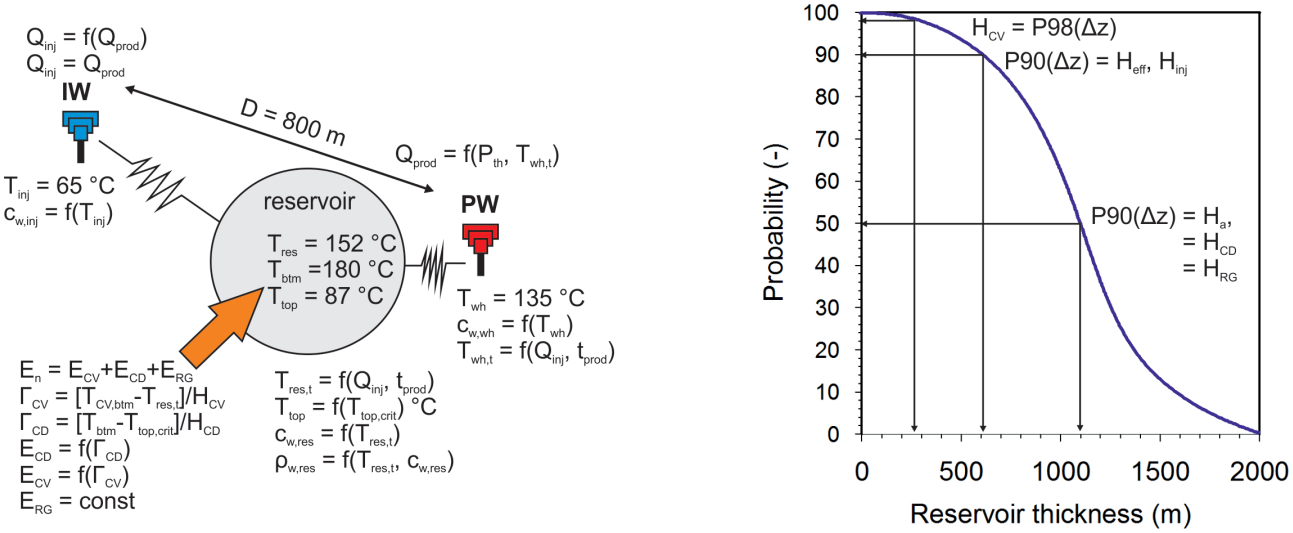

Fig. 3.5. *Basic visualization of lumped parameter model scenario (left) and CDF for reservoir thickness – Δz (right).*

et al., 2019) – see "Part II" paper for more detailed discussion. Because both models work as non-isothermal, i.e. $P_{th} = f(T_{wh,t})$ and $T_{wh,t} = f(T_{res,t})$, an objective demand on increase yield is solved through (45):

$$P_{th,t} = Q_{prod,t}.c_{w,wh}.\left(T_{wh,t} - T_{inj}\right) \quad (45)$$

Reservoir (w,res), wellhead (w,wh), and reinjection (w,inj) parameters such is the specific heat capacity (e.g. $c_{w,wh}$) and reservoir density (e.g. $\rho_{w,wh}$) are set as function of temperature to response for cooling or heating after the shut-in (46 to 47). All fluids invoke Bousinesq's approximations (e.g. Holzbecher, 1998; Rabinowitz et al., 1999; O'Sullivan, 2010; Pasquale et al., 2011; Lipsey et al., 2016):

$$\rho_{w,wh} = \rho_0.\left[1 - \beta_{vw}.\left(T_{wh,t} - 25\right)\right]$$
$$\text{where}: \beta_{vw} = 1.6.10^{-5} + \left(9.6.10^{-6}.T_{wh,t}\right) \quad (46)$$

$$c_{w,wh} = \frac{4245 - \left[1.841.\left(T_{wh,t} + 273.15\right)\right]}{\rho_{w,wh}}.10^{-3} \quad (47)$$

3.4.2 Boundary conditions: parameter "a" – reservoir production

The entire solution of reservoir prediction meets sparse exploration grid density, i.e. 3 geothermal wells per 33.6 km^2 of a total delineated area of the system. An obligatory objection is, thus, consideration of Mid Triassic carbonates as a solid (although fairly dissected) homogeneous body. Selection of effective *reservoir area for production* A_a is set to respect an energy balance in definition of parameter "a", providing desired energy exploitation to the total energy stored in a reservoir (see -24). So that A_a = 33.6 km^2.

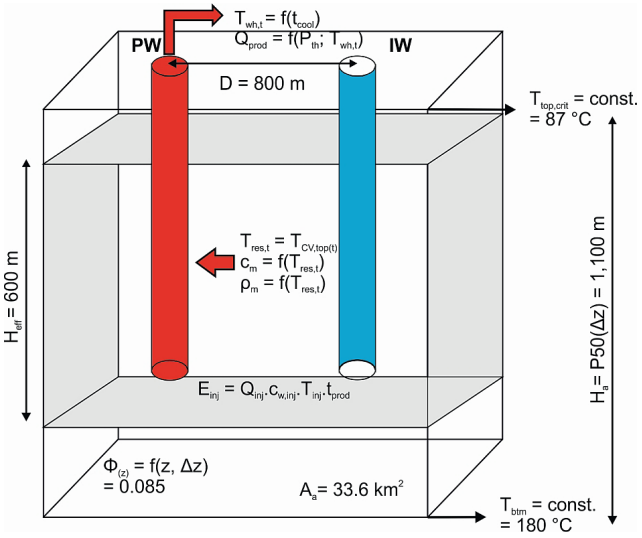

Fig. 3.6. *A simple conceptual model depict of ALPM production "parameter a" component.*

Definition of *effective reservoir thickness for production* H_a is based on Monte Carlo simulation of system's geometry used for sustainable thermal energy potential (Fričovský et al., 2019). At given CDF of total reservoir thickness, the H_a represents its 50th-percentile, i.e. $H_a = P50(\Delta z)$ = 1,100 m, as representative value at still tolerable level of confidence (Fig. 3.6).

The *effective reservoir volume available for production* V_a is function of A_a and H_a, so that $V_a = A_a.H_a$ of matrix associating saturated single phase reservoir fluid – geothermal brine. The fluid and the matrix contribute on total *specific heat capacity of the reservoir,* $\gamma_{a,a}$, generally described as (48):

$$\gamma_a = \left(1 - \phi_{(z)}\right).\rho_m.c_m + \phi_{(z)}.\rho_w.c_w \quad (48)$$

3.4.3 Boundary conditions: parameter "g" – reinjection

3.4.3.1 Geometry

According to a model (Fig. 3.4 and 3.5) the reinjection is set at the periphery of a single tank. Instead of considering the entire system, pressure drop in a reservoir defines a primary flow path towards the production zone. A cylindrical flow is assumed, turning cone-shaped towards producers (Fig. 3.7). As long as the distance is D = 800 m, the *effective distance of propagation* D_g equals the boundary distance, i.e. $D_g = D$ = 800 m. Unlike to previous case, *effective propagation thickness* H_g can not be described through a total reservoir thickness, as either effective porosity and permeability decreases with depth, i.e. $\Phi_{(z)} = f(z)$.

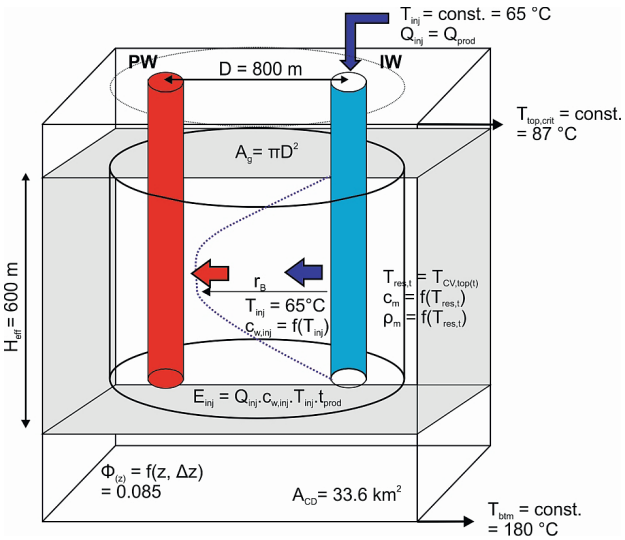

Fig. 3.7. *A simple conceptual model depict of ALPM reinjection "parameter g" component.*

Thus, a minimum thickness of Mid Triassic carbonates available to transmit the cold front is found at CDF (Fig. 3.7), at corresponding rate of probability, i.e. $H_a = P90(\Delta z)$ = 600 m. According to a flow geometry the *effective volume for reinjection* $V_g = \pi.D_g^2.H_g$ = 1.2 .10^9 m^3 of reservoir available for advective cooling or thermal exchange between stored and reinjected fluid that is of an impact on overall mean reservoir temperature $T_{res,t}$.

3.4.3.2 Reinjection rate

According to a fixed pressure conditions in reservoir under exploitation given by a tank model we consider the reinjection rate equal to that of production, i.e. $Q_{prod} = Q_{inj}$.

Then, both, the production and reinjection are given by energy balance under designed modeled scenario (45). Onset of cooling within production zone means, thus, increase in yieldrates ($Q_{prod,t}$) necessary to balance for loss of temperature to maintain desired thermal output (P_{th} = const.).

3.4.4 Boundary conditions: parameter "g'" – heat flux

The heat flux increment "g'" parameter stands for thermal gradient formation and destruction derived flow of energy available to correct for cooling during production or to enhance recovery after shut-in.

The DDHS is a conduction dominated CD2 play-type, i.e. conduction-dominated, orogenic belt type (Moeck, 2014). Indices do, however, exist on insulated convection cells formation restrained in extention to individual tectonic blocks (Fričovský et al., 2018a,b,c). Although of minor effect on a deep geothermal field distribution, consideration of their increment on heat flux due to cooling-induced gradient is, though, obligatory as long as all heat flow endmembers are invoked (40).

3.4.4.1 Conduction

Because of conductive environment, the stationary geothermal model has been constructed according to Fourier's equations (49) on heat conduction (Haenel et al., 1988) per individual stratigraphic layer, i.e. for Sarmatian, Badenian, Karpatian, and Mid Triassic carbonates. Because of insufficient spatial data available, grid refinement led to recalculation of a bulk thermal conductivity λ_B (50) based on temperature-related approximation for fluid λ_w (51) and depth-derived matrix λ_m conductivity (52) combining cubic mixing model (Sclater & Christie, 1980) with global porosity model for carbonates and siliciclastic lithofacies (Baldwin & Buttler, 1985). A reference thermal conductivity λ_{ref} for (52) is set as a mean of available data from GTD-1 and GTD-3 per each strata. A same procedure has been applied to yield distribution of radiogenic heat production Q_{RG} modifying (53) when using surface heat measurements ($Q_{RG(z=0)}$) in the Western Carpathians (Lizoň & Jančí, 1979).

$$T_{i+1} = T_i + \left(\frac{q_i.\Delta z_i}{\lambda_B}\right) - \left(\frac{Q_{RG,i}}{2\lambda_i}.\Delta z_i^{\,2}\right) \tag{49}$$

$$\lambda_B = \left\{\left[\left(1-\phi_{(z)}\right).\sqrt{\lambda_m}\right] + \left(\phi_{(z)}.\sqrt{\lambda_w}\right)\right\}^2 \tag{50}$$

$$\lambda_w = -922.47 + \left[2{,}839.8\left(\frac{T}{273.15}\right)\right] - \left[1{,}800.7\left(\frac{T}{273.15}\right)^2\right] + \left[527.77\left(\frac{T}{273.15}\right)^3\right] - \left[73.44\left(\frac{T}{273.15}\right)^4\right] \tag{51}$$

$$\lambda_m = \lambda_{ref} + 0.2.\left[\left(\frac{z_i}{1{,}000}\right) + \left(0.5\frac{\Delta z_i}{1{,}000}\right)\right] \tag{52}$$

$$Q_{RG,i} = Q_{RG(z)}.e^{-\frac{z_i}{D_{(RG)}}} \text{ where } D_{(RG)} = \frac{z - z_0}{\ln\left(\frac{Q_{RG(z=0)}}{Q_{RG(z=i)}}\right)} \tag{53}$$

At steady-state a stable conductive heat flux (54 – Haenel et al., 1988) within reservoir is a function of thermal gradient between reservoir base T_{btm} and reservoir top T_{top} temperature over a block thickness H_{CD} = P50(Δz) = 1,100 m (Fig. 3.8). In 1TIQ, the T_{btm} = const. = 180 °C, however, T_{top} modifies to $T_{top,crit}$ once production zone is subjected to cooling. Due to energy balance, thermal conductivity is assumed to realize across the entire system, so that A_{CD} = 33.6 km^2:

$$E_{CD} = A_{CD}.\lambda_B.\left(\frac{T_{btm} - T_{top}}{H_{CD}}\right) \tag{54}$$

Temperature at a top of a reservoir is function of time as borehole measurements already proven inflow from Karpatian basal clastics, so that effect of reinjection on recharge from a top can not be neglected. The reservoir top temperature is calculated using undisturbed environment (Axelsson et al., 1995) function (55). Hence $Q_{prod} = Q_{inj}$ = 1:1 according to fixed pressure boundary condition, a ratio of total over effective profile thickness is substituted (56):

$$T_{top} = T_{top,(t=0)} - \frac{Q_{inj}}{Q_{prod}}.\left(T_{res} - T_{res,t}\right) \tag{55}$$

$$T_{top} = T_{top,(t=0)} - \frac{\mathrm{P90}(\Delta z)}{\mathrm{P50}(\Delta z)}.\left(T_{res} - T_{res,t}\right) \Big| \begin{matrix} T_{top} = T_{top(t=0)} = 87°C \\ T_{top} = T_{top,crit} \end{matrix} \tag{56}$$

At a steady state, the T_{top} = 87 °C as a minimum reservoir top temperature according to a stationary geothermal model (Fričovský et al., 2018a). Solving for critical reservoir top temperature (57) means setting a boundary condition a temperature can not decay beyond at maximum rate of cooling, turning $T_{top} \in (T_{top(t=0)}; T_{top,crit})$. Further on, we assume conductive environment between reservoir top and top of the effective heat exchange profile. A vertical observation distance, i.e. a zone where cooling becomes negligible (Bjornsson et al., 1994; Axelsson, 2012b) is $L_{(z)}$ = 0.5ΔH where ΔH = P50(Δz) – P90(Δz) = (1,100-600)/2 = 250 m:

$$T_{top,crit} = T_{top,(t=0)} - \left(T_{top,(t=0)} - T_{inj}\right).\left\{1 - erf\left[\frac{\zeta_{CD} + L_{(z)}}{2.\sqrt{\frac{\lambda_m}{\rho_m.c_m}.t}}\right]\right\} \Big| \begin{matrix} T_{top,crit} = T_{top,(t=0)} = 87°C \\ T_{top,crit} = T_{inj} = 65°C \end{matrix}$$

$$\text{where}: \zeta_{CD} = \frac{2\lambda_B}{Q_{inj}.\rho_{w,inj}}.A_g \; ; \; A_g = \pi.D^2 \tag{57}$$

Provided setup allows conduction to increase in time as long as cooling realizes in profile of effective thermal exchange during production and reinjection, as well as to decay with progressive recovery. Hence thermal gradient is balanced to top of a reservoir, where temperatures can nod drop below reinjection temperature and neither they can recover above initial conditions, conduction appears fixed within reasonable interval.

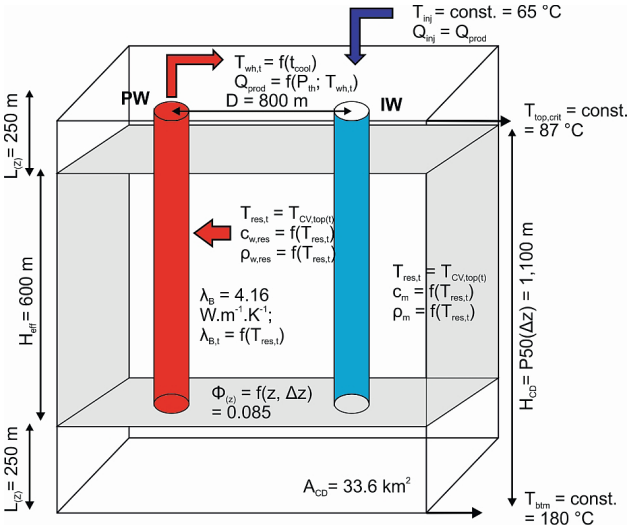

Fig. 3.8. *Depict of conceptual model for conductive heat flux increment to ALPM.*

3.4.4.2 Convection

Unlike conduction, convective heat increment into a profile of effective heat exchange due to reinjection remains questionable. Numerical indices calculated for horizontal (Fričovský et al., 2018b) and inclined (Fričovský et al., 2018c) homogeneous porous media did imply existence of 2 separate cells in deepest parts of produced block that can be of some contribution. Other studies, such as use of geochemical mixing models (e.g. Fournier et al., 1974; Fournier & Potter, 1982), solute (e.g. Fournier & Potter, 1978, 1979; Giggenbach, 1988) or multicomponent (e.g. Neupane et al., 2014; Spycher et al., 2014; Peiffer et al., 2014) geothermometry, able to track plausible convection through re- or un- equilibration of macrocomponents, solutes or mineral phases (e.g. Fričovský et al., 2016) haven't yer been conducted to prove or disprove the idea of vertical reservoir heat and mass flux through convection.

Disturbances to conductive environment (58) were studied for total reservoir area where actual Rayleigh number Ra exceeded that critical (Rac) corrected by a model unit cell inclination (φ = 2 – 52 ° increasing in SW-NE direction) and overheat ratio τ (Fričovský et al., 2018b). The (58) was solved for z = 0 at a top of the zone and z = H_{CV} towards the base, with boundary conditions given by magnitude of convective gradient $0 < \Gamma_{CV} < 2\Gamma_{CD}$ and zone thickness $H_{CV} > H_{CV,crit}$ calculated using (59) (Sheldon et al., 2011). Positive Rayleigh number anomaly in horizontal and vertical direction has been substituted as plausible convection zone width L_{CV}, oriented in W-E direction to follow general trend of thermal field distribution anisotropy (Fig. 3.9):

(58)

$$\frac{dT}{dz} = \frac{T_{i+1} - T_i}{H_{CV}} \cdot \left\{ \begin{array}{l} 4\pi 2\sqrt{\frac{Ra - Rac}{Ra} \cdot \left[\cos\left(\pi \frac{z}{H_{CV}}\right)\right]} \\ \cdot \left[\cos\left(\frac{L_{CV}}{H_{CV}}\right)\right] - 1 \end{array} \right\} \Bigg| \begin{array}{l} z = 0 \\ z = H_{CV} \end{array}$$

$$H_{CV,crit} = \frac{\frac{38.71 e^{-4.176\tau}}{\cos\varphi} \cdot \nu_D \cdot \lambda_m}{g_G \cdot K_m \cdot \rho_{w,CV} \cdot c_{w,CV} \cdot \beta_{vw} \cdot (T_{i+1} - T_i)} \qquad (59)$$

The linear stability analysis (e.g. Kassoy & Zebib, 1975; Garg & Kassoy, 1981) yields Ra = 42-117 within a block where Ra > Rac (Fričovský et al., 2018b,c). Solving for (59), temperature at a base of convective zone is given by $T_{CV,base}$ = 175 °C as a mean. Because towards the base the reservoir is expected undisturbed, $T_{CV,base}$ = const.

After (59), the representative convection zone height is H_{CV} = 270 m. As $H_{CV} > 0.5\Delta H$, where ΔH = P50(Δz) – P90(Δz) = (1,100-600)/2 = 250 m (distance between effective heat exchange profile and simulated reservoir base depth), temperature at a top of convection zone must vary in time (35), so that $T_{CV,top} = T_{res}$ and $T_{CV,top,t} = T_{res,t}$ (Fig. 3.10).

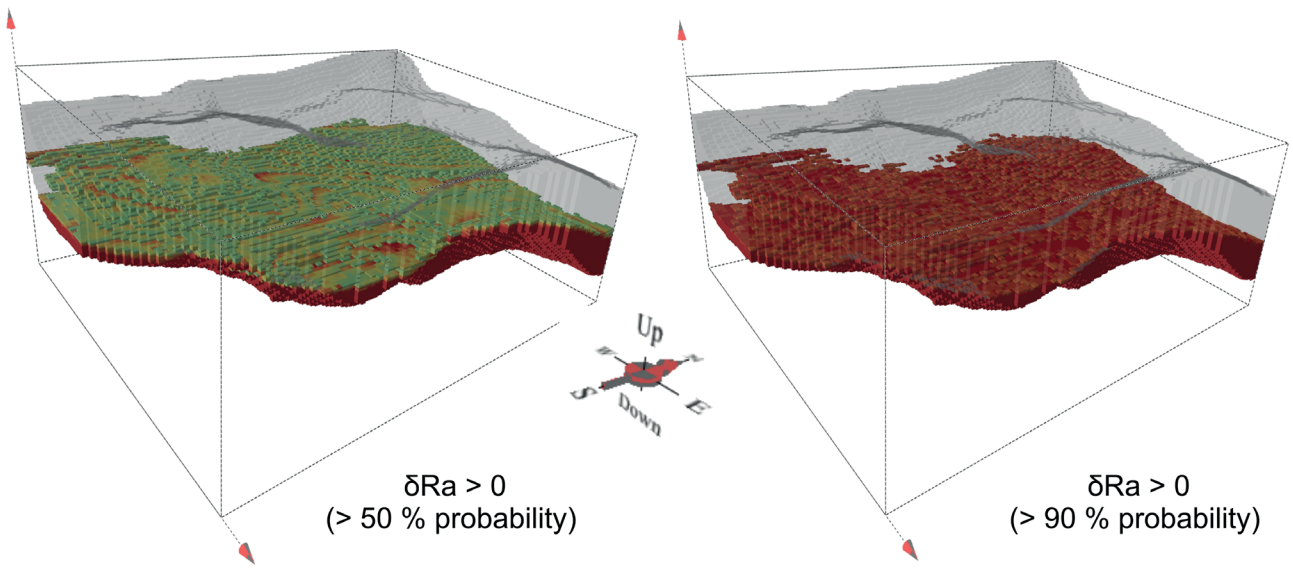

Fig. 3.9. *Conditioned Turning-bands simulation of δRa = Ra - Rac > 0 distribution in reservoir environment, indicating plausible zone for convection development.*

The whole model uses a constant permeability of $K_m = 9.912 .10^{-15}$ m^2 (Vranovská et al., 1999b) as fixed constant, because data from depths below those targeted by wells are not available yet. Obviously, new drillings may generate more inputs into the model. Again, most of parameters are set as function of temperature at a base of convection cell. Dynamic fluid viscosity ν_D (60) has been approached using model by Lipsey et al. (2016):

$$\nu_D = 2.4141.10^{-5}.10^{\frac{247.8}{\left[\left(T_{CV,btm}+273.15\right)-140\right]}} \quad (60)$$

Finally, the convective heat increment (Haenel et al., 1988) to the effective profile is governed by (61) for which influenced area is $A_{CV} = 8.1$ km^2 equal to extension of the block, geothermal parameters are set function of reservoir temperature $T_{res,t}$ and vertical fluid filtration velocity ν_z is given by a difference between viscous and buoyant forces along a convective profile (62 – Lippsey et al., 2016):

$$E_{CV} = A_{CV}.\phi_{(z)}.\rho_{w,res}.c_{w,res}.\nu_z.\left(T_{CV,btm} - T_{res,t}\right) \quad (61)$$

$$\nu_z = \frac{\nu_D.H_{CV}.\lambda_m}{\phi_{(z)}.\rho_{w,res}.c_{w,res}.H} \quad (62)$$

Fixing E_{CV} controls a rate of heat increment according to change in initial conditions, as the gradient forms between fixed convection zone bottom and dynamic convection zone top temperature. Thus, heat increment can not exceed a rate given by predicted change in reservoir environment, either considering cooling or recovery.

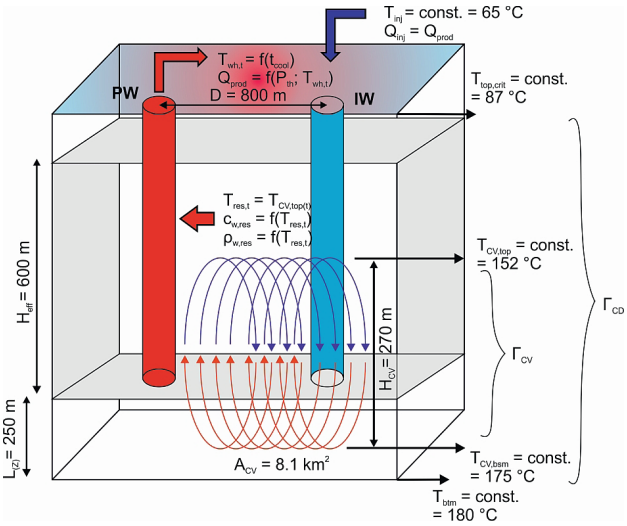

Fig. 3.10. *Simplified conceptual model of convective heat flux increment in ALPM parameter g'.*

3.4.4.3 Radiogenic heat generation

Both, the convection and conduction are controlled by thermal gradient (54 and 62). The radiogenic heat generation is, however, of a minor heat contribution, but kept constant in time, as at low temperatures, the rate of heat generated is independent on temperature (Čermák et al., 1991). Another difference to the convection and conduction is a fact that the radiation generates, not only transfers a heat. As such, the heat generated is later on transported conductively.

Equation (53) defines unit heat generated in steady environment. The $Q_{RG(z)}$ that stands for energy produced through radioactive isotope decay at representative depth can, however, be approximated as long as concentration of isotopes is known (63 – Čermák et al., 1991):

$$Q_{RG(z)} = \rho_{m(z)}.\left[\left(9.7.10^{-5}C_U\right)+\left(2.63.10-9C_{Th}\right)+\left(3.57.10-9C_K\right)\right] \quad (63)$$

(Unless concentrations can be found in literature (e.g. Lizoň & Jančí, 1979), the formulation reflects distribution of heat generation with depth. Area of interest where generation applies is limited to $A_{RG} = 16.3$ km^2 that corresponds to thermal field anomaly at a site, because of consequent heat diffusivity. For thickness H_{RG} we select the entire modeled thickness at corresponding probability for the block, i.e. $H_{RG} = P50(\Delta z) = 1{,}100$ m. Straight forward is then calculation of constant heat increment E_{RG} (64) into the profile of effective heat exchange during production and recovery (Haenel et al., 1988):

$$E_{RG} = Q_{RG,i}.H_{RG}.A_{RG} \quad (64)$$

3.4.5 Reservoir state conditions

3.4.5.1 Steady state and pseudo-steady state

Distinguishing the steady- and pseudo-steady- state in 1TIQ/1TER ALPM algorithm is secured through a cold-front diameter r_B spatial extension (Fig. 3.11), that is practically a function of Q_{inj} ($Q_{inj} = Q_{prod}$) and t_{prod}, as long as T_{inj} = const. = 65 °C, so that $c_{w,inj}$ = const. (43).

The *steady state* is given at $t_{prod} = 0$, i.e. where $Q_{prod} = Q_{inj} = 0$ kg.s^{-1}, representing a time prior launching reservoir production and reinjection, assuming in ALMP equal time of turn-on. The *pseudo-steady state* (PSS) represents a reservoir state off any cooling at any distance from reinjection site ($t_{cool} = 0$). Essentially, $t_{prod} < t_B$ is a general description. For an instance, the pseudo-steady state for production zone (D = 800 m) can be rewritten as $r_B < D$ or $r_B < 800$ m. Although there is no breakthrough towards production zone, $t_{cool} = 0$ for D = 800, it is not a case for parts of the system closer to the reinjectors, where cooling ($t_{cool} \neq 0$) is controlled by $r_B \geq D$ according to (43).

Reservoir temperatures prior breakthrough equal initial conditions, thus for $t_{cool} = 0$ $T_{wh,t} = T_{wh} = 135$ °C, $T_{res,t} = T_{res} = 152$ °C (Fig. 3) and $T_{top,crit} = T_{top} = 87$ °C (Fig. 8). Then, each parameter X that is a function of temperature (see the section with critical input data tables) is defined through $X = f(T_{(t=0)})$. If there is no thermal breakthrough yielded in 1TIQ, the 1TER model is set off, as no recovery is needed.

Distribution of conductive and convective heat increment and distribution in a reservoir equals the initial state during PSS as at distance D that meets $D > r_B$ there is no thermal gradient induction. Considering a system as CD2 play-type (Moeck, 2014; Fričovský et al., 2018a, 2019), a ratio of convective Γ_{CV} to conductive gradient Γ_{CD} (65)

yields $\Delta\Gamma_{CV}/\Gamma_{CD} = 0.4$, that characterizes a stable, diffuse reservoir conditions where (if any) convection occurs at natural conditions according to linear stability analysis. As long as radiogenic heat production is independent on temperature variation, it remains constant, not related to any changes in a reservoir state:

$$\Gamma_{CV} / \Gamma_{CD} = \frac{\left[\frac{\left(T_{CV,btm} - T_{CV,top}\right)}{H_{CV}}\right]}{\left[\frac{\left(T_{CD,btm} - T_{CD,top}\right)}{H_{CD}}\right]} = \frac{\left[\frac{\left(T_{CV,btm} - T_{res}\right)}{H_{CV}}\right]}{\left[\frac{\left(T_{btm} - T_{top}\right)}{P50(\Delta z)}\right]} \quad (65)$$

3.4.5.2 Transient state

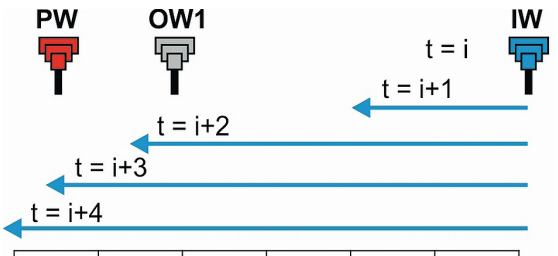

point	t= i	t= i+1	t= i+2	t=i+3	t=i+4
IW	SS	TRS	TRS	TRS	TRS
OW	SS	PSS	TRS	TRS	TRS
PW	SS	PSS	PSS	TRS	TRS

Explanations: ***IW*** - injector, ***OW*** - observation well, ***PW*** - production well, ***SS*** - steady state, ***PSS*** - pseudo-steady state, ***TRS*** - transient state

Fig. 3.11. *Schematic time-domain visualization on variation in reservoir states during pre-production and field exploitation related to a distance D.*

The transient state replaces the pseudo-steady state as long as a cold front propagates at a distance D from a reinjector described as $D \leq r_B$ and $t_B < t_{prod}$ (Fig. 3.11). A breakthrough initiates instant cooling, so that $t_{cool} \neq 0$, turning PSS conditions invalid. For 1TIQ model, decay of a mean reservoir temperature Tres starts immediately according to (35), i.e. $T_{res,t} \neq T_{res}$. Hence wellhead temperature $T_{wh,t}$ is function of $T_{res,t}$, the $T_{wh,t} \neq T_{wh}$. Securing energy and mass balance according to (35) requires a progressive increase in withdrawals Q_{prod}, i.e. $Q_{prod} = f(P_{th})$, so that $Q_{prod} = f(T_{res,t})$ to maintain constant thermal output. Because $Q_{prod} = Q_{inj}$, the rate of injection increases simultaneously, i.e. $Q_{inj,t} > Q_{inj}$.

A period of cooling is easily determined as $t_{cool} \epsilon < t_B$; $t_{si} >$, i.e. $t_{cool} = t_{si} - t_B$, i.e. for $t_{prod} = 100$ yrs a cooling stage is $t_{cool} = 100 - t_B$. When a critical cooling rate is introduced (some discussion is below), set in 1TIQ model as a shut-in according to $t_{si} = t_{Twh,t(crit)}$ where $T_{wh,t(crit)} = 0.9T_{wh} = 122$ °C, the $t_{cool} = 100 - t_B$ as long as $T_{wh,t} > T_{wh,t(crit)}$, otherwise $t_{cool} = t_{si} - t_B$ as a shut is expected prior end of desired period of production if wellhead temperature intercepts the set boundary condition. Unlike an instant decrease in mean reservoir and wellhead temperature, temperature at a top of the reservoir transits from T_{top} to $T_{top,crit}$ considerably slower, following (56 to 57). A lag in the transition is given by $L_{(Z)}$, as there is some thermal diffusion of cooling accounted between reservoir top and an upper boundary of effective thermal exchange profile, i.e. $L_{(z)} = 250$ m. Temperature at a base of the reservoir T_{btm} is not submitted to any change in a model, expecting a rapid decay of cooling effect from the effective heat-exchange profile.

Both, 1TIQ and 1TER ALPMs are constructed and upscaled as unisothermal. Thus, reservoir (res) and wellhead (wh) geothermal properties become a function of decay in temperature, so that for each parameter X that relates to a dynamic change in temperature, the general formula to describe such a link becomes $X = f(T_{(t\neq0)})$, following e.g. (46) or (47). Yet reinjection properties (inj) do not change during transition between PSS and transient state as $T_{inj} = \text{const.} = 65$ °C.

As long as $T_{res,t} = T_{CV,top(t)}$ causes a convective gradient to increase (65) proportionally to a cooling rate. The 1TIQ solution expects, thus, initiation of induced convection extending in a height H_{CV} (59) and a relative heat increment (66), so that $\Gamma_{CV}/\Gamma_{CD} \neq 0.4$:

$$Q_{CV} = A_{CV}.H_{CV}.\phi.\rho_{w,res(t)}.c_{w,res(t)}.\nu_{(z)}.\left(T_{CV,btm} - T_{res,t}\right) \quad (66)$$

Unlike $T_{res,t}$, trend in $T_{top,crit}$ is of much lower magnitude, i.e. conductive heat flux Q_{CD} (67) increases inproportionally (65) to the Q_{CV}, because of a lag in expected time of cooling temperature at a top of a reservoir ($T_{top,crit} = T_{top,CD}$):

$$Q_{CD} = A_{CD}.\lambda_B.\left(\frac{T_{btm} - T_{top,crit(t)}}{H_{CD}}\right) \quad (67)$$

The Γ_{CV}/Γ_{CD} allows to assess a relative rate of a change in reservoir geothermal field unstationarity due to cooling. After Sheldon et a. (2011) the convection occurs at $0 < 2\Gamma_{CD}$ that is an exact case of situation at DDHS. Yet considering stability of convective energy and mass flux, we consider a ratio $\Gamma_{CV}/\Gamma_{CD} \leq 0.5$ an indice on quiet, normal-gradient driven convection, not compromising conduction-dominated environment. Then, for $\Gamma_{CV}/\Gamma_{CD} = 0.5 - 1$ the induced convection gains proportion, yet a field may still be considered conduction dominated. Increase in the gradient ratio to $\Gamma_{CV}/\Gamma_{CD} = 1 - 1.5$ is considered a sign of convective reservoir conditions prevailing over conduction, where convection cells conserve their phase and symmetry stability. However, for $\Gamma_{CV}/\Gamma_{CD} = 1.5 - 2.0$ the ALPM classifies a reservoir environment as convective, yet with destruction of cells' symmetry, while we assume that at $\Gamma_{CV}/\Gamma_{CD} > 2$ a convection is self-destroyed through massive cooling of the cell. Provided stability analysis give accent to assess impact of production not only geothermal field, but stationarity of a system that controls consequent reservoir heat and mass processes, such is modification of brine chemistry or equilibration, playing a role in evaluation of corrosion or scaling.

3.4.5.3 Critical cooling rate

The 1TIQ ALPM starts at $t_{prod} = 0$ (steady state). At any time between $t_{prod} = 0$ and $t_{prod} = t_{si}$, the PSS controls reservoir response as described above. For theoretical considerations

it is possible to fix the 1TIQ solution for $T_{wh,t} \rightarrow \lim T_{inj}$, $T_{top,crit} \rightarrow \lim T_{inj}$ and $T_{res,t} \rightarrow \lim T_{inj}$. However, as long as difference in wellhead ($T_{wh,t} - T_{inj}$) or mean reservoir ($T_{res,t} - T_{inj}$) is zero, there is no gradient accessible, turning $Q_{prod,t} \rightarrow \lim\infty$ to balance production capacity demands (45), that makes such fixation unrealistic. Moreover, intense cooling often leads to more or (rather) less reversible changes in reservoir conditions and environment, taking excessive time to recover just after production stops. It is, obviously, because of multiple technical and reservoir engineering issues.

Instead, we accredit a compromise between reservoir sustainability, renewability of a resource and economical feasibility for a theoretical field operator, following a tolerable (critical) cooling rate in 1TIQ model. This has already been in multiple guidebooks and "best practices" (Tester et al., 2006; Sutter et al., 2011; Fox et al., 2013; Williams, 2007, 2014). A tolerated cooling rate is set for $T_{wh,t(crit)} = 0.9T_{wh}$, i.e. a production stops at $t_{si} = t_{Twh,t(crit)}$. Because $T_{wh} = 135$ °C, the $T_{wh,t(crit)} = 122$ °C, so each scenario in 1TIQ model is ran until $T_{wh,t} \geq T_{wh,t(crit)} = 122$ °C. Thus, if $T_{wh,t} < 122$ °C at $t_{prod} < 100$ yrs, production is shut-in ahead of desired period ($t_{si} = t_{Twh,t(crit)}$) of production, not considering such a scenario sustainable. Otherwise $t_{si} = t_{prod}$ for scenarios of $T_{wh,t} \geq 122$ °C at $t_{prod} = 100$ yrs. For both cases, reaching the t_{si} gives $Q_{prod} = Q_{inj} = 0$ kg.s^{-1} and the 1TER model for temperature and energy recovery starts instantly.

3.4.5.4 Thermal recovery

The 1tank energy-recovery model starts at t_{si}, turning Q_{prod} and Q_{inj} instantly to zero, because of no natural recharge to the reservoir system. While for 1TIQ the steady-state is described through reservoir parameters at initial-state, initial conditions for 1TER model correspond to a situation of a transient-state at t_{si}. For each parameter X that is a function of temperature there is, thus, a clear definition $X = f(T_{t(si)})$, no matter on whether the $T_{t(si)}$ stands for a state at $t_{si} = t_{prod} = 100$ yrs or $t_{si} \leq 100$ yrs.

The time of shut-in is, however, crucial in setting a period a system is evaluated for reclamation. As renewability of a resource is defined as ability of a system to gain or approach initial conditions at time of comparable to that it was utilized (e.g. Rybach & Mongillo, 2006), a time the 1TER runs reclamation predicting equals the time of production, i.e. $t_{reco} = t_{si}$. This allows then evaluation of its renewability, i.e. to mark a scenario as of renewable approach to the resource as long as $t_{reco} \leq t_{si}$ with positive renewable capacity ($\Delta t_{reco} = t_{prod} - t_{si} \geq 0$) or non-renewable for $t_{reco} > t_{si}$ with negative renewable capacity ($\Delta t_{reco} < 0$). Obviously, the longer is the production, the longer is a time accessible for recovery, yet maximum time corresponds to a desired period of production, i.e. $t_{prod} = 100$ yrs according to a sustainable reservoir management concept.

With no natural hot-water recharge into system ($Q_{rech} = 0$ kg.s^{-1}) the 1TER model accounts natural heat increment from a basis of the system. During the reclamation, temperature recovers according to $T_{wh,r} \epsilon < T_{wh,t} = T_{wh,t(si)}$; $T_{wh} = T_{wh(t=0)} >$ and $T_{res,r} \epsilon < T_{res,t} = T_{res,t(si)}$; $T_{res} = T_{res(t=0)} >$ and $T_{top,r} \epsilon < T_{top,crit}$; $T_{top} = T_{top(t=0)} >$. Fixing $T_{wh,r} \leq T_{wh}$, $T_{res,r} \leq T_{res}$ and $T_{top,r} \leq T_{top}$ restrains disruptions in energy and mass balance in the system, not exceeding initial settings. During reclamation, every parameter that is a function of temperature follows $X = f(T_{reco})$.

A progressive recovery erases, however, an induced convective or conductive gradient generated previously through cooling in 1TIQ model. Keeping $T_{CV,btm}$ and T_{btm} constant, increase in $T_{CV,top} = T_{res,r}$ and $T_{CD,top} = T_{top,r}$ reduces temperature difference (65), causing a heat increment to fall towards initial conditions. Simultaneously, $\Gamma_{CV}/\Gamma_{CD} \rightarrow \lim 0.4$ with t_{reco}. Obviously, for scenarios where $T_{top,r} = T_{top}$ and $T_{res,r} = T_{res}$ at $t_{reco} = t_{si}$, restoration of initial conduction-dominated environment with natural (plausible) convection may occur, depending on a rate of convection / conduction ratio.

3.5 Scenario selection approach

3.5.1 Review on geothermal reserves booking and constant production strategies selection

3.5.1.1 USGS volume method

The USGS volume (or stored-heat) method (Muffler & Cataldi, 1978) became one of most utilized in geothermal resource assessment as not requiring field production data and history matching (Sanyal, 2007), at least in early stages of evaluation process. The method counts the total thermal energy stored in the reservoir H_T (68) be it a sum of heat stored in the rock H_R and reservoir fluid H_W (Grant, 2014; Garg & Combs, 2015) as a function of reservoir heat capacity γ_a; herein a single-phase saturated geothermal water in Mid Triassic carbonates in hydraulic connection to the Karpatian basal conglomerates (Vranovská et al., 1999, 2002):

$$H_T = H_M + H_W = \gamma_a . V . \left(T_{res} - T_{inj} \right)$$

where (68)

$$\gamma_a = \rho \bar{c}_w + \rho \bar{c}_m = \phi . \rho_w . c_w + \left(1 - \phi\right) . \rho_m . c_m$$

The H_T acknowledges not only to a heat that is stored, but to the heat that is in a flow through the reservoir as well (Axelsson et al., 2005), i.e. the heat flux driven by a gradient between reservoir base and a top. A risk of misestimates on a scale of multiples to folds arises, if only "known" values are being substituted to Monte Carlo simulations (Grant, 2000, 2014) addressing booking the geothermal reserves (Sanyal & Sarmiento, 2005; Garg & Combs, 2015). Critical moment of a method is, however, definition of recoverable heat in place H_0 (69), i.e. a part of a heat reasonably exploitable (Doveri et al., 2010; Grant, 2014):

$$H_0 = R_0 . H_T \tag{69}$$

Obviously, the recovery factor R_0 is of essential impact on H_0 assessment. Instead of a standard method on R_0 estimate comparing energy produced at the wellhead over that accumulated in a reservoir (Garg & Combs, 2010, 2015; Williams, 2014; Takahashi & Yoshida, 2016) working with

fluid enthalpies (well applicable in assessment of potential for power production) a concept of production-based recovery efficiency has been used (Ungemach et al. 2005, 2007, 2009). This is exactly designed for doublet field operation. The production efficiency (η_{prod}) measures (70) energy produced ($Q_{prod}.\rho_{w,wh}.c_{w,wh}$) during a given period of time (t_{prod}) over energy stored in reservoir ($\gamma_a.A.\Delta z$). Then, accessible recovery R0 is derived through a gradient to production (T_{inj}) and reservoir (T_s) conditions (71):

$$\eta_{prod} = \frac{Q_{prod}}{A.\Delta z}.\frac{\rho_{w,wh}.c_{w,wh}}{\gamma_a}.t_{prod} \tag{70}$$

$$R_0 = \eta_{prod}.\frac{T_{res} - T_{inj}}{T_{res} - T_s} \tag{71}$$

3.5.1.2 Geothermal reserves booking

A concept of geothermal reserves booking – GRB (Sanyal & Sarmiento, 2005) is based on probabilistic Monte Carlo simulation – MCS (Rubinstein & Kroese, 1991), involving 5,000 iterations prior obtaining inverse distribution function (IDF) for H_0 (69) through 10,000 iterations of H_T. For R_0, the MCS yields $R_0 = 0.053$ from IDF curve, representing a median of $P90(R_0)$ to $P50(R_0)$ interval, obviously being more conservative estimate than using arbitrary set constants, i.e. $R_0 = 0.1$ (Fendek et al., 2005) or $R_0 = 0.075$ (Vranovská et al., 1999a). MCS simulation of H_T (68) yielded an IDF function converted to H_0 using (69). Booking (Fig. 3.12) is then based on following determinations (Sanyal & Sarmiento, 2005; Garg & Combs, 2015):

- geothermal resources: $RS_T = [P10(H_T) – P10(H_0) / t_{prod}]$
- inferred reserves: $R_{inf} = [P10(H_0) – M(H_0) / t_{prod}]$ if $M(H_0) < P50(H_0)$
- inferred reserves: $R_{inf} = [P10(H_0) – P50(H_0) / t_{prod}]$ if $M(H_0) > P50(H_0)$
- probable reserves: $R_{pb} = [M(H_0) – P90(H_0) / t_{prod}]$ if $M(H_0) < P50(H_0)$
- probable reserves: $R_{pb} = [P50(H_0) – P90(H_0) / t_{prod}]$ if $M(H_0) > P50(H_0)$
- proven reserves: $R_{pv} = (P90(H_0) / t_{prod})$

Note the booking based on probabilistic simulation using IDF through percentiles and mode well reflects certainty levels in definition of McKelvey's scheme (for reading we refer to: Muffler – Cataldi, 1978; Clotworthy et al., 2006; Williams et al., 2011; Falcone et al., 2013; Falcone & Beardsmore, 2015; Sarmiento et al., 2013). Introduction of a period for balancing the reservoir available energy content, i.e. $t_{prod} = 100$ yrs, the booking counts:

- geothermal resources: $RS_T = 3{,}015$ MWth
- geothermal reserves: $RE_T = 180$ MWth
- inferred reserves: $R_{inf} = 83$ MWth
- probable reserves: $R_{pb} = 60$ MWth
- proven reserves: $R_{pv} = 37$ MWth

3.5.1.3 Reserve capacity ratio

The reserve capacity ratio approach is based on a balance evaluation between accessible energy stored in the reservoir and energy removed through desired or installed capacity, be it thermal output in conditions of the DDHS. In its origin (Bjarnadottir, 2010), the method accounts on a reserve capacity (R_{cap}) defining differences between a part of energy expected and the one that has already been proven. Then, the reserve capacity ratio (72) assesses a proportion between energy left in the reservoir and that assumed to be accumulated:

$$r_{cap} = \frac{R_{cap}}{R_{pb}} = \frac{R_{pb} - R_{pv}}{R_{pb}} \tag{72}$$

In her work Bjarnadottir (2010) developed 5-level scheme to evaluate sustainability of Icelandic geothermal fields operation as given by an energy balance. The scheme

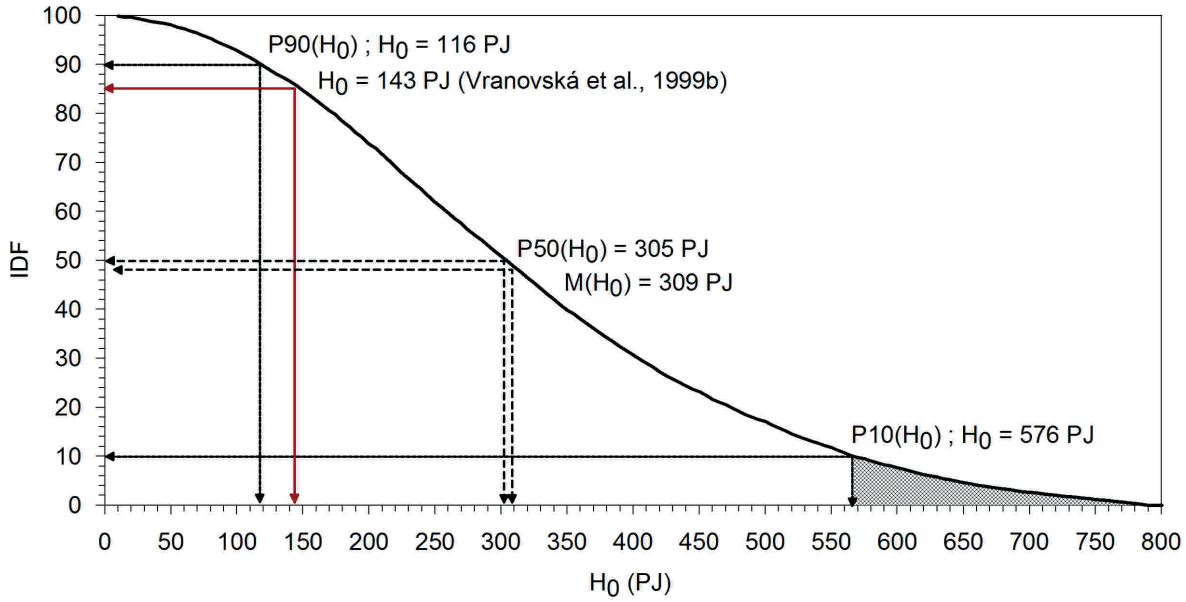

Fig. 3.12. *Review on geothermal reserves booking scheme for the DDHS.*

has been modified (Fričovský et al., 2019) to delineate 4-levels only. The $r_{cap} > 0.5$ describes a field which at least same portion of energy that is removed is still stored in the reservoir, moreover, for $r_{cap} > 0.75$, production capacity or longevity may be extended up to doubling.

3.5.1.4 Definition of sustainable levels of production

A detailed study on reserve capacity ratio analysis is provided in paper of Fričovský et al. (2019). Note this is an energy-balanced approach suitable for tentative reservoir analysis, where insufficient production and monitoring data restrain more precise estimates. However, a strong advantage of the method is its applicability at a scale (e.g. Fričovský et al., 2020b).

The results obtained combining reserve capacity ratio analysis with the USGS method give (Fig. 3.13):

- a maximum thermal output that correspondents to a sustainable level when balanced for $t_{prod} = 100$ yrs is $P_{th(0.5)} = 49$ MWth corresponding to $r_{cap} = 0.5$, equal to $H_0 = 154$ PJ at P85(H_0) confidence level (Fig. 3.12)
- a thermal output opting for doubling the production or prolonging a period of production up to by two when balanced for $t_{prod} = 100$ yrs is $P_{th(0.75)}$ at $r_{cap} = 0.75$ level
- each production higher than $P_{th} = 49$ MWth compromises, thus, an energy balance in within a system and so with longevity of a production

cases where $t_{si} \geq t_{prod} = 100$ yrs because of $t_B \geq t_{prod}$ ($t_{cool} = 0$), the 1TER model does not apply, as there is no cooling. If scenarios are described according to $t_B < t_{prod}$ ($t_{cool} \neq 0$) but $T_{wh,t} \geq T_{wh,t(crit)} = 122$ °C, recovery starts at $t_{si} = 100$ yrs, as the critical cooling rate boundary condition has not been reached in 1TIQ model. Otherwise, the module simulates shut-in at production zone at $t_{prod} = t_{si} < 100$ yrs.

3.5.2 Review on potential-based resource classification and stepwise scenario selection

Unlike the USGS volume method, evaluation of reservoir according to a thermal potential stored in rock, exploitable at certain technical limits is less presented, with some studies already conducted in Australia (Williams et al., 2010; Beardsmore et al., 2010) or Canada (Deibert et al., 2010). The scheme has been proposed as being more familiar to field operators and investors through identified categories rather than referring to a geological probability (Beardsmore et al., 2010, Falcone & Beardsmore, 2015).

A worldwide praxis has shown that stepwise field operation has many advantages if compared to produce at constant withdrawal or output. The essential amongst is minimizing a risk of an unexpected resource deterioration as stepwise development provides the operator with time to conduct a long-term monitoring during early stages of production and assess possibilities of reservoir response when opting to increase the rate (Stefansson & Axelsson, 2005; Bromley et al., 2006). It may, thus, contribute slightly

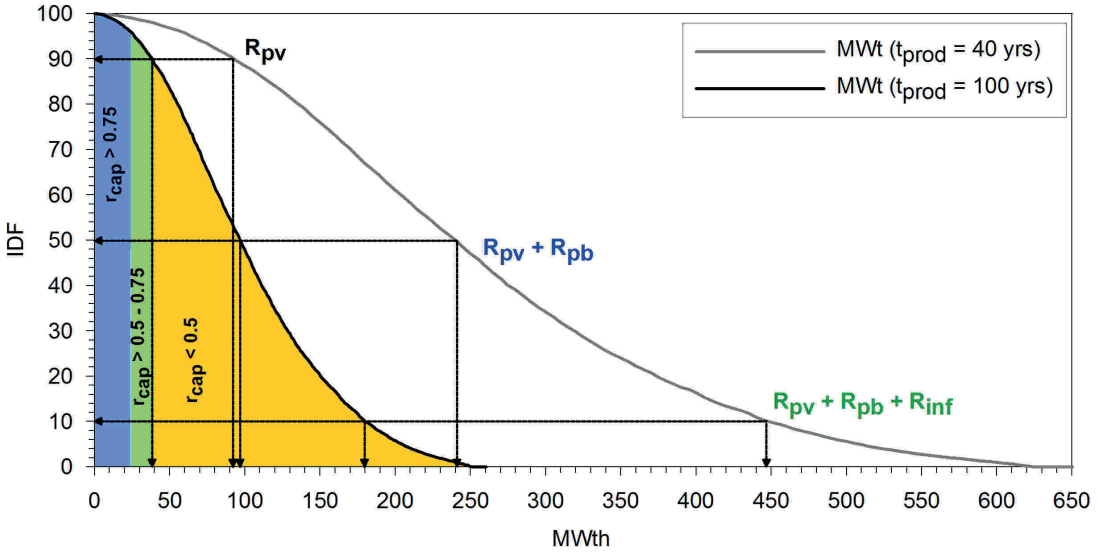

Fig. 3.13. *Review on geothermal reserves booking scheme for the DDHS.*

3.5.1.5 Constant production scenarios considerations

ALPMs application aims to analyze reservoir response on production through breakthrough and induced cooling after cold-front propagation to the production zone. A wide range of scenarios, i.e. $P_{th} = 1 – 240$ is selected to cover plausible changes in reservoir thermal conditions and heat flow dynamics, explaining importance of sustainable production. Constant thermal output strategies (P_{th} = const.) are expected to maintain desired P_{th} during $t_{prod} = 100$ yrs, and to switch between 1TIQ and 1TER model at t_{si}. For more to what stands beyond a principle of sustainable geothermal energy production.

To compare effects of stepwise and constant production on reservoir, a model of sustainable P_S and developable P_D potential assessment has been applied in following.

3.5.2.1 Sustainable and developable potential assessment

A *theoretical potential* P_M (73) accounts energy stored in a reservoir up to a 10 km depth and available for given longevity of extraction under certain geothermal

settings, considering thermal efficiency η_{th} when used either for power production or heat exchange (Falcone & Beardsmore, 2015):

$$P_M = \frac{A.\Delta z.\gamma_a.\Delta T_{res}.\eta_{th}}{t_{prod}} \quad (73)$$
$$\text{where}: \Delta T_{res} = T_{res} - T_{ref} \text{ and } T_{ref} = T_s + T_{inj}$$

As long as thermal efficiency of heat conversion or exchange is not known, the cycle efficiency η_{th} (74) is approached as function of a critical temperature T_c between a reference and definition point (DiPippo, 2007):

$$\eta_{th} = 5.2.10^{-4} T_c + 0.032$$
$$\text{where } T_c = \frac{T_{res} + T_{ref}}{2} = \frac{T_{res} + (T_{inj} + T_s)}{2} \quad (74)$$

A *technical potential* P_T (75) gives energy up to 6.5 km available for extraction with current or predictable technology in no far than 30 years (Beardsmore et al., 2010). To yield, a theoretical potential is corrected according to tolerable reservoir cooling rate (R_{TD}; set to 10 % to initial conditions), recoverability ($R_0 = 0.053$) and resource accessibility R_a; the latter defined as a ratio of area with no limits on development to the entire area of a system, including any urban or natural restrains (Agemar et al., 2012):

$$P_T = P_M.R_0.R_a.R_{TD} \quad (75)$$

There is, however, no general guide on sustainable and developable thermal potential assessment and methods differ between national codes. Hereafter, analogue to a booking scheme (Sanyal & Sarmiento, 2005) has been adopted, with baseline provided by MCS obtained IDF of technical potential P_T.

The *sustainable potential* P_S represents part of P_T that can be produced and maintained during desired t_{prod} with minimizing risk of reservoir and energy production collapse (Rybach, 2015). Obviously, such category calls a high confidence level. As such, we approached the P_S to proven reserves determination in booking, i.e. $P_S = P90(P_T)$, obtaining robust certainty in an estimate. The *developable potential* P_D sums energy available for increase in production at sustainable conditions, i.e. available to develop the P_S more at a minimum risk on production longevity (Rybach, 2015).

Now let us assume the $P_S + P_D$ must not compromise the longevity (sustainability) of production. While probabilistic aspect of P_D definition can be solved through IDF construction for P_T (Fig. 3), the aspect of sustainability is somewhat approached through an entire concept beyond the reserve capacity ratio. Thus, $P_S + P_D \leq M(P_T)$, so that $P_S + P_D > P50(P_T)$. This secures a minimum acceptable risk of failure. Substitution of reserve capacity ratio concept gives the potential difference (analogue to R_{cap}) as $\Delta P_D = M(P_T) - P90(P_T)$ or $\Delta P_D = M(P_T) - P_S$. Now knowing that at least an equal part of potential is supposed to remain left in a reservoir to provide safe reserves for a future, the P_D is accessed through (76):

$$P_D = \frac{M(P_T) - P90(P_T)}{2} = \frac{\Delta P_D}{2} \quad (76)$$

Note that P_D is in its principle analogous to $P_{th(0.5)}$, i.e. to the maximum thermal output available in a reservoir at $r_{cap} = 0.5$ representing a critical capacity for sustainable production.

3.5.2.2 Stepwise production scenarios considerations

Inverse distribution function of P_T (Fig. 3.14) yields: $P90(P_T) = 43$ MWth that corresponds to definition of sustainable potential P_S. Although $M(P_T) > P50(P_T)$, striking IDF curve's skewness to the left conditions use of median $M(P_T)$ instead of $P50(P_T)$ not to underestimate further computations. The $M(P_T) = 101$ MWth. The potential difference is then $\Delta P_D = 101 - 43$ MWth and thus $\Delta P_D = 58$ MWth. As long as the same amount of potential must remain in a reservoir available as the one that can be

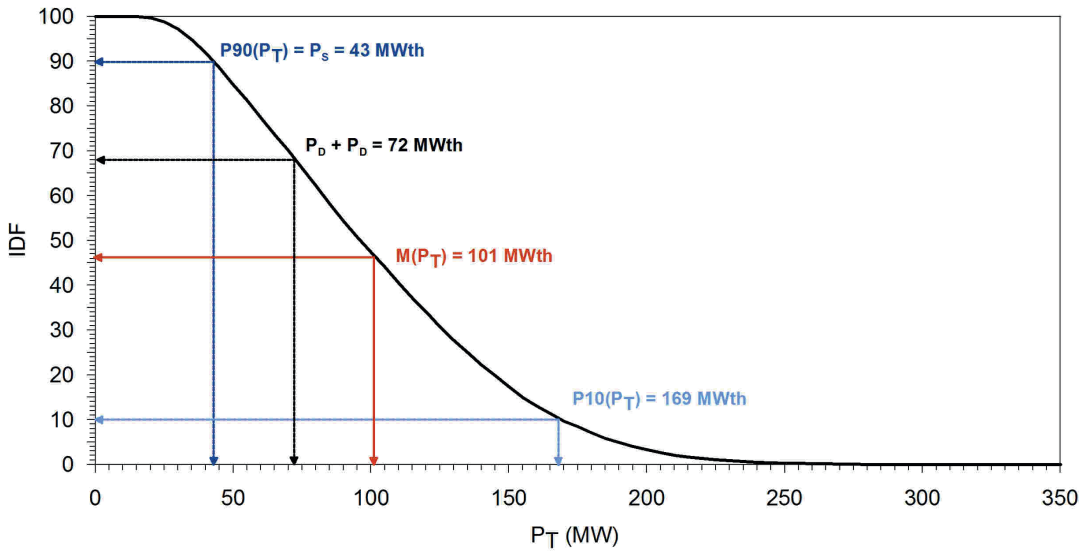

Fig. 3.14. *Technical potential IDF distribution with interpretation of PT, PS and PD.*

extracted more, the $P_D = 0.5\Delta P_D$, so that the developable potential is assessed for $P_D = 29$ MWth.

Definition of P_S and P_D expects a stepwise field development in its principle, opening a production at the P_S first. To demonstrate an interaction of such field development, we set:

- increase in production from P_S to $P_S + P_D$ at steps of $t_{prod,1}/t_{prod,2}$ = 70/30, 80/20 years
- decrease in production from $P_S + P_D$ to P_S at steps of $t_{prod,1}/t_{prod,2}$ = 20/80, 30/70 years

AS $P_S + P_D$ = 72 MWth, a comparison is run for case-studies to option operating a field at P_{th} = 72 MWth constantly.

3.6 Symbols and indexes for heads 3.3 to 3.5

3.6.1 Symbols

Symbol	Unit	Explanation
a	-	production parameter in 1TIQ / 1TER model
A	m^2	area
c	$J.kg^{-1}.K^{-1}$	specific thermal capacity
C	$J.kg^{-1}.K^{-1}$	thermal capacity
C_U, C_{TH}, C_K	$kg.kg^{-1}$	radioactive isotopes concentration
D	m	Horizontal distance between producer / reinjector
$D_{(RG)}$	-	radiogenic heat capacity depth distribution function
E	J, W	energy
$E_{TH(122)}$	TWh,th	cumulative production of GTE at $T_{wh,t}$ = 122 °C
g	-	reinjection parameter in 1TIQ / 1TER model
g’	-	heat influx parameter in 1TIQ / 1TER model
g_G	$m.s^{-2}$	gravity acceleration
H	m	height, thickness
H	J	heat
K_m	m^2	critical permeability for conductive flow onset
$L_{(Z)}$	m	observation vertical distance
m^*	$kg.s^{-1}$, $m^3.s^{-1}$	mass flow rate
M	kg, m^3	total (reservoir fluid) mass
p	Pa	pressure
P_D	MWth	developable potential
P_M	MWth	theoretical potential
P_S	MWth	sustainable potential
P_T	MWth	technical potential
P(X)	-	percentile
q	$W.m^{-2}$	heat flow density
Q	$kg.s^{-1}$	yieldrate, withdrawal, reinjection
r_B	m	cold-front appron, cold-front diameter
r_{cap}	-	reserve capacity ratio
R_0	-	coefficient of reduction (coefficient of recovery)
R_a	-	resource accessibility coefficient
R_{cap}	MWth	reserve capacity
R_{pb}	MWth	probable reserves
R_{pv}	MWth	proven reserves
R_{TD}	-	tolerated cooling rate coefficient
Ra	-	actual Rayleigh number
Rac	-	critical Rayleigh number
t	s, yrs	time
t_B	yrs	thermal breakthrough
T	°C	temperature

Symbol	Unit	Explanation
V	m^3	volume
x	-	net heat increment in 1TIQ / 1TER model
z	m	depth
Symbol	Unit	Explanation
z	m	depth
βvw	K^{-1}	coefficient of volumetric heat expansion
γ	$J.m^3.K^{-1}$	total heat capacity
Γ	-	gradient
Δz	m	thickness
ζ	-	conductive diffusion ratio
η	-	production efficiency
η_{th}	-	thermal (triangle) efficiency
κ	$kg.MPa^{-1}$	storage capacity
λ	$W.m^{-1}.K^{-1}$	thermal conductivity
Λ	-	coefficient of diffuse cooling retardation (heat exchange)
ν_D	$Pa.s^{-1}$	thermal viscosity
ν_z	$m.s^{-1}$	vertical filtration velocity
ρ	$kg.m^{-3}$	specific density
τ	-	overheat ratio
φ	°	angle of inclination
Φ	-	porosity
ψ	$kg.MPa^{-1}.s^{-1}$	productivity index

3.6.2 Indexes

Index	Explanation
0	reference conditions
a	aquifer, reservoir
B	bulk
c	current (energy and/or mass in reservoir)
cool	cooling
crit	critical
CD	(related to) conduction
CV	(related to) convection
eff	effective
i	i-th (observed) layer
i+1	top-wall layer
ini	initial
inj	reinjection
IN	(energy) influx
m	matrix, rock
M	reservoir matrix
n	renewable
net	net mass and/or volume
OUT	(energy, mass) losses
prod	production
PROD	energy produced, withdrawn
rech	natural recharge
ref	reference

Index	Explanation
reco	recovery
res	reservoir
RG	(related to) radiogenic heat production
si	shut-in
S	surface, ambient
t	(with) time
T	total
th	thermal
top	reservoir top, convection cell top
w	water (reservoir fluid)
wh	wellhead
W	geothermal fluid
(z)	(related to) depth

3.7 Results – production scenarios

3.7.1 Thermal breakthrough

The thermal breakthrough (t_B) accounts for a time the reinjected fluid at considerably lower temperature as is that of the reservoir environment arrives to the producer, instantly launching cooling of the effective zone; theoretically up to a moment at which the fluid and geothermal reservoir reach thermal equilibrium.

We used an advective model with a diffuse retardation to assess velocity of breakthrough propagation, as this yields a time at which 1TIQ applies. Setting $Q_{prod} = Q_{inj}$ = 1:1, for a given reservoir geometry (H_{eff} = 600 m, D = 800 m), production parameters ($Q_{prod} = f(P_{th})$; $\rho_{w,inj}$ $c_{w,inj} = f(T_{inj})$; $\gamma_a = f(T_{res}, \Phi)$ and designed period of a fluid withdrawal / reinjection (t_{prod} = 100 years), the model assumes yieldrates at $Q_{prod} \leq 158$ kg.s^{-1} safe of breakthrough (Fig. 3.15). Assuming mean annual wellhead temperature T_{wh} = 135 °C and T_{inj} = 65 °C, the rate corresponds to P_{th} = 38 MWth. Introducing conservative error of estimation at a scale of +/- 1/10t_{prod} = 100 +/- 10 years, the recommended opening production rate would rather not exceed Q_{prod} = 140 – 158 kg.s^{-1} (P_{th} = 36 – 38 MWth) to mitigate breakthrough. Then, the plot demonstrates some cooling even for P_{th} = 49 MWth (critical sustainable production capacity according to r_{cap} analysis), hence t_{cool} = 100 – 79 = 21 years. Obviously, cooling rate controlled through $Q_{inj}.c_{w,inj}.t_{prod}$ (where $c_{w,inj} = f(T_{inj})$ = const.) increases with demand on production ($Q_{prod} = Q_{inj}$), progressively taking over an effect of diffuse retardation along effective heat exchange profile within reservoir. Some caution must, however, be paid for $P_{th} = R_{pv}$ = 37 MWth ($Q_{prod} = Q_{inj}$ = 147 kg.s^{-1}) too, as t_B = 103 years in the model. Although $t_B > t_{prod}$, i.e. cooling is expected after production terminates, the calculated t_B is still within a set error of estimate, thus, left to account on uncertainties.

Reinjection temperature reduction to T_{inj} = 25 °C results in less withdrawal demand on wellhead due to building up a thermal gradient, so that critical production for cold-front propagation increases for Q_{prod} = 154 kg.s^{-1} or P_{th} = 61 MWth. A same effect in increasing production capacity ahead of breakthrough is obtained shortening a desired period of production. For t_{prod} = 40 years the P_{th} = 90 MWth, Q_{prod} = 382 kg.s^{-1} even with T_{inj} = 65 °C. This is in somewhat match to TOUGH2 based model presented by e.g. Giese (1998, 1999), estimating accessible potential of P_{th} = 92 MWth at comparable time scale. Although probability of cooling prior shut-in may be considered low in absolute values, position of cold-front apron moves dramatically towards producers, calling to account on uncertainties too.

The breakthrough model is sensitive to variation in effective thickness of heat exchange profile (HEP), as long as D = const., $Q_{inj} = Q_{prod}$, $c_{w,inj}$, $\rho_{w,inj}$ are constant functions of return temperature, and γ_a is derived through T_{res} according to a mean reservoir temperature model. For H_{eff} = 800 m at P73(Δz), production of P_{th} = 51 MWth ($Q_{prod} = Q_{inj}$ = 205 kg.s^{-1}) would be still capable to restrain a breakthrough, with the potential increased to P_{th} = 64 MWth ($Q_{prod} = Q_{inj}$ = 205 kg.s^{-1}) if H_{eff} = 1000 m estimated as P54(Δz). Otherwise, for reduced thickness of H_{eff} = 400 m corresponding to P96(Δz) the capacity is assumed to drop to P_{th} = 26 MWth or $Q_{prod} = Q_{inj}$ = 105 kg.s^{-1}).

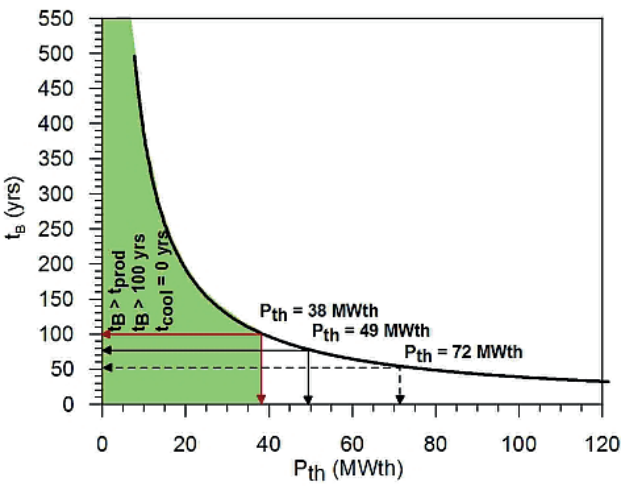

Fig.3.15. *Thermal breakthrough model: constant production summation curve.*

To demonstrate impact of production on breakthrough, we compared constant production of P_{th} = 72 MWth and a stepwise production development given by potential analysis, i.e. from P_S = 43 MWth to $P_S + P_D$ = 43 + 29 = 72 MWth (Fig. 3.14). The constant strategy yields t_B = 53 years (t_{cool} = 47 years). To reach $t_B \geq t_{prod}$ or $t_B \geq 100$ years, a model setup would require $H_{eff} > 1100$ m (P43(Δz)), or extension of a distance between producer and injector to D ≥ 1000 m.

Step-wise development as considered ($t_{prod,1}/t_{prod,2}$ = 70/30 and 80/20 years) from P_S to $P_S + P_D$ instantly prolongs a time of breakthrough, reducing, thus, time of production zone cooling. Although cold front arrives to producers at t_B < 100 yrs, the delay is long enough to perform relevant field monitoring and field developments to reduce risk of cooling (Fig. 3.16). Shortening t_{cool} limits, then, drop in mean reservoir and wellhead temperature in 1TIQ model, so that the scenario can be maintained in production for t_{prod} = 100 years, introducing the critical cooling rate as boundary condition for shut-in (see case study below).

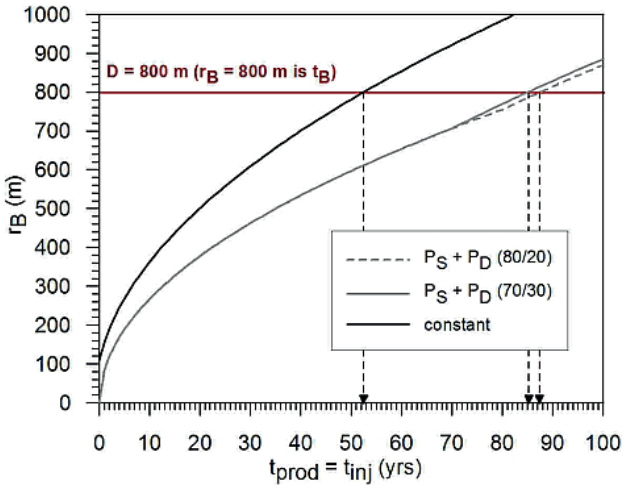

Fig. 3.16. Thermal breakthrough: comparison between constant and step-wise production strategies – visualization of cold-front apron propagation.

3.7.2 Reservoir response

At a time of cold-front arrival to producer(s), the cooling realizes during the t_{cool} period, changing reservoir and wellhead attributes instantly. This is when 1TIQ model of the entire ALPM module estimator applies, transiting from pseudo-steady state to transition state. Use of 1TIQ gives a hint on what production scale can be considered to at least open a production, keeping longevity of resource utilization in scope through mitigation of negative impacts on reservoir fluid and its energy balance.

3.7.2.1 Reservoir cooling

Reservoir cooling prediction is carried through application of 1-tank closed analytical pseudo lumped-parameter model with dynamic heat flux and reinjection (1TIQ). Although no history matching was applied, future upscaling for monitoring data is available as soon as their quality becomes sound, avoiding errors plausible at a recent state of their completion.

For each production option, the model starts at $t = t_{prod} = 0$. As long as $t_B > t_{prod}$, there is no cooling induced, so that $T_{res,t} = T_{res}$ and so it is for $T_{wh,t} = T_{wh}$ ($t_{cool} = 0$). After a cold-front arrival ($t_B < t_{prod}$), the cooling of production zone starts, so that $t_{cool} \neq 0$. Consequent change in $T_{res,t} \neq T_{res}$ and $T_{wh,t} \neq T_{wh}$ modifies reservoir parameters set as analytical functions of temperature, yielding non-isothermal reservoir response forecasting in a model. Drop in reservoir temperature inducing decay of temperature at a wellhead recalls consideration of constant production (P_{th} = const.) or withdrawal (Q_{prod} = const.) maintaining. The first management requires increase in Q_{prod} due to decline of thermal gradient at a wellhead, increasing the Q_{inj} at a same time ($Q_{prod} = Q_{inj}$), however, it also allows to maintain optimized thermal output up to a point where tolerable cooling boundary condition is reached, or the system is produced due to desired period of production. Hence reinjection equals the withdrawal, the cooling of production zone is expected intense and progressive. The latter management considers maintaining set Q_{prod} and thus the Q_{inj}, however, thermal output at the wellhead is reduced with drop in thermal output due to cooling, so field management and project strategies must opt for optimized output at terminal stages of production. Although this management usually leads to less intense cooling, it is rarely applied in praxis, and so is skipped in this paper.

The boundary condition of maximum allowed cooling at a wellhead by 10 % has been applied to all cases, i.e. for T_{wh} = 135 °C at $t = t_{prod} = 0$, the critical temperature was set to $T_{wh,t(crit)}$ = 122 °C. Then, for $T_{wh,t} < T_{wh,t(crit)}$ the production is supposed to shut-in (t_{si}), i.e. $t_{si} < t_{prod}$ and $t_{si} < 100$ yrs respectively. For scenarios of $T_{wh,t} \geq T_{wh,t(crit)}$ at $t_{prod} = 100$ yrs, the $t_{si} = t_{prod} = 100$ yrs, defining it sustainable.

Running the algorithm on a t_{prod} = 100 yrs scale, the critical capacity a system is capable to hold for a desired period of production is P_{th} = 51 MWth (t_{si} = 100 years), increasing the production / reinjection

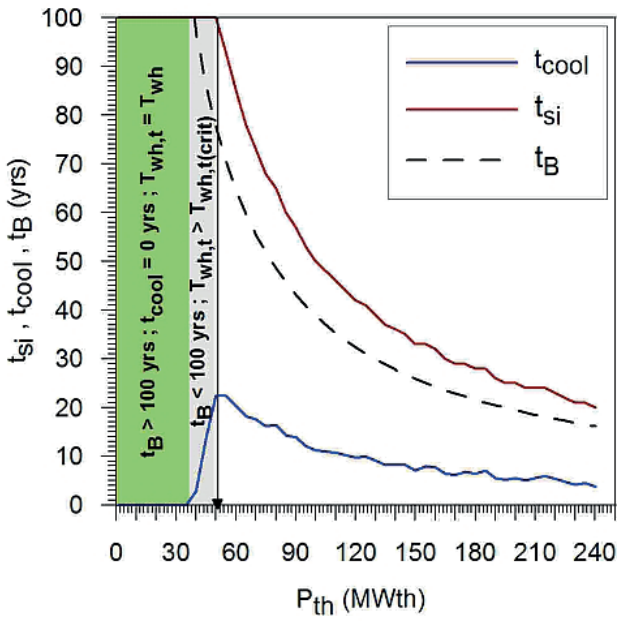

Fig. 3.17. Reservoir cooling prediction: shut-in (tsi) and cooling (tcool) variation.

rate from Q_{prod} = 214 kg.s^{-1} to Q_{prod} = 262 kg.s^{-1} at the end of production. However, because of an analytical character of a model in use, we rather recommend not to exceed the initial production of P_{th} = 49 MWth, i.e. Q_{prod} = 194 kg.s^{-1} (t_{prod} = 0) and Q_{prod} = 230 kg.s^{-1} at $t_{prod} = t_{si}$ = 100 yrs, prior gaining detailed monitoring data for model calibration (Fig. 3.17). This matches well to a sustainable capacity given by r_{cap} analysis, implying such production safe for opening (for further scenario analysis see case studies section in following). Figure 3.17 explains that with invoking the critical cooling boundary condition, the $t_{si} = t_{prod}$ = 100 yrs for P_{th} = 38 – 51 MWth ($T_{wh,t}$ at t_{prod} = 100 years is above 122 °C), increasing t_{cool} with shortening the t_B, hence $t_{cool} = t_{si} - t_B$. At higher production rates, the t_{si} falls along with t_{cool}, due to rapid cooling in production zone as thermal breakthrough shortens. The model expects, thus, that all production exceeding P_{th} = 51 MWth would cause drop in $T_{wh,t}$ far below 122 °C at t_{prod} = 100 yrs, turning such scenarios unsustainable.

Cooling of HEP changes not only T_{res}, but dispersively decays temperature at a top of the reservoir (Fig. 3.18), though the deviation is apparently less intense. Where t_B > 0 yrs and $t_{si} \geq$ 100 yrs, the $T_{top,crit}$ = 75 – 87 °C for constant production, as an effect of long-term, whatever weak in an impact, cooling. Unlike, for scenarios short in shut-in period, i.e. defined at $t_B < t_{prod}$ and t_{si} < 100 yrs, the $T_{top,crit}$ = 75 – 82 °C respectively, due to considerable shorter t_{cool}. Yet some heat flux from overburden to balance a loss in temperature can not be excluded in considerations.

Any drop in $T_{top,crit}$ generates conductive heat flux increment from a base of the reservoir, while decrease in $T_{res,t}$ triggers convection expected to occur between a reservoir base and effective heat exchange profile. According to (40), combination of both, along with radiogenic heat production (constant at given temperature conditions) poses effect of induced cooling retardation. Hence dispersed, it is not intense enough to mitigate and stop cooling itself at high production rates. Such non-linearity in thermal field explains, however, why modeled drop in t_{si} is not strictly proportional to increase in P_{th}.

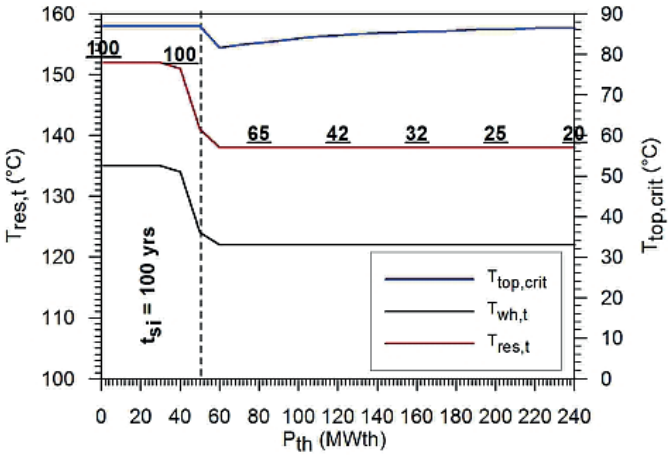

Fig. 3.18. *Thermal field ($T_{res,t}$; $T_{top,crit}$) and wellhead conditions ($T_{wh,t}$) at a shut-in (tsi; in underlined numbers)*

3.7.2.2 1TER lumped/analytical model: reservoir thermal recovery

For cases where t_B < 100 yrs, so that $t_{cool} \neq$ 0 yrs, the 1TER, i.e. one-tank closed energy recovery model) has been applied. The model accounts on reservoir dynamics, including variation in mean reservoir and reservoir top temperature in time that are of an effect on conductive and convective heat increment distribution as the system recovers from production. Unlike 1TIQ, the $Q_{prod} = Q_{inj}$ = 0 kg.s^{-1}, leaving a reservoir to recover due to a natural heat increment only. Distribution of conduction and convection in a reservoir ("tank") is not equal. While conduction is expected to cover entire reservoir body (see 3.4.4.1), convection controls thermal field in deepest parts of the system, limited to a profile between HEP and reservoir base (see 3.4.4.2). Then, while $T_{top,r}$ recovers due to conduction only, the $T_{res,r}$ recovery is accelerated through convection and conduction, involving constant heat increment from radiogenic heat production.

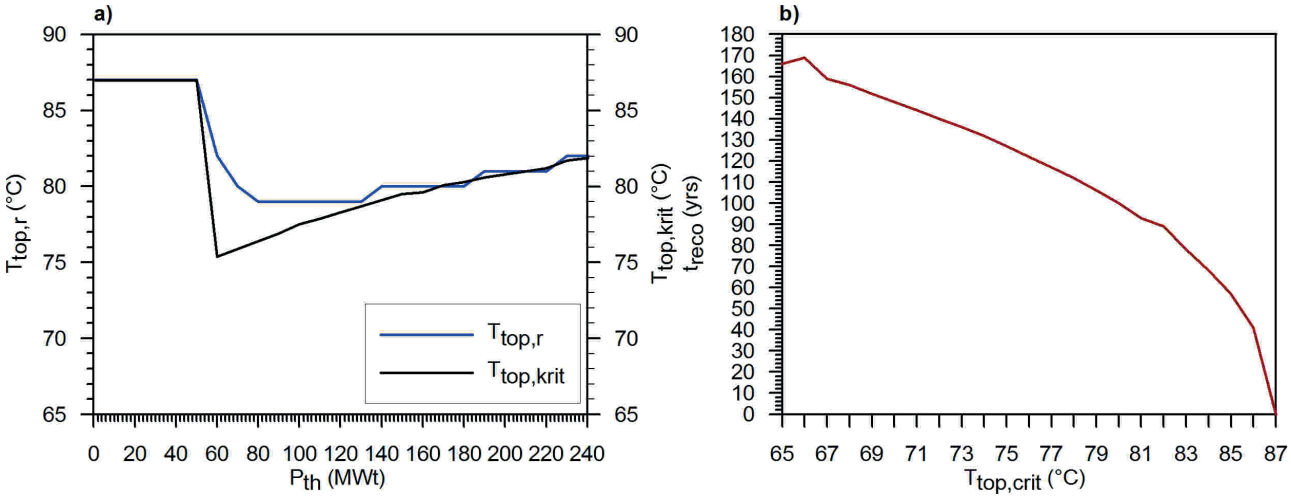

Fig. 3.19. *Reservoir top temperature ($T_{top,r}$) and recovery period (t_{reco}) for critical reservoir top temperature at variable rates (a) and $T_{top,crit}$ at t_{si} (b).*

We let the recovery to start at a time of shut-in, so that $t_{reco} = 0 = t_{si}$. Again, for scenarios where $t_B > 100$ yrs, the $t_{cool} = 0$, and so that $t_{reco} = 0$. For scenarios of $P_{th} < 51$ MWth, the breakthrough-caused cooling ($t_{cool} \neq 0$) generates a reclamation period of reservoir top temperature at $t_{reco} < 30$ yrs (Fig. 3.19). Obviously, 1TER implies a system is capable to recover initial (pseudo-initial) conditions, i.e. $t_{reco} \leq 100$ yrs as long as $T_{top,crit} \geq 80$ °C at t_{si}.

While recovery of temperature at a top of the reservoir is in control of diffuse heat transfer in the reservoir body, response of mean reservoir temperature gives an impact to both, convective heat increment and wellhead temperature. It is, thus, the reservoir temperature recovery that is used to trace renewability of a resource and somewhat renewability of a production prior a time of reclamation.

The 1TIQ model yields $T_{res,t} = T_{res} = 152$ °C for $P_{th} \leq 38$ MWth ($t_B \geq 100$ yrs, $t_{si} = 100$ yrs and $t_{cool} = 0$ yrs), so that no recovery is required ($t_{reco} = 0$). This is, however, related to production zone only. At reinjection site, the cooling starts at time of production / reinjection opening – analysis of reinjection zone is not included in this paper.

As long as production is between $P_{th} = 38 – 51$ MWth, the $t_B \leq 100$ yrs and $t_{cool} \neq 0$ yrs. Due to expected cooling, mean reservoir temperature declines, assumed $T_{res,t} = 138 – 152$ °C at t_{si}. Then, the 1TER model estimates a system as able to recover between $t_{reco} = 0 – 60$ yrs, depending on $T_{res,t}$. In turn, the $T_{res,r} = T_{res}$ at $t_{reco} \leq t_{si}$. With time required for mean reservoir temperature recovery assumed shorter than that of production, a renewable capacity ($\Delta t_{reco} = t_{si} – t_{reco}$) is positive (Fig. 3.20). A model predicts the $P_{th} = 51$ MWth as maximum capacity considered sustainable ($t_{si} \geq 100$ yrs) and renewable ($\Delta t_{reco} > 0$). This matches well to the 1TIQ model, increasing reliability of carried upscaling.

At production rates greater than $P_{th} = 51$ MWth, the recovery starts at $t_{si} \leq 100$ yrs. It does, however, shorten the time available for reclamation due to $t_{reco} \leq t_{si}$ criterion on a resource renewability. Hence $T_{res,t} = 138$ °C at a time of shut-in, the 1TER expects temperature to recover at $t_{reco} = 30 – 65$ yrs depending on rate of variation in $T_{top,crit}$. Setting $t_{reco} = t_{si}$ as a condition, the 1TER yields $T_{res,r} < T_{res}$, so estimating $\Delta t_{reco} < 0$ for production rates over 90 MWth. Thus, production at higher capacity than the critical can neither be considered sustainable ($t_{si} < 100$ yrs), nor of renewable impact on reservoir and a resource.

A relation between mean reservoir temperature recovery and a diffuse heat flux is depicted on Figure 3.21. The greater is a thermal gradient between reservoir base (constant $T_{btm} = 180$ °C) and reservoir top at production termination, the shorter is a period required for recovery. Obviously, the lower is $T_{top,crit}$, the longer it takes to recover, maintaining increased conductive gradient when compared to initial (steady-state) conditions. Now

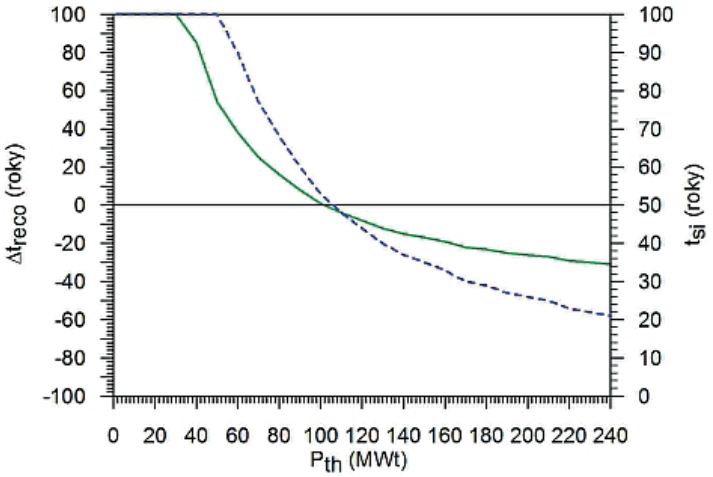

Fig. 3.20. Model solution on reservoir recovery and renewable capacity for $t_{reco} = t_{si}$. Green line: Δt_{reco}, blue line: t_{si}.

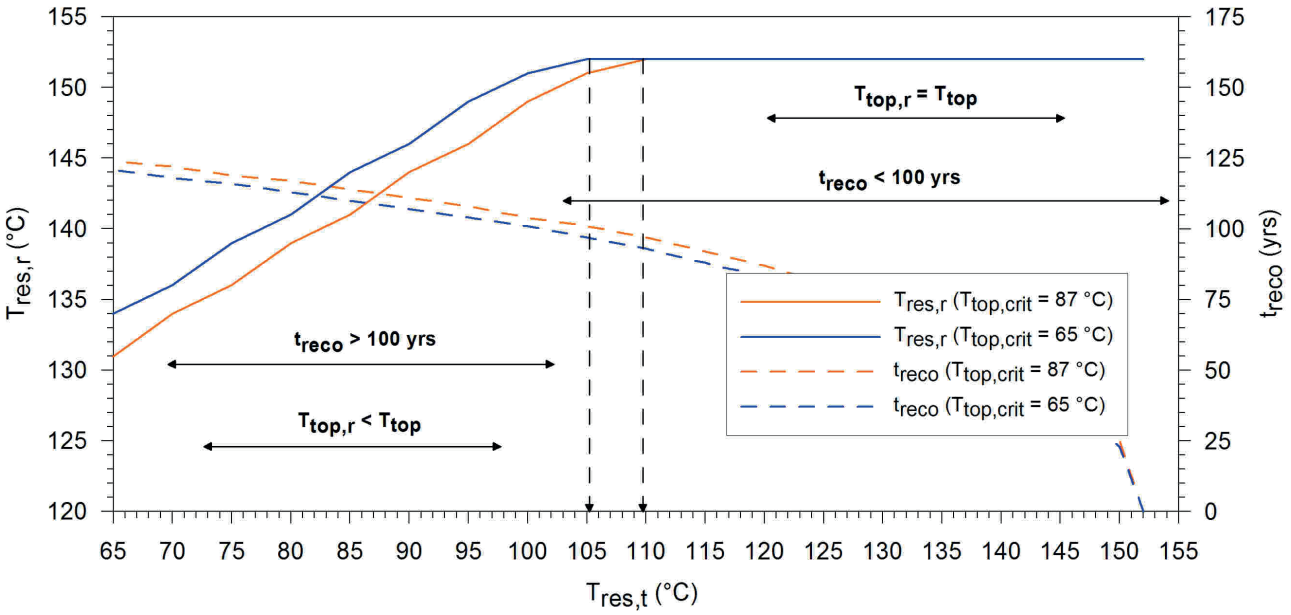

Fig. 3.21. Relation between mean reservoir temperature at t_{si} ($T_{res,t}$), at $t_{reco} = t_{si}$ ($T_{res,r}$) and critical reservoir top temperature ($T_{top,crit}$) at t_{si}.

consider a situation the production is maintained constant for t_{prod} = 100 yrs, though a critical cooling rate boundary condition is omitted in the model. This allows to extend available reclamation time for $t_{prod} = t_{si} = t_{reco}$ = 100 years. According to 1TER estimate, a system will not be able to recover to steady-state conditions ($T_{res,r} < T_{res}$) at t_{reco} = 100 years if $T_{res,t}$ < 105 °C at t_{si}, scoring negative renewable capacity for such a case.

3.7.3 Reservoir dynamics

An accent towards conductive play-type (Moeck, 2014; Fričovský et al., 2018a) is given in upscaling of the model for DDHS. Both, the 1TIQ and 1TER model assume dominant diffuse heat transfer between reservoir base and its top, driven by conductive gradient. So far, numerical indices analysis (Fričovský et al., 2018b, Vizi et al., 2020) propose creation of separate convection cells in deepest parts of reservoir, limited to tectonic blocks, owing to plausible upwelling and sink vectors along faults that dissect the Mid Triassic profile.

To account on different proportion of a diffuse and convective heat flux in a model, we introduced the relative conductive ($\Gamma_{CD} = (T_{btm}-T_{top,crit}) / H_{CD}$) and convective ($\Gamma_{CV} = (T_{btm}-T_{top,crit}) / H_{CV}$) gradients, equal to Γ_{CD} = 42.3 °C.km^{-1} and Γ_{CV} = 17 °C.km^{-1} respectively, i.e. Γ_{CV}/Γ_{CD} = 0.4 at initial conditions. Thus, while any change in mean reservoir temperature due to cooling gives an increment to convection ($T_{res} > T_{res,t}$) as $\Gamma_{CV,t} > \Gamma_{CV}$, drop in critical reservoir top temperature triggers conductive heat flux through a model, i.e. $T_{top,crit} < T_{top}$, so that $\Gamma_{CD,t} > \Gamma_{CD}$. However, results yielded by 1TIQ show clearly the $T_{res,t}$ is predicted to decline more rapidly than that at a top of a reservoir, driving a robust increase in Γ_{CV} when compared to Γ_{CD}.

In case $t_B > t_{prod}$, there is no cooling induced in production zone (D = 800 m) and the system remains in pseudo-steady state. This describes conduction-dominates system with quiet, stable convection due to a gradient within a cell, thermally equilibrated with a reservoir – in its deepest parts. Breakthrough expects induced convection to take part in response to reservoir cooling (Fig. 3.22) for P_{th} > 38 MWth. Generated convection is unlikely to extend vertically to cover entire reservoir profile, rather we assume a cell growth rate of a few to tens of meters. At this amplitude, convection phase and stability of geometry is likely maintained, not placing a rapid impact on reservoir geothermal fluid chemistry. Besides, there are dramatic changes expected in 1TIQ model close to reinjection zone – note presented in this paper. At D = 200 m ($T_{res,t}$ << 138 °C), the return may cool down a reservoir to a state at which convection prevails over conduction, stability of cells' geometry and its phase changes, gaining potential to cause major changes in reservoir fluid mobile phase and chemistry.

Reservoir recovery, including building up $T_{res,r}$ and $T_{top,r}$ after shut-in is definitely a progressive process lacking any linearity as long as heat fluxes are accounted in 1TER algorithm. Instead, when a $T_{res,r}$ and $T_{top,r}$ temperature rise, the gradient slowly ceases and so does recovery. However, the model for D = 800 m shows that a system is able to gain initial, diffusion-dominated conditions as long as a production is not greater than 90 MWth, consequent to combination of a reservoir state at time of shut-in, including $t_{si} = t_{prod}$ = 60 yrs. Though, scenarios considered sustainable and renewable ($P_{th} \leq$ 51 MWth) may recover initial state of heat flux endmembers. To compare, for D = 200 m simulating proximity to reinjector, the system will not recover initial conduction-dominated state for $P_{th} \geq$ 60 MWth, instead, convection at variable stability rate should be still expected. For production rates between at a range of P_{th} = 37 – 60 MWth, combination of diffuse environment with still induced convection should be taken into account while performing further reservoir analysis, especially reservoir chemistry.

3.8 Results – case studies

One reason of 1TIQ and 1TER model application was to study a maximum constant capacity a reservoir can hold for a desired t_{prod}, to meet criteria of sustainable production ($t_{si} = t_{Twh,t(crit)} \geq t_{prod}$ = 100 yrs), and renewable approach

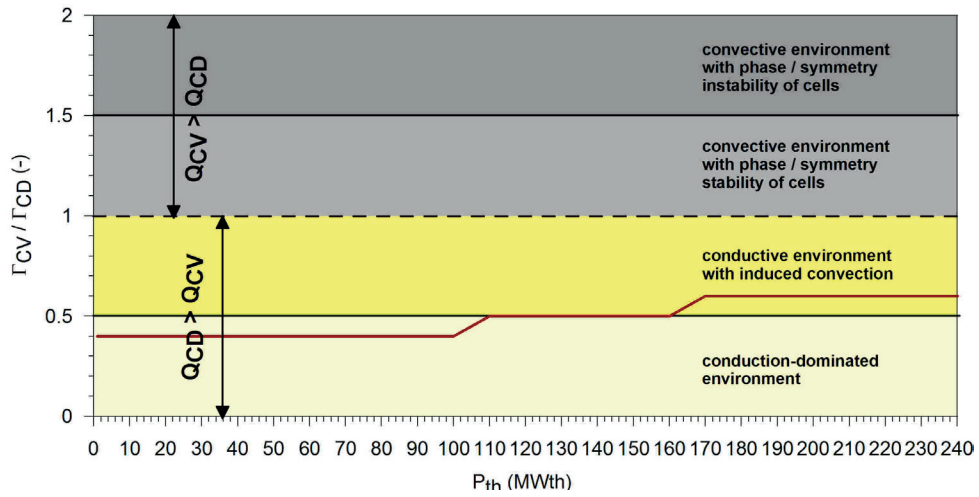

Fig. 3.22. *Reservoir state dynamics depiction as based on relative convective / conductive gradient at $t_{prod} = t_{si}$ and $t_{reco} = t_{si}$.*

($t_{reco} \leq t_{si}$ = 100 yrs) to the system. However, we used both models to test strategies obtained from reservoir energy balance studies, such is:

- derivation of maximum sustainable rate (P_{th} = 49 MWth) through reserve capacity ratio application (Bjarnadottir, 2010) to geothermal reserves booking scheme of the DDHS (Fričovský et al., 2019a)
- definition of sustainable (P_S) and developable (P_D) potential, i.e. P_S = 43 MWth, P_D = 29 MWth as based on potential-balance classification (e.g. Rybach, 2015).

The latter case has then been used to demonstrate a difference of reservoir response on stepwise and constant production.

3.8.1 Constant production scenario: P_{th} = 49 MWth

A given constant production rate represents a critical capacity a system is supposed to hold for desired production period (t_{prod} = 100 years) posing any compromise on reservoir sustainability (r_{cap} = 0.5). At such, it has also been proposed as an output recommended for production given by a reservoir response analysis (Fig. 3.17), accenting rather conservative approach due to unability to carry on a history matching for the model.

According to a thermal breakthrough model (Fig. 3.15), a cold front is assumed to propagate towards production zone at t_B = 79 yrs. For a t_{prod} = 100 yrs baseline, 1TIQ model applied a cooling period of t_{cool} = 21 yrs (by $t_{cool} = t_{prod} - t_B$) to predict changes in reservoir thermal settings because of a response to production.

After breakthrough at D = 800 m, the reservoir cools progressively in a model (Fig. 3.23). Expected drop of reservoir $T_{res,t}$ = 141 °C and wellhead $T_{wh,t}$ = 124 °C temperature implies, though, the capacity can constantly be maintained through the desired t_{prod}, as $T_{wh,t} > T_{wh,t(crit)}$, i.e. $t_{prod} = t_{si}$ = 100 yrs. Because of cooling, withdrawals are supposed to increase, i.e. Q_{prod} = 194 kg.s^{-1} at t_{prod} = 0 and Q_{prod} = 230 kg.s^{-1} at t_{si}. Drop in $T_{res,t}$ and $T_{top,crit}$ ($T_{top,crit}$ = 79 °C) stimulates Γ_{CV}/Γ_{CD} = 0.55 at t_{si}, changing a diffusion-dominant environment to a reservoir with induced convection. However, at D < 600 m, a system may experience rapid cooling ($T_{res,t} = T_{inj}$ = 65 °C), and consequent intense change in reservoir heat flow dynamics.

A 1TER model of thermal recovery after shut-in yields optimistic assumptions. Fixing $T_{res,t}$ = 141 °C at t_{si}, a system may be able to recover a mean reservoir temperature at t_{reco} = 53 yrs. As $t_{reco} < t_{si}$, the model yields positive renewable capacity ($\Delta t_{reco} = t_{si} - t_{reco} > 0$). Because both, the $T_{res,t}$ and $T_{top,r}$ approach initial conditions at D = 800 m, a system is expected to return into a conduction-dominated environment, with quiet, steady ("steady state" thermal gradient driven) convection.

3.8.2 Constant production scenario: P_{th} = 72 MWth

Although a total capacity of P_{th} = 72 MWth has been calculated as combining the sustainable and developable potential, i.e. P_S and P_D, expecting a stepwise approach in a principle, we add a constant output scenario model as comparative in presenting on how both strategies may differ on reservoir response.

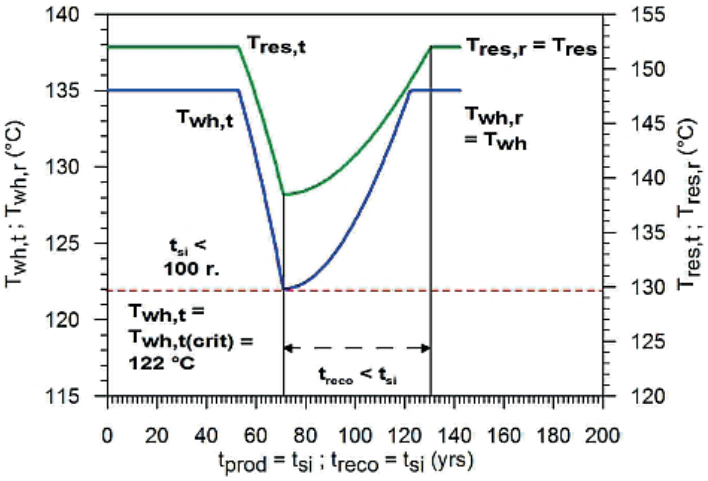

Fig. 3.24. Preview on 1TIQ / 1TER reservoir response model estimation for constant P_{th} = 72 MWth production strategy.

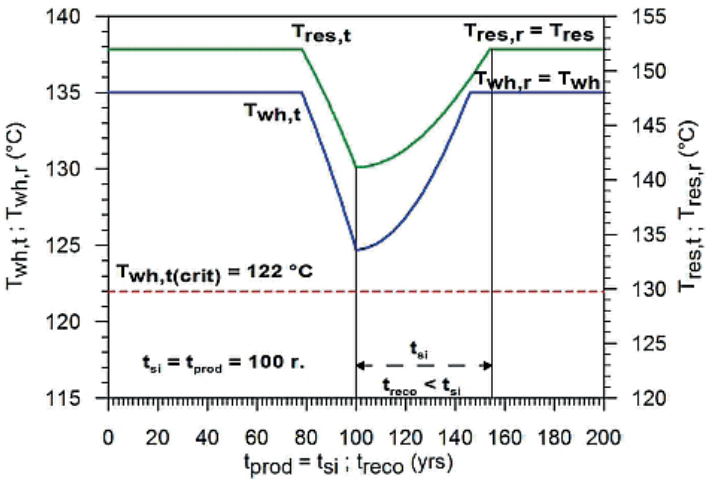

Fig. 3.23. Preview on 1TIQ / 1TER reservoir response model estimation for constant P_{th} = 49 MWth production strategy.

If the capacity is held constant since t_{prod} = 0, a breakthrough is expected to happen at around t_B = 53 yrs (Fig. 3.15). For t_{prod} = 100 yrs, a 1TIQ model cools, thus, a reservoir for t_{cool} = 47 yrs. However, the model predicts interception of $t_{si} = t_{Twh,t(crit)}$ at t_{si} = 71 yrs, where $T_{wh,t}$ = 122 °C and $T_{res,t}$ = 138 °C for D = 800 m (Fig. 3.24). Due to cooling, an initial yield of Q_{prod} = 285 kg.s^{-1} increases to Q_{prod} = 350 kg.s^{-1} at t_{si}, prompting a question on how recent 3-wells scheme can hold such deliverability.

An instant recovery is calculated for t_{reco} = 60 yrs for $T_{res,r}$, so that $t_{reco} < t_{si}$, and an approach can be considered renewable in interaction with reservoir. Yet a fact that t_{si} < 100 yrs means a strategy compromises principle of sustainable reservoir operation.

3.8.3. Stepwise field development: P_{th} = 43 → 72 MWth

Energy potential classification (Rybach, 2015) is rather a producer- or field operator- oriented scheme, working with more understandable classes then is a certainty-based McKelvey's diagram. In principle, a sustainable potential P_S = 43 MWth represents a part of total potential a system is supposed to maintain for a desired period of production, not compromising energy balance in a reservoir. The developable potential P_D = 29 MWth gives amount of energy recoverable under sustainable potential to supply a sustainable potential for some part of desired period of production. A stepwise approach in field management is, thus, in essential principles of both.

We tested stepwise field development first, considering $t_{prod,1}/t_{prod,2}$ schemes as 70/30 and 80/20 yrs. Unlike a constant production variant, both schemes appear as sustainable (Fig. 3.25), as for $t_{prod} = t_{si}$ = 100 yrs the $T_{wh,t}$ = 125 °C and $T_{wh,t}$ = 128 °C respectively, i.e. the critical boundary condition $T_{wh,t} \leq T_{wh,t(crit)}$ has not been reached through t_{prod} = 100 yrs, consequent to a calculated breakthrough at t_B = 85 and 87 yrs. Initial yield of $Q_{prod} = Q_{inj}$ = 285 kg.s^{-1} at t_{prod} = 0 yrs is forecasted to increase to Q_{prod} = 333 kg.s^{-1} and Q_{prod} = 320 kg.s^{-1}, balancing loss of thermal gradient at the wellhead. Immediate recovery after shut-in is supposed as capable to generate return of initial conditions at t_{reco} = 62 yrs and t_{reco} = 59 yrs, turning renewable capacity positive, i.e. $t_{reco} < t_{si}$. Both stepwise field development variants can, thus, be classified as sustainable and renewable approaches.

3.8.4. Stepwise field reduction: P_{th} = 72 → 43 MWth

In following, we tested mirroring of field development strategies, i.e. proceeding from a full development at $P_S + P_D$ = 72 MWth to P_S = 43 MWth, simulating field is operated at all pace first to shorten a payback, and then left easing impact of production on reservoir. A time-step scheme is given by $t_{prod,1}/t_{prod,2}$ = 20/80 and 30/70. Higher initial production (P_{th} = 72 MWth ; Q_{prod} = 285 kg.s^{-1}) accelerates cold front arrival in 1TIQ at t_B = 71 and 64 yrs respectively, resulting in a cooling period prolongation. Then, model estimates reaching $T_{wh,t}$ = 122 °C at t_{si} = 100 yrs and $T_{wh,t}$ = 121 °C at t_{si} = 99 yrs respectively, questioning both options in their sustainability ($T_{wh,t} \approx T_{wh,t(crit)}$). These absolute values do not account on uncertainties, yet compromising sustainability of this strategy even more. Use of 1TER algorithm predicts recovery of initial conditions for both scenarios at t_{reco} = 61 yrs, so that $t_{si} \geq t_{reco}$, classifying the approach renewable (Fig. 3.26).

Obviously, when opting for a safe strategy for initial field operation, a stepwise development is highly recommended. This provides time enough to study field response under detailed production monitoring, including multiple recalibrations of model. Unlike, a straight-forward peaking production, maximizing reservoir economics, is easy to compromise production longevity, and, thus, sustainability of a resource production and use.

3.9 Discussion

3.9.1. ALPM model limitations

Obvious importance of the DDHS requires application of multiple approaches to study conditions securing longevity and renewability of resource production. Analytical and lumped parameter models are capable to carry simulations on reservoir response and reclamation, yielding tentative guide for opening a field production. This may, however, be enough at early stages of reservoir opening, providing field operator sufficient time for further field and production monitoring, consequently leading to reliable data collection allowing use of more sophisticated, numerical models. Otherwise, with a few and unsound data, numerical models yield robust errors of estimates. In use of ALPMs, it is, however, necessary to respect and understand its limits.

3.9.1.1 Model calibration and history matching

A fact that model has not been calibrated using history matching has repeatedly been commented in the paper. Authors are not convinced that available data from uncomplete pumping tests, including multiple drawdown stages, are representative enough. This is instantly a case of temperature response and deliverability. To mitigate effects

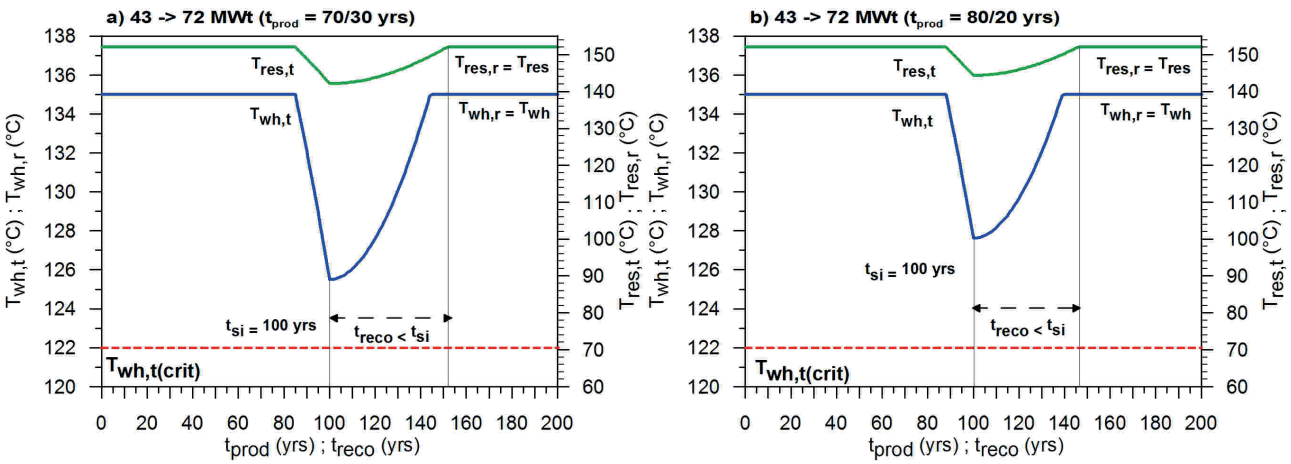

Fig. 3.25. Preview on 1TIQ / 1TER reservoir response model estimation for stepwise P_S to $P_S + P_D$ development strategies

of inadequate input data, and to strengthen reliability of the model, several actions were conducted during model calibration and upscaling:

Monte Carlo simulation of effective heat exchange profile (Heff) accounts on maximum thickness a reinjection can interact with HEP through; obtained from tectonic model of the structure at highest probability rate P90(Δz)

- adjustment of reservoir parameters as function of temperature helps avoiding constants; fixes model logs within realistic conditions, easy to be subjected for future recalibration and history matching; and secures non-isothermal reservoir behavior, so that recovery logs can not exceed values at initial conditions
- use of sampled bottomhole and wellhead temperatures from exploration provides fixed margin boundary for recovery too
- mass-balance function is defined through (1) to (14) is now fixed at $Q_{prod} = Q_{inj} = 1{:}1$, as long as tracer tests are performed, yielding relevant data on effective connectivity between reinjector and producer, now securing 1-tank pressure regime

3.9.1.2 Production scheme

At a recent state, three wells are considered to contribute on geothermal energy production at a site, drilled during a hydrogeothermal exploration campaign in 1999 (Vranovská et al., 1999a,b). A distance between wells has been calculated for D = 800 m concerning deep reservoir position. Thus, thermal breakthrough and reservoir response and recovery algorithms calculate with the given horizontal distance. It is, however, ingenuous expecting new wells not to come, as long as technical installations are supposed to wear fast exposed to chemistry of local geothermal fluids. Some studies on decline curve analysis (Reyes et al., 2004) and economical capacity (Sanyal, 2005) have also been carried for the DDHS (Fričovský et al., 2020c), showing a need on new boreholes emplacement at a time not shorter than 24 yrs. Assuming position of new wells is unreal at now. Opting for new coordinates give a field operator a good chance to enlarge a horizontal distance between reinjection and production site, further increasing safety of a long-term production. A caution must be paid on geothermal settings at a new position.

3.9.1.3 Heat flow balance

Correction for temperature, i.e. wellhead T_{wh} or borehole inflow to represent a mean reservoir temperature T_{res} can reduce assumptions on relevant conductive and convective heat increment during production. Use of advective cooling ($Q_{inj}.c_{w,inj}.t_{prod}$) in thermal breakthrough and ALPMs accredits the magnitude of cooling dramatically (compared to a case where cooling is reduced to a diffuse). This is, however, balanced through introduction of convective (advective) heat increment (62) in a gross E_n (40) determination for both, the 1TIQ and 1TER model once the cold front arrives to production zone. Building-up the E_{CV} during production eases the effect of advective cooling as long as Γ_{CV} (58) increases with drop in $T_{CV,top} = T_{res,t}$. Starting the reclamation at t_{si} for scenarios where $t_B < t_{prod}$ and $T_{res,t} \leq T_{res}$ accounts for maxima in E_{CV} and Γ_{CV}, promoting recovery in early stage, while progressively decaying as long as $T_{res,r} \rightarrow \lim T_{res}$ in 1TER model. This allows a model to adjust towards reservoir dynamics that are function of change mean reservoir temperature.

Importance of conduction can not be questioned at local conditions. Convection is, however, assumed from indirect indices, such is local thermodynamics (e.g. Fričovský et al., 2018a) or linear stability analysis (e.g. Fričovský et al., 2018b,c; Vizi et al., 2020). To support the idea, several adiabatic boiling and phase stability models have also been carried (Fričovský et al., 2020c), limiting plausible

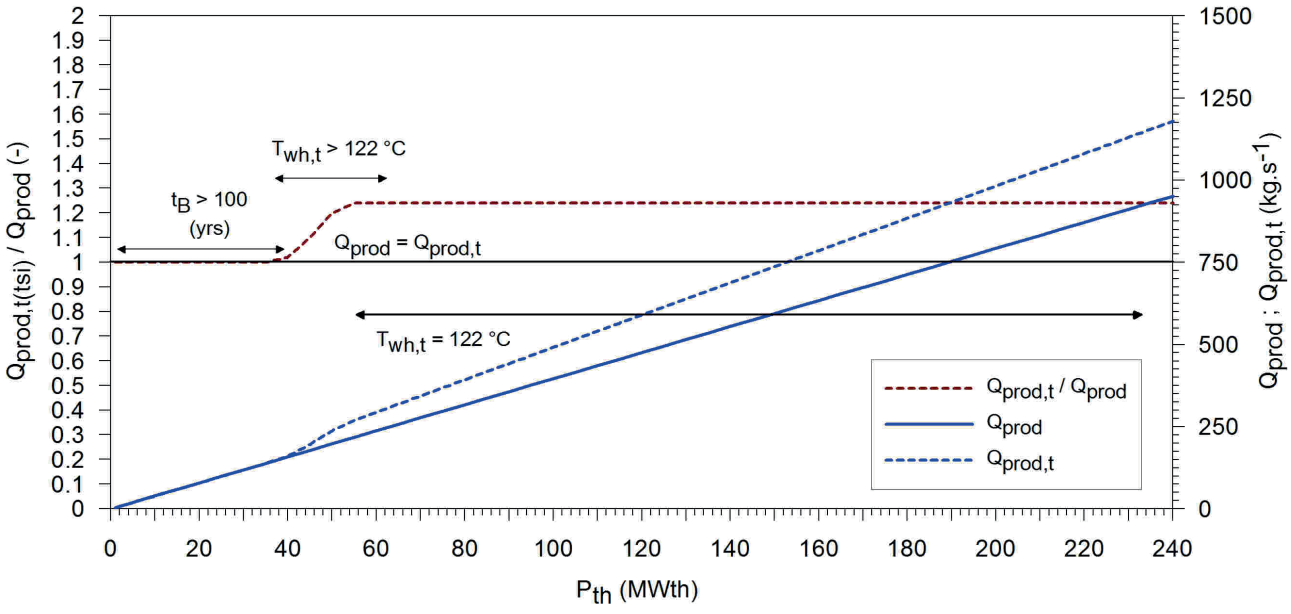

Fig. 3.26. *Preview on 1TIQ / 1TER reservoir response model estimaton for stepwise field reduction from $P_S + P_D$ to P_S strategies.*

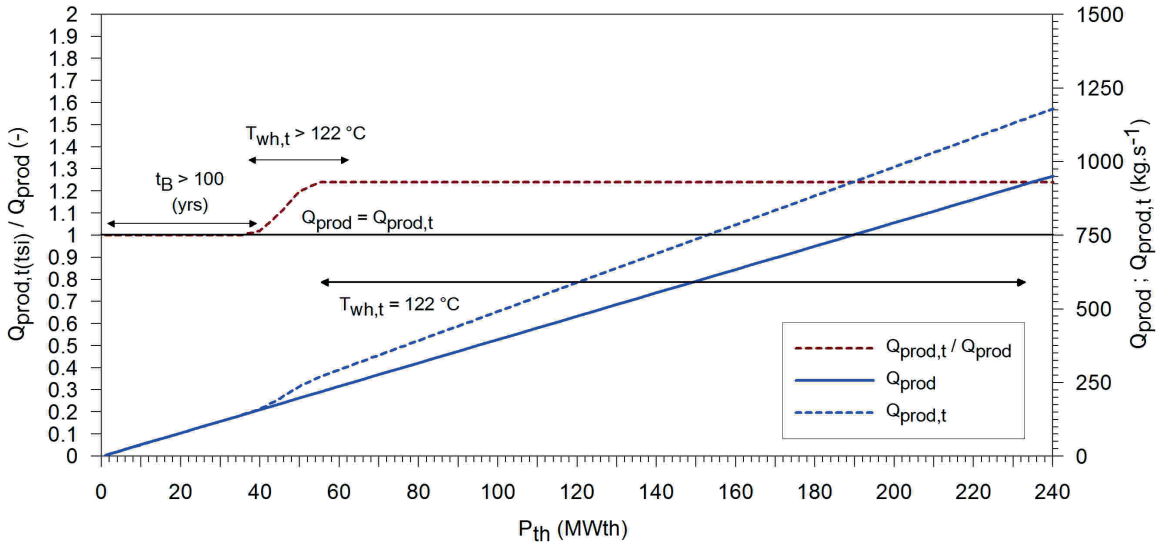

Fig. 3.27. *Desired yieldrates (Q_{prod}) at t_{si} for constant thermal output strategies.*

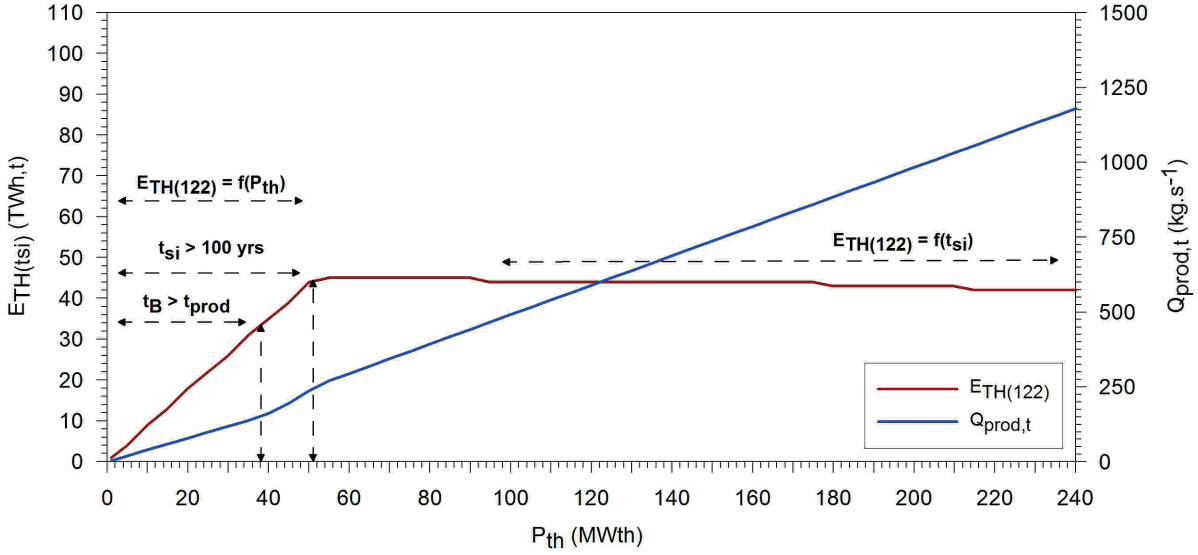

Fig. 3.28. *Cumulative geothermal energy production $E_{TH(122)}$ for constant thermal output strategies.*

convection as quiet at a steady-state in deepest parts of reservoir. However, more studies are required, such is use of geothermometry and mixing / boiling models, capable to address vertical geothermal brine movements in reservoir through thermal equilibrium recalibration.

3.9.2. Cumulative production of geothermal energy at sustainable conditions

One of most critical parameters when concerning a field development with consecutive investments into geothermal infrastructure, operation and maintenance costs etc. is a potential of energy that can be generated over a desired period of time, an operator can sell to the market. This is even more pronounced, as environmental subsidies from carbon dioxide mitigation can play a role in total investments – income balance.

The level of sustainable cumulative production of geothermal energy is approached introducing the $E_{TH(122)}$ parameter, representing ideal (theoretical) cumulative amount of energy produced at a time of shut-in (t_{si}), yet not including engineering considerations, such is thermal efficiency of heat exchange processes, assuming the thermal output constant in a model.

Any cooling calls for a necessary increase in yield to balance loss in $T_{res,t}$ and $T_{wh,t}$ paying an instant impact on deliverable energy at a wellhead through specific heat capacity of geothermal brine at the wellhead, i.e. $c_{w,wh} = f(T_{wh,t}, \rho_{w,wh})$, where $\rho_{w,wh} = f(T_{wh,t}, p_{wh})$, assuming constant wellhead pressure. As long as $Q_{prod} = Q_{inj} = 1{:}1$ is set in the 1TIQ model, the Q_{prod} or Q_{inj} rates increase up to 20 % depending on a decay in $T_{res,t}$ and $T_{wh,t}$ (Fig. 3.27), yet fixed through shut-in at $T_{wh,t} \leq T_{wh,t(crit)} = 122$ °C and $t_{si} = t_{Twh,t(crit)}$. As based on 1TIQ model, the boundary that corresponds to a maximum increase in desired productivity is, thus, $P_{th} \geq 51$ MWth. Following the boundary condition, a maximum sustainable thermal energy production that can be produced from a reservoir $E_{TH(122)} = 45 – 46$ TWh,th at $t_{si} = 100$ yrs (Fig. 3.28). Any constant thermal output

strategy above the threshold level of P_{th} = 51 MWth yields slow decay in $E_{TH(122)}$ as period of production shortens with t_{si} due to critical cooling rate boundary condition interception. The 1TIQ summation plot thus demonstrates a fair compromise between longevity of production and a cumulative energy recovery from a reservoir to turn investments reasonable.

Obviously, higher production rates can generate the same output in considerably shorter time, yet on considerable costs on a resource and reservoir environment. An example of such comparison is a constant management operating P_{th} = 49 MWth and P_{th} = 72 MWth. A first scenario generates $E_{TH(122)}$ = 43 Twh,th at $t_{si} = t_{prod}$ = 100 yrs, so that at such a rate, a system can be considered sustainable and renewable. The latter, maintained constant, does, however, generate $E_{TH(122)}$ = 45 TWh,th, yet a system terminates at t_{si} = 71 yrs, compromising a principle beyond what sustainability and sustainable development means. A total difference is, thus, 2 TWh,th between both, yet impact on a reservoir and production longevity is huge in a difference. At least for resources repeatedly considered "renewable" an income-only approach should not always be introduced.

3.10 Conclusions

A complete module on thermal breakthrough, production response and reclamation, is presented in this paper, providing theory beyond necessary for its reconstruction, upscaling and application. Assessing thermal breakthrough is approached through a doublet, advective cooling model with a diffuse / conductive retardation (e.g. Ungemach et al., 2005, 2009). Reservoir response to production forecasting is governed by analytical, pseudo lumped-parameter model 1TIQ (1-tank ALPM with heat flux and reinjection), set to run since beginning of production at D = 0 (position of reinjector), and since $t_B \leq t_{prod}$, i.e. if $t_{cool} \neq 0$ at D = 800 m (position of producers). A similar ALPM model is applied in simulation of reservoir reclamation after production shut-in with 1TER (1-tank closed energy recovery) model.

The entire model is precisely upscaled to local conditions, including reservoir geometry (e.g. simulation of HEP thickness, total "tank" thickness) and doublet scheme (e.g. D = 800 m), geothermal field (mean reservoir temperature, heat flux), and reservoir dynamics (convection contribution). A necessary mass balance (1 to 14) functions (e.g. Sarak et al., 2003a,b, 2005) secure a closed-tank (Axelsson, 1989) behavior of the model. Pressure is controlled through 1:1 production – injection ratio, i.e. $Q_{prod} = Q_{inj}$, assuming ideal connectivity within HEP as part of a reservoir profile, and no natural / induced recharge (Vranovská et al., 2015). The energy flux introduces the radiogenic heat production (64), conduction (54) and convection (61) into the balance (37). Given setup allows non-isothermal reservoir conditions during production and recovery, except constant radiogenic heat production E_{RG}, assumed stable at shallow crustal depths and given temperatures (Čermák et al., 1991). This reduces (40) impact of applied advective cooling on effective heat exchange profile in 1TIQ model (28 or 36) where convective Γ_{CV} and conductive Γ_{CD} gradients (65) are induced due to cooling ($T_{res,t} \rightarrow \lim T_{res,t(si)}$; $T_{top,t} \rightarrow \lim T_{top,crit}$) as long as there is some breakthrough i.e. $t_B < t_{prod}$. For recovery, the dynamic setup reduces heat flow density progressively as a reservoir reclaims (pseudo) initial conditions in 1TER model. Fixing the energy flux restrains exceeding initial, steady-state conditions during and after recovery from production. Analytical functions are adjusted rather to mean reservoir $T_{res,t}$, wellhead $T_{wh,t}$ or reinjection T_{inj} temperature, the less to the system geometry, i.e. depth (z) or thickness (H or Δz respectively). A given model does not include iterative techniques for history matching, such the least-square or Levenberg-Marquardt (Sarak et al., 2003), hence history matching is skipped in the model due to unreliable long-term monitoring data. However, the entire module can easily be equipped with history fitting function, depending on a parameter to match – yet Q_{prod} and T_{res} are the most likely.

Geothermal resources are repeatedly addressed as sustainable and renewable in once, presented to society as one of tools to approach sustainable development. Praxis has, however, repeatedly shown that both, sustainability and renewability can easily be compromised through depletive field management. It is, however, not a question of a geothermal fluid quantity. Instead, temperature, mobile phase stability and change, reservoir thermodynamics (exergy, enthalpy), and heat flux dynamics are frequently concerned. Each production that causes irreversible changes to a geothermal system is, thus, all but sustainable. To mitigate such a human impact, numerous approaches to study reservoir sustainability and renewability emerged in last decades, turning sustainability one of the most important issues of reservoir engineering. In fact, this topic has long been omitted in Slovakia, lacking any support in essential enactments, such is Act. No. 569/2007 Coll. (Geology act) and its related Regulation N. 51/2008 Coll., or Act. No. 364/2004 Coll. (Water Act). Neither balance based, nor analytical and numerical solutions on a resource sustainability in its energy capacity, potential and fluxes are set mandatory in hydrogeothermal assessments or prior field opening.

The Ďurkov Depression hydrogeothermal structure (DDHS) is considered one of the most perspective amongst geothermal systems in Slovakia. TOUGH2 code based model has been already carried to search for sustainable production (Giese, 1998, 1999), yielding several limits (purely conductive environment, orthogonal / regular grid atc.), however, assuming reinjection at T_{inj} = 25 °C. Under given geothermal fluid chemistry (e.g. Vranovská et al., 1999a,b, 2015; Bodiš & Vranovská, 2012), rather a fluid return at T_{inj} = 65 °C (Vranovská et al., 1999a) is more realistic. Multiple studies have also shown there is at least limited, quiet convection likely within deepest parts of a system that must be accounted. Authors also conclude, that at given thermal field setup, relying only on conductive cooling / heating balance becomes fairly optimistic assumption (local temperatures along effective heat exchange profile are simply too low).

Instead, a model on breakthrough, reservoir response and recovery has been adopted as part of a complex study

on reservoir sustainability at a site, funded by Ministry of Environment of the Slovak Republic (Fričovský et al., 2020c), balancing and modeling at a desired period of production equal to t_{prod} = 100 yrs according to a concept of sustainable reservoir production (Axelsson et al., 2001).

In cold-front progression analysis using advective breakthrough model with simultaneous conductive retardation, a thermal capacity of P_{th} = 38 MWth has been found a limit to avoid cooling within production zone during desired period of production (Fig. 3.16). At given conditions (T_{inj} = 65 °C and $Q_{prod} = Q_{inj}$ = 1:1 = const.), the capacity equals $Q_{prod} = Q_{inj}$ = 158 kg.s^{-1}. The model calculates with effective reservoir heat-exchange profile, assumed H_{eff} = 600 m as 90-th percentile of reservoir thickness simulation. As it is given by a theory beyond, reduction of return temperature increases the threshold value for a cold-front to arrive (e.g. P_{th} = 61 MWth for T_{inj} = 25 °C), and so an increase in H_{eff} does.

Thermal breakthrough is, however, frequently observed phenomena at geothermal fields, not necessarily terminating field production as long as there aren't changes in reservoir phase or quality, or, rather, if geothermal infrastructure has been optimized for some optional cooling. Several approaches have already been introduced to answer a rate of tolerable cooling that secures feasibility of a project and minimizes impact on a reservoir performance. For that case, the model adopts a 10 % tolerated cooling limit (Williams, 2004, 2007) prior shut-in. This allows temperature at a wellhead to be a principal boundary condition, i.e. $T_{wh,t(crit)} = 0.9T_{wh}$ = 122 °C (T_{wh} = 135 °C; Halás Sr et al., 2016), and so the 1TIQ model stops simulation at a time the drop in temperature intercepts the boundary condition, i.e. $t_{si} = t_{Twh,t(crit)}$. Each simulation has been run for a desired period of production, i.e. t_{prod} = 100 yrs to find out the realistic time of shut-in.

Plot of t_{si} development (Fig. 3.17) shows that for t_{prod} = 100 yrs, the critical thermal output is P_{th} = 51 MWth (Q_{prod} = 214 kg.s^{-1}) to maintain constant field operation. Because the model is not matched with the production history, production of P_{th} = 49 MWth is recommended. This is a value obtained from reserve capacity ratio application to geothermal reserves booking performed through Monte Carlo simulation of recoverable heat in place (Fig. 3.13). A given rate yields t_B = 79 yrs, so that t_{cool} = 21 yrs. At t_{prod} = 100 yrs, the wellhead temperature is expected above the critical, i.e. $T_{wh,t}$ = 124 °C, not intercepting introduced boundary condition, so $t_{si} = t_{prod}$ = 100 yrs. Due to t_{cool}, 1TIQ model assumes necessary increase in deliverability up to $Q_{prod,t} = Q_{inj}$ = 230 kg.s^{-1} at production termination (Fig. 3.23). The 1TER model for reclamation has been initiated as t_{reco} = 0 at $t_{prod} = t_{si}$, setting $Q_{prod} = Q_{inj}$ = 0 kg.s^{-1} in an algorithm. Obviously, a system is able to recover at $t_{reco} \leq t_{si}$, so that $\Delta t_{reco} = t_{si} - t_{reco} > 0$, classifying such strategy sustainable and of a renewable interaction with the reservoir. Generally, the reservoir (a geothermal system) is able to recover initial conditions nearby the production zone as long as $T_{res,t} \geq$ 138 °C and $t_{reco} \geq$ 60 yrs with $T_{top,crit} \geq$ 80 °C.

1TIQ model analysis also implicated that the conductive play-type of the DDGS, may only be generally preserved at initial state. A long term production and reinjection can, apparently, generate convective gradient through cooling high enough to make quiet, stable convection towards induced (D = 800 m) and unstable (D ≤ 600 m), optionally with convective regime prevailing over conductive close to reinjector (D ≤ 200 m). However, as long as a system is able to recover initial geothermal field, it is also able to return into quiet, conductive environment at a final stage of recovery.

The 1TIQ model has also been equipped with algorithm to calculate sustainable cumulative geothermal energy production – termed herein $E_{TH(122)}$, not accounting engineering efficiencies, such as optional heat exchanger station. The computation worked for a period between t_{prod} = 0 to t_{si} (Fig. 3.28). Obviously, a maximum amount of geothermal energy production under sustainable and renewable conditions may count no more than $E_{TH(122)}$ = 46 TWh,th, assuming constant production. It well represents an example of a compromise between maximizing long-term output and restraining irreversible or major risks posed onto reservoir.

Slovakia is still fossil-fuels oriented economics, though there is a political and social call on transition towards carbon-neutral primary energy mix. The DDHS is, obviously, amongst resources of contributable potential. Yet instead of excessive installments and depletion, concern must be acknowledged towards sustainability of geothermal energy production, the more, in case of sites of such energy potential. Obtained results must not be taken as absolute. Authors are aware of limits of the model, even constructed under precise upscaling to local conditions. Instead, gained analysis should provide background reliable enough to, first, open a field production at recommended limits (P_{th} = 49 MWth), followed by detailed field analysis, including tracer tests (assessing connectivity), production monitoring, model calibration (such using history matching), and transition towards complex numerical models. Just after yielding good certainty, the production should be increased, i.e. towards P_{th} = 72 MWth, as given by combination of sustainable (P_S) and developable (P_D) potential. Such a step-wise development is, indeed, a worldwide applied praxis, mitigating unexpected reservoir or production failure.

References

Agemar, T., Schellschmidt, R. & Schulz, R., 2012: Subsurface temperature distribution in Germany. Geothermics, 44, p. 65-77.

Alkan, H. & Satman, A., 1990: A new lumped parameter model for geothermal reservoirs in the presence of carbon dioxide. Geothermics, 19, p. 469-479.

Arevalo, A.S., 2003: Rapid environmental assessment tool for extended Berlin geothermal field project. In: Proceedings International Geothermal Conference, Reykjavik, Iceland, p. 1-7.

Axelsson, G., 1989: Simulation of pressure response data from geothermal reservoirs by lumped parameter models. Proceedings 14th Workshop on Geothermal Reservoir Engineering, Stanford University, CA, p. 1-7.

Axelsson, G., 2010: Sustainable geothermal utilization – Case histories; definitions; research issues and modelling. Geothermics, 39, p. 283-291.

Axelsson, G., 2011: Using long case histories to study hydrothermal renewability and sustainable utilization. Geothermal Resource Council Transactions, 35, p. 1393-1400.

Axelsson, G.., 2012a: Modelling sustainable geothermal energy utilization. Proceedings the 53rd Scandinavian Simulation and Modelling Society Conference, Reykjavik, Iceland, p. 1-14.

Axelsson, G., 2012b: The physics of geothermal energy. In: Sayigh, A. (Ed.) 2012: Comprehensive renewable energy. Elsevier Ltd., p. 1-52.

Axelsson, G., Bjornsson, G., Flovenz, O.G., Kristmansdóttir, H. & Sverrisdottir, G., 1995: Injection experiments in low-temperature geothermal areas in Iceland. Proceedings World Geothermal Congress 1995, Florenze, Italy, p. 1-5.

Axelsson, G., Gudmundsson, A., Steingrímsson, B., Palmasson, G., Armansson, H., Tilinius, H., Flovenz, O.G., Bjornsson, S. & Stefansson, V., 2001: Sustainable production of geothermal energy: suggested definition. International Geothermal Association News Quaterly, 43, p. 1-2.

Axelsson, G., Stefansson, V. & Xu, Y., 2002: Sustainable management of geothermal resources. Proceedings Beijing International Geothermal Symposium, Beijing, China, p. 277-283.

Axelsson, G., Stefansson, V. & Björnsson, G., 2004: Sustainable utilization of geothermal resources. Proceedings 29th Workshop on Geothermal Reservoir Engineering, Stanford University, CA, p. 1-8.

Baldwin, B. & Butler, C.O., 1985: Compaction curves. American Association of Petroleum Geologists Bulletin, 69 (4), p. 622-626.

Beardsmore, G.R., Rybach, L., Blackwell, D. & Baron, Ch., 2010: A protocol for estimaping and mapping global EGS potential. Geothermal Resource Council Transactions, 34, p. 301-312.

Bielik, M., 1999: Geophysical features of the Slovak Western Carpathians: a review. Geological Quaterly, 43 (3), p. 251-262.

Bjornsson, G., Axelsson, G., Flóvenz, O.G., 1994: Feasibility study for the Thelamork low-temperature system in Iceland. Proceedings 19th Workshop on Geothermal Reservoir Engineering, Stanford University, CA, p. 1-9.

Blöcher, M.G., Zimmermann, G., Moeck, I., Brandt, W., Hassanzadegan, A., Magri, F., 2010: 3D numerical modeling of hydrothermal processes during the lifetime of a deep geothermal reservoir. Geofluids, 10 (3), p. 406-421.

Bjarnadottir, R., 2010: Sustainability evaluation of geothermal systems in Iceland. Indicators for sustainable production [manuscript – Master's Thesis], Reykjavik Energy Graduate School of Sustainable Systems, Reykjavik.

Bodiš, D. & Vranovská, A., 2012: Genéza anomálneho obsahu arzénu v hydrogeotermálnej štruktúre Ďurkov [*Genesis of anomalous arsenic content in the hydrogeothermal structure of Ďurkov*]. Podzemná voda, XVIII (2), p. 123-136, in Slovak, English resume.

Brehme, M., Moeck, I., Kamah, Y., Zimmermann, G. & Sauter, M., 2014: A hydrotectonic model of a geothermal reservoir – A study in Lahedong, Indonesia. Geothermics, 51, p. 228-239.

Bromley, Ch., Rybach, L. & Mongillo, M., 2006: Sustainable utilization strategies and promotion of beneficial environmental effects: having your cake and eating it too. Proceedings New Zeeland Gegothermal Workshop.

Bujakowski, W., Tomaszewska, B. & Miecznik, M., 2016: The Podhale geothermal reservoir simulation for long-term sustainable production. Renewable Energy, 99, p. 420-430.

Burnell, J., O'Sullivan, M., O'Sullivan, J., Kissling, W.., Croucher, A., Pogacnik, J., Pearson, S., Caldwell, G., Ellis, S., Zarrouq, S. & Climo, M., 2015: Geothermal Supermodels: The next generation of integrated geophysical, chemical and flow simulation modelling tools. Proceedings World Geothermal Congress 2015, Melbourne, Australia, p. 1-7.

Clotworthy, A.W., Ussher, G.N.H., Lawless, J. V. & Randle, J.B., 2006: Towards an industry guideline for geothermal reserves determination. Geothermal Resource Council Transactions, 30, p. 852-859.

Čermák, V., Bodri, L. & Rybach, L., 1991: Radioactive heat production in the continental crust and its depth dependence. In: Čermák, V. – Rybach, L. (Eds.): Terrestrial Heat Flow and the Litosphere Structure. Springer – Verlag, Berlin Heidelberg, DE, p. 23-70.

Činčura, J. & Köhler, E., 1995: Paleoalpine karstification: the longest paleokarst period in the Western Carpathians (Slovakia). Geol. Carpathica, 46 (5), p. 343-347.

Deibert, L., Hjartarson, A., McDonald, I., McIlveen, J., Thompson, A., Toohey, B. & Yang, D., 2010: The Canadian geothermal code for public reporting – 2010 Edition. The Canadian Geothermal Code Committee, 34 p.

DiPippo, R., 2005: Geothermal power plants – principles, applications and case studies. Butterworth – Heinemann, New York, 445 p.

DiPippo, R., 2007: Ideal thermal efficiency for geothermal binary plants. Geothermics, 36, p. 276-285.

Doveri, M., Lelli, M., Marini, L. & Raco, B., 2010: Revision, calibration, and application of the volume method to evaluate the geothermal potential of some recent volcanic areas of Latium, Italy. Geothermics, 39, p. 260-269.

Falcone, G. & Beardsmore, G.R., 2015: Including geothermal energy within a consistent classification for renewable and non-renewable energy resources. Proceedings World Geothermal Congress 2015, Melbourne, Australia.

Falcone, G., Gnoni, A., Harrison, B. & Alimonti, C., 2013: Classification and reporting requirements for geothermal resources. Proceedings, European Geothermal Congress 2013, Pisa, Italy.

Fendek, M., Remšík, A. & Fendeková, M., 2005: Metodika vyhľadávania, hodnotenia a bilancovania množstva geotermálnej vody a geotermálnej energie [*Methodology of searching, evaluation and balancing of the amount of geothermal water and geothermal energy*]. Mineralia Slovaca, 37 (2), p. 117-121, [in Slovak, English summary].

Flóvenz, O.G., Árnason, F., Finnsson, M. & Axelsson, G., 1995: Direct utilization of geothermal water for space heating in Akureyri, N-Iceland. Proceedings World Geothermal Congress 1995, Firenze, Italy, p. 1-6.

Flóvenz, O.G., Arnason, F., Gautason, B., Axelsson, G., Egilson, T., Stendórsson, S.H. & Gunnarsson, H.S., 2010: Geothermal District Heating in Eyjafjördur, N-Iceland; Eighty Years of Problems, Solutions and Success. Proceedings World Geothermal Congress 2010, Bali, Indonesia, p. 1-8.

Fournier, R.O. & Potter, R.W. II., 1978: A magnesium correction for the Na-K-Ca chemical geothermometer. U.S. Geological Survey Open-File Report No. 78-986, 24 p.

Fournier, R.O. & Potter, R.W. II., 1979: Magnesium correction to the Na-K-Ca chemical geothermometer. Geochimica Cosmochimica Acta, 43, p. 1543-1550.

Fournier R.O. and Potter R.W.II., 1982: A revised and expanded silica (quartz) geothermometer. Geothermal Resources Council Bulletin 11, p. 3-12.

Fournier R.O., White D.E. & Trusdell A.H., 1974: Geochemical indicators of subsurface temperature - Part 1, basic assumptions. J. Res. U. S. Geol. Survey, 2, p. 259-261.

Fox, D.B., Sutter, D., Beckers, K.F., Lukawski, M.Z., Koch, D.L., Anderson, B.J. & Tester, J.W., 2013: Sustainable heat farming: modelin extraction and recovery in discretely fractured geothermal reservoirs. Geothermics, 46, p. 42-54.

Fričovský, B., Jacko, S. Jr., Popovičová, M. & Tometz, L., 2013: Substitution approach in cabron dioxide emission reduction evaluation: case study on geothermal power station project plan – Ďurkov (Košice Basin, Slovakia). International Journal of Environmental Science and Development, 4, 2, p. 124-129.

Fričovský, B., Tometz, L. & Fendek, M., 2016: Geothermometry techniques in reservoir temperature estimation and conceptual site models construction: principles, methods and application for the Bešeňová elevation hydrogeothermal structure, Slovakia. Mineralia Slovaca, 48, 1, p. 1-60.

Fričovský B., Vizi, L., Surový, M. & Mižák, J., 2018a: Numerical indices implications on reservoir convection for the Ďurkov Depression hydrogeothermal structure, Košice Basin. Geologické Práce, správy, 132, p. 3-30, in Slovak, extended English resume.

Fričovský B., Vizi, L. & Surový, M., 2018b: Vplyv segmentácie rezervoáru na formovanie priaznivých podmienok konvekcie: model ukloneného pórovitého prostredia; príklad hydrogeotermálnej štruktúry Ďurkovská depresia, Košická kotlina [*Influence of reservoir segmentation on the formation of favourable convection conditions: model of inclined porous medium; example of hydrogeothermal structure Ďurkov Depression,* Košice Basin]. Proceedings, 19. Slovak hydrogeological conference, Nimnica Spa, Slovakia, in Slovak.

Fričovský, B., Vizi, L., Gregor, M., Zlocha, M., Surový, M. & Černák, R., 2018c: Thermodynamic analysis and quality mapping of a geothermal resource at the Ďurkov hydrogeothermal structure, Košice depression, Eastern Slovakia. Proceedings 43rd Workshop on Geothermal Reservoir Engineering, Stanford University, CA, p. 1-9.

Fričovský, B., Vizi, L., Fordinál, K., Surový, M. & Marcin, D., 2019: A reviewed hydrogeothermal evaluation of the Ďurkov Depression hydrogeothermal structure: insights from probabilitstic assessment and sustainable production optimization. Proceedings 44rd Workshop on Geothermal Reservoir Engineering, Stanford University, CA, p. 1-14.

Fričovský, B., Černák, R., Marcin, D., Blanárová, V., Benková, K., Pelech, O., Fordinál, K., Bodiš, D. & Fendek, M., 2020a: Geothermal Energy Use – Country Update for Slovakia. Proceedings World Geothermal Congress 2020, Reykjavik, Iceland, p. 1-12 (fulltext accepted, in press).

Fričovský, B., Vizi, L., Marcin, D., Černák, R., Blanárová, V., Ujjobbágyová, Z., Bodiš, D., Benková, K., Pelech, O. & Fordinál, K., 2020b: Geothermal energy utilization in Slovakia: First insights from sustainability prospective. Proceedings World Geothermal Congress 2020, Reykjavik, Iceland, 1-12 (fulltext accepted, in press).

Fričovský, B., Vizi, L., Surový, M., Fordinál, K., Zlocha, M., Gregor, M. & Fričovská, J., 2020c: Hydrogeotermálne hodnotenie Ďurkovskej depresie: aplikácia princípov trvalo udržateľného rezervoárového manažmentu. Manuscript, Technical Report, SGIDŠ, Bratislava, 167 p. [in Slovak, in print].

Fridleifsson, I.B., Bertani, R., Huenges, E., Lund, J.W., Ragnarsson, A. & Rybach, L., 2008: The possible role and contribution of geothermal energy to the mitigation of climate change. In: Hohmeyer – Trittin (Eds): IPCC Scoping Meeting on Renewable Energy Sources Proceedings, Luebeck, Germany, p. 59-80.

Garg, S.K. & Kassoy, D.R., 1981: Convective heat and mass transfer in hydrothermal systems. In: Rybach, L., Muffler, L.J.P. (Eds.), Geothermal Systems. Principles and Case Histories. Wiley, p. 37–76.

Garg, S.K. & Combs, J., 2010: Appropriate use of USGS volumetric "heat in place" method and Monte Carlo simulations. Proceedings, 34th Workshop on Geothermal Reservoir Engineering, Stanford University, Stanford, California.

Garg, S.K. & Combs, J., 2015: A reformulation of USGS volumetric „heat in place" resource estimation method. Geothermics, 55, p. 150-158.

Giese, L., 1998: Report on the evaluation of well test data – geothermal well GTD-2, Ďurkov geothermal field, Košice Basin. Manuscript, Geothermia, Geochimica, Berlin.

Giese, L., 1999: Report on the evaluation of well test data – geothermal well GTD-3, Ďurkov geothermal field, Košice Basin. Manuscript, Geothermia, Geochimica, Berlin.

Giggenbach, W.F., 1988: Geothermal solute equilibria. Derivation of Na-K-Mg-Ca geoindicators. Geochimica Cosmochimica Acta, 52, p. 2749-2756.

González, Z., González, D. & Kretzchmar, T., 2015: First approach of Environmental Impact Assessment of Cerro Prieto geothermal power plant, BC, Mexico. In: Proceedings World Geothermal Congress 2015, Melbourne, Australia, p. 1-9.

Grant, M.A., 2000: Geothermal resource proving criteria. Proceedings World Geothermal Congress 2000, Kyushu-Tohoku, Japan.

Grant, M.A., 2014: Stored-heat assessments: a review in the light of field experience. Geothermal Energy Science, 2, p. 49-54.

Grant, M.A. & Bixley, P.F., 2011: Geothermal Reservoir Engineering, 2nd Edition. Elsevier – Academic Press, Amsterdam, NL, 359 p.

Gringarten, A.C., 1978: Reservoir lifetime and heat recovery factor in geothermal aquifers for urban heating. Pure and applied geophysics, 117, p. 297-308.

Gringarten, A.C. & Sauty, J.P., 1975: A theoretical study of heat extraction from aquifers with uniform regional flow. Journal of geophysical research, 80 (35), p. 4956-4962.

Gungor, A., Erbay, Z. & Hepbasli, A., 2011: Exergetic analysis and evaluation of a new application of gas-engine heat pumps (GEHPs) for food drying processes. Applied Energy, 88, p. 882-891.

Gutiérrez-Negrín, L.C.A., Maya-González, R. & Quijano-Leon, J.L., 2015: Present situation and perspectives of geothermal in Mexico. Proceedings World Geothermal Congress 2015, Melbourne, Australia, p. 1-10.

Haenel, R., Rybach, L. & Stegena, L., 1988: Fundamentals of geothermics. In: Haenel et al. (Eds.): Handbook of terrestrial heat-flow density determination with guidelines and recommendations of the International Heat Flow Commission. Kluwer Academic Publishers, Dordrecht, NL, p. 9-56.

Halás, O., Drozd, V. & Vranovská, A., 1999: Investigation of Ďurkov geothermal structure in Košice Basin for geothermal energy utilization. Proceedings XXIX IAH Congress: Hydrogeology and Land Use Management, Bratislava, Slovakia, p. 689-695.

Halás Sr. O., Halás Jr. O., Drozd, V. & Výboch, M., 2016: Košická kotlina – geotermálna energia: Čiastková záverečná správa a výpočet množstiev vôd [*Košice Basin - geothermal energy: Partial final report and calculation of water quanti-*

ties]. Manuscript – Technical report SLOVGEOTERM a.s., Bratislava, 58 p. In Slovak.

Holzbecher, E.O., 1998. Modeling Density-driven Flow in Porous Media: Principles, Numerics, and Software. Springer, Berlin, Germany.

Hosgor, F.B., Cinar, M., Kaklidir, F.T., Tureyen O.I. & Satman, A., 2013: A new lumped parameter (tank) model for reservoirs containing carbon dioxide. Proceedings 38th Workshop on Geothermal Reservoir Engineering, Stanford University, CA, p. 1-7.

Hyashi, K., Willis-Richards, J., Hopkirk, R.J. & Niibori, Y., 1999: Numerical models of HDR geothermal reservoirs – a review of current thinking and progress. Geothermics, 28, p. 507-518.

Ijäs, A., Kuitunen, M.T. & Jalava, K., 2008: Developing the RIAM method (rapid impact assessment matrix) in the context of impact significance assessment. Environmental Impact Assessment Review, 30, p. 82-89.

Jacko, S., Fričovský, B., Pachocká, K. & Vranovská, A., 2014. Reverse stationary temperature modeling and geothermal resource calibration for the Košice depression (eastern Slovakia). Geological exploration technology, geothermics, sustainable development, 1 (2014), p. 3 - 25.

Kassoy, D.R. & Zebib, A., 1975: Variable viscosity effects on the onset of convection in porous media. The Physics of Fluids, 18 (12), p. 1649-1651.

Kukurugyová, M., Jablonský, G., Nalevanková, J. & Dzurňák, R., 2015b: Production, profit and return of ORC-CHP geothermal power plant model at Ďurkov area, Slovakia. Proceedings, ISET 2015, Bratislava, Slovakia.

Lipsey, L., Pluymaekers, M., Goldberg, T., van Oversteeg, K., Ghazaryan, L., Cloetingh, S. & van Wees J.-D., 2016: Numerical modelling of thermal convection in the Luttelgeest carbonate platform, the Nederlands. Geothermics, 64, p. 135-151.

Lizoň, I. & Jančí J., 1979: Základný výskum priestorového rozloženia zemského tepla v Západných Karpatoch [*Basic research of spatial distribution of terrestrial heat in the Western Carpathians*]. Manuscript – Technical report. Bratislava: Geofyzika, Archív Geofond, 35 p. [in Slovak].

Majcin, D., Král, M., Bilčík, D., Šujan, M. & Vranovská, A., 2017: Deep geothermal sources for electricity production in Slovakia: thermal conditions, Contributions to Geophysics and Geodesy, 47 (1), p. 1-22.

Menjoz, A. & Sauty, J.P., 1982: Characteristics and effects of geothermal resource exploitation. Journal of Hydrogeology, 56, p. 49-59.

Moeck, I.S., 2014: Catalog of geothermal play types based on geologic controls. Geothermics, 37, p. 867-882.

Moeck, I. & Beardsmore, G., 2014: A new „Geothermal Play Type" catalog: streamlining exploration decision making. Proceedings 39th Workshop on Geothermal Reservoir Engineering, Stanford University, CA, USA, p. 1-10.

Muffler, L.P.J. & Cataldi, R., 1978: Methods for regional assessment of geothermal resources. Geothermics, 7, p. 53-89.

Neupane, G., Mattson, E., McLing, T., Palmer, D., Smith, R.W. & Wood, T.R., 2014: Deep Geothermal Reservoir Temperatures in the Eastern Snake River Plain, Idaho, using Multicomponent Geothermometry. In: Proceedings 39th Workshop on Geothermal Reservoir Engineering, Stanford University, California, p. 1-12.

O'Sullivan M.S., 2010: Geothermal fluid dynamics. Proceedings the 17th Australian Fluid Mechanics Conference, Auckland, New Zeeland, p. 1-6.

O'Sullivan, M.J., Bullivant, D.P., Follows, S.E. & Mannington, W.I., 1998: Modelling of the Wairakei – Tauhara geothermal system. Proceedings of the TOUGH Workshop '98, Lawrence Berkeley National Laboratory, California, USA, p. 1-6.

O'Sullivan, M.J., Pruess, K. & Lippmann, M.J., 2001: State of art of geothermal reservoir simulation. Geothermics, 30, p. 395-429.

Onur, M., Sarak, H., Tureyen, I., Cinar, M. & Satman, A., 2008: A new non-isothermal lumped-parameter model for low temperature, liquid dominated geothermal reservoirs and its application. Proceedings 33th Workshop on Geothermal Reservoir Engineering, Stanford University, CA, p. 1-10.

Ozgener, L., Hepbasli, A., Dincer, I. & Rosen, M.A., 2007: A key review on performance improvement aspects of geothermal district heating systems and applications. Renewable and Sustainable Energy Reviews, 11, p. 1675-1697.

Pachocká, K., Jacko, S. & Pachocki, M., 2010: 3D modeling of a geothermal reservoir in Eastern Slovakia. VDM Verlag Publ. Saarbrücken, 62 p.

Pasquale, V., Gola, G., Chiozzi, P. & Verdoya, M., 2011: Thermophysical properties of the Po Basin rocks. Geophysical Journal International, 186, p. 69-81.

Pastakia, C.M.R. & Jensen, A., 1998: The Rapid Impact Assessment Matrix (RIAM) for EIA. Environmental Impact Assessment Reviews, 18, p. 461-482.

Peiffer, L., Wanner, C., Spycher, N., Sonnenthal, E.L., Kennedy, B.M. & Iovenitti, J., 2014: Optimized multicomponent vs. classical geothermometry: Insights from modeling studies at the Dixie Valley geothermal area. Geothermics, 15, p. 154-169.

Pereszlenyi, M., Pereszlenyiova, A. & Masaryk, P., 1999: Geological setting of the Košice Basin in relation to geothermal energy resources. Bulletin d'Hydrogeologie, 17, p. 115-122.

Phillips, J., 2010a: The advancement of a mathematical model of sustainable development. Sustainable Science, 5, p. 127-142.

Phillips, J., 2010b: Evaluating the level and nature of sustainable development for a geothermal power plant. Renewable and Sustainable Energy Reviews, 14, p. 2414-2425.

Popovičová, M. & Holoubek, D., 2011: Binary geothermal power plant using n-pentane at Ďurkov, Slovakia. Acta Metallurgica Slovaca, 2, 1, p. 172-175.

Rabinowitz M., Sempéré J-Ch. & Genthon P., 1999: Thermal convection in a vertical permeable slot: Implications for hydrothermal circulation along mid-ocean ridges. Journal of Geophysical research, 104, B12, p. 29275-29292.

Reyes, J.L.P., Lee, K., Chen, Ch.Y. & Horne, R.N., 2004: Calculation of steam and water relative permeabilities using field production data, with laboratory verification. Geothermal Resource Council Transactions, 28, p. 1-12.

Rubinstein, R.Y. & Krosese, D.P., 1991: Simulation and Monte Carlo method, 2nd Edition. Wiley-Interscience, USA.

Rybach, L., 2007: Geothermal sustainability. Proceeding European Geothermal Congress 2007, Unterhaching, Germany, p. 1-5.

Rybach, L., 2010a: The future of geothermal energy and its challenges. Proceedings World Geothermal Congress 2010, Bali, Indonesia, 8 p.

Rybach, L., 2010b: Status and prospects of geothermal energy. Proceedings World Geothermal Congress 2010, Bali, Indonesia, 8 p .

Rybach, L., 2015: Classification of geothermal resources by potential. Geothermal Energy Science, 3, p. 13-17.

Rybach, L. & Mongillo, M., 2006: Geothermal sustainability – a review with identified research needs. Geothermal Resource Council Transactions, 30, p. 1083-1090.

Rybach, L., Mégel, T. & Eugster, W.J., 1999: How Renewable are Geothermal Resources? Geothermal Resources Council Transactions, 23, p. 563-567.

Sanyal, S.K., 2005: Sustainability and renewability of geothermal power capacity. Proceedings World Geothermal Congress 2005, Antalya, Turkey, p. 1-13.

Sanyal, S.K. & Sarmiento, Z.F., 2005: Booking geothermal energy reserves. Geothermal Resource Council Transactions, 29, p. 467-474.

Sarak, H., Onur, M. & Satman, A., 2003a: Application of lumped parameter models for simulation of low-temperature geothermal reservoirs. Proceedings 28th Workshop on Geothermal Reservoir Engineering, Stanford University, CA, 9 p.

Sarak, H., Onur, M. & Satman, A., 2003b: New lumped parameter models for simulation of low-temperature geothermal reservoirs. Proceedings 28th Workshop on Geothermal Reservoir Engineering, Stanford University, CA, 8 p.

Sarak, H., Onur, M. & Satman, A., 2005: Lumped-parameter models for low-temperature geothermal fields and their application. Geothermics, 34, 6, p. 728-755.

Sarmiento, Z.F., Steingrímsson, B. & Axelsson, G., 2013: Volumetric resource assessment. Proceedings, Short Course V on Conceptual Modelling of Geothermal Systems, UNU-GTP, Santa Tecla, El Salvador.

Satman, A., 2010: Sustainability of a geothermal reservoir. Proceedings World Geothermal Congress 2010, Bali, Indonesia, p. 1-13.

Satman, A., 2011: Sustainability of geothermal doublets. Proceedings 36th Workshop on Geothermal Reservoir Engineering, Stanford University, CA, p. 1-6.

Satman, A. & Tureyen, O.I., 2012: Sustainability factors for doublets and conventional geothermal systems. Proceedings 37th Workshop on Geothermal Reservoir Engineering, Stanford University, CA, p. 1-6.

Sauty, J.P., Gringarten, A.C., Landel, P.A. & Mejoz, A., 1980: Lifetime optimization of low enthalpy geothermal doublets. In: Strub A.S., Ungemach, P. (Eds.): Advances in European Geothermal Research. D. Reidel Publications Co., NL, p. 706-719.

Sclater, J.G. & Christie, P.A.F., 1980: Continental stretching: an explanation of the post Mid-Cretaceous subsidence of Central North Sea Basin. Journal of Geophysical Research, 85, p. 3711-3739.

Sheldon, H.A., Reid, L.B., Florio, B. & Kirkby, A.L., 2011: Convection or conduction? Interpreting temperature data from sedimentary basins. Proceedings Australian Geothermal Energy Conference, Melbourne, Australia, p. 1-4.

Shortall, R., Davidsdottir, B. & Axelsson, G., 2015a: Geothermal energy for sustainable development: A review of sustainability impacts and assessment frameworks. Renewable and Sustainable Energy Reviews, 44, p. 391-406.

Shortall, R., Davidsdottir, B. & Axelsson, G., 2015b: Methodology for designing a sustainability assessment framework for geothermal energy developments. Proceedings World Geothermal Congress 2015, Melbourne, Australia, p. 1-10.

Spycher, N., Peiffer, L., Sonnenthal, E.L., Saldi, G., Reed, M.H. & Kennedy, B.M., 2014: Integrated multicomponent solute geothermometry. Geothermics, 51, p. 113-123.

Stefansson, V., 2005: World Geothermal Assessment. Proceedings World Geothermal Congress 2005, Antalya, Turkey.

Stefansson, V. & Axelsson, G., 2005: Sustainable utilization of geothermal resources through stepwise development. Proceedings World Geothermal Congress 2005, Antalya, Turkey, p. 1-6.

Sutter, D., Fox, D.B., Anderson, B.J., Koch, D.L., von Rohr, P.R. & Tester, J.W., 2011: Sustainable Heat Farming of Geothermal Systems: a Case Study of Heat Extraction and Thermal Recovery in a Model EGS Fractured Reservoir. Proceedings 36th Workshop on Geothermal Reservoir Engineering, Stanford University, CA, USA, p. 1-11.

Takahashi, S. & Yoshida, S., 2016: Improvement of calculating formulas for volumetric resource assessment. Geothermics, 64, p. 187-195.

Tester, J.W., Anderson, B.J:, Batchelor, A.S., Blackwell, D.D., DiPippo, R., Drake, E.M., Garnish, J., Livesay, B., Moore, M.C., Nichols, K., Petty, S., Toksoz, M.N. & Veatch Jr., R.W., 2006: The future of geothermal energy. Massachusetts Institute of Technology, 372 p.

Tureyen, O.I. & Akyapi, E., 2011: A generalized non-isothermal tank model for liquid dominated geothermal reservoirs. Geothermics, 40, p. 50-57.

Tureyen, O.I., Onur, M. & Sarak, H., 2009: A generalized nonisothermal lumped-parameter model for liquid dominated geothermal reservoirs. Proceedings 34th Workshop on Geothermal Reservoir Engineering, Stanford University, CA, p. 1-10.

Tureyen, O.I., Kirmaci, A. & Onur, M., 2014: Assessment of uncertainty in future performance predictions by lumped-parameter models for single-phase liquid geothermal systems. Geothermics, 51, p. 300-311.

Ungemach, P., Antics, M. & Papachristou, M., 2005: Sustainable geothermal reservoir management. Proceedings, World Geothermal Congress Antalya, Turkey.

Ungemach, P., Papachristou, M. & Antics, M., 2007: Renewability versus Sustainability. A reservoir management approach. Proceedings, European Geothermal Congress 2007, Unterhaching, Germany.

Ungemach, P., Antics, M. & Lalos, P., 2009: Sustainable geothermal reservoir management practice, Geothermal Resources Council Transactions, 33, p. 885-891.

Utlu, Z. & Hepbasli, A., 2008: Energetic and exergetic of the industrial sector at varying dead (reference) state temperatures: A review with an illustrative example. Renewable and Sustainable Energy Reviews, 12, p. 1277-1301.

Vizi, L., Fričovský, B., Zlocha, M. & Surový, M., 2020: Use of geostatistical simulation in reservoir thermodynamics assessment and interpretation at the Ďurkov hydrogeothermal structure, Slovakia. Slovak Geological Magazine, 20 (1), [this issue].

Vranovská, A. & Bodiš, D., 1999: Survey for prospective utilization of geothermal energy in Košice Basin. Bulletin d'Hydrogeologie, 17, p. 106-113.

Vranovská, A., Bodiš, D. & Drozd, V., 1999a: Zhodnotenie hydrogeotermálnej štruktúry Ďurkov na základe vrtov GTD-1,2 a 3 [*Evaluation of hydrogeothermal structure Ďurkov based on wells GTD-1,2 and 3*]. Podzemná voda, V (2), p. 45-53.

Vranovská A., Bondarenková,Z., Král M. & Drozd, V., 1999b: Košická kotlina - štruktúra Ďurkov - hydrogeotermálne zhodnotenie, vyhľadávací prieskum. [*Košice Basin – Ďurkov structure, hydrogeothermal evaluation, exploratory survey*]. Manuscript – Technical report. Bratislava: SLOVGEOTERM, Geofond Archive, 90 p. [in Slovak].

Vranovská, A., Beňovský, V., Drozd, V., Halás, O. & Váňa, O., 2000: Investigation for geothermal energy utilization in the town Košice, Slovak Republic. Proceedings World Geothermal Congress 2000, Kyushu-Tohoku, Japan, p. 1-6.

Vranovská, A., Beňovský, V., Drozd, V., Halás, O. & Váňa, O., 2002: The results of pilot test in Ďurkov hydrogeotermal structure. Geol. Carpathica, 53 (2), p. 1-6.

Vranovská, A., Bodiš, D., Šráček, O. & Ženišová, Z., 2015: Anomalous arsenic concentrations in the Ďurkov carbonate

geothermal structure, eastern Slovakia. Environmental Earth Science, 73, p. 7103-7114.

Williams, C.F., 2007: Updated methods for estimating recovery factors for geothermal resources. Proceedings, 32nd Workshop on Geothermal Reservoir Engineering, Stanford University, CA.

Williams, C.F., 2014: Evaluating the volume method in the assessment of identified geothermal resources. Geothermal resource council transactions, 38, p. 967-974.

Williams, C.F., Lawless, J.V., Ward, M.A., Holgate, F.L. & Larking, A., 2010: A code for geothermal resources and reserves reporting. Proceedings world geothermal congress 2010, Bali, Indonesia.

Williams, C.F., Reed, M.J. & Anderson, A.F., 2011: Updating the classification of geothermal resources. Proceedings, 36th Workshop on Geothermal Reservoir Engineering, Stanford University, Stanford, California.

Yasukawa, K. & Sasada, M., 2015: Country update of Japan: Renewed Opportunities. Proceedings World Geothermal Congress 2015, Melbourne, Australia, p. 1-6.

Yousefi, H., Ehara, S., Yousefi, A. & Seiedi, F., 2009: Environmental impact assessment of Salaban geothermal power plant, NW Iran. In: Proceedings 34th Workshop on Geothermal Reservoir Engineering, Stanford University, CA, p. 1-9.

Slovak Geol. Mag., 20, 1 (2020), 85 – 98

4. Use of Geostatistical Simulation in Reservoir Thermodynamics Assessment and Interpretation at the Ďurkov Hydrogeothermal Structure, Slovakia

Vizi Ladislav, Fričovský Branislav, Zlocha Marian & Surový Martin

State Geological Institute of Dionýz Štúr, Mlynská dolina, Bratislava, Slovak Republic, ladislav.vizi@geology.sk

Abstract: Geothermal energy in Slovakia is under a systematic research since 70's of the last Century. Out of 27 identified prospective geothermal fields within a territory of the Western Carpathians, the Ďurkov hydrogeothermal structure in the Košice Depression is repeatedly accented as of the most enormous potential for a heat (and in some, rather wishful, plans for power) production. Unlike a conventional evaluation of thermal potential and temperature, this study aims at description of the reservoir under an exergy concept; quantifying reservoir enthalpy, exergy and specific exergy index based on geostatistical modelling prior classifying a system according to a thermodynamic quality.
Geostatistical simulations have become very popular in different areas of spatial modelling for spatial simulation of properties, geometries or heterogeneities. The geostatistical approach is supportive to quantification and interpretation necessary to understand for reservoir engineering and construction of reservoir prediction and response models. Turning band method of simulation was used to create multiple realisations of the convection indicators within the reservoir body due to evident non-stationary behaviour, mainly in vertical direction, which made it impossible to use Gaussian type model. Non-conditional simulations were tested conditioned by universal kriging using modelled variograms of global trend residuals with respective drift functions for each studied variable. The risk volumetric curves were derived from final numerical models and probable reservoir volumes above different boundary conditions (cut-offs) were calculated and visualised. Based on numerical models, reservoir enthalpy greater than 800 $kJ.kg^{-1}$ has been identified in deeper parts of a system with very small proportion of specific exergy index above 0.2. Thermodynamic data, and models based on them, show the resource is rather suitable for a large-scale heat (district heating) production – supply.
Key words: thermodynamic quality, reservoir enthalpy, geostatistics, simulation, volumetrics

4.1 Foreword

The Slovak Republic is a low atmosphere harmful substances (AHS) country with mean yearly emissions of 25 % below a ratified level. Although, national economy is still fossil-fuels oriented. Indeed, renewables contribute only 23 % on domestic electricity and 19 % on domestic heat primary energy consumption. By a contrast, onset of systematic research and development of geothermal energy dates back to the 70's of the last Century, progressively increasing a number of geothermal installations in a direct-use from 43 MWt in 1980 (Franko et al., 1990) to 149 MWt in 2015, not including heat pumps (Fendek & Fendeková, 2015). Recent global environmental constraints prompt, however, the country towards renewables. With 27 geothermal water bodies covering roughly 40 % of the country identified (Fendek & Fendeková, 2010), the geothermal energy appears of a significant potential, assumed app. 6,500 MWt in probable reserves.

The Ďurkov hydrogeothermal structure has been recognized the most prospective system amongst the all (e.g. Vranovská et al., 2000). Even several plans on district heating individual (e.g. Halás et al., 1999) or binary geothermal power plants bound (Kukurugyová et al., 2015) exist already, a conceptual, engineering approach to analyze the geothermal resource is still missing. Preliminary studies based on a borehole data classified the structure as of moderate-low exergy (Fričovský et al., 2016a, b). This paper presents a first insight into local reservoir thermodynamics and thermodynamic quality mapping.

4.2 Background

4.2.1 General consideration

Hydrogeological conditions triggering evolution of geothermal resources in Slovakia owe to lateral extension and vertical position of prospective Middle Triassic carbonates organized in multiple superpositioned nappes, resultant to Alpine tectonics; and Neogene Germanic-type neotectonics, forming deep sedimentary basins associating a resource with sands and sandstones in major (Franko & Melioris, 1999). Heat flux and accumulation outlines as consequent to different structure and depths of neotectonic blocks, overall crustal thickness and non-uniform mantle propagation, seating and depth of major crustal faults; and spatial distribution of Neogene – Early Pleistocene neovolcanism (Fendek et al., 1999). Still, geothermal plays in the Western Carpathians (Slovakia) are conduction-dominated, orogenic belt-type (Moeck, 2014).

Two different regions of geothermic activity are distinguished within the Western Carpathians. Intramountain depressions show rather low to moderate heat flux density (q = 60 – 90 $mW.m^{-2}$). This increases within Neogene deep sedimentary basins towards q = 90 – 120 $mW.m^{-2}$ (Franko & Melioris, 1999), classified moderate-high to high in local conditions. Amongst the latter is the Košice Depression (Fig. 4.1), terminated along Neogene volcanic range of the Slanské vrchy Mts. to east and a core-mountain massif of the Slovenské Rudohorie Mts. to the west (e.g. Vranovská et al., 2015).

4.2.2 Site description

The Ďurkov hydrogeothermal structure (DDHS) represents a depressed morphostructure of Mesozoic carbonates beneath, in vast majority, Neogene sedimentary basin fill in the western part of the Košice Depression. To the west, the structure terminates along a N-S trended fault zone parallel with the line connecting towns of Vyšný Čaj – Olšovany – Ďurďošík – Trsťany. Eastern margin corresponds with deep extension of the Neogene volcanites. A northern limit corresponds to the tectonic contact with the pre-Tertiary Bidovce Depression, whilst to the south, the system is delineated arbitrary to the uplifting blocks of Mesozoic carbonates along a Ruskov – Vyšný Čaj line (Fig. 4.1).

4.2.3 Deep geological structure

The Košice Depression as a neotectonic morpho-structure is resultant to the Neogene Germanic-type tectonics. In general, Quaternary exclusively terrestrial accumulations, Neogene sedimentary to minor volcanosedimentary formations and Mesozoic carbonates form a relevant deep geological structure. A crystalline beneath has not been subjected to a study yet. Obviously, the Quaternary accumulations (fluvial, proluvial and deluvial forms) are only several meters thick; thus, are usually neglected in vertical and horizontal extension. A thickness of the Neogene profile reaches up to 2,000 – 3,000 m within the structure. Atop, Sarmatian clays with rare rhyolite and andesite volcanoclastics are 200 – 1,000 m thick (Vranovská et al., 1999a). Beneath, carbonate sandy clays alternating sparsely with tuffites form up to 1,500 m thick Badenian part of the profile. Carbonate claystones with minor sandstones and basal brecciated conglomerates represent a bottom 400 – 600 m thick base of the Neogene succession (Vranovská et al., 2015).

Middle Triassic dolomites represent an analogue to the Krížna Nappe series of the Western Carpathians. Because of the tectonic dissection of the Košice Depression, a thickness of the Mesozoic profile varies between 200 – 2,000 m (Vranovská et al., 1999a), increasing pseudo-axially in the NW-SE and SW-NE direction. It is generally assumed that the greatest thickness corresponds to the major depression of the DDHS in the Ďurkov town area. However, the entire structure is dissected into several elevated and depressed blocks of the Mesozoic carbonates beneath the Neogene sedimentary cover along multiple faults; i.e. those of N-S and SW-NE trend in major.

A geochemical modelling conducted to explain high arsenic concentrations (cAs = 19 – 36 mg.l^{-1}) in Na-Cl type geothermal water associated with the DDHS (TDS = 20,000 – 30,000 mg.l^{-1}) has proven the system as hydrogeologically closed (Bodiš & Vranovská, 2012; Vranovská et al., 2015). A lack of natural reservoir recharge is amongst the most pronounced in considering of closed-loop systems at the site.

4.3 Methodology and approach

Under theoretical considerations, renewability of a geothermal resource at natural (initial, reservoir, etc.) conditions can be attributed to the closed thermodynamic

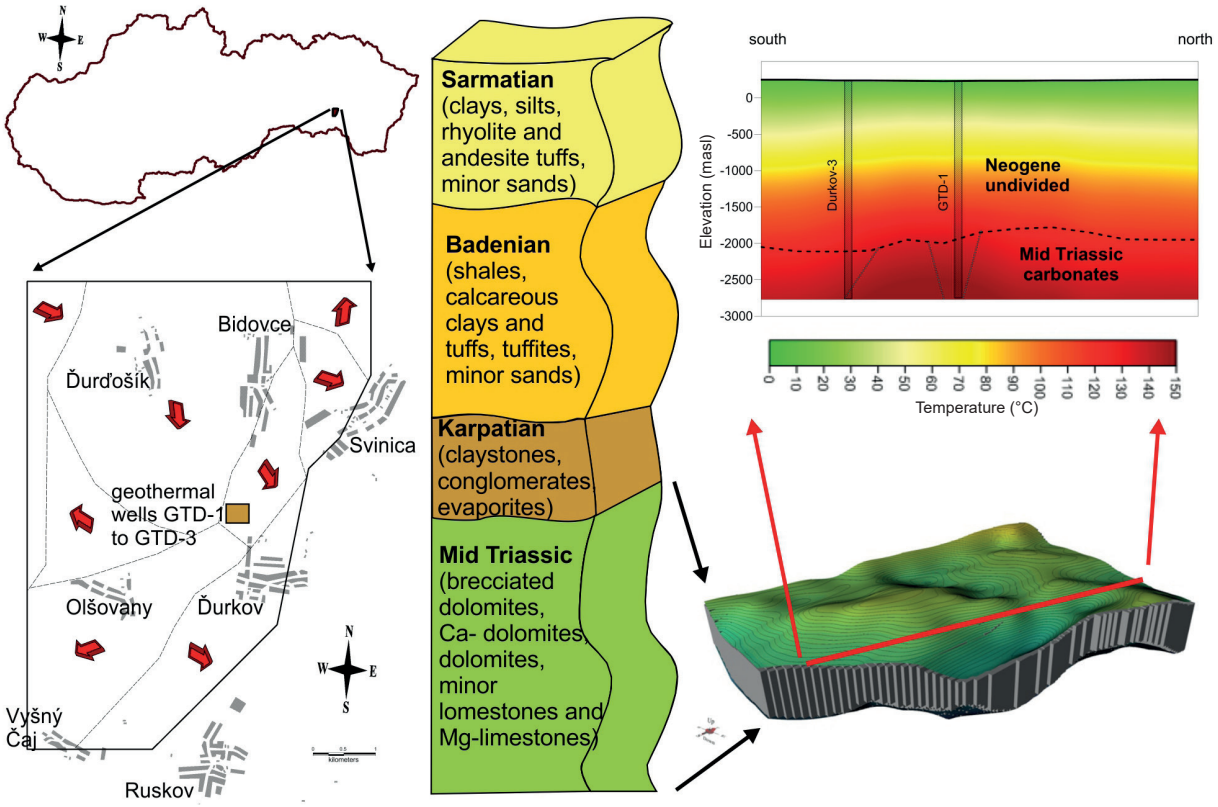

Fig. 4. 1. *Site definition of the Ďurkov Depression hydrogeothermal structure; tectonic segmentation with direction and slope of tectonic blocks; vertical profile and lithology, temperature profile and a reservoir body.*

system. As such, the 1st Law of Thermodynamics is adequate enough, whilst the resource and the system can easily be described according initial-state conditions; i.e. the temperature. However, resource production is an artificial aspect of geothermal energy utilization, far beyond a thermodynamic concept of a closed system. Indeed, multiple irreversibilities apply, the 2nd Law of Thermodynamics must be considered.

4.3.1 A concept of exergy

According to the 1st Law of Thermodynamics, the energy of the closed system at initial (natural) conditions is a conservative measure (1) well described along a balanced enthalpy flow (2). The latter neglects heat and work transfers (Ozgener et al., 2005, 2007):

$$\dot{Q}_{in} - \dot{Q}_{out} + \sum m_{in}.h_{in} = \dot{W}_{in} - \dot{W}_{out} + \sum m_{out}.h_{out} \quad (1)$$

$$\sum m_{in}.h_{in} = \sum m_{out}.h_{out} \quad (2)$$

where $\dot{Q}$ is heat transfer rate, is the mass flow, is the work rate, and h is the enthalpy; symbols "in" and "out" refer to system inlet/outlet conditions.

Under artificial production, the state of the system changes, and multiple irreversibilities apply as the entropy generates. Then, only a part of an energy can be sufficiently converted into a useful work – the exergy (DiPippo, 2005), also denoted as a thermodynamic quality (Lee, 1996). Unlike the energy, the specific exergy (3) is rather consumed or destroyed during a resource utilization due to entropy generation (Ozgener et al., 2005):

$$e = \left(h_{DP} - h_{RC}\right) - T_{RC}\left(s_{DP} - s_{RC}\right) \quad (3)$$

where e is the specific exergy, h is the enthalpy, T is the temperature, and s is the entropy; indexes "*DP*" and "*RC*" refer to a definition and reference point respectively.

A maximum thermodynamic quality (exergy) is achieved if the system transfers from definition to the dead-state p-T conditions. The latter corresponding to the triple-point (4):

$$e = h_{DP} - 273 s_{DP} \quad (4)$$

where e is the specific exergy, h is the enthalpy, and s is the entropy; index "*DP*" refers to a definition point.

Otherwise, pseudo-dead state conditions can be specified (Ozgener et al., 2006) variously; whether at reinjection or spill, a condenser etc. A definition point is typically defined to the borehole inlet or wellhead, as this takes an advantage in a fact that this is a first point where the resource can actually undergo a conversion process or can generate work (Lee, 2001).

4.3.2 A concept of specific exergy index classification

Geothermal resources (fields) tend to get subjected both for quantitative and qualitative analysis. In exergy concepts, the quantitative definition of thermodynamic quality relates to the specific exergy index – *SExI* (Lee, 1996, 2001) calculation. Instead of some arbitrary criteria, such as it is with the temperature, this is a normalized parameter (5) relating a maximum exergy of the system theoretically available, to the maximum exergy of a saturated steam at p = 90 Bar-abs and T = 303 °C with a triple point sink condition; i.e. e = 1,192 kJ.kg^{-1} (Lee, 2001):

$$SExI = \frac{h - 273.16s}{1192} \quad (5)$$

where *SExI* is the specific exergy index, and h and s refer to the geothermal resource enthalpy and entropy at a definition point.

To map thermodynamic quality, Lee (1996, 2001) introduced several limits: a *SExI* = 0.5 represents a thermodynamic quality of saturated steam at p = 0.1 MPa and T = 100 °C, whilst a *SExI* = 0.05 describes a thermodynamic quality of saturated water at T = 100 °C and p = 0.1 MPa. Thus, the *SExI* = 0.2 represents a limit for double-phase system at p = 2 MPa and h = 1,000 kJ.kg^{-1}. Under given criteria set, geothermal resources can be classified as:

a) low thermodynamic quality exergy; *SExI* < 0.05 (typically single-phase, water dominated geothermal fields)
b) moderate-low thermodynamic quality / exergy; 0.05 ≤ *SExI* < 0.2 (two-phase, water dominated geothermal fields)
c) moderate-high thermodynamic quality / exergy; 0.2 ≤ *SExI* < 0.5 (typically two-phase, vapour dominated geothermal fields)
d) high thermodynamic quality / exergy; *SExI* ≥ 0.5 (single phase dry steam, two-phase vapour dominated geothermal fields).

Along with numerical consideration, geothermal resources are frequently analyzed using Mollier's and Rant's diagrams, plotting enthalpy to entropy and entropy to the specific exergy of the resource respectively. Since introduction, the concept of exergetic (engineering) classification has been successfully applied in analyses of geothermal fields in Turkey (Etemoglu & Can, 2007), Poland (Barbacki, 2012), Japan (Jalilinasrabady & Itoi, 2013), Mexico (Ramajo et al., 2010) or in Slovakia (Fričovský et al., 2016a, b).

4.4 Geostatistical modelling

Geostatistics is a rapidly evolving scientific branch of applied statistics and mathematics that studies the spatial-temporal phenomena and thus extends the concept of traditional statistical methods of data processing in a spatial form. It was originally developed by George Matheron of Centre de Morphologie Mathématique in France for solving the problems of the ore reserve estimation in the mining industry but it is nowadays very popular not only in geology but also in many other areas of the natural science. Spatial data, in the framework of geosciences, exhibit some degree of spatial correlation, which is a function of the distance – the greater distance between samples, the lower

similarity between the data, but on the contrary, the higher is their variability (Matheron, 1963). The paper does not intend to present a deep review of geostatistics with all its algorithms and methods. A number of geostatistical books are available that document the principles, methods and techniques, including for instance Journel & Huijbregts (1978), Isaaks & Srivastava (1989), Clark & Harper (2000), Armstrong (1998), Goovaerts (1997), Webster & Oliver (2001), Wackernagel (2003), Chilès & Delfiner (2000), Olea (1999), Lantuéjoul (2002), Leuangthong et al. (2008), etc. Tonnes of notes, courses and papers have been published to study the topic. Since its definition in 1962 by George Matheron, initially developed for ore reserve estimation problems in the mining industry, geostatistics has evolved extremely, including many methods, techniques and approaches for spatial modelling of natural phenomenon in the Earth sciences. From mining, geostatistics has spread and has become an important methodology in many fields of application like petroleum industry, geology, climatology, agriculture, soil science, forestry etc. For these reasons, only a very brief introduction of geostatistics and very basic principles and terms will be given in this section.

Geostatistics provides a wide variety of tools to quantify and model the degree of spatial similarity and spatial variability. The aim of geostatistical methods for modelling of spatial variability is a random variable Z distributed in space and/or time. In geostatistical applications, a random variable is a function of spatial coordinates at any point of the studied area, in which each point $\mathbf{u}$ is determined by geographic (and/or time) coordinates in one, two or three-dimensional space; $\mathbf{u}$ = (X, Y, Z). Set of such random variables at each point $\mathbf{u}$ of the studied domain D represents a random function $Z(\mathbf{u})$. One realisation of a random function, or one realisation of each random variable in the space, consists of a set of values $z(\mathbf{u})$ called a regionalised variable (Matheron, 1971).

In geostatistical application, a random function $Z(\mathbf{u})$ can be expressed as the sum of two parts (Dowd, 2004):

1. A deterministic part $m(\mathbf{u})$, called *drift* or *trend*, represented by a deterministic function of location (linear, quadratic, etc.).
2. A stationary random function $R(\mathbf{u})$ with a constant mean that represents the deviation from the mean $m(\mathbf{x})$, so called residuals, and can be estimated by the standard techniques of stationary methods.

The above terms yield to the following expression of the random function $Z(\mathbf{u})$:

$$Z(\mathbf{u}) = R(\mathbf{u}) + \underbrace{m(\mathrm{u})}_{\mathrm{E}[Z(\mathbf{u})]}. \tag{6}$$

If we assume that the mean $m(\mathbf{u})$ is constant, then we have the basis for the geostatistical methods of overcoming the problems imposed by stationarity. A decision of stationarity of available data used for spatial modelling is necessary for all geostatistical modelling. However, as stated by Journel (1986), stationarity is a constitutive property of the random function and not an intrinsic property of the studied phenomenon and therefore a decision about stationarity is, in fact, a model itself.

4.4.1 Variogram

The variogram is the basic structural tool to model spatial continuity in geostatistical applications. It represents bivariate statistics, which express the variability of increments of the values z of random variables Z at points $\mathbf{u}$ separated by a vector $\mathbf{h}$. This direct variogram can be expressed as follows:

$$2\gamma_Z(\mathbf{h}) = \mathrm{E}\lfloor \{Z(\mathbf{u}) - Z(\mathbf{u}+\mathbf{h})\}^2 \rfloor = 2[\mathrm{C}_Z(0) - \mathrm{C}_Z(\mathbf{h})] \tag{7}$$

where $\mathrm{C}_Z(\mathbf{h})$ represents covariance between $Z(\mathbf{u})$ and $Z(\mathbf{u} + \mathbf{h})$ with constant mean m and $\mathrm{C}_Z(0) = \mathrm{Var}[Z(\mathbf{u})] = \sigma^2$ represents apriori variance of $Z(\mathbf{u})$. The variogram in (7) is valid only for stationary or weak stationary random processes (Matheron, 1971).

The expression (7) simply describes how the values of Z at two points $\mathbf{u}$ and $\mathbf{u} + \mathbf{h}$ become different as the separation vector $\mathbf{h}$ between pairs of points increases. Graphically, the variogram is a positive function increasing with $\mathbf{h}$ and it describes the change of the spatial variability of the studied features in the studied area for any distance and any direction of space (Armstrong, 1998).

The final model of the variogram describes the change of the spatial variability and, consequently, it is used in the geostatistical modelling. The main role of geostatistics is to make an estimation of the unknown value at unsampled locations.

4.4.2 Kriging

The geostatistical estimation procedure is called kriging, developed by George Matheron in 1963, and it is named in honour of Daniel G. Krige, following his university thesis. Nowadays, under kriging we understand "a collection of generalized linear regression techniques for minimizing an estimation variance" (Olea, 1991) that is used to estimate unknown values at unsampled locations using surrounding data $z(\mathbf{u}_\alpha)$. It is beyond the scope of the paper to present all different kriging techniques due to their wide variation. The paper presents the general model named universal kriging (abbr. UK). Matheron (1971) assumes that the mean in (1) can be written in a form of finite polynomial of order K, or trend, in practise of first or second order:

$$m(\mathbf{u}) = \sum_{k=0}^{K} a_k \mathbf{u}^k \tag{8}$$

Since kriging is a method of a linear regression, a weighted linear estimator at unsampled location $\mathbf{u}_\mathrm{o}$ in the stationary case where the mean m is known can be written as:

$$z^*(\mathbf{u}_\mathrm{o}) - m = \sum_{\alpha=1}^{n(\mathbf{u}_\mathrm{o})} \omega(\mathbf{u}_\alpha)\big(z(\mathbf{u}_\alpha) - m\big) \qquad \text{or shortly}$$

$$z^*_\mathrm{o} = \sum_{\alpha=1}^{n_\mathrm{o}} \omega_\alpha \underbrace{\big(z_\alpha - m\big)}_{\text{residuals } r_\alpha} \tag{9}$$

where ω_α are the weights assigned to the n_o data z_α within a search neighbourhood available for estimation. The estimation variance for universal kriging is given by (Dowd, 2004):

$$\sigma_e^2 = \mathrm{Var}\left[Z_o^* - Z_o\right] = 2\sum_{\alpha=1}^{n_o}\omega_\alpha\gamma_{\alpha o}^R - \sum_{\alpha=1}^{n_o}\sum_{\beta=1}^{n_o}\omega_\alpha\omega_\beta\gamma_{\alpha\beta}^R - 2\sum_{k=0}^{K}\lambda_k\left(\sum_{\alpha=1}^{n_o}\omega_\alpha\mathbf{u}_\alpha^k - \mathbf{u}_o^k\right) \quad (10)$$

with sample-to-sample variogram of residuals $\gamma_{\alpha\beta}^R$, sample-to-target variogram $\gamma_{\alpha o}^R$ and a set of Langrange multipliers λ_k for a given trend order K.

The weights ω_α in equation (9) are derived by minimizing of the estimation variance (10) and solving a kriging system of linear equation:

$$\begin{cases} \sum_{\beta=1}^{n_o}\omega_\beta\gamma_{\alpha\beta}^R + \sum_{k=0}^{K}\lambda_\alpha^k f_\alpha^k = \gamma_{\alpha o}^R \quad \forall\alpha \\ \sum_{\alpha=1}^{n_o}\omega_\alpha f_\alpha^R = f_o^k \quad \forall k \end{cases} \quad (11)$$

Associate kriging variance, independent of available data values, becomes:

$$\sigma_K^2 = \sum_{\alpha=1}^{n_o}\omega_\alpha\gamma_{\alpha o}^R - \sum_{k=0}^{K}\lambda_k\mathbf{u}_o^k. \quad (12)$$

4.4.3 Geostatistical simulations

The aim of kriging is to produce the best accurate estimation of the mean value of a random variable Z at an unsampled location $\mathbf{u}_o$, $E[Z(\mathbf{u}_o)]$ in the sense of the least-square method because of minimizing the local estimation variance σ_e^2. The spatial structure of the estimated values differs from that of the actual ones (de Fouquet, 1993). The map of kriged estimates is interpreted as a set of expectations of the random variables at all locations $\mathbf{u}_o$ and tends to smooth out the local variability of the data. That means that low values are overestimated whereas high values are underestimated. The smoothing effect of kriging is a serious disadvantage when trying to reproduce the extreme values. One important fact is that the smoothing effect of kriging depends on the data location – smoothing is smaller close to the data location and conversely. The final kriged map is therefore less variable than the data.

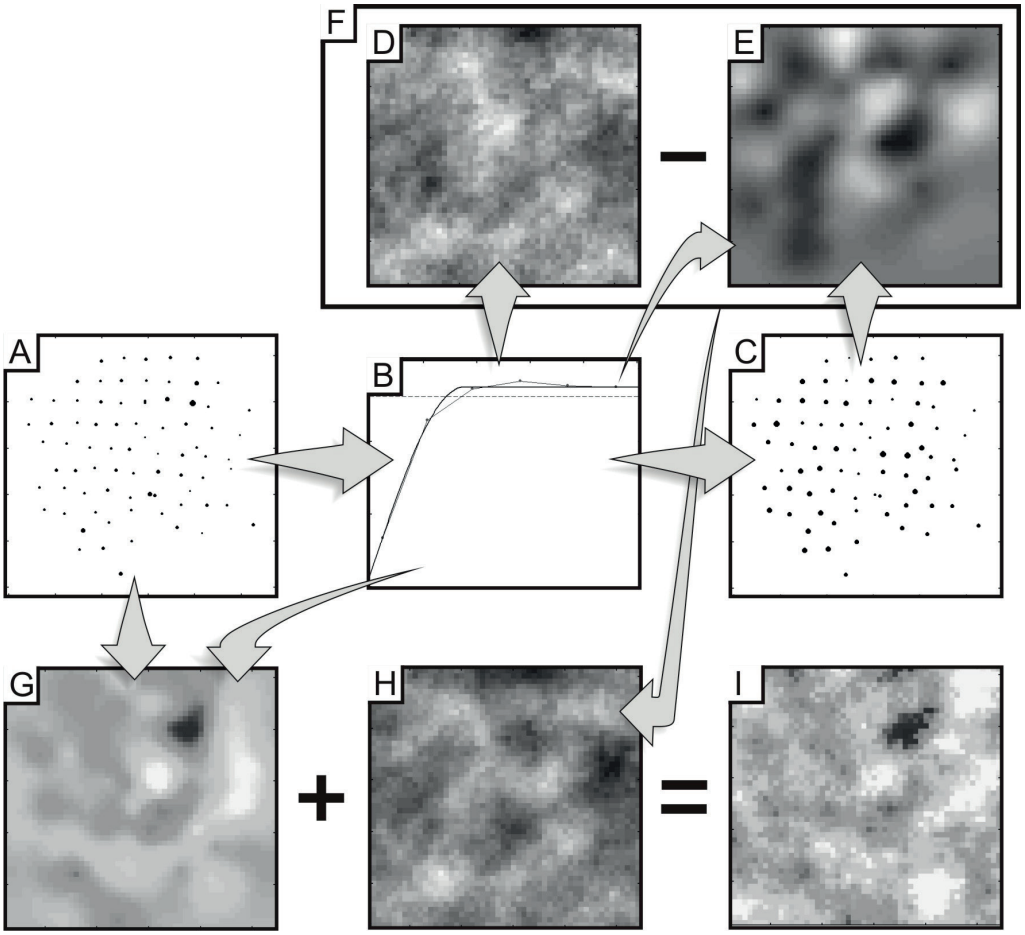

Fig. 4.2. *The values at sampling locations (A) are used to construct a variogram model (B). The model of variogram is used to simulate the values of the non-conditional simulation at the sample location to obtain $z_{NS}(\mathbf{x}_\alpha)$ (C) as well as on the grid nodes to get non-conditional simulation $Z_{NS}(\mathbf{x})$, which represents a reality with the same variability pattern as the sample values (D) Non-conditional simulation values at the sample locations $z_{NS}(\mathbf{x}_\alpha)$ are kriged on the grid nodes using the variogram model (B) to get a smooth estimation of the non-conditional simulation (E). Difference between non-conditional simulation and kriged non-conditional simulation gives a kriging error – a natural error, which appears when a reality is estimated from the samples (F). Conditional simulation (I) is finally built up by adding the simulated kriging error (H) to the kriging estimation of a regionalized variable (G) using the sample data (A) and the variogram model (B).*

Stochastic simulation produces the maps of realisations $z_s(\mathbf{u}_o)$ of a set of random variables $Z(\mathbf{u}_o)$ at all unsampled locations $\mathbf{u}_o$. The aim of the simulation is to randomly draw several realisations of the random function that reflect the variability of the sample values (data histogram and variogram). Each simulated realisation represents a possible version of reality coherent with the data values and a used model of variability as well. A simulation that does not honour the experimental data values is called non-conditional simulation (NS). There are many methods for generating a realisation of the non-conditional simulation (for example sequential methods, spectral methods, LU covariance matrix decomposition, turning bands, etc.). Each method has its own advantages and disadvantages, as may be seen for example in Chilès & Delfiner (1999) or Lantuéjoul (2002). In general, non-conditional simulation is one possible realisation of a random function that has the same variogram model as the one modelled from the sample data, but it is otherwise totally unrelated to them (Chilès & Delfiner, 1999). Non-conditional simulation is conditioned by kriging. Conditioning is a process by which we can pass from a non-conditional simulation Z_{NS} to a conditional simulation Z_{CS} that match the sample points $z(\mathbf{u}_\alpha)$ of random function $Z(\mathbf{u})$. Non-conditional and conditional simulations are independent, but with the same variogram model. Conditional simulation $Z_{CS}(\mathbf{u})$ is built by adding the kriging error $[Z(\mathbf{u}) - Z_K^*(\mathbf{u})]$ to the kriging estimation $Z_K^*(\mathbf{u})$. However, the kriging error is unknown because $Z(\mathbf{u})$ is not known. Therefore the kriging variance is replaced by non-conditional simulation of the kriging variance $[Z_{NS}(\mathbf{u}) - Z_{NS}^*(\mathbf{u})]$ where non-conditional simulation $Z_{NS}(\mathbf{u})$ is known on a simulated grid and is based on the variogram modelled from the sample data. Estimation of the non-conditional simulation $Z_{NS}^*(\mathbf{u})$ is based on kriging of the values of the non-conditional simulation at the sample locations $\mathbf{x}_\alpha$ using the same variogram model (Fig. 4.2).

A set of L independent and equal probable realisation of random function from conditional simulation constitutes a numerical model. Simulation post-processing and ranking of the realisations from the smallest realisation to the largest one enables us to construct an inverse distribution curve for any single cell of simulated grid, a group of cells or the entire area under consideration. The curve represents a probability, or risk curve.

The Turning Band (TB) algorithm was selected for simulation of the studied variables. It was the earliest algorithm for simulation of autocorrelated random processes in two or three dimensions (Deutch & Journel, 1998). The principle is to produce a non-conditional simulation that reflects the variogram but does not honour the input data. Independent one-dimensional realisations are first simulated along lines radiating from central points. Then, each point in 3D space is orthogonally projected into every line and the simulated values nearest to the projected points are averaged. The non-conditional simulation is then conditioned by kriging, which is used to interpolate the experimental error between data and non-conditional simulated values at the data points. The TB algorithm is suitable for all covariance models, does not assume Gaussian type model (Chilès & Delfiner, 1999) and it is great compromise between quality and computing time.

4.4.4 Input data and output geometry

Creation of final model began with a primary reservoir body dissection into 150 points regularly spaced of 500x500 m located on the top surface of the reservoir. Then, the reservoir was vertically divided into proportionally distributed 10 sublayers according to an overall reservoir thickness at given point on top reservoir surface. Thus, the studied hydrogeothermal reservoir Ďurkov was subdivided into 1,650 calculation points **u** in total.

Figs. 4.3 A and D show experimental histograms of both studied variables with used boundary conditions (or cut-offs):

1. Enthalpy h being equal or greater than 800 kJ.kg^{-1} ($h \geq 800$ kJ.kg^{-1}),
2. Specific exergy index *SExI* being equal or greater than 0.05 and 0.2 ($SExI \geq 0.05$, $SExI \geq 0.2$).

The experimental histogram of enthalpy shows approximately 10 % of its values above 800 kJ.kg^{-1} (166 calculated values of total 1,650) with their mean value 873 kJ.kg^{-1}. The histogram of specific exergy index shows almost 99 % its values above 0.05 (1,634 of 1,650) with the mean value 0.11 but it gets only 2 % values above 0.2 (34 of 1,650) with the mean value 0.215.

Fig. 4.4 shows spatial pattern and distribution for both studied variables. The spatial distributions look the same; differ only in scale. There is also a strong trend in the values increasing from the top to the bottom of the reservoir. That indicates a non-stationary phenomenon. As a matter of fact, the calculated variables of the specific enthalpy h and specific exergy index *SExI*, described in section 3, are function of temperature, which is, in fact, function of depth. Therefore, a non-stationary model was considered during spatial modelling phase under assumption of systematic increasing the values of studied variables in vertical direction. To build the non-stationary model, the first step consisted in modelling a trend function by means of the least square polynomial method fitting. Under assumption of stationarity in a horizontal plane XY; a linear model in form of $m(z) = a_0 + a_1 Z$ was fitted to obtain a stationary residual variables $R_h(\mathbf{u}_\alpha)$ and $R_{SExI}(\mathbf{u}_\alpha)$ The final residuals follow a normal distribution with zero means (Figs. 4.3 B and E, respectively).

Reservoir geometry is based on a multi-parametric model with inputs from borehole lithology, logging, seismic profiles and morphostructural maps (Vranovská et al., 1999b) and other hardcopy or grid data (Pachocká et al., 2010). Stationary thermodynamic data derivation succeeded geothermic calculations (temperature, heat flux, radiogenic heat production, etc).

The points with calculated variables under study served to model reservoir matrix prior processing in a refined 3D model with more than 1.4 million grid nodes with regular spacing 50x50x10 m for using of geostatistical simulations

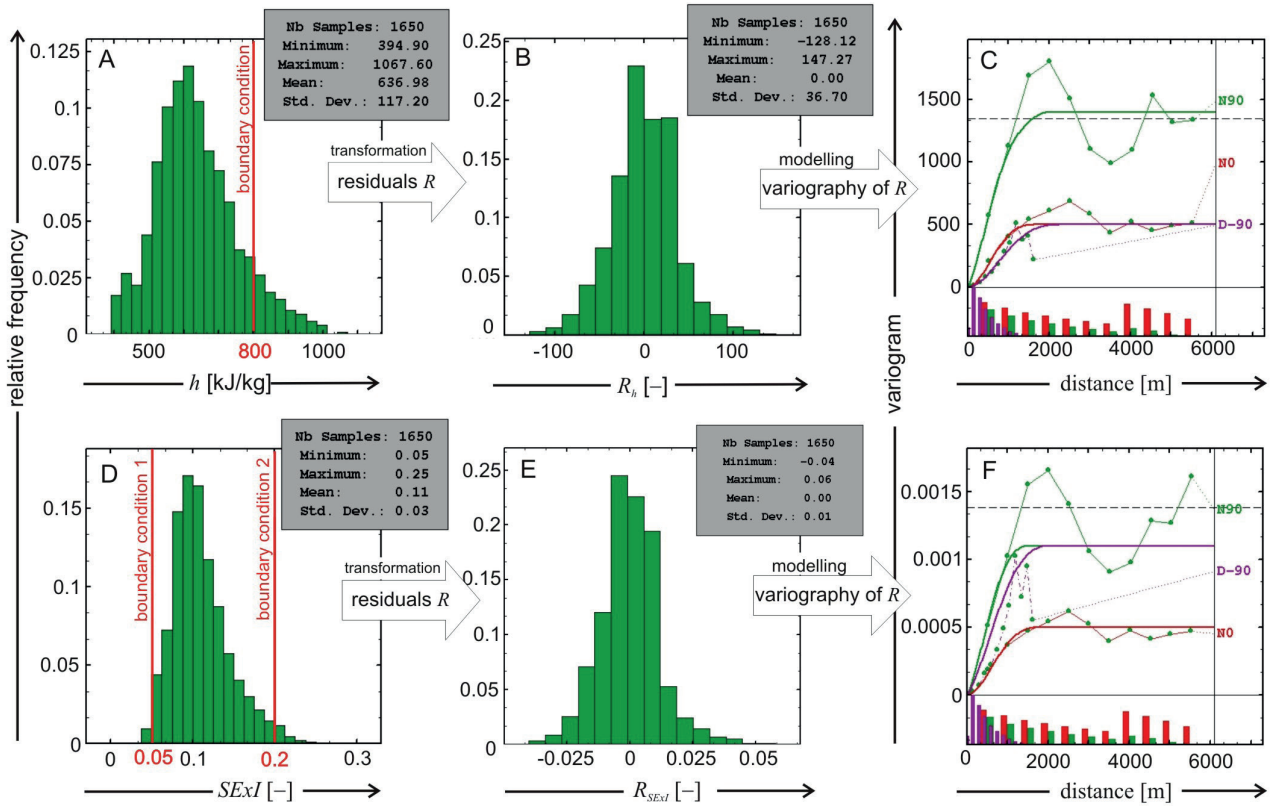

Fig. 4.3. *Experimental histogram of raw calculated data (A, D) their respective histograms of residuals (B, E) and final variogram models of residuals (C, F).*

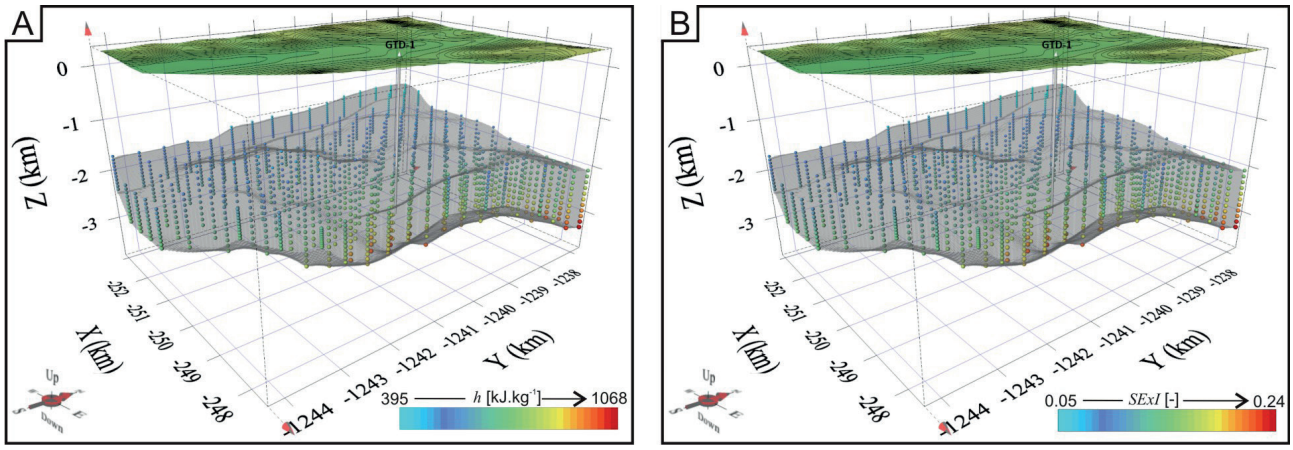

Fig. 4.4. *Spatial arrangement of 1,650 calculated sample points within 3D regular grid of Ďurkov reservoir shown in transparent grey. The sample points are coloured in accordance with the studied variable values for enthalpy (A) and specific exergy index (B).*

to create numerical models of the variables. It gives more than 35 milliards m^3 of total gross volume of the Ďurkov reservoir.

The experimental variograms were calculated for the residual variables: two experimental variograms in N-S and E-W directions in horizontal planes with lag distance 500 m in accordance with the sample spacing, and one experimental variogram in vertical direction. Nested basic structures of spatial variability were fitted to the directional experimental variogram to build variogram models. The final variogram models of calculated residuals are shown in Fig. 4.3 C for $R_h(\mathbf{u}_\alpha)$ and Fig. 4.3 F for $R_{SExI}(\mathbf{u}_\alpha)$. Both variogram models perfectly fit the directional experimental variograms with low nugget effect values and parabolic behaviour at the origins of models. They also exhibit a strong anisotropical pattern with apparent zonal anisotropy in horizontal plane prolonged in N-S direction, coincident with reservoir body and direction of main geological faults, and vertical direction toward the north, which is in accordance with stratified structure of the calculated variables under study. There is also presence of geometrical anisotropy between E-W and vertical directions and with higher continuity in E-W, which indicates the lowest continuity of studied variables in vertical direction, higher continuity in E-W direction and the highest continuity in N-S direction.

By adding the variogram models of residual variables to the linear trend model initialized at the trend modelling stage, the required non-stationary models are obtained, and subsequently used during geostatistical simulations.

4.5. Results

4.5.1 Geostatistical simulations

As stated previously, simulated grid consists of more than 1.4 million points on a 3D regular grid 50x50x10 m with total gross volume more than 35 milliards m^3. One hundred realisations in total were simulated by Turning Bands method using a given model variogram and search neighbourhood. Non-conditional simulations were conditioned by universal kriging due to using non-stationary structural model. The final numerical model consists of 100 simulated reservoir bodies filled by simulated values of studied variables specific enthalpy *h* and specific exergy index *SExI*.

Fig. 4.5 shows an example of reproduction of the statistical parameters of 1,650 input data and the same skewed shape of the input histogram for SExI shown in Fig. 4.4 D. In general, the individual simulations of the numerical model slightly exceeded experimental minimal and maximal values observed from the input data for both studied variables due to using non-stationary modelling approach. It is well know that the non-stationary approach often exceeds input data range mainly in extrapolation areas of studied domain. The mean values and standard deviation for the individual simulations of numerical model are well reproduced.

Fig. 4.6 shows the mean realisations for both studied variables, representing the spatial distribution of the variable values within the reservoir. The both models clearly show a reproduction of the spatial trend with the simulated values that increase with depth.

One hundred simulated values of the studied variables per each 3D grid node have been used to determine a value of parametric estimation either for enthalpy or specific exergy index in a 3D resolution. We used the given cut-off to detach a part of subpopulation estimated as under the criteria. This allowed delineation of local anomalies meeting a given criteria. Moreover, the cut-offs use also allowed probabilistic determination of distribution of selected variables and target values within the reservoir. Simulation post-processing consists in splitting each of 100 realisations into two parts – above and below a boundary condition (cut-off). On the grid node basis, post-processing continues with counting the number of times when the simulated values of each realisation exceed the boundary condition. This number is normalized by total number of realisations to obtain probability values ranging from 0 to 1. Figs. 4.7, C and D show such probability models. As can be seen, there is very tight transition in vertical direction among zero probability to exceed a given cut-off in the upper part of the reservoir and the very high probabilities at the lower part or at the bottommost parts of the reservoir for *SExI*.

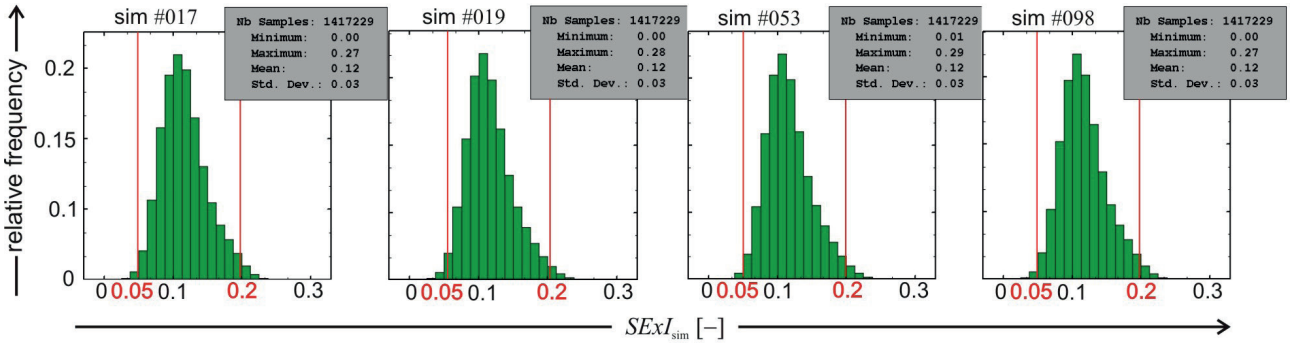

Fig. 4.5. *Experimental histograms of four randomly selected realisations of SExI simulation.*

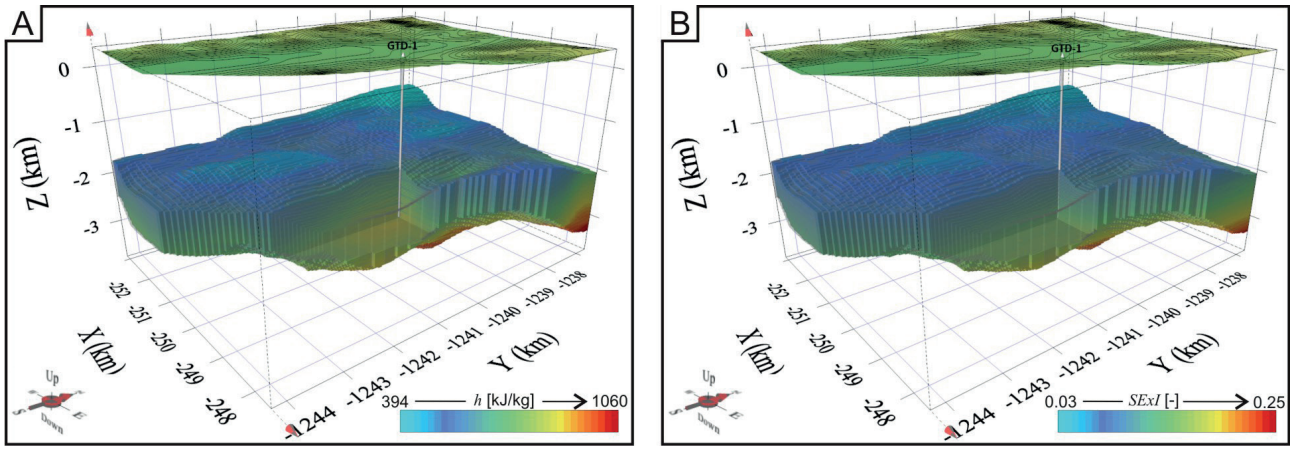

Fig. 4.6. *3D visualization of the mean realisations of the studied variables showing their spatial distribution within the Ďurkov reservoir.*

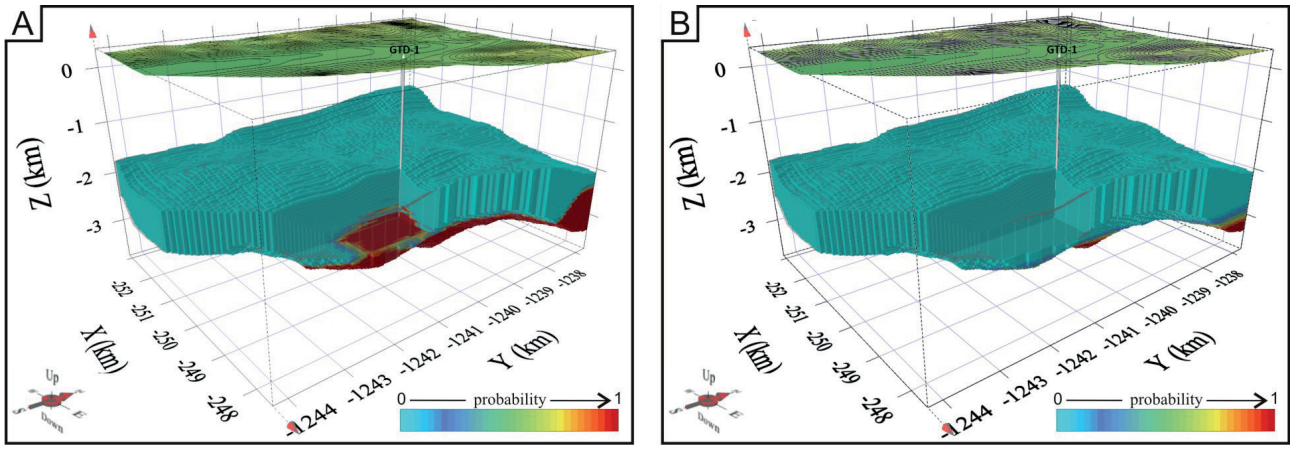

Fig. 4.7. *Probability models for* $h \geq 800$ kJ.kg^{-1} *(A) and* $SExI \geq 0.2$ *(B).*

In fact, there is approximately 5.8 milliards m^3 of volume within the reservoir where enthalpy exceed 800 kJ.kg^{-1} what gives only 16 % of total reservoir volume. Similarly, there is only 7 % (2.55 milliards m^3) of total reservoir volume with specific exergy index above 0.2.

Final probability models were used to construct the volumetrics risk curves as described in 4.3. The volumetrics curves for the studied variables are shown in Fig. 4.8. The final risk curves help to build different risk scenarios for the reservoir volume. For instance, there is only less than 10 % probability or less to get more than 609 Mm^3 of the reservoir volume with specific exergy index higher than 0.2. Or, there is less than 492 Mm^3 of reservoir volume with 90 % probability to get specific exergy index higher than 0.2. In other words, the reservoir volume will decrease with increasing probability to get values above a cut-off. Fig. 4.9 demonstrates the concept where we can clearly see that with increasing probability becomes the reservoir volume with $SExI \geq 0.2$ divided into two distinguishable zones.

4.5.2 Reservoir specific enthalpy

Most of studies on DDHS promote the system as of moderate to high temperature, according to local classification schemes (e.g. Fendek et al., 1999). Temperature (T_{gw}), total dissolved solids (M_{gw}) and calculated hydrostatic pressure (p_{gw}) were used to determine specific enthalpy in reservoir conditions; so that $h_{(z)} = f(T_{gw}, M_{gw}, p_{gw})$ where $T_{gw} = f(z)$, $M_{gw} = f(T_{gw})$ and $p_{gw} = f(z)$.

It is a clear SE trend observed for increase in specific enthalpy within the reservoir body as a function of depth and proximity to the Slanské vrchy Mts. The top of the reservoir extends in depths of 1,660 – 2,600 m, so that the reservoir enthalpy at a top varies h_{top} = 390 – 740 kJ.kg^{-1}. Approximately 50 % of the calculated enthalpy is less than h = 540 kJ.kg^{-1}. Towards the base at z = 1,960 – 4,000 m, the enthalpy fairly increases, i.e. h_{btm} = 440 – 1,060 kJ.kg^{-1}. As given by the model, a mean enthalpy at the base of the reservoir is h = 710 kJ.kg^{-1}. A most significant rise in enthalpy is estimated for the SE part of the system, where

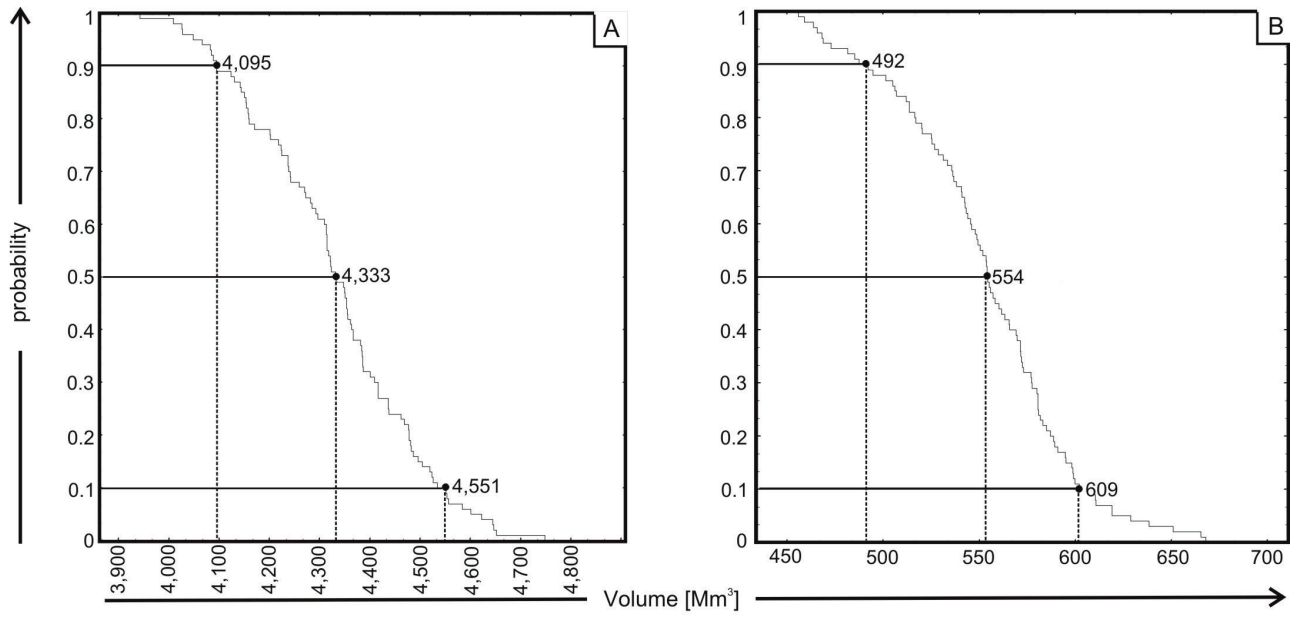

Fig. 4.8. *Final volume risk curves for* $h \geq 800$ kJ.kg^{-1} *(A) and* $SExI \geq 0.2$ *(B).*

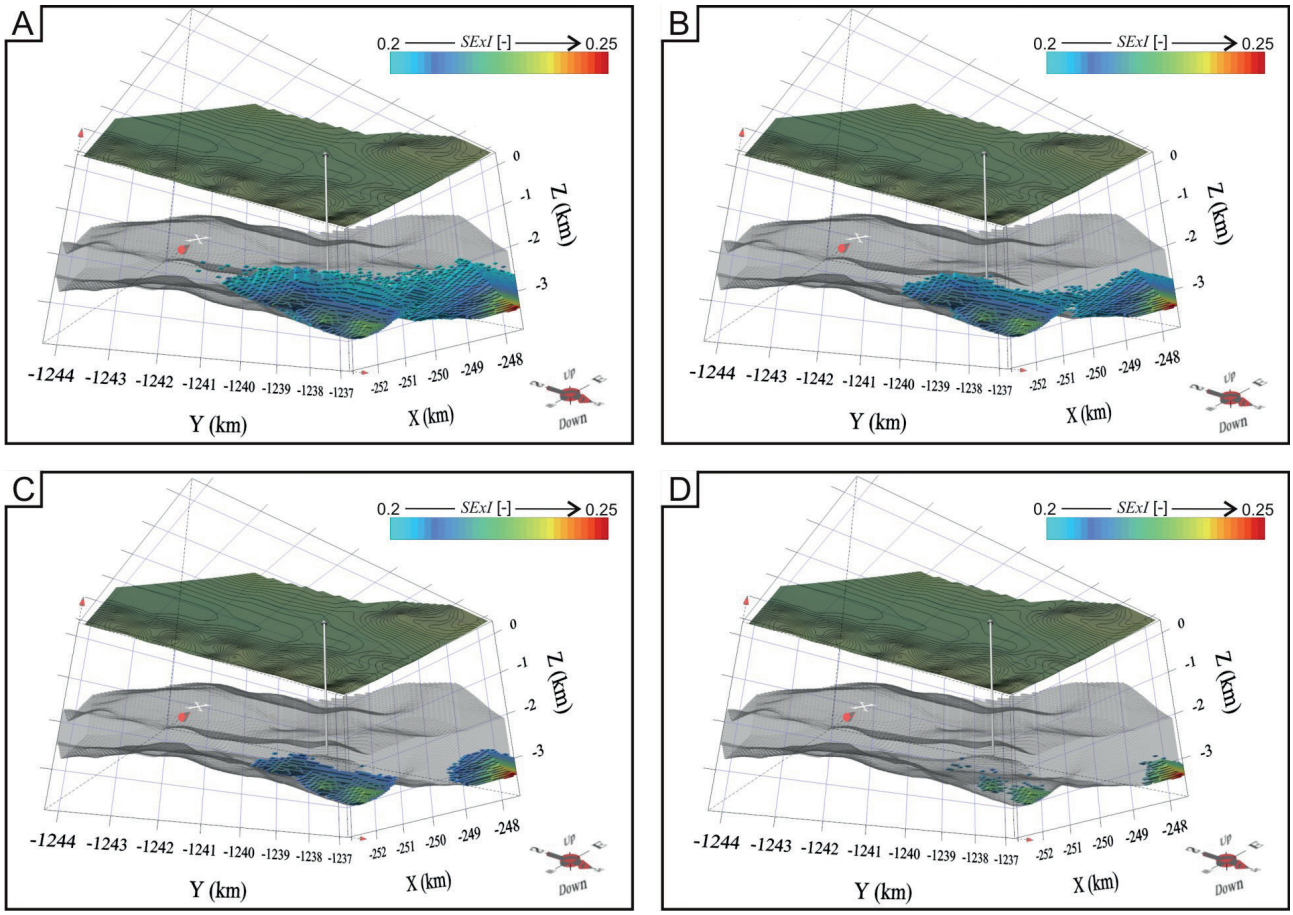

Fig. 4.9. *Probability models of SExI with extracting the non-zero probabilities (A), probabilities higher than 0.1 (B), 0.5 (C) and 0.9 (D).*

the gradient in enthalpy is δh_{res} = 200 – 260 kJ.kg^{-1}.km^{-1}. An overall thickness of the Middle Triassic carbonates in this part is assumed for Δz = 500 – 1,500 m.

Unlike general assumptions, only 16 % of the entire reservoir exceed the arbitrary given limit of h_{res} > 800 kJ.kg^{-1} criteria to distinguish between low and moderate (high) enthalpy geothermal waters. Distribution within the reservoir is uneven, skewed left. A zone of h_{res} > 800 kJ.kg^{-1} locates at the SE margin of the reservoir, in depths of z = 2,870 – 4,000 m below the surface. The zone of elevated, moderate (high) enthalpy, is most probably located east from the Ďurkov municipality. It corresponds to the tectonic block hit by geothermal wells GTD-1, GTD-2 and GTD-3. A vicinity to the neovolcanic Slanské vrchy Mts. and possible metamorphism plays a huge uncertainty to hydraulic properties in that zone though, increasing a risk of failure when tapping for geothermal water and deliverability. Instead of focusing to the E, we propose to delineate the prospective zone along a depressed block of carbonates running N and NE from geothermal wells.

4.5.3 Specific exergy index

By definition, the specific exergy index relates exergy of the given fluid described at a triple point conditions over a maximum exergy available, i.e. e = 1,192 kJ.kg^{-1}. Similar to specific enthalpy, we set the specific entropy; so that the $s = f(T_{gw}, M_{gw}, p)$. Thus, the specific entropy varies s_{top} = 1.2 – 2.1 kJ.kg^{-1}.K^{-1} for the top and increases to s_{btm} = 1.4 – 2.8 kJ.kg^{-1}.K^{-1} at a base of the reservoir. For the entire reservoir body, a mean specific entropy is estimated for s = 1.75 kJ.kg^{-1}.K^{-1}.

Quantitatively, the specific exergy index is calculated for *SExI* = 0.05 – 0.25, with a mean of *SExI* = 0.095 if the reservoir is taken as a solid body. This is strikingly different compared to other hydrogeothermal systems in the Western Carpathians. Based on local geometry and geothermics, a specific exergy index fairly increases between a top ($SExI_{top}$ = 0.04 – 0.06) and bottom ($SExI_{btm}$ = 0.1 – 0.25); so, a mean at a top and a base do (*SExI* = 0.08 and *SExI* = 0.14). A tendency of *SExI* to increase follows the trend of reservoir specific enthalpy; i.e. a clear trend with depth and a direction, the SE margin of the structure, is well expectable. Thus, for what is called the prospective zone in this paper, the specific exergy index interval reduces to *SExI* = 0.11 – 0.25 at depths of z = 2,870 – 4,000 m. However, *SExI* > 0.2 occupies a minimum depths of 3,100 m rather to the east. This part has not been documented yet, bearing a huge risk of failure when targeting to tap the geothermal resource there.

4.5.4 Thermodynamic quality classification

Under a given range of specific exergy index calculated, 99 % of the reservoir exceeds the *SExI* = 0.05 criterion to consider an associated resource as of moderate-low thermodynamic quality. Exception is the NW periphery of

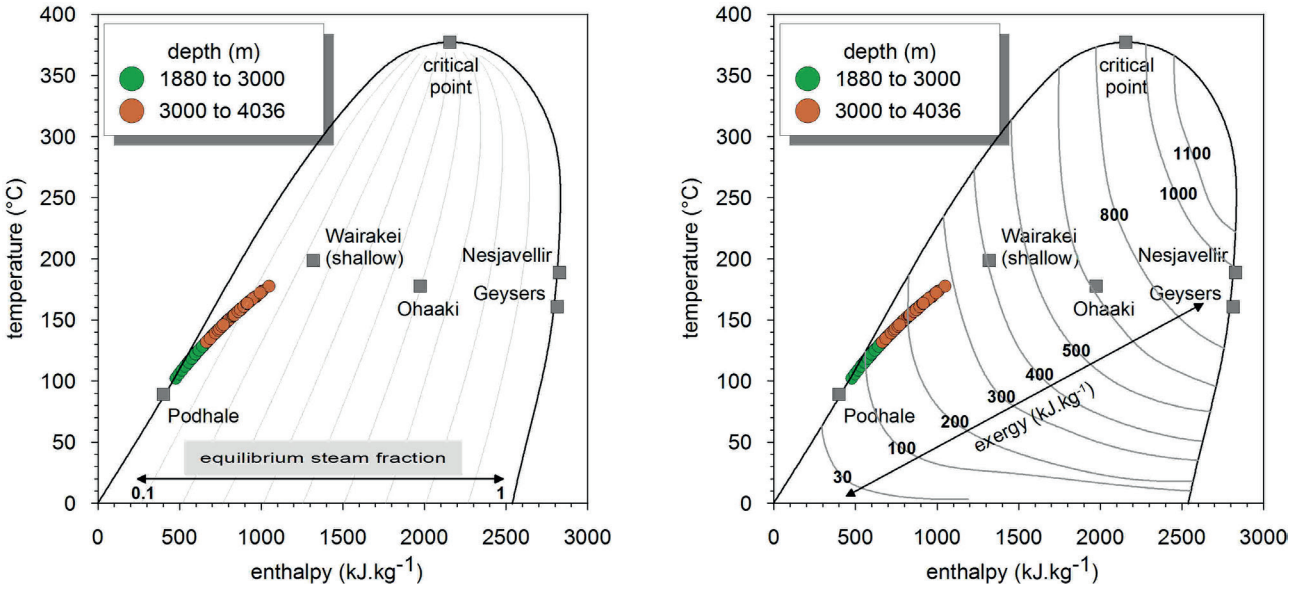

Fig. 4.10. The Ďurkov hydrogeothermal structure – "prospective zone"; T-h diagrams

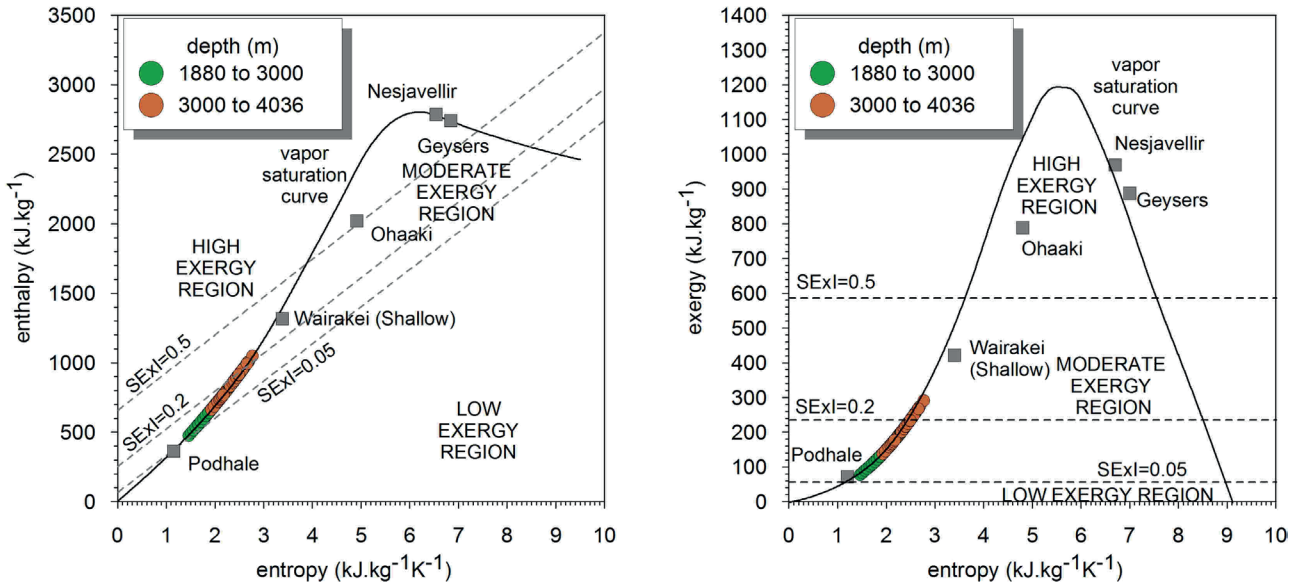

Figure 4.11. The Ďurkov hydrogeothermal structure – "prospective zone"; Mollier's (left) and Rant's (right) diagrams

the structure at depths of z = 1,660 – 1,780 m west from the municipality of Ďurďošík, where carbonates are fairly elevated (z_{top} = 1,600 – 1,800 m; z_{btm} = 1,800 – 4,000 m).

A second standard given by Lee (1996, 2001) recognizes moderate-high thermodynamic quality geothermal resources if *SExI* > 0.2. In geothermic conditions at the DDHS, approximately 7 % of the reservoir exceeds the level of specific exergy index only. Obviously, the zone of elevated thermodynamic quality correlates well to the zone of highest reservoir specific enthalpy, concentrated along E margin of the structure. When considering depths, zones, where moderate-high geothermal resource can be found with 90 % probability of success locates in depths of z = 3,100 – 3,900 m.

Indeed, a skepticism arises when evaluating the elevated thermodynamic quality, at least as implied by *SExI* calculation. A vicinity of neovolcanites triggers geothermic activity there. Meanwhile, an effect of metamorphism and reduction in permeability cannot be omitted. Thus, when considering an anomaly hunting / stacking approach (Cumming, 2009) for a future exploration of the entire geothermal structure, a focus on a tectonic block running NE between Ďurkov and Bidovce/Svinica towns is strictly recommended, as this has been sampled already. This should limit a risk of failure apparent where targeting for highest *specific enthalpy index* or enthalpy.

4.5.5 Thermodynamic quality mapping

To map thermodynamic quality of the geothermal resource associated with the Middle Triassic reservoir, we used state diagrams for enthalpy versus temperature (Fig. 4.10) and entropy versus enthalpy and exergy (Fig. 4.11); both plotting calculation results for a prospective zone of the reservoir only. This should be delineated as a part of the reservoir following a tectonic block hit by GTD-1 to GTD-3 wells in 1999 (Vranovská et al., 1999),

running N of the Ďurkov town and arching NE between the towns of Bidovce and Svinica (Fig. 4.1). Vertically, the zone is limited along a top and bottom of the reservoir. So, if we consider this part as elevated in geothermic and thermodynamic parameters, a rest of the reservoir is, consequently, of lower exergetic quality.

A plot of reservoir enthalpy to reservoir temperature shows only a minor equilibrated steam fraction up to X_S = 0.18, increasing with depth. In fact, recently unpublished sustainable reservoir management evaluation for the structure questions presence of a steam cap in the reservoir and so a possibility of a double phase at depths does. However, for a prospective zone, a resource specific exergy at a triple point conditions ranges $e = 90 – 290$ kJ.kg^{-1}. A reservoir out of the prospective zone does not reach the saturation curve at all. A difference between the DDHS and some geothermal systems worldwide is striking (Fig. 4.10), even if reservoir temperature is comparative. Indeed, with higher steam fraction at Wairakei ($X_S \approx 0.23$) or Ohaaki ($X_S \approx 0.6$), both record higher specific exergies; i.e. e = 400 kJ.kg^{-1} and e = 650 kJ.kg^{-1}, respectively; and are used for geothermal power production. It would, thus, be thermodynamically inefficient (if not impossible) to consider a direct or flashing power generation systems at the DDHS, even temperatures may imply some potential.

Evident is also the difference between the DDHS and selected geothermal fields on the Mollier's and Rant's plot (Fig. 4.11). Even within the prospective zone delineated by heat flux and temperature anomalies, when stacked, only a few percentages exceed a *SExI* = 0.2 (moderate-high exergy) line, although reservoir temperatures between the DDHS and, e.g. Ohaaki, are approximately the same. Rather is the system comparable to Podhale, Fuzhou, Tianjin or Balcova geothermal fields.

Thus, we recommend the system of DDHS to be classified as of moderate-low thermodynamic quality (moderate-low exergy).

4.6 Discussion and conclusions

The presented paper describes and applies geostatistical methodology of spatial modelling and risk assessment thermodynamic conditions of the Ďurkov hydrogeothermal structure in Slovakia. The DDHS is repeatedly reported as the most prospective geothermal system in the Western Carpathians. Three geothermal wells (GTD-1 to GTD-3) have been installed there in 1999 (Vranovská et al., 1999a, b; Beňovský et al., 2001) targeting the prospective tectonic block north from the Ďurkov village. The analysis and spatial modelling were based on calculated spatial data with enthalpy and specific exergy values in 1,650 points within the reservoir body. Geostatistical simulations were used to model the studied variables that are functions of temperature and depth under non-stationary assumption. For that reason, the turning bands simulation technique was chosen to create a 3D numerical model. Final numerical model constituted 100 simulated realisations that were used to delineate probable volume of the reservoir with the enthalpy above 800 kJ.kg^{-1} and specific exergy index above 0.05 and 0.5, respectively. The complete numerical model of the Ďurkov reservoir was used to construct probability risk curves for reservoir volume above the mentioned boundary conditions.

The Ďurkov structure includes about 16 % of the total reservoir volume with the enthalpy above 800 kJ.kg^{-1}. In accordance with the volume risk curve there is less than 13 % of the total volume with more than 10 % probability. For higher probabilities such as 50 % or 90 % there is only 5 % or 10 % reduction of the reservoir volume above the boundary condition.

The specific exergy index above 0.05 occupies almost the entire reservoir with negligible proportion below that values in NW part of the reservoir. On the other side, there is only 7 % of the total reservoir volume with specific exergy exceeding 0.2 in the east and north-east part of the Ďurkov reservoir, mostly with very low probabilities. Indeed, from the volume risk curve it can be conclude that for probability above 10% there is more than 75 % reduction of the original reservoir volume above 0.2 of the specific exergy index. Similarly, for median probability (50 %) there is another almost 10 % reduction of that volume and more than 20 % reduction for probability 90 % with clear separation of the volume into two distinguishable zones.

Thermodynamic conditions for the Ďurkov depression hydrogeothermal structure imply its similarity to several moderate enthalpy, liquid (water) dominated geothermal fields worldwide. Indeed, the Podhale (Barbacki, 2012), Tianjin (Axelsson & Dong, 1998), Fuzhou (Pang et al., 2015) or Balcova (Ozgener et al., 2006) systems produce a geothermal resource for large-scale utilization, such is the district heating or individual space heating in combination with agriculture and recreation. All are also classified of moderate-low or simply a moderate (*SExI* = 0.05 – 0.5) exergy. In fact, no project operates the Ďurkov Depression until now. Thermodynamically, the system is not adequate for power production, lacking a sufficient steam fraction. However, with a cumulative discharge of Q = 115 l.s^{-1} and thermal output of 28 MW$_t$ as proven over closed-looped pumping test, with GTD-1 serving as reinjection well (Vranovská et al., 1999b; Beňovský et al., 2001), utilization of a geothermal resource for geothermal district heating appears outright energetically and exergetically. The more is the fact accented with a town of Košice a 13 km to the west only, still served with coal and natural gas in district heating systems (Fričovský et al., 2013). Thus, instead of increasing a share of geothermal resources on a primary energy mix in the country; reducing energetic dependency of a state on foreign resources; CO_2 mitigation; and transition towards the sustainable development at least on a municipal scale, the geothermal resource is set stand-by, somewhat ignoring its potential.

The thermodynamic study on DDHS reservoir conditions has proven the site as of moderate-low thermodynamic quality. A low equilibrium steam fraction disqualifies other than direct use of the resource, proven by moderate *SExI* values above depths of 3,000 m. Beneath, a risk of failure when targeting that zone increases dramatically. Suitability of the resource for a large-scaled, district heating and cascaded projects is also proven along

a similarity of reservoir (and wellhead) conditions with geothermal fields worldwide.

References

Armstrong, M., 1998: Basic Linear Geostatistics. Springer, ISBN-10 3-540-61845-7.

Axelsson, G. & Dong, Z., 1998: The Tanggu geothermal reservoir (Tianjin, China), Geothermics, 27 (3), p. 271-294.

Barbacki, A., 2012: Classification of geothermal resources in Poland by exergy analysis – Comparative study, Renewable and Sustainable Energy Reviews, 16, p. 123-128.

Beňovský, V., Drozd, V., Halás, O., Vrana, O., & Vranovská, A., 2018: Investigation of the Ďurkov geothermal structure for utilization of geothermal energy, Bulletin d'Hydrogeologie, 17, p. 1-11.

Bodiš, D. & Vranovská, A., 2001: Genéza anomálneho obsahu arzénu v hydrogeotermálnej štruktúre Ďurkov [*Genesis of anomalous arsenic content in the* Ďurkov *hydrogeothermal structure*], Podzemná voda, XVIII (2), p. 123-136, in Slovak, English resume.

Bories, S.A. & Combarnous, M.A., 1973: Natural convection in a sloping porous layer, Journal of Fluid Mechanics, 57 (1), p. 63-79.

Bodvarsson, G.S., Benson, S.M. & Witherspoon, P.A., 1982: Theory of the development of geothermal systems charged by vertical faults, Journal of Geophysical Research, 87 (B11), p. 9317-9328.

Chilès, J. & Delfiner, P., 1999: Geostatistics: Modelling Spatial Uncertainty. John Wiley and Sons, Inc. New York. ISBN 0-471-08315-1.

Clark, I. & Harper, W.V., 2000: Practical Geostatistics 2000. Greyden Press, U.S.A. ISBN 0-9703317-0-3.

Cumming, W., 2009: Geothermal resource conceptual models using surface exploration data, Proceedings, 34th Workshop on Geothermal Reservoir Engineering, Stanford University, CA.

De Fouquet, C., 1993: Reminders on the conditioning kriging. In: Geostatistical simulations, p. 131-145. Edited by Armstrong M, Dowd, P., A. Kluwer Academic, Dordrecht.

Deutsch, C.V. & Journel, A.G., 1998: GSLIB Geostatistical Software Library. 2nd edition. Oxford University Press Inc. New York. ISBN 0-19-510015-8.

DiPippo, R., 2005: Geothermal power plants – principles, applications and case studies, Butterworth – Heinemann, New York.

Dowd, P.A., 2004: MINE5260 Non-Stationarity. MSc. in Mineral Resources and Environmental Geostatistics. University of Leeds, Leeds. 2004. U.K.

Etemoglu, A.B. & Can, M., 2007: Classification of geothermal resources in Turkey by exergy analysis, Renewable and Sustainable Energy Reviews, 11 (7), p. 1596-1606.

Fendek, M. & Fendeková, M., 2010: Country update of the Slovak Republic, Proceedings, World Geothermal Congress 2010, Bali, Indonesia.

Fendek, M. & Fendeková, M., 2015: Country update of the Slovak Republic, Proceedings, World Geothermal Congress 2015, Melbourne, Australia.

Fendek, M., Remšík, A. & Král, M., 1999: The nature of geothermal resources in Slovak Republic, Slovak Geological Magazine, 5 (1-2), p. 121-131.

Franko, O. & Melioris, L., 1999: Conditions for formation & extension of mineral and thermal waters in the Western Carpathians, Slovak Geological Magazine, 5 (1-2), p. 93-109.

Franko, O., Bodiš, D., Fendek, M. & Remšík, A., 1990: Outline of geothermal activity in Czecho-Slovakia, Geothermal Resource Council Transactions, 14 (I), p. 31-40.

Fričovský, B., Jacko Jr., S., Popovičová, M. & Tometz, L., 2013: Substitution approach in carbon dioxide emission reduction evaluation: case study on geothermal power station project plan Ďurkov (Košice Basin, Slovakia), International Journal of Environmental Science and Development, 4 (2), 2, p. 124-129.

Fričovský, B., Černák, R., Marcin, D. & Benková, K., 2016a: A first contribution on thermodynamic analysis and classification of geothermal resources of the Western Carpathians (an engineering approach), Slovak Geological Magazine, 16 (1), p. 94-117.

Fričovský, B., Černák, R., Marcin, D., Benková, K., Remšík, A. & Fendek, M., 2016b: Engineering approach in classification of geothermal resources of Slovakia (Western Carpathians), Proceedings, the 41st Stanford Geothermal Workshop on Reservoir Engineering, Stanford University, CA.

Fričovský B., Vizi, L., Gregor, M., Zlocha, M., Surový, M. & Černák, R., 2018: Thermodynamic Analysis and Quality Mapping of A Geothermal Resource at the Ďurkov Hydrogeothermal Structure, Košice Depression, Eastern Slovakia. Proceedings, 43rd Workshop on Geothermal Reservoir Engineering Stanford University, Stanford, CA.

Goovaerts, P., 1997: Geostatistics for Natural Resources Evaluation. Oxford University Press, Inc. 1997. London. ISBN 0-19-511538-4.

Halás, O., Drozd, V. & Vranovská, A., 1999: Investigation of Ďurkov geothermal structure in Košice Basin for geothermal energy utilization, Proceedings, XXIX IAH Congress: Hydrogeology and Land Use Management, Bratislava, Slovakia.

Hanano, M., 1998: A simple model of two-layered high-temperature liquid-dominated geothermal reservoir as a part of large-scale hydrothermal convection system, Transport in Porous Media, 33, p. 3-27.

Hanano, M. & Kajiwara, T., 1999: Permeability associated with natural convection in the Kakkonda Geothermal Reservoir, Geothermal Resources Council Transactions, 23, p. 351-360.

Isaaks, E.H. & Srivastava, R.M., 1989: An Introduction to Applied Geostatistics. Oxford University Press, Inc. New York. ISBN 0-19-505013-4.

Jalilinasrabady, S. & Itoi, R., 2013: Classification of geothermal energy resources in Japan applying exergy concept, International Journal of Energy Research, 37, p. 1842-1850.

Journel, A.G. & Huijbregts, C.J., 1978: Mining Geostatistics. Academic Press, Inc. London. ISBN 0-12-391050-1.

Journel, A.G., 1986: Geostatistics: Model and Tools for the Earth Sciences. Mathematical Geology, Vol. 18, No. 1, p. 110-130.

Kassoy, D.R. & Zebib, A., 1975: Variable viscosity effects on the onset of convection in porous media, The Physics of Fluids, 18 (12), p. 1649-1651.

Kukurugyová, M., Jablonský, G., Nalevanková, J. & Dzurňák, R., 2015: Production, profit and return of ORC-CHP geothermal power plant model at Ďurkov area, Slovakia, Proceedings, ISET 2015, Bratislava, Slovakia.

Kühn, M., Dobert, F. & Gessner, K., 2006: Numerical investigation of the effect of heterogeneous permeability distributions on free convection in the hydrothermal system at Mount Isa, Australia, Earth and Planetary Science Letters, 244, p. 655-671.

Lantuéjoul, Ch., 2002: Geostatistical Simulations. Models and Algorithms. Springer-Verlag Print, Berlin. ISBN 3-540-42202-1.

Lee, K.C., 1996: Classification of geothermal resources – an engineering approach, Proceedings, 21st Workshop on geothermal reservoir engineering, Stanford University, CA, USA.

Lee, K.C., 2001: Classification of geothermal resources by exergy, Geothermics, 30, p. 431-442.

Ledru, P. & Gillou-Frottier, L., 2010: Reservoir definition. In: Huenges, E. (Ed.): Geothermal Energy Systems. Exploration, Development and Utilization. Wiley-VCH Verlag, Weinheim, DE, p. 1-37.

Leuangthong, O., Khan, K.D. & Deutsch, C.V., 2008: Solved problem in geostatistics. John Wiley & Sons, Inc.. New Jersey. ISBN 978-0-470-17792-1.

Lipsey, L., Pluymaekers, M., Goldberg, T., van Oversteeg, K., Ghazaryan, L., Cloetingh, S. & van Wees J.-D., 2016: Numerical modelling of thermal convection in the Luttelgeest carbonate platform, the Nederlands, Geothermics, 64, p. 135-151.

Matheron, G., 1963: Principles of Geostatistics. Economical Geology, p. 1246-1266. Vol. 58.

Matheron, G., 1971: The theory of regionalized variables and its application. Les Cahiers du Centre de Morphologie Mathématique. École Nationale Supérieure des Mines Paris. Fontainebleau, Paris, France.

Moeck, I.S., 2014: Catalog of geothermal play types based on geologic controls, Geothermics, 37, p. 867-882.

Olea, R.A., 1991: Geostatistical Glossary and Multilingual Dictionary. Oxford University Press, Inc. ISBN 0-19-506689-9.

Olea, R.A., 1999: Geostatistics for Engineers and Earth Scientists. Kluwer Academic Publishers. ISBN 0-7923-8523-3.

Ozgener, L., Hepbasli, A. & Dincer, I., 2005: Energy and exergy analysis of geothermal district heating systems: an application, Building and Environment, 40, p. 1309-1322.

Ozgener, L., Hepbasli, A. & Dincer, I., 2006: Effects of reference state on the performance of energy and exergy evaluation of geothermal district heating system: A Balcova example, Building and Environment, 41, p. 699-709.

Ozgener, L., Hepbasli, A., Dincer, I. & Rosen, M.A., 2007: A key review on performance improvement aspects of geothermal district heating systems and applications, Renewable and Sustainable Energy Reviews, 11, p. 1675-1697.

Pachocká, K., Jacko, S. & Pachocki, M., 2010: 3D modeling of a geothermal reservoir in Eastern Slovakia, VDM Verlag Publ. Saarbrücken, 62 p.

Pang, Z., Luo, J., & Pang, J., 2015: Towards a new classification scheme of geothermal systems in China, Proceedings, World Geothermal Congress 2015, Melbourne, Australia.

Pasquale, V., Chiozzi, P. & Verdoya, M., 2013: Evidence for thermal convection in the deep carbonate aquifer of the eastern sector of the Po Plain, Italy, Tectonophysics, 594, p. 1-12.

Pereszlenyi, M., Pereszlenyiova, A. & Masaryk, P., 1999: Geological setting of the Košice Basin in relation to geothermal energy resources, Bulletin d'Hydrogéologie, 17, p. 1-8.

Rabinowicz, M., Sempéré, J-Ch. & Genthon, P., 1999: Thermal convection in a vertical permeable slot: Implications for hydrothermal circulation along mid-ocean ridges, Journal of Geophysical research, 104 (B12), p. 29275-29292.

Ramajo, H., Tritlla, J., Levresse, G., Tello-Hinojosa, E., Ramírez, G. & Pérez, H., 2010: New SExI tool to evaluate the evolution and anthropic disturbance in geothermal fields: the case of Los Azufres geothermal field, México, Revista Mexicana de Ciencias Geológicas, 27 (3), p. 520-529.

Ravenscroft, P.J., 1994: Conditional Simulation for Mining: Practical Implementation in an Industrial Environment. In Geostatistical Simulations. Armstrong, M.; Dowd, P.A.(Eds.), p. 79-89. Kluwer Academic Publishers. ISBN 0-7923-2732-2.

Rees, D.A.S. & Postelnicu, A., 2001: The onset of convection in an inclined anisotropic porous layer, International Journal of Heat and Mass Transfer, 44, p. 4127-4138.

Sclater, J.G. & Christie, P.A.F., 1980: Continental stretching: an explanation of the post Mid-Cretaceous subsidence of Central North Sea Basin, Journal of Geophysical Research, 85, p. 37111-3739.

Tóth, A.N., 2012: Heat losses in geothermal reservoir, Geosciences and Engineering, 1 (2), p. 321-327.

Vranovská, A., Bodiš, D. & Drozd, V., 1999: Zhodnotenie hydrogeotermálnej štruktúry Ďurkov na základe vrtov GTD-1,2 a 3 [*Evaluation of hydrogeothermal structure* Ďurkov *based on wells GTD-1,2 and 3*], Podzemná voda, V (2), p. 45-53, in Slovak, English resume.

Vranovská, A., Bondarenková, Z., Král, M. & Drozd, V., 1999: Košická kotlina - štruktúra Ďurkov - hydrogeotermálne zhodnotenie, vyhľadávací prieskum [*Košice Basin* – Ďurkov *structure, hydrogeothermal evaluation, exploratory survey*]. Manuscript – Final Report, Slovgeoterm / SGIDŠ, Bratislava, Slovak Republic. 90 p. In Slovak,

Vranovská, A., Beňovský, V., Drozd, V., Halás, O. & Váňa, O., 2000: Investigation for geothermal energy utilization in the town Košice, Slovak Republic, Proceedings, World Geothermal Congress 2000, Kyushu-Tohoku, Japan.

Vranovská, A., Bodiš, D., Šráček, O. & Ženišová, Z., 2015: Anomalous arsenic concentrations in the Ďurkov carbonate geothermal structure, eastern Slovakia, Environmental Earth Science, 73, p. 7103-7114.

Wackernagel, H., 2003: Multivariate Geostatistics. 3rd edition. Springer-Verlag Print, Berlin. ISBN 3-540-44142-5.

Wang, C.T. & Horne, R.N., 2000: Boiling flow in horizontal structure, Geothermics, 29, p. 759-772.

Webster, R. & Oliver, M.A., 2001: Geostatistics for Environmental Scientists. John Wiley & Sons, Inc. 2001. New York. ISBN 0-471-96553-7.

Instructions to authors

General instructions

The Editorial Board of the Slovak Geological Magazine accepts manuscripts in English language.

The Editorial Board accepts or refuses a manuscript with regard to the reviewers` opinions. The authors are informed about a refusal within 14 days after receiving the decision of the Editorial Board. Accepted manuscripts are prepared for a publication in an appropriate issue of the magazine. The author(s) and the publishers enter a contract establishing the rights and duties of both parties during editorial preparation and printing, until the time of a paper publishing. Simultaneously with article the editorial office must receive the corresponding author's proclamation that no part of the manuscript was already published and figures are original as well. Copied figures must be legalized by obtaining the copyright. The proclamation must contain the name of author (authors), title and the address of residence.

Text layout

The text should be arranged as follows: full name of the author(s); title of the paper, number of supplements (in brackets, below the title, e.g. 5 figs., 4 tabs.); key words - maximum 6 key words arranged successively from general to special terms; abstract (max. 300 words presenting principal results, without references); in a footnote of the first page, name of the author(s) as well as her/his/their professional or private address.

The extent of the article is limited to 30 manuscript pages including references, figures and explanations. Publishing of longer articles must be agreed by the Editorial Board.

The text of the paper should be logically divided. Text must be sectionalized by headlines, the position of the main headlines is in the centre of the page, associated headlines start from the left side of the page. The hierarchy of headings can contain maximum three levels (1 - highest level, 2 - lower, 3 - lowermost), being indicated by pencil at the particular heading. Text of the article has to contain the introduction, characterization (state) of investigated problem, used methodology, obtained data, discussion, conclusion and references.

The references in the text should be used preferably in parentheses. Names of cited authors in the text are written without first names or initials (e.g. Matula, 1969); the names of the co-authors are divided (e.g. Mišík & Sýkora, 1981). The name(s) is followed by a comma. If there are more authors, the first one, or the first two only are cited, adding et al. and publication year.

Mathematical and physical symbols of units, such as m, °C should be preceded by a space, e.g. 20 m, 50 °C, etc. In the case of % and ‰, the exemption shall be made: 10%, 2‰. SI units are preferred. Abbreviations of the units such as second, liter, etc. should be written without a period. Compass readings may be substitute by the abbreviations E, W, NW, SSE, etc. Brackets (parentheses) are to be indicated as should be printed, i.e. square brackets, parentheses or compound. Dashes should be typed as double hyphens. Please, use comma, as a 3-digit group separator (10,000) and decimal point, as separator of the fractional part of decimal number (0.1)

Text of the article must be sent to Editorial office printed in two copies with line spacing 2, as well as on CD. Please for using preferable MS Word editor for PC. Figs. and Tabs. must be delivered in digital form in separate files. Paragraphs are marked with 1 tab space from the left margin, or by a typographic symbol. Greek character in the text must be visualized in the text by its name [e.g. ʊ (omega)]. Indices and exponents should be properly marked.

Figures and tables

The high quality of illustrations is required. Their aim is the most effective documenting and explaining the text. When drawing them by hand or computer their maximum width 81 mm (width of column) or 170 mm (width of page) must be taken into account. Properly adapted figure (dimensions of letters, thickness of lines) can be reproduced also in the scale 1: 1, but there is recommended to prepare figures in larger scale. The pen-drawn figures must be prepared by black ink using the template for figures. The minimum acceptable size of capitals and numbers in camera-ready figure is 2 mm. Maximum dimension of illustration in journal is 170 x 240 mm. Overlapping of illustrations should be avoided.

Figures compiled using the computer must be printed by high resolution laser printer (min. 300 DPI). For figures drawing the editorial office recommends the Corel Draw software. The very thin lines (hair lines) as well as automatic filling of objects are not allowed. The filling must consist from separately set objects. The raster-type filling of planes is either appropriate.

Each illustration including photographs must contain graphic (metric) scale. Grouped figures, e.g. photographs and diagrams must be compiled as one figure with separate parts designated a, b, c, etc. They are referred to as one picture.

Photographs must be sharp, preferably black & white, contrast, in the form of JPG or TIFF files having resolution of at least 600 DPI.

All figures must contain their number, description and name of author; in the case of maps and sketches an arrow indicating their orientation, and scale.

The explanations used for a series of several maps and profiles should correspond to that in the first figure. Description to figures should be inserted in the text on their proper place.

Each illustration and table must be referred in the text.

The high quality colour illustrations can be published after agreement by editorial office. The costs incurred will be charged to the account of the author (50 EUR for one page).

The Publisher reserves the right to return the graphic supplements back to author after language correction, resp. demand him to replace them by the higher quality ones.

Tables are submitted on separate page. Their layout is accepted in a size of up to A4. More widespread tables are not accepted.

Data are incorporated into table only when there is no possibility to incorporate them into text. The numbering of tables shall be gradual. Short explanation to a table should be included on the same sheet. If the text is longer, it should be typed on a separate sheet.

References

The list of references should only include the works cited in the text. The references are stated in alphanumeric order, with hanging indent in the second and following lines. The denotation "in press" can be used only in the cases of acceptance of reviewed version of article by editorial board. The denotation "personal information" can be cited only in the text (e.g. Kováčik, pers. information, 2008). When referring the data by other author not being the co-author of referred publication, in the text he is cited in the following form: (Gerda in Kubka, 1975), though in the list of literature is stated only Kubka J., 1975.

Examples of referring:

Book

Gazda, L. & Čech, M., 1988: Paleozoic of the Medzev nappe. Bratislava, Alfa, 155 p.

Journal

Vrba, P., 1989: Shear zones in the metapelite complexes. Mineralia Slov., 21, p. 135 –142.

Anniversary volume

Návesný, D., 1987: High-potassium rhyolites. In: Romanov, V. (ed.): Stratiform deposits of Gemericum. Spec. publ. Slov. Geol. Soc. Košice, p. 203 – 215.

Manuscript

Radvanský, F., Slivka, B., Viktor, J. & Srnka, T., 1985: Vein deposits of the Jedľovec nappe of Gemericum. Final report from the project SGR-geophysics. Manuscript-archive ŠGÚDŠ Spišská Nová Ves, 28 p.

Proofs

The authors are obliged to correct the errors, which are due to typing and technical arrangements. The first proof is sent to author(s). The second proof is provided only to the editorial office. It can be sent to authors upon request.

The proofs must be marked clearly and intelligibly, to avoid further errors and doubts. Common typographic symbols are to be used; their list and meaning will be provided by editorial office. Each used symbol must also appear on the margin of the text, if possible on the same line where the error occurred. The deadline and conditions for proof-reading are subject to the contract, which is governed by the Chairman of the Editorial Board.

Final remarks

These instructions are obligatory to all authors. Exceptions can be made by the Editorial Board or the Scientific Editor. Manuscripts not complying with these instructions shall be returned to the authors.

The Editorial Board reserves the right to publish preferentially invited manuscript and to assemble thematic volumes.

The manuscripts should be sent by e-mail to the address:
slovak.geological.magazine[at]geology.sk.

Contents

www.geology.sk/slovak-geological-magazine/